The Structural Behaviour of Horizontally Curved Prestressed Concrete Box Girder Bridges

Alyaa Shatti Mohan Alhamaidah

School of Computing, Science and Engineering
University of Salford, Salford, United Kingdom

Submitted in Partial Fulfilment of the Requirements of the Degree of Doctor of Philosophy, September 2017

Abstract

Bridges are important and efficient structures which are comprised of a number of elements and substructures, namely the deck, abutment and foundation and possibly additional intermediate supports. Recently the horizontally curved box girder bridge has become more desirable in modern motorway systems and big cities. Even though numerous amounts of research have been in progress to analyse and understand the behaviour of all types of box-girder bridges, the results from these different research projects are unevaluated and dispersed.

Therefore, a clear understanding of an accurate study on straight and curved box-girder bridges is needed. In this study, a three dimensional straight and horizontally curved prestressed box section has been analysed with shell elements using the finite element analysis program ANSYS to examine structural behaviour and load carrying capacity. The box girder under static gravity, pre-stressed and gravity + pre-stressed loading has been analysed. The model which has been investigated in this report is taken from a published paper and expanded to study the effects of curvature under different loads applied (UDLs). The report concludes that the FEA using shell elements is able to predict the behaviour of box girders with adequate accuracy through the comparisons made between stress results from analytical hand calculations and published work, both for the straight and curved box girder bridges.

Further theoretical and analytical investigations have been carried out to study the effects of parameters such as horizontal curvature, prestressing, and traffic patterning. For this purpose, a new model was created, modelled with an accurate prestress representation and analysed as a three-dimensional model using the ANSYS.

This thesis presents a complete description of the bridge system, addressing the aforementioned parameters and presenting the results through graphs of stress distribution, and displacement. Recommendations for the practical use of FE for bridge design are discussed.

Table of Contents

List of Figures

List of Tables

Acknowledgements

In the name of Allah, Most Gracious, Most Merciful

All praise and glory to Almighty Allah who gave me strength, courage and patience to carry out this research.

This study would not have been possible without the Iraqi government financial support, my sponsor (HCED) and Iraq Ministry of Higher Education and Scientific Research.

I would like to express profound gratitude to my advisor Dr Lawrence Weekes for his patient and helpful supervision. Without his careful feedback, the present work would not have been possible.

I would like to express my gratitude to Mr. Haynes, Neil Currie for their help.

I also wish to thank my colleagues at the University of Salford and University of Basra, and the administrative and library staff, for their kind support.

Finally, I would like to thank my mother and my two sisters, my relatives (my mum's brothers and my aunties) and my love ones, as well as my close friends in the UK, without whose loving support this often arduous journey would have been much more difficult.

I lovingly dedicate this thesis to my mum, my sisters and my loved ones who supported me each step of the way

Declaration

I declare that this thesis has been composed solely by myself and that it has not been submitted, in whole or in part, in any previous application for a degree. Except where states otherwise by reference or acknowledgment, the work presented is entirely my own. The data analysis is entirely by own work.

……

Alyaa Alhamaidah Date

Chapter One

Introduction

Prestressed curved box girder bridges are amongst the most common types of highway bridges. These bridges allow long spans to be achieved due to the prestress (as an economic solution), and are excellent in resisting torsion due to their 'closed' sectional nature. The design of these bridges has evolved over time, and the design of prestressed bridges which are horizontally straight in form is a well understood process. However, the client and/or engineer may well be faced with the situation where a horizontally curved deck solution is preferable.

The conventional design consideration for prestressing is the resistance of vertical load actions, hence prestressing cables are usually curved in the vertical plane to produce bending moments which oppose those produced by the loading (effectively causing an opposing 'equivalent' load). A horizontally curved bridge, by its geometric nature, will require the prestressing cable to follow the curve in the horizontal plane. This does not necessarily require the prestress to have deviation of horizontal distance from the section centroid which would otherwise cause prestressing moments in the horizontal plane. However, as curved bridges will suffer from torsion as well as vertical loading effects, the presence of the prestress may well prove beneficial in resisting any additional torsional effects, coupled with the sectional geometry of the box girder.

1.1 Box girder

Box girder bridges comprise girders with a hollow box shape and are constructed from materials such as concrete, steel, or a composite of steel and reinforced concrete. Figure (1.1) shows a photograph of a typical horizontally curved prestressed concrete bridge.

Figure (1.1) Curved box girder bridge (Civil Engineering, 2015)

The first box girder bridges were usually built using cantilever construction. Examples show the history of box girder cross sections figure (1.2) where box girders started as a solid section then for economic reasons box girders became open sections till the box girder shapes reached this stage with closed sections, (Schlaich & Scheef, 1982).

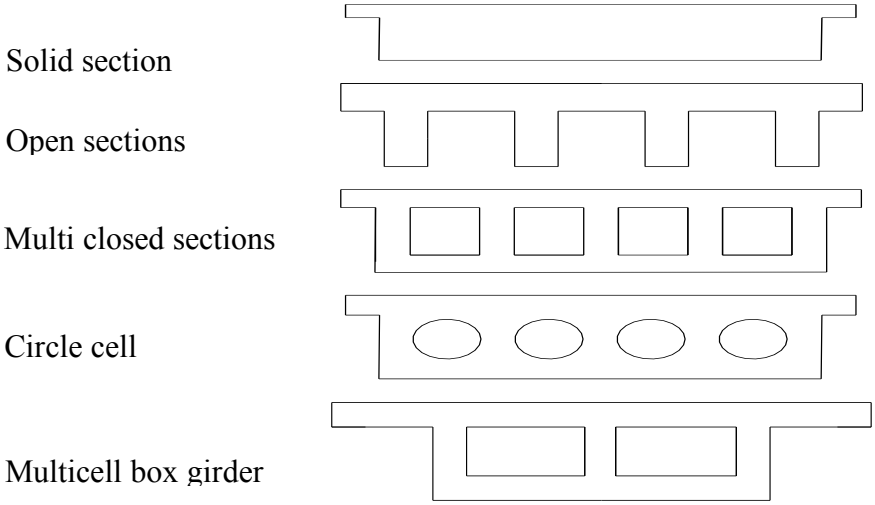

Figure (1.2) Development of the box girder cross- section

I-girder prestressed concrete bridges started to be used when the first one was built at the end of 1920'S and then the biggest achievement happened later when Magnel constructed in 1948 The Sclayn Bridge over the river Maas, figure (1.3). It comprised two spans of 62.70 m of continuous prestressed concrete box girder construction.

Figure (1.3) The Sclayn bridge (International Database for Civil and Structural Engineering, 2015).

Box girder bridges have become a popular construction in recent highway systems. There are many reasons for their desirability, such as rise of traffic volume, economics and aesthetic design choices. The use of straight segmental construction has decreased compared with curved girders because in urban areas where elevated highways and multi-level structures are necessary, modern highway bridges are often subjected to severe geometric restraints; consequently, there must be constructed as a curved alignment. Even though the cost of building the superstructure as a curved girder is higher, the total cost of the curved girder system has reduced significantly since the number of intermediate supports, expansion joints and bearing details has reduced. The continuous curved girder also offers a more aesthetically pleasing structure. In spite of the advantages stated above, horizontally curved girders are more complex than straight girders. Curved girders are subjected to vertical bending plus torsion caused by the girder curvature. In the 1960's, researchers started to focus attention on curved girder complexities and formulated

approximate assumptions that deal with the analysis of curved bridges. Previously curved girders were assumed as a series of straight segments that were used as chords in forming a curved alignment. With the availability of analytical software, the analysis of curved bridges is relatively straightforward.

1.2 Curved box girder

Box girder cross sections may take the form of single cell (one box), multi-spline (separate boxes) or multi-cells with a common bottom flange. Box girders offer better resistance to torsion, which is particularly of benefit if the bridge deck is curved in plan. Due to the high torsional stiffness of the closed cross section of the box girders, which often ranges from 100 to 1000 times larger than the torsional stiffness of comparable I-shaped sections, the torsional moment induced by the curvature of the girder can be resisted by the box girder. The fabrication of the box girder is more expensive compared to the I-shaped girder, but this additional cost is usually balanced by the reduction in substructuring for the box girder, the top of the box girder will work as the deck. Additionally, for long span bridges, where the segmental method of construction is chosen, prestressed concrete box girders have proved to be economical.

The main reason for box sections becoming more popular is that for eccentrically placing the live loads on the deck slabs while the distribution of longitudinal flexural stresses across the section remains more or less identical to that produced by symmetrical transverse loading. In other words, the high torsional strength of the box section makes it very suitable for long span bridges. Torsional moments are produced in vertically loaded horizontally curved bridges, in addition to bending and shear, and for this reason box girder sections are now frequently used in highway bridges. Twisting moments have the tendency to deform the bridge cross section and produce non-uniformly distributed longitudinal flange stresses in addition to the secondary flexural stress in the plates. Therefore, when shear is applied as a torsional component, the section will twist without distorting the cross section and this will cause small longitudinal warping stresses without producing any transverse flexural distortional stresses. When a point load applied on a box like in (a, b & c) the results for warping, shear lag, and cross-sectional distortion will be as (d to i) figure (1.4). In straight box sections under symmetrical loading, the stresses produced by warping, shear lag, and cross-sectional distortion are usually small as these loads create only a slight twist, figure (1.4). However, in curved box bridges, twisting/torsional moments are created

for even symmetrical loading and a small amount of distortional deformations will occur. Warping and distortion in cross-sections have major effects on stress distributions along the bridge. One of the effects is the ability to create a complex bending pattern and non-uniform flange stresses in the longitudinal direction at the corner of the box where stresses will reach their highest values. Higher resistance values can be achieved by adding intermediate diaphragms or by providing extra stiffeners in the cross-section (Prayash Gomdenn, 2012).

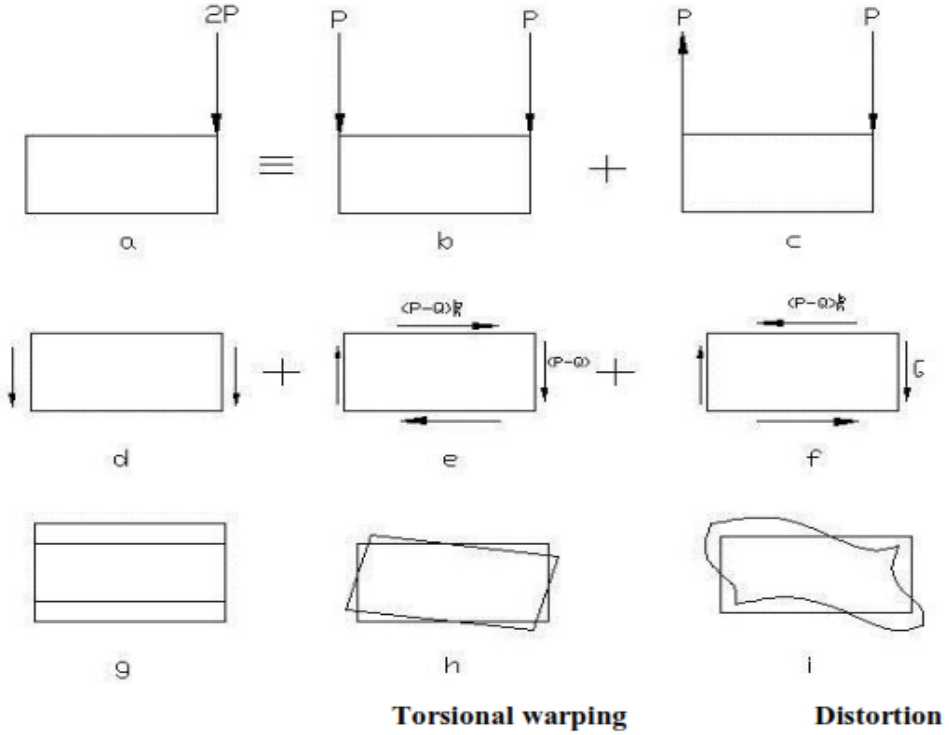

Figure (1.4) Behaviour of box girder subjected to eccentric loading (Prayash Gomdenn, 2012).

Curved girders are usually employed for long spans to decrease substructure costs and the number of expansion joints and bearing details. Deterioration around the joints and bearings can result in leakage which is the main servicing problem related to these common details. Furthermore, curved girders provide a more convenient way to satisfy the response of highway structures for prearranged roadway curves and fitted geometric boundaries provided by the accumulation of right-of-way restrictions. The box girder comprises various types of geometries and forms, but the cross-section can generally be divided into single-cell, multi-cell or spread box beams as shown in figure (1.5). (Associates, inc & Zocon consulting engineers, inc., 2008).

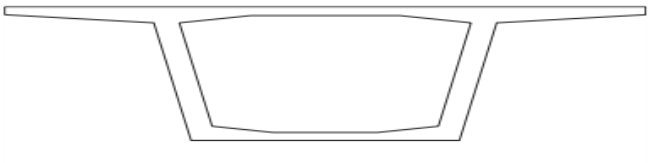

Single cell-box girder

Multi-cell box girder

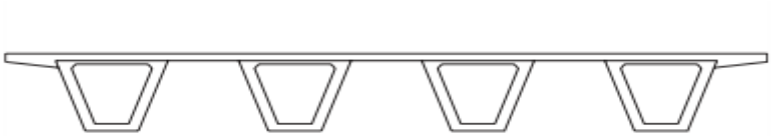

Spread box beams

Figure (1.5) Types of cross sections (National Cooperative Highway Research Program, 2008).

In addition to normal static loading, curved box bridges are subject to dynamic loads while they are under construction or during service. These loads can be as a result of winds, waves, earthquakes and traffic movements.

Bridge design codes also consider the dynamic loading occurring from vehicles moving over the bridge such as those caused by traffic frictional transfer of braking forces. Recently, various parametric studies have been carried out to investigate the behaviour of curved girder bridges due to length, loading and radius. Research has focused on this area with consideration of dynamic loading from highway traffic (Sarode & Vesmawala, 2014), while seismic effects have only received modest research, therefore, seismic behaviour requires more investigation. The dynamic response of a structure is reliant on the modal characteristics of the structure and the characteristics of the dynamic load to which it is subjected. However, dynamic loads including the earthquake loads are commonly defined in the form of a time history or a response spectrum.

Curved box girders have many advantages in addition to the fact that they have high strength and are more resistant to torsional effects. The construction depth of box girders is smaller than plate girders and provides a space for the passage of maintenance and services such as gas pipes, cables, and water because of their closed shapes. Also, they are good in resisting corrosion.

Moreover, the shape of horizontally curved bridges is more aesthetically pleasing than the shape of similar chorded structures, traffic design speeds can be maintained with less land space needed and undoubtedly, the upper flange of box sections can act as part of the deck structure. On the other hand, the disadvantages reported include the difficulty of casting in-situ because of the unavailability of the bottom slab and the need to remove the internal shutter. In addition, the box sections require higher manufacturing costs compared with I-steel girder. Box girder bridges which are more suitable to use for long spans (range from 12 m to 300 m) especially in the case of curved girders there is higher torsion and lower depth requirement.

1.3 Prestressing

Prestressed concrete is a commonly used construction technique typically employed in the construction of long and medium span bridges. The prestress is usually applied through prestressing tendons (generally of high tensile steel cable or rods) providing an axial clamping load which produces a compressive stress (and usually bending stresses) that balances the bending stresses that compression member of concrete would otherwise experience due to a transverse load. Traditional reinforced concrete is based on the use of steel reinforcement bars (rebar) inside poured concrete. In 1930, Freyssinet developed the idea of using prestress reinforcement, and this material was extensively applied for long-span bridge construction to replace the use of normal reinforcing steel which could cost more for maintenance under changing environmental conditions, (Engineeringcivil.com, 2013).

1.4 Aim

Due to the increased need for curved bridges in modern cities and the complexity of curved bridge design and analysis, this research has been carried out to investigate the structural behaviour of horizontally curved prestressed concrete box girder bridges by changing the prestressing values under different load capacities and different traffic patterns.

1.5 Objective

The aims will be achieved by creating a three-dimensional finite element analysis model (3D FEA) of a typical box girder bridge using two-dimensional shell elements and including prestress

effects. The 3D FEA model will be verified against traditional hand calculations for stresses, and these will be used not only as a marker for validation, but to confirm load carrying capacities. The bridge will be modelled as both straight and curved (with varying curvature) with the inclusion of prestress. Self-weight will be accounted for in the analysis and the capacity for additional live load at varying curvatures will be assessed from allowable stresses. The commercial finite element program ANSYS will be used for this study.

This thesis will study:

1- The structural behaviour of a prestressed curved box girder under static loading.
2- From numerical studies, determine the stress distribution in a typical prestressed concrete box girder bridge and compare with published results.
3- The effect of changing the horizontal curvature on the load carrying capacity of the bridge starting from a straight deck, then changing the radius of curvature.
4- The effects of load and traffic patterning on the stresses induced in the bridge for different curvatures, using a parametric study.
5- To verify the structural model against hands calculations, allowing the performance of the prestressed curved box girder to be evaluated.

Chapter Two

Prestressed Concrete

2.1 The principles of prestressed concrete

Bridges are considered to be one of the most important constructions in any society, and due to modern lifestyle, artistic and economic progress, they have had a lot of attention from designers around the world. A bridge design is usually more complex when compared to other structures, therefore to accomplish this goal there should be a full knowledge of the structural behaviour of the bridge and the bridge responses for different geometries, loading or environmental conditions.

The main load carrying element of the bridge structure is the deck which can be constructed of different materials, one of which may typically be a prestressed concrete box girder. Pre-stressed concrete is a common form of construction for bridges, especially when the span length ranges between 25m to 450m. Precompressive stresses in a pre-stressed concrete member are created first before the member is subject to service loading to decrease tensile stresses (Mosley et al., 2012); as a result of this, the need to reinforce the tension zone will be reduced in a concrete section through converting the direct stresses in the section to compression. Concrete is known to be weak in tension so by introducing pre-stressing, the concrete will be able to carry more bending moments by reducing (or eliminating) the tensile stresses in the concrete.

2.2 Prestressed concrete

In industry, the demand to innovate and achieve new ideas which are quicker to construct, more durable and economic is the goal. In the same way, the aim of creating pre-stressed concrete was to fulfil the need in order to produce structures with higher load capacity, longer spans less deflection, with less material. Pre-stressing is the artificial creation of beneficial permanent compressive stresses in a concrete member to improve its load capacity (Lin & Burns, 1981).

To understand the theory of pre-stressing, the concept will be explained in more detail in the following section.

2.3 The concept of prestressing

When a beam is under load, the stresses result from loading will be distributed as compressive on the top face of the beam and tensile stresses on the bottom face (Benaim, 2008). The material properties of concrete are well known for being strong in compression, but will only take a small amount of tensile stress before cracking. Hence the concept of prestress was conceived to reduce (if not remove) any tensile stress in any structural member by preforcing it to experience precompression before loading – in the knowledge that the material being prestressed has a high compressive capacity (Mosley et al., 2012). The same concept works for beams and bridges constructed of concrete.

The assumed bending moment for a rectangular concrete simply supported beam under the effects of gravity alone is shown in figure (2.1). If the same beam is now prestressed with a steel cable (which is placed under tension and subsequently transferred to compression in the concrete) the bending moment diagram will change due to the prestress as shown in figure (2.2). As a result of these two cases, the resulting bending moment will change through the beam as figure (2.3) shows. These cases of loading will also affect the stresses acting on the member. Looking specifically at the midspan location, the first case (self-weight) creates a linearly varying compressive to tensile stress distribution from top to bottom of the section. For the second case, the application of prestress through a cable creates a bending moment equal to (P x e), where P is the prestress and e is the downward eccentricity from the centroid of the section. If the tendon is straight and has deviated by the same amount of eccentricity along the entire length of the beam, the prestress bending moment will be hogging and constant along it's length also. In addition to this the presence of the prestress ensures that there is a uniform axial stress component across the depth of the section. Hence the stress distribution in the section will also be linearly varying across the depth from top to bottom, but as the bending moment is now in the opposite sense to that caused by self weight effects, there is a combination of axial and bending stress which varies linearly from a minimum at the top of the section (minimum compression, possible tension) to a maximum at the bottom of the section. If the prestress is designed such that the prestress bending moment balances the bending moment from self-weight at midspan, then a uniform compressive stress of (P/A) is created in the section where (P) is the prestressed load and (A) is the cross-sectional area (as shown in figure (2.1)). The resultant stresses are a summation of both tensile stresses on the bottom of the span member and compression stresses

along the top of the member. The stresses can be calculated from (My/I) where (M) is moment (y) the distance from the centroid to the extreme fibre and (I) is the second moment of area of the section. After this, it is apparently clear that the structural beam will carry loads with the member predominantly acting in compression where the dead loads are usually balanced by the prestress and live loads are usually dealt with by limiting stresses (i.e. no tension or small value), figure (2.4).

L: length of the beam member,

H: height of the beam member

P: prestressed force

and (e) is the eccentricity.

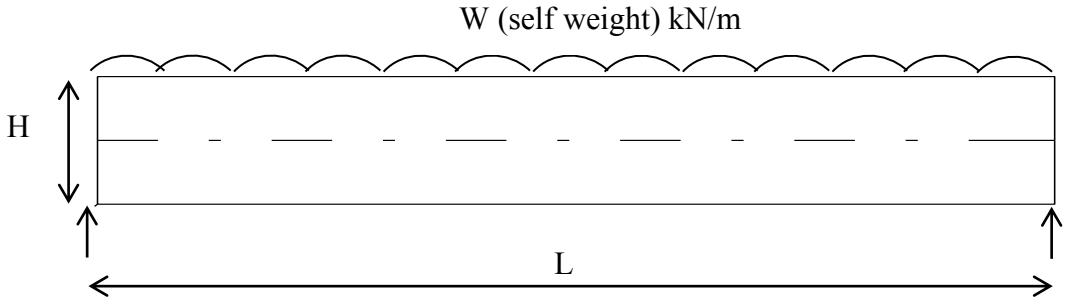

Simply supported beam

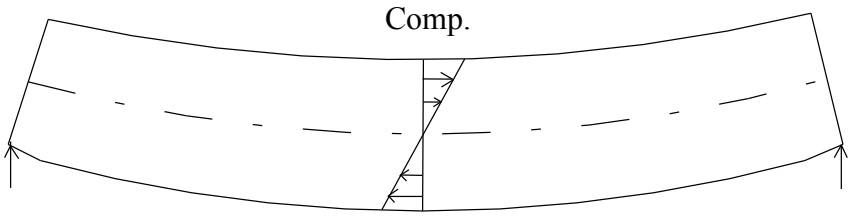

Simply supported beam under gravity

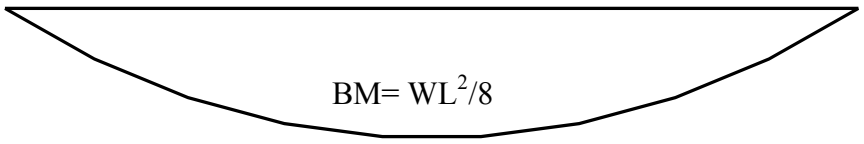

Bending moment for simply supported beam under gravity action

Figure (2.1) Simply supported beam

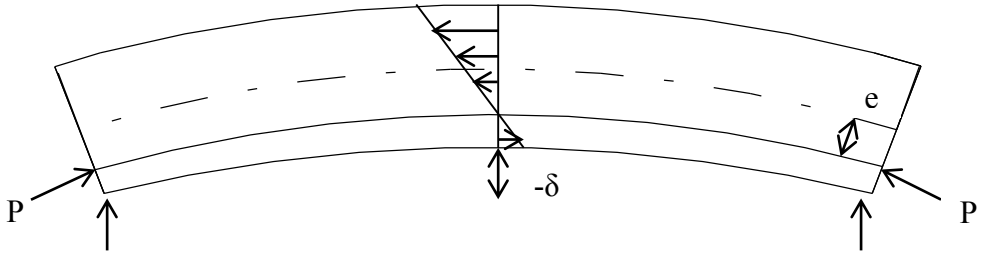

Prestressed simply supported beam

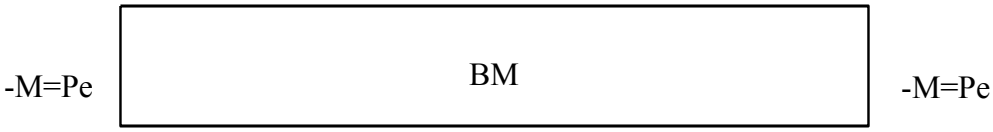

Bending moment for prestressed simply supported beam

Figure (2.2) Prestressed simply supported beam

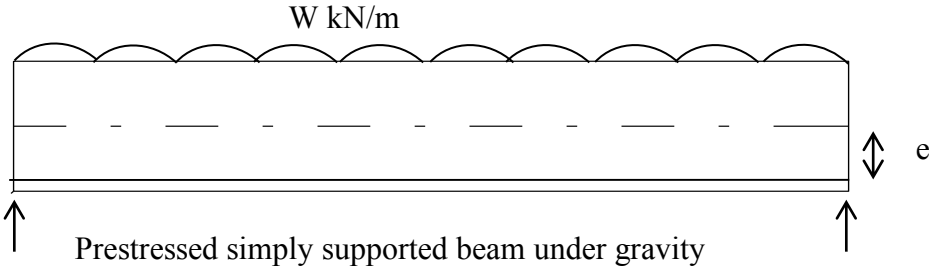

Prestressed simply supported beam under gravity

Bending moment for prestressed simply supported beam under gravity

Figure (2.3) Bending moment distribution of a prestressed beam

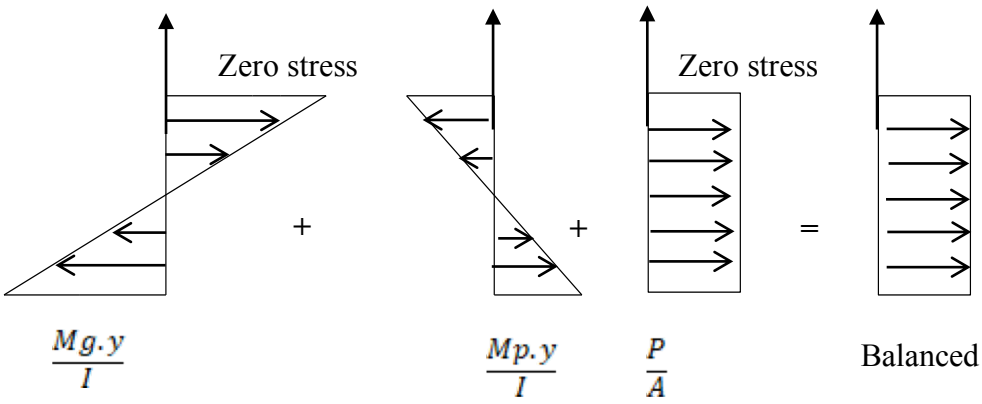

$Mg = \frac{WL^2}{8}$, W: **load due to gravity** Mg : Gravity moment, $\boldsymbol{Mp = P \times e}$, $\boldsymbol{Mp}$: Prestressed moment

Figure (2.4) Stress distribution of a prestressed beam when the bending stresses are balanced

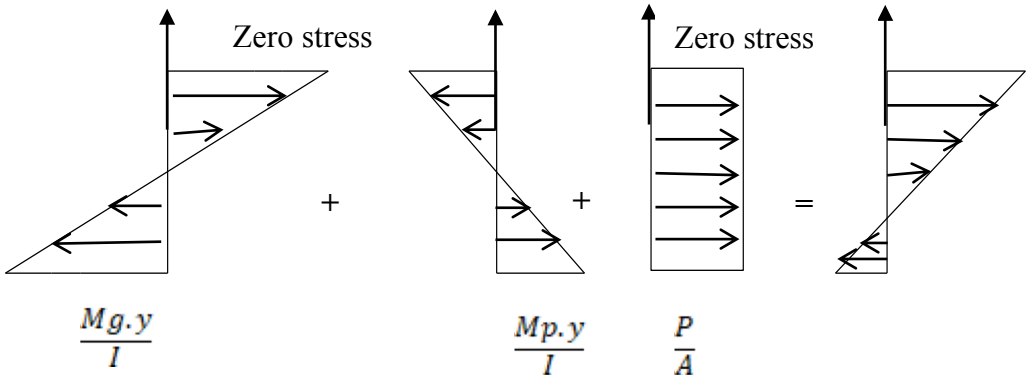

Figure (2.5) Stresses distribution of a prestressed beam when the stresses are unbalanced

If the same member is subject to a uniform load in addition to its own weight, then the stresses at midspan will follow the bending moment, which is due to the total uniform load plus the precompression. The resulting stress distribution is shown in figure (2.5) (Hurst, 1998).

The tendon profile shown in the previous example is for a straight tendon only, so it can be seen that the only position where the bending moments are balanced is at midspan. Hence if the tendon is converted to a parabolic profile downward from the centroid, the bending moment from the UDL can be completely balanced along the entire length of the span (see figure (2.6)).

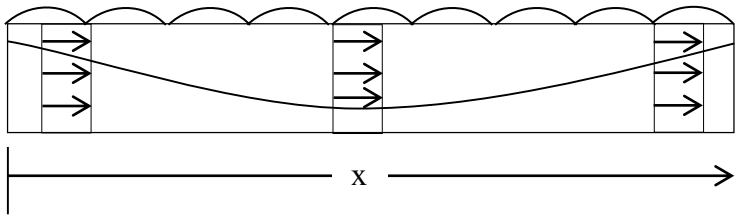

Figure (2.6) Prestressed simply supported balanced beam

Note that the resulting stress distribution has been shown with a net tensile stress at the beam soffit. This tension can be eliminated and a crack-free member produced. This clearly illustrates the advantages of using pre-stressed concrete. To explain this advantage, when compared with reinforced concrete, a certain degree of cracking of the concrete is expected, but with prestressed concrete it can be eliminated entirely. When reinforced concrete simply supported beams are designed, the maximum ultimate load governs the structural design (ultimate limit state) and the service load on the beam is then checked. With prestressed concrete members the service load is the important loading condition (serviceability limit state). Figure (2.7) shows the stresses that occur due to both (the prestress force and the self-weight). A net tension might exist at the top, rather than at the soffit as is the case with the maximum load. This is particularly important since the minimum load condition usually occurs soon after transfer (the point when the prestress force is transferred from the tensioning equipment to the concrete and is at its maximum value), (Hurst, 1998).

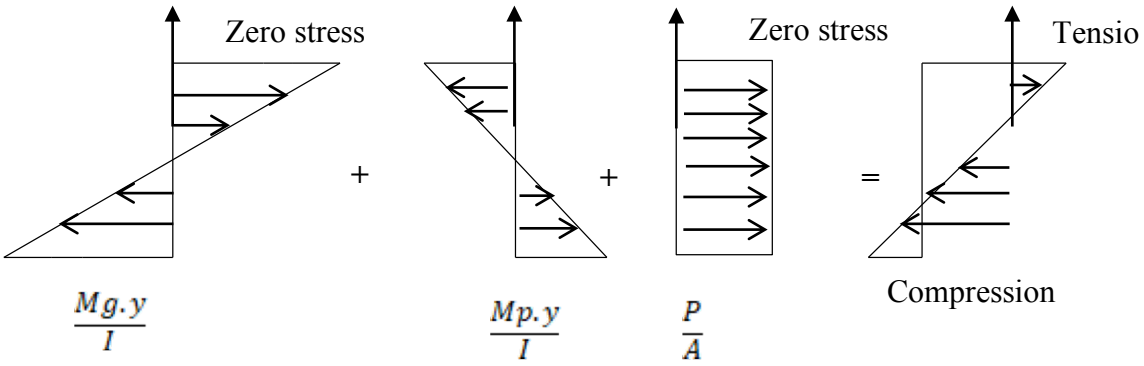

Figure (2.7) Stresses distribution of a beam under prestressed and self-weight when the stresses are unbalanced (Hurst, 1998).

2.4 Pre-stress methods

Pre-stress methods can be classified into two main types which are pre-tensioned and post-tensioned (Rajagopalan, 2002). They will be briefly explained here.

2.4.1 Pre-tensioning

In this method the prestress cables are stressed by jacking in steel moulds before placing the concrete. As the concrete cures and reaches its strength, the jacks are released. The cables try to return to the original length, and the bond between the steel and the concrete means that a

compressive force is applied to the concrete (Hurst, 1998).

2.4.2 Post-tensioning

This method is specified for use on site for structures with continuous spans and irregular member shapes. The pre-stress is applied to the cables after the concrete has reached adequate strength levels. Pre-stress tendons pass through ducts that were already placed before casting; the tendons are stressed and anchored. Ducts are usually subsequently filled with a grout of high strength to provide bonding and thereby increase the ultimate strength capacity of the structure. This helps to eliminate the effects of corrosion and reduce long term force losses in the cable. The post-tension process in this case is known as bonded post-tensioning. When the ducts are not filled with grout and are alternatively filled with grease to reduce friction force losses, then this procedure is known as unbounded post-tensioning. In this process, the pre-stress force is fully transferred by bearing into the anchorages, figure (2.8).

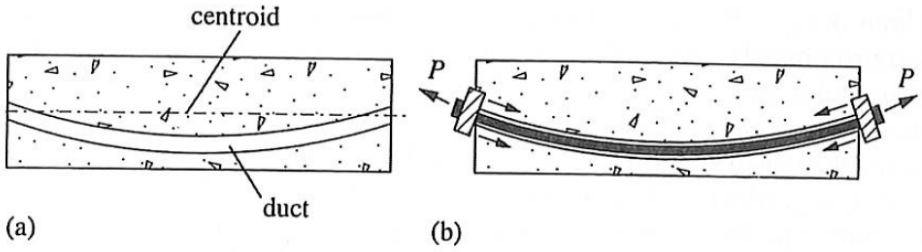

Figure (2.8) Post-tensioning system (O'Brien et. al, 2012)

2.5 Concrete box girder bridges

Due to the demand for improving structural behaviour, stability, economic efficiency, construction and aesthetics, box girders have become widely used in motorway and bridge systems. However, the analysis and design of box girder bridges is complex and needs more attention, especially in relation to three-dimensional analysis, because of the effect of torsion, distortion and bending in vertical and horizontal directions.

There are many ways to classify box girders, i.e. by the method of construction, shape and how is it used. As a result of the high torsional strength and stiffness, horizontally curved box girders are becoming convenient to use thereby allowing changes in direction. This high torsional rigidity makes the box girders effective in minimizing torsional deformations that occur in curved thin-walled beams. When bridges have a lower degree of curvature, the effect of curvature on shear, bending and torsional shear stresses can be ignored. Horizontally curved bridges can usually be considered as straight with certain limitations and modifications.

Recently, these bridges are commonly analysed using the finite element methods (F.E.M) especially when the radius of curvatures is investigated (such as closed box girders).

2.6 Development of curved bridge design approach

The response of curved bridges was first investigated in the mid-nineteen sixties and it focused on analysis work for the behaviour of linear elastic statics of an isolated curved section (Sennah & Kennedy, 2002). This mainly depended upon the material strength assumptions, which are that the cross section would not deform anticlastically, obeys Hooke's law, and conforms to small deflection theory. Therefore, curved girder research investigations were launched in Japan and the United States, which tended to focus on the experimental use of curved beam theory to investigate curved bridge design. In 1965, U.S. Steel Highway (1965), a comprehensive evaluation of theoretical and experimental investigations on box-girder bridges was started by Maisel (1970) in England and it was extended by Swann, (1972), Maisel et al., (1973), and Maisel, (1982). By developing the technology appropriate mathematical formulations were programmed into software to solve complex mathematical models and produce numerical solutions for structures added through the last 20 years, this has pushed both theoretical and analytical investigations to focus on identifying and analysing the behaviour of curved girders. For example, the finite difference method is used to set the solutions for systems of differential equations. Recently, finite element analysis has been introduced and it can provide accurate approximations, therefore the whole curved bridge superstructure can be analysed as a system of finite elements and enhanced to design a curved bridge (Sennah & Kennedy, 2002).

2.7 Behaviour of prestressed curved box girder

A box girder has its main beams comprising of girders in the shape of hollow boxes. The cross section may take the form of single cell (one box) or multi-cell box girder (when the depth of a box girder bridge exceeds 1/6 or 1/5 of the bridge width then it is recommended to be designed as a single cell box girder bridge), (Schlaich & Scheef, 1982). A single cell box girder has the mechanism to twist, deform and bend its cross section under loading. Thin walled closed box girders are stiffer and stronger in torsion than assumed by the designer where the calculations are based on the elemental torsional theory. When the loading component of torsion is applied such as a shear on a plate element according to St. Venant torsion shear flows, the beam will twist

without any deformations occurring in the cross section. As a result, a small longitudinal warping stress will show, and no sign of transverse flexural distortion stresses will arise. For horizontally curved bridges, bending will occur with shear stresses as well as torsional stresses, all due to the horizontal curvature even if they are only acting under gravity (self-weight). Furthermore, the closed cell has a greater torsional stiffness and strength than an open section and it is the main reason for choosing a box girder configuration.

According to the previous explanation, it can be clearly seen that there are two types of torsion subjected to cross-sections; the first is Saint-Venant torsion and the second one is warping torsion. Saint-Venant torsion causes a shear flow around the cross-section figure (2.9), while the warping torsion causes bending distortion of the cross-section. In closed cross-sections, warping torsion is neglected (Kolbrunner & Basler, 1969).

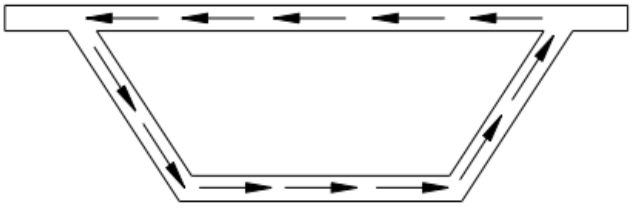

Figure (2.9) Shear flow in a box girder bridge

At the inner piers of a continuous bridge hogging moments will be present; therefore, a wide compression flange is required. Box girders consist of a typical wide flange which is referred to as the soffit and slab, connected by webs figure (2.10). The dimensions of the box section are thin walled dimensions and in most cases the depth of the box section is unchangeable throughout the length.

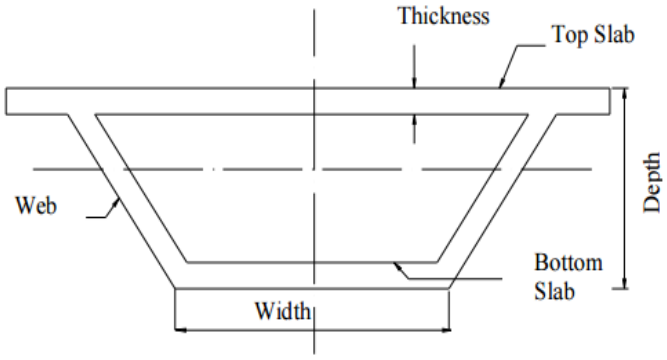

Figure (2.10) Single cell box girder

For prestressed bridges, larger deflections occur under static and dynamic loads due to a lesser depth to span (D/L) ratio in comparison with other bridge constructions. To make sure sufficient stiffness is present to limit deflections, the (D/L) ratio must be greater than 0.04 for prestressed concrete and 0.055 for reinforced concrete bridges.

2.8 Structural action of box girders

Bending and shear actions occur in the longitudinal direction of the box girder. The top slab serves as a road in carrying traffic loads and works as a top flange for longitudinal bending stresses. In comparison to T-sections, flanges are more convenient in resisting sagging and hogging due to the bigger size flanges. The box section being closed is considered to have high torsional stiffness and strength (Chapman et al, 1971). This is more useful in curved and in straight structures carrying eccentric loads.

The structural response of a box girder consists of a combination of longitudinal bending, transverse bending, torsion and warping.

2.8.1 Longitudinal bending

The self-weight and other superimposed dead loads like the self-weight of the kerb, footpath, parapet and wearing course are usually symmetrical about the central vertical axis of the box, hence they do not create any torsional effects. These are resisted by simple bending action of the rigid cross section of the box girder. This longitudinal bending causes flexural stresses, which are considered as membrane forces in the plates.

2.8.2 Transverse bending

Transverse bending of the box section is the bending of the top and bottom of the slab around the neutral axis at the level of the common centre of gravity, as if they are connected by a rigid shear web. Transverse bending of top and bottom slabs causes distortion of the cell.

2.8.3 Torsion

The wheel loads from vehicular traffic are mostly placed asymmetrically. They thus cause torsion in the section as well as longitudinal and transverse bending. The vertical reactions p_1 and p_2 at the web positions due to live loads can be resolved into a statically equivalent combination of a set of symmetrical and asymmetrical loads as shown in figure (2.11). The symmetrical component of the load $(p_1+p_2)/2$ causes only longitudinal bending and asymmetrical component $(p_1-p_2)/2$ creates the torsional and 6 distortion effects. The effect of asymmetrical loading is represented in figure (2.12). The torsional load component gives a resultant torque and it tends to

rotate the section as rigid body about the longitudinal axis of the box. The considerable strength of the box allows little twist.

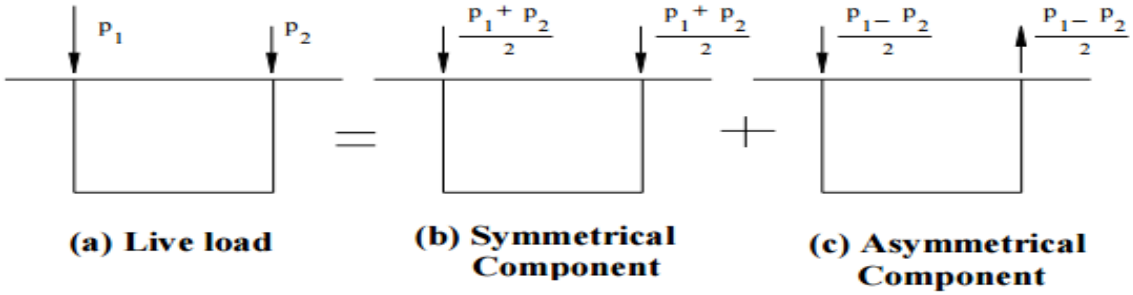

Figure (2.11) Resolution of asymmetrical live load (https://theconstructor.org/structures/behaviour-of-box-girder-bridges/2194/)

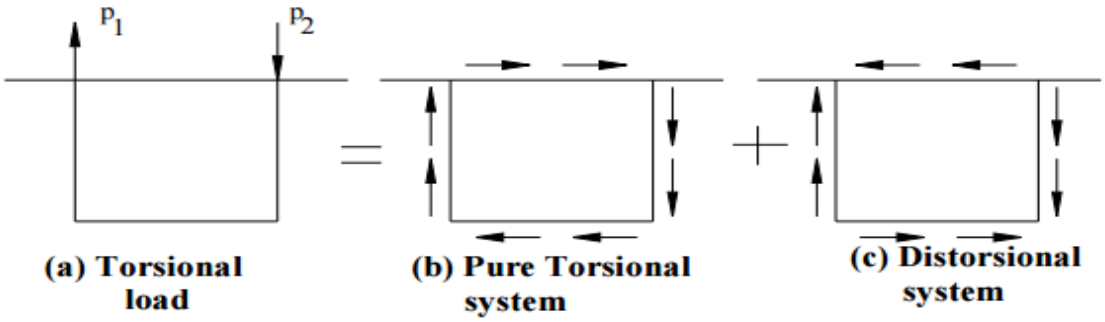

Figure (2.12) Resolution of torsional load (https://theconstructor.org/structures/behaviour-of-box-girder-bridges/2194/)

2.8.4 Shear leg

In a box girder, a large shear flow is normally transmitted from vertical webs to horizontal flanges, which causes in-plane shear deformation of flange plates. The consequence of which is that the longitudinal displacements in the central portion of a flange plate lag behind those near the web. Whereas, bending theory predicts equal displacements which produce out-of-plane warping of an initially planar cross section, resulting in the *shear lag* effect.

Another form of warping can arise in a box girder subject to bending without torsion, i.e. symmetrical loading, is known as *shear lag in bending*.

Detailed information on shear leg effects in bridge designs like box girders, is given in EN 1993-1-5 (Eurocode 1: Design of steel structures, Part 1-5: Plated structural elements).

2.8.5 Effect of horizontal loading

Different load conditions must be considered, acting either singly or in combination. Box girder bridges will have different forms of loading, such as, superimposed dead loads, moving live

loads and horizontal loads (e.g. braking forces on bridges or braking force due to the horizontal movement of cranes).

2.9 Bridge superstructure

Box girders are a part of the whole bridge with various support types, Schlaich & Scheef (1982) and can be designed to be continuous depending on the intended bridge length. For curved bridges, box girders are preferred and can also be adopted for arch, cable-stayed and suspension bridges. In 1911 the Risorgimento Bridge, figure (2.13), was constructed as a box girder with a three-hinged arch technique. As development occurred in the theory of reinforced concrete, bridges became longer and the arch shape began to disappear. Pre-stressed concrete was being developed with the Sclayn Bridge being built with a prestressed and continuous box girder.

Figure (2.13) Risorgimento bridge (International Database for Civil and Structural Engineering., 2015).

To understand the load carrying structural mechanism of the box girder, the piers and abutments will also need to be addressed. When the piers are quite thin and the superstructure is heavy, especially when the cross-section of the bridge is big and the depth of the span changing along the span (from the biggest depth at the support to the smallest in the middle of the bridge span) then the pier cap must be slightly bigger than the bottom of the flange of the box girder to carry the whole superstructure weight and this will reduce the stresses. The highest point of the embankment is the location of the abutment

Loads from the superstructure are transferred to the soil by (Schlaich & Scheef, 1982):

1- Abutment 2- Pier 3- Foundation

These will be examined in more detail in the following sections

2.9.1 Abutment

The main job of the abutment is to connect the superstructure parts with the embankment and provide the lateral support to the embankment also. The back walls of the abutments provide a free space for a future displacement in the superstructure. Normally, the superstructure sits on the bearing which is made to carry the loads through the support walls to finally transfer it to the foundation and soil with well compacted earth filling. The location for any drainage line and bearings should be covered by diaphragm ends and a gap about 100 mm between diaphragm ends and the box girder soffit should be left. The top of abutments is the location to place the expansion joint and bearing, figure (2.14).

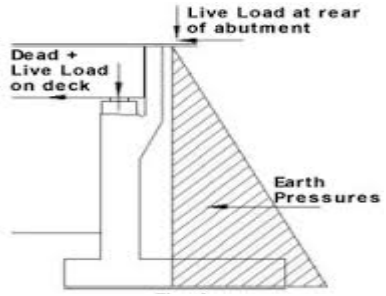

Figure (2.14) Abutment (Childs, 2015)

2.9.2 Pier

The pier is the structural wall support between any two spans. For a single span bridge, the abutment plays the main role in supporting the bridge weight and also works as a retaining wall, for multi span bridges the supports between the ends of the span need to have some intermediate supports which are in this case the piers. Bridges with small height mostly consist of two columns working as piers (in any case good soil conditions are required to resist any differential settlement between two columns which are adjacent to each other). These columns would be designed to fulfil the fundamental design criteria so would be safe even for a large box girder, figure (2.15).

Figure (2.15) A bridge pier (Adel et al., 2007).

2.9.3 Foundation

The design of the bridge foundation depends on the soil conditions; spread foundations generally work for shallow surfaces. If the soil is not strong enough, then piles will be needed to support the bridge.

2.10 Design loads

This section lists the loading on a pre-stressed concrete box girder bridge which can be divided into:

1- Dead load (i.e. concrete self-weight, parapets and roads weight) and live loads (i.e. traffic loading, wind and earthquake)
2- Braking and acceleration forces (as the traffic accelerate breaks it causes a horizontal friction)
3- Temperature
4- Differential settlement
5- Impacts (i.e. vehicles crushes)

2.11 Historical development of the analysis of curved box girder bridges

In this section, some of the research is presented which has focused on the structural development of the curved box girder. The research covers the time line from 1968 until the present day.

Dabrowski (1968) introduced an open section supported by lateral bracing at the top theoretically as a closed section with a plate on top. This was considered to be the first attempt to analyse the box section.

Figure (2.16) Bracing system in a composite box girder bridge (Chan & Teng, 2002)

Then, Cheung (1976) used the finite strip method to define the natural frequencies and mode shapes for a continuance with changeable thickness deck or box girder bridges.

Dey et al. (1984) defined the dynamic behaviour of a simply support deck curved bridge subject to moving vehicles. The finite strip method had been used to analyse the deck with an assumption of elastic material properties. The homogeneous differential equation of an orthotropic plate in polar coordinates was used to derive the stiffness and the mass matrix for every element. As a result, there was significant variation in response across the transverse section of the bridge, and dynamic investigation was carried out with the same finite strip method which also gave reasonable and accurate results.

Harik & Pashanasangi (1985) developed a more accurate method for the analysis of horizontal curved and orthotropic bridge decks subjected to patch, uniform, line and concentrated loads. The bridge was idealized as a curved strip and the deflection of each plate strip was expressed as a levy type Fourier series and the loads are expressed as a corresponding series also. The present method could predict good deflection results by considering only three significant terms of the Fourier series. Kou et al. (1989) studied the response of the dynamic continuous curved box girder, also, Kou (1992) developed a theory that assimilates a solution of warping in the analysis of free vibration of curved continuous thin-walled girders.

Shanmugam et al. (1995) studied the ultimate load behaviour of I-beams curved in plan. Experimental results were presented and agreement reached in relation to deformations and ultimate strength results, with a consideration to the effects of residual stresses and radius of curvature to span-length ratio (R/L) on ultimate strength. A concentrated load was applied on each beam at the midpoint where the beam was laterally fixed. The load-carrying capacity decreases as the R/L ratio decreases.

Galambos et al. (2000) explained a system of curved steel I-girder bridge behaviour during the construction phase. The longitudinal stresses in the bridge are represented well by linear elastic analysis represented by F.E analysis software and the longitudinal stress was determined. A comparison was made between stresses and deflections with the results for full construction. Also, Linzell et al. (2004) studied nine simply supported bridges consisting of three curved steel I-girders with lengths of 27.4 m. The analysis attempted to predict the dynamic response of the bridges during erection. The resulting stresses and deflections were compared and showed that analysis tools can be useful in predicting loads and deformations during the construction stage.

DeSantiago et al. (2005) analysed a simple model of beam and plate elements using the finite element method. The model consists of five horizontal curved bridges with span lengths of about 30.5 m and with an angle of curvature between10° to 30°. From the analysis of the curved bridges, the deflection in the vertical direction was about 80% higher than the vertical deflection calculated on the straight bridge when the angle of curvature was 30°, the girder bending moment of the curved bridge was about 32.5% higher compared with straight girder moments which had the same span length and design configuration. Also, the magnitude of the torsional moment reached to about 10.3% of the peak bending moment in the straight girders of a straight bridge with a similar span length and design.

Khaloo & Kafimosavi (2007) tested the allowable bend for curved pre-stressed (post-tensioned) box bridges using the finite element method. The 3D finite element sample was modelled and studied for bridge length, section geometry, and material properties and these were the same as used in all models, while the angle of curvature was changing from 0° to 90°. As a result of this, the distribution of stresses for the curved bridges changed significantly compared with the straight bridges (this is expanded in Chapter Three).

Abeer et al. (2013) presented a method to calculate the torsional capacity and behaviour of R.C multi-cell box girders strengthened with carbon fibre reinforced polymer (CFRP) sheets depending on the 'Modified Softened Truss Model' for Torsion (MSTM). The theory was first mentioned by Hsu (1988) which emphasizes the importance of incorporating of the softened constitutive laws of concrete in the analysis of RC structures. Later this method has been developed by Fu and Yang (2001) to resolve torsional problem based on STM, especially for RC box girder bridge superstructures with multiple-cell sections.

As a result, the suggested algorithm for solving the related equations for torsional analysis of the strengthened girders is particularly suitable for practical applications.

Bourne (2013) studied prestressed concrete bridge behaviour and construction in the UK. In this paper, there was a comparison between using reinforced concrete and prestressed and why prestressed is preferable. The study was based on EC2 and BS5400. The author concluded that using prestressed sections is more economical. The best prestressed sections are those with fully prestressed or partially prestressed scheme. Bourne explained that he best section is closer to the fully compressed prestressed or partially prestressed scheme with high levels of prestress (i.e. 80% or 100%) and without cracking.

Shen et al. (2015) presented a multi span curved box girder with external prestressed tendons and compared it with regular internal tendons design. As a conclusion, the external prestressed layout design reduces the peak torsion, introduced a uniform torsion distribution and there was no impact on shear or moment see figure (2.17).

Horizontal layout of tendons.

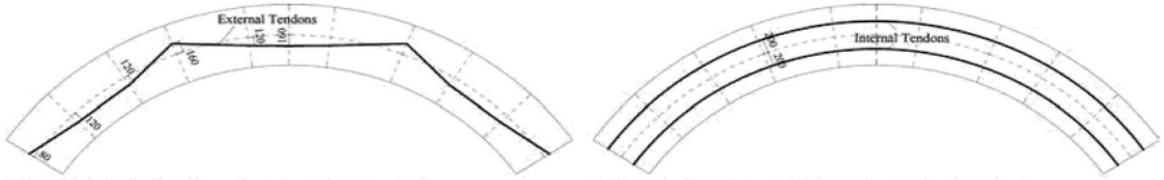

(a) External prestressing tendon design (b) Internal prestressing tendon design

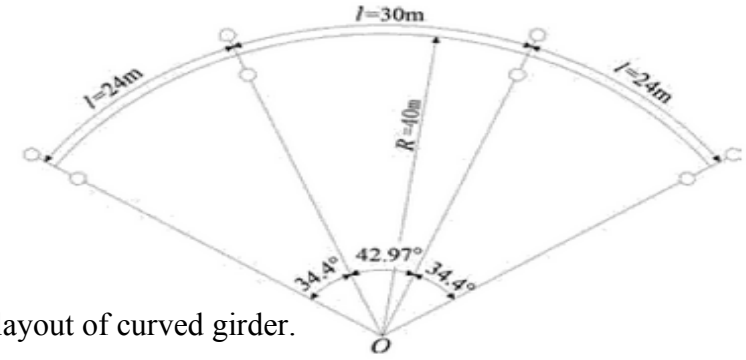

c. Plan layout of curved girder.

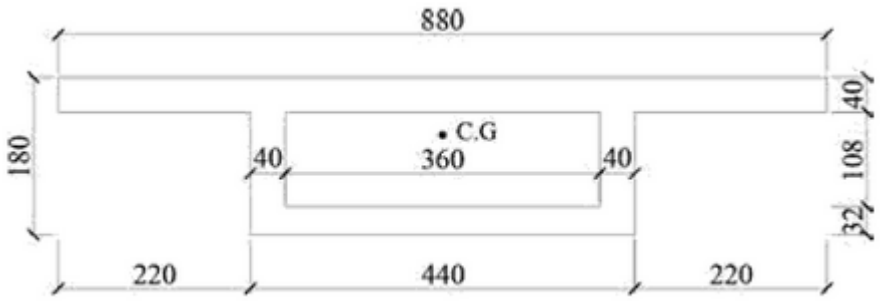

d. Box girder cross-section.

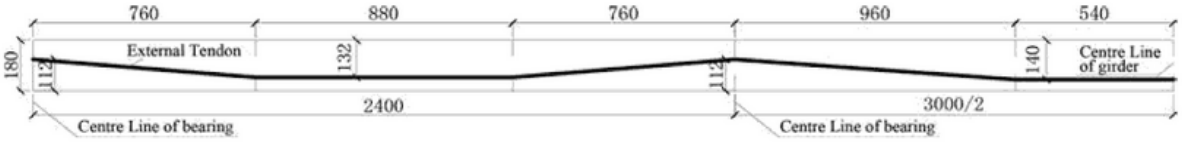

e. Vertical layout of external tendons.

Figure (2.17) Box girder bridge, (Shen et al.2015) all units are in (cm).

Gupta et al. (2010) presented a parametric study of a cross section (rectangular, trapezoidal and circular) of a box girder bridge using the finite element method for analysis. SAP-2000 was utilized throughout this study with three-dimensional shell element models being used. Linear analyses were carried out with dead and live loads based on Indian codes to investigate deflection, stresses and shear lag for those different cross sections. A validation was carried out from previous literature to compare the results with their finite element predictions. The results showed that a rectangular section has the best results when compared with the performance of other sections due to the section simplify, modelling and accurate results also rectangular section was stiffer than the trapezoidal section, so deflection was lower in the rectangular section.

Angomas (2009) investigated the behaviour of prestressed concrete bridge girders. In this Master's thesis, Angomas investigated prestress losses in six HPC (High Performance Concrete) bridge girders. Those losses were compared to the predictions of camber losses from the AASHTO code of practice. Prestress loss predictive methods considered for this research were: 1- AASHTO LRFD 2004, 2- AASHTO LRFD 2004 Refined, 3- AASHTO LRFD 2007, and 4- AASHTO LRFD Lump Sum method. Nevertheless, the camber prediction methods were: 1- Time dependent method described in NCHRP Report 496, 2- PCI multiplier method, and 3- Improved PCI Multiplier method. In conclusion, the AASHTO LRFD 2004 Refined Method was most accurate in predicting the prestress loss. All the assumed methods performed well in estimating the loss for the larger girders.

Chourasia & Akhtar (2015) conducted a parametric study of two different cross-sections of a box-girder with the same loading conditions to determine the best economical cross-section. The study was based on the design standard of India, IRC used in designing box-girder superstructures according to the IRC class AA loading. To determine the best cross-sections, a comparison was made for the different design parameters. As a result, bending moment and stresses for self-weight and superimposed dead load were different for various cross-sections. The result showed that multi cell box girders were expensive (time and constructions) compared to the single cell box girder, under the same loading and support conditions. The MIDAS (finite element method) software was utilized for this study.

Shah et al. (2016) presented a parametric study of curved box girders designed in accordance with IRC: 112 code of practice for concrete road bridges and considering curved geometry for analysis. The details of the curved bridge models were as follows:

- 35 m long, single cell, with a width of 7.5 m with two lanes
- 35 m long with two cells with a width of11.25 m with three lanes.

Analysis and design for eight complete models with differing radius of curvature were 100 m, 75 m, 50 m and a straight span with similar depth equal to 2.4 m of the box girder cross section. The grade of concrete was assumed to be 50 N/mm^2 (compressive strength) and the grade of steel was taken as 500 N/mm^2 (tensile strength). Analysis and design was conducted using the software CSI Bridge 2015. Graphical relations between various parameters were optimized with the intention of providing designers with a clear understanding of structural and economic aspects of curved box girder bridges. The results showed increasing curvature will increase bending moment and in required quantity of prestressing steel.

Ahirwar et al. (2016) summarized papers that dealt with box girder bridge behaviour. In this study, the author focused on papers which presented different analytical methods to understand the behaviour of box girder bridges. It was concluded that further study was needed, a study that focused on the analysis and behaviour of three dimensional models of box girder bridges with the use of FE analysis.

Patil, & Shinde, (2013) studied the two standards AASHTO and IRC under the effect of traffic loading conditions during the construction of superstructures. In order to determine the best cross section, different checks were utilized. The results showed that bending moment and stress predictions for self-weight and superimposed weight are the same for both codes, however those

for the moving load consideration exhibited some variance, and this was because of the fact that the IRC codes provided design for heavier traffic loads in contrast to the AASHTO codes. Furthermore, although the AASHTO code has higher factors of safety, it is more economical due to the characteristic loading being less than required by the IRC code. Hence for the same dimensions of section, the numbers of prestressing strands required in the web will be less for the AASHTO code. The MIDAS CIVIL software was used for the finite element analysis.

Sali et al. (2016) analysed a 32m span prestressed trapezoidal box girder from a flyover in Trivandrum, Kerala. The analysis was carried out for five cases with differing radius of curvature under the effect of dead load, superimposed dead load and live load according to the IRC Standard. In this paper, the box girder had the same span length, cross sectional shape and material properties for all the models. The straight and curved trapezoidal box girders were modelled using CSI Bridge software. The parametric study investigated how changing the radius of curvature would affect the behaviour of the box girders and how the deflection, longitudinal bending stresses and torsion would develop. Bending moment increased with decreasing radius of curvature under all loading conditions. Deflection along the span for the box girder showed the same response as the bending moment under all loading conditions. The torsion along the span of the box girder increased as the radius of curvature decreased, and torsion is negligible for straight box girders under all loading conditions. The longitudinal stress at the top and bottom of the centre part of the cross section increases with decrease in radius of curvature of the box girder.

Sasidharan & Johny (2015) investigated box girders curved on plan with rectangular cross-sections, figure (2.18). The finite element software ABAQUS was utilized for the analysis. The box girder was analysed for different loading conditions, namely the dead load, superimposed load and live load based the IRC Class A loading. A parametric study of curved box girders was carried out by changing the span and radius of curvature and keeping the span to depth ratio constant. The results for different reactions, bending stress, shear stress and mid-span deflections were presented and showed that when the radius of curvature decreased the bending stresses increased and shear stresses increased (torsion started to occur).

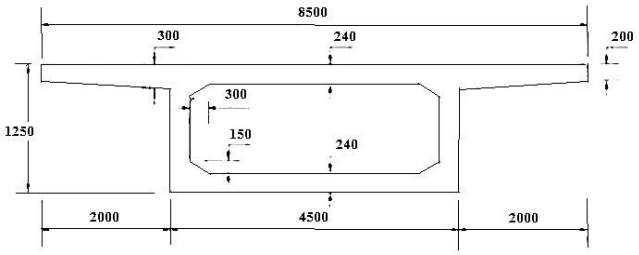

Figure (2.18) Box girder cross-section with span lengths equal to 20m, 30m and 40m, L/D ratio of 16 and 7 different radii, Sasidharan & Johny (2015).

Thakai et al. (2016) studied box-girder bridges with rectangular and trapezoidal cross-sections. In this paper, SAP 2000 was adopted for the finite element analysis. The box girder was analysed under dead load (self-weight) and live load in accordance with IRC 70R loading for zero eccentricity (centrally placed) for both simply supported and continuous spans. The results for rectangular and trapezoidal cross-section were graphed and presented for bending moment and longitudinal bending stress in the top and bottom flange along the span. It can be concluded that:

i. When the depth of box-girder decreased the longitudinal bending stress in top and bottom flange along the span increased.

ii. The bending moment was highest in trapezoidal girder under the load combination of dead load and live load and least in the rectangular girder.

iii. The rectangular section was stiffer than the trapezoidal section, so deflection was lower in the rectangular section.

Jain & Singh (2016) analysed curved box girders and compared the results for the bending moments, torsion and shear in relation to the change of curvature. They also compared the maximum and minimum reactions and checked the stability against overturning. The parameters span length, depth, deck width, radius of curvature and loading were modelled by using a LUSAS Finite Element Analysis software. The results showed that there was no change in bending moments and shear forces for a span with different radii, however, torsional moments increased significantly as the span radius decreased.

Darji et al. (2016) summarized some of literature dealing with elastic analysis experimental studies of prestressed concrete (PSC) box girders looking at type, span, live load, curved box girders, shear lag and torsion due to curvature. A comparison of the literature was made for both

analysis and design of PSC T-girders with PSC box girder using STAAD – PRO, for normal and skew box girders.

Corven (2016) introduced a manual (Federal Highway Administration's National Technology Deployment Program), the *Post-Tensioned Box Girder Design Manual* related to the analysis and design of cast-in-place concrete box girder bridges prestressed with post-tensioned tendons. The Manual displayed the types of the construction of cast-in-place concrete box girder bridges, material features that impact design, principles of prestressed concrete, and losses in prestressing force related to post-tensioned construction. The manual also considered the longitudinal and transverse analysis of the box girder superstructure. Both single-cell and multi-cell box girders were discussed and some design examples were inserted in the Appendices. The manual can be considered as a training manual.

Khairmode & Kulkarni (2016) analysed a horizontally curved prestressed concrete box girder bridge deck, figure (2.19). The SAP program was utilized to model the bridge as a three-dimensional finite element model. The angle of curvature was varied 0° to 90° and the radius of curvature was changed from 25m to 50m. The material properties remained unchanged. Analysis was based on using the IRC Class AA loading. The results of stresses have been represented by graphs in the paper. The deflection was caused due to the different loadings and the mid-span deflection for all the models were computed. These longitudinal stresses were obtained for prestress loading case. The values of stresses were negative which meant that stresses were in compression. When the radius of curvature and angle of curvature increased the stresses at the top of the prestressed curved bridges increased but stresses at the bottom of the bridges decreased and midspan vertical deflection decreased also.

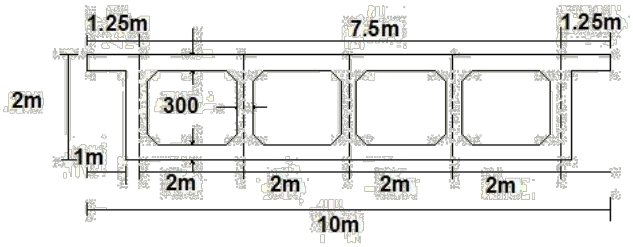

Figure (2.19) Cross-section of multi-cell box girder, Khairmode and Kulkarni (2016).

Fangping & Jianting (2012) investigated changing the radius of curvature for prestressed box girder bridges as shown in figure (2.20). A spiral bridge in Chongqing was analyzed using the finite element program ANSYS. Five different curved bridge models subject to self-weight and

prestressing were modelled and analysed. The deformations in all directions of the curved box girder bridges were presented but the vertical deformation was still dominant. The vertical displacement of the mid-span of continuous curved box girder bridges increased as the radius of curvature increased. For example, when the radius was 10-150 m the vertical displacement has changed most quickly, while when the radius was over 200 m, the displacement-curvature graphs tends to an asymptote, the force characteristics were the same as for a straight bridge.

(A) The whole spiral bridge model

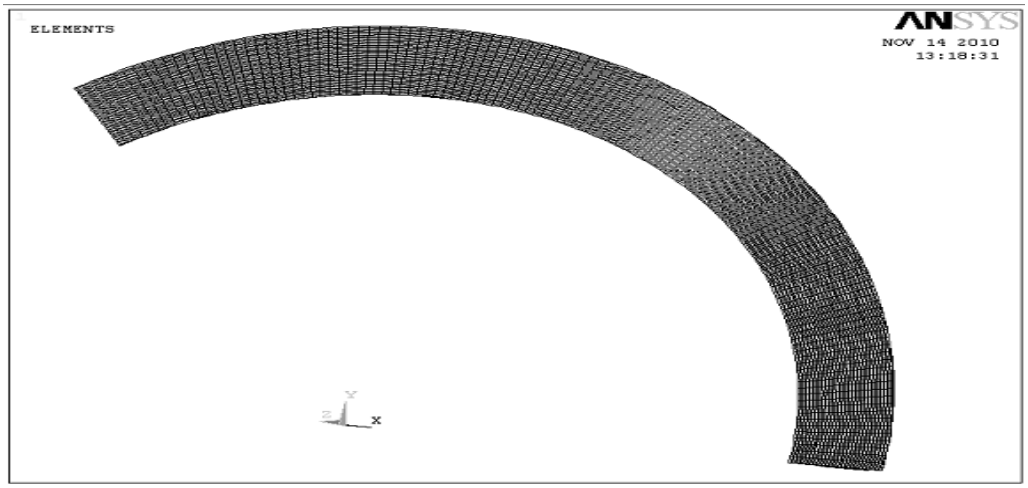

(B) The finite element model

Figure (2.20) Spiral bridge model, Fangping & Jianting (2012)

Sennah & Kennedy (2002) extensively studied previous research that dealt with straight and curved box girder bridges in the form of single-cell, and multi-cell cross sections. This literature dealt with elastic analysis and experimental works on the elastic response of box girder bridges.

As a result, they suggested that the finite-element method was the best method for analysis and more finite element investigations are needed in future.

Ch et al. (2016) conducted the analysis and design of straight prestressed concrete bridges (deck slab, T-girder and box girder) in accordance with the Indian code IRC:112-2011. A sample of these box girder bridges was investigated using SAP 2000 software. The results for different span to depth ratios were compared with code specifications. The deflection and stresses results represented in the paper were within the permissible limits according to the authors.

Alawneh (2013) studied a new system for curved precast prestressed concrete girder bridges at University of Nebraska. The author used relatively short girder segments in a straight line, then those segments were joined and post-tensioned to form a curved girder. This system showed economic advantages. The forms can be used in straight-line prestressing beds and in lower cost production.

Okeil & El-Tawil (2004) analysed a detailed study of warping-related stresses in 18 composite steel-concrete box girder bridges. The bridge was in the state of Florida and the parametric study included many parameters such as the horizontal curvature, cross-sectional properties, and number of spans. Forces were estimated from the mathematical model, including the effects of warping. Loading was based on the 1998 AASHTO-LRFD. Warping stress was considered, however it was ignored in some cases. As a result, analysis showed that warping has little effect on both shear and normal stresses in all bridges.

Sali & Mohan (2017) compared straight and curved box girder bridges with trapezoidal cross sections. Dead load, superimposed dead load, live load of IRC Class A tracked vehicle and prestressed loads were investigated. The span, cross sectional shape and material properties were unchanged. The aim of the study was to investigate the behaviour of box girders by changing the radius of curvature. Five models were investigated one straight and four curved and the comparison were made in deflection, torsion and longitudinal stresses. The results showed that increased the radius of curvature will decreased deflection, torsion and longitudinal stresses.

John & Prasad (2017) summarized literature that dealt with the behaviour of straight and curved box girder bridges. The objective of this documentary study was to provide a better understanding for the behaviour of box girders with different variations in parameters such as curvature and shape. This study will help the bridge engineer to better understand the behaviour of straight and curved box girder bridge

Chapter Three

Numerical Analysis

3.1 Analysis methods

This chapter presents the numerical analyses which have been utilized to investigate the prestressed concrete box girder bridge behaviour and the methodology of how the box girder for this study will be analysed. Complex bridge design needs to identify the internal forces within the bridge which are generated by the applied loading and how the bridge material will behave structurally. Analysing the stresses acting in the bridge elements is the aim of the analysis of such structures and to verify that the bridge material properties have the required stiffness and strength (these are related to the constitutive modelling of the basic materials in the numerical analyses). The accuracy of the structural analysis is dependent upon the choice of a particular method and its assumptions. Many methods have been used to analyse box girders, starting from the curved beam theory by Saint-Venant (1843), the thin-walled beam theory by Vlasov (1965) through to the big advancements made by using the finite element method.

The main methods of analysis can be summarized as:

1- Orthotropic plate theory
2- Grillage analogy
3- Folded plate
4- Finite strip
5- Thin walled curved beam theory
6- Finite elements

1- Orthotropic plate theory

The orthotropic plate theory method addresses the interaction between the concrete deck and the curved girder of a box girder bridge. In this method the stiffnesses of the diaphragms are divided over the girder length and the stiffness of the flanges and girders are lumped into an orthotropic

plate of equivalent stiffness. However, the estimation of the flexural and torsional stiffness is considered to be one of the major problems with this method. Also, adopting this method has another disadvantage in which the stresses in the slab and girder are hard to estimate. This method has been recommended for multiple-girder straight bridges and curved bridges with high torsional rigidity, but the Canadian Highway Bridge Design Code CHBDC (2000) has claimed this method should only be used for the analysis of straight box-girder bridges of multispine cross section and not multicell cross section.

2- Grillage analogy method

In the case of multiple cell boxes with vertical and inclined webs and voided slabs, the grillage method has usually been adopted for analysis. In this method, the bridge deck is assumed as a grid assembly, where each slab of the box section is converted to a series of orthogonal slab/beam strips. The grid assembly members are assumed to have axial, bending and torsional stiffness, which approximate the two-way plate response by considering the plates are fully connected with the joints of the three-dimensional rigid frame.

There are some drawbacks with this method, the first is in calculating the effective width of the slab to include the shear lag effects. Another is in finding the torsional stiffness of closed cells. Evans & Shanmugam (1984) estimated approximate results for torsional stiffness for a single cell closed section by modelling as an equivalent I-beam. As a result, the Canadian Highway Bridge Design Code CHBDC (2000) has restricted using this method for analyses of box-girder bridges where the number of cells or boxes are greater than two.

3- Folded plate method

Linear elastic analysis of a box girder bridge can be solved using this method, considering the assumptions of elastic theory. According to this method a box girder bridge will be modelled as a folded system which is an assemblage of longitudinal plate elements connected at their corner joints (two adjacent plates share one joint) and both ends are simply-supported by diaphragms. These diaphragms are infinitely rigid in plane and perfectly flexible perpendicular to the

orthogonal planes. This method provides a solution for simply supported straight or curved box-girder bridges for any subjective longitudinal load function. Scordelis (1960) produced an analytical method to determine the longitudinal stresses, transverse moments and vertical deflections in folded plate structures by adopting matrix algebra. The method can be easily programmed for digital computers. The procedure has been utilized to model cellular structures by Meyer & Scordelis, (1971), Al-Rifaie & Evans, (1979), and Evans, (1984). Marsh & Taylor (1990) introduced a method that incorporates a classical folded plate analysis consisting of an assembly of orthotropic or isotropic plates to form box girders. This method has a major disadvantage in that it is complicated and also tedious. The Canadian Highway Bridge Design Code CHBDC (2000) suggested that the applicability of this method should be limited to bridges with support conditions which are close enough to line supports at both ends and line intermediate supports in the case of multi-span bridges.

4- Finite strip method

In the finite strip method of analysis, which is a particular type of finite element analysis in its special form of the formulation of displacement, the box girder is assumed to be organized into annular finite strips that span from one end support to another. These 'strips' are linked transversely through their edges by longitudinal nodal lines. The stiffness matrix for the box girder using this method is calculated for every strip and depends on a displacement function assuming an analytical distribution such as a Fourier series.

The finite strip method is considered as a midway between the folded plate method and the finite element method. The finite element method is different from the strip method in terms of the assumed displacement interpolation functions. Contrasting the finite element method, the displacement functions according to the finite strip method are produced as a combination of harmonic variation longitudinally and polynomial variation in the transverse direction.

Strip stiffness was developed to solve equations of equilibrium to estimate displacements, stresses and strains. Curved geometry and orthotropic material properties can be incorporated in such formulations. The finite strip method has advantages over the finite element method in that it reduces the number of degrees of freedom and therefore the computer solution time is shorter and therefore storage requirements are less. However, the main disadvantage of using this

method is that it cannot be utilized for bridges with skew ends and with non-simply supported bridges. Differences in geometrical or material properties of the bridge cannot be considered in this method (CHBDC, 2000).

5- Thin walled curved beam theory

In the case of the solid curved bar, Saint-Venant (1843) has proved that the theory of curved beams can be utilized, especially when the load is applied in a direction normal to the curved plane. The advantage of using the curved beam theory is that it can provide us with the correct distribution of the bending moment, shear and torque resultant in any part of the curved beam when the accurate bending, axial and torsional rigidities have already been identified. However, this method cannot be applied to curved box girders and for the reason that it does not consider the effect of distortion, warping and bending deformation of each element in the wall of the box.

6- Finite element method

The finite element method can be described as a method of dividing the structure into many small elements, these elements are connected with each other through nodes. The strain displacement matrix, the element stiffness matrix and nodal load vectors have to be calculated for each individual element. The global stiffness matrix consists of numbers of local element matrices which are assembled according to orientation and connectivity. In the finite element method the equations of equilibrium are solved to find the nodal displacement for each node these are then back subtitled to calculate the element stresses, Zienkeiwicz (1977).

To analyse problems with different geometry, thickness and material properties through the length of the bridge, the finite element method is considered the best choice for analysis. The advantage of using FEA is that it can be used for any type of loading and any boundary condition. An accurate approximation of the structural behaviour can be provided by this method which makes it the most versatile of all the available methods.

The analysis of concrete structures can be readily solved using the finite element method. However, if the FE method is utilized to analyse reinforced concrete structures, there will be a lack of consistency of results between different structural forms (different element and

nonlinearity). This usually happens due to the use of approximate assumptions adopted to describe the material, and also, the computational difficulty that arises as a consequence of numerical instabilities associated with nonlinear effects such as, cracking of concrete and yielding of reinforcement. Until now, the most powerful method to be used in the analysis of the box girder bridge is the finite element method. The finite element method has provided the designer with an accurate result for static and dynamic analyses. For example the Canadian Highway Bridge Design Code CHBDC (2000) has recommended the finite element method for all types of bridges.

A large number of element types have been investigated using the finite element analysis for two dimensional elements such as beams, plates or shell elements, and three-dimensional elements such as solid elements. Since the structure consists of many finite elements connected at nodal points, each element has a stiffness matrix, which approaches the behaviour in the continuum. It is assumed to be an assemblage depending on presumed displacement or stress patterns, then the nodal displacements and the internal stresses on the finite element are achieved by using the overall equation of equilibrium. Also, the FE method is available in many commercially written programs such as ANSYS and ABAQUS. The finite element analysis has been adopted for this study.

3.2 Numerical study of prestressed box girder bridges

Complex geometries, such as those of multi-cell straight and curved prestressed box girder bridges can readily be modelled using the FEA technique. The method is also capable of solving structures with different material properties, boundary conditions and various load conditions. The structural response of such bridges can be predicted with good accuracy using this method.
In this chapter of the thesis, a single- span box girder bridge section is investigated, the details of which are shown in figure 3.1. The box girder in question is produced from the published work of Khaloo & Kafimosavi (2007) for verification purposes and extended into further study. The length of the span is 54m, the depth is 3.3m and the deck width is 12m. The material properties and structural arrangements are as follows:

- Modulus of Elasticity E= 17×10^9 N/m^2
- Density ρ= 2400 kg/m^3
- Nine prestressed tendons located at the girder soffit.
- The modulus of elasticity for the tendons is 200×10^9 N/m^2.

FE analyses were carried out on this sample subject to gravity, prestressing and different arrangements of additional loading to determine the load capacity for various ranges of curvature using the finite element analysis programme ANSYS12.

In this study the box girder investigation begins with a straight box girder bridge, and then proceeds to curved box girder bridges. Both models are subjected to self-weight (gravity loading) and prestressing. This section presents the verification work on a static model of straight and curved box girder bridges to ensure that the modelling and prestress is applied in the correct manner. Additional load is then applied to the bridge over a range of horizontal curvatures, and the load capacity is then based on stresses criteria at serviceability limit state.

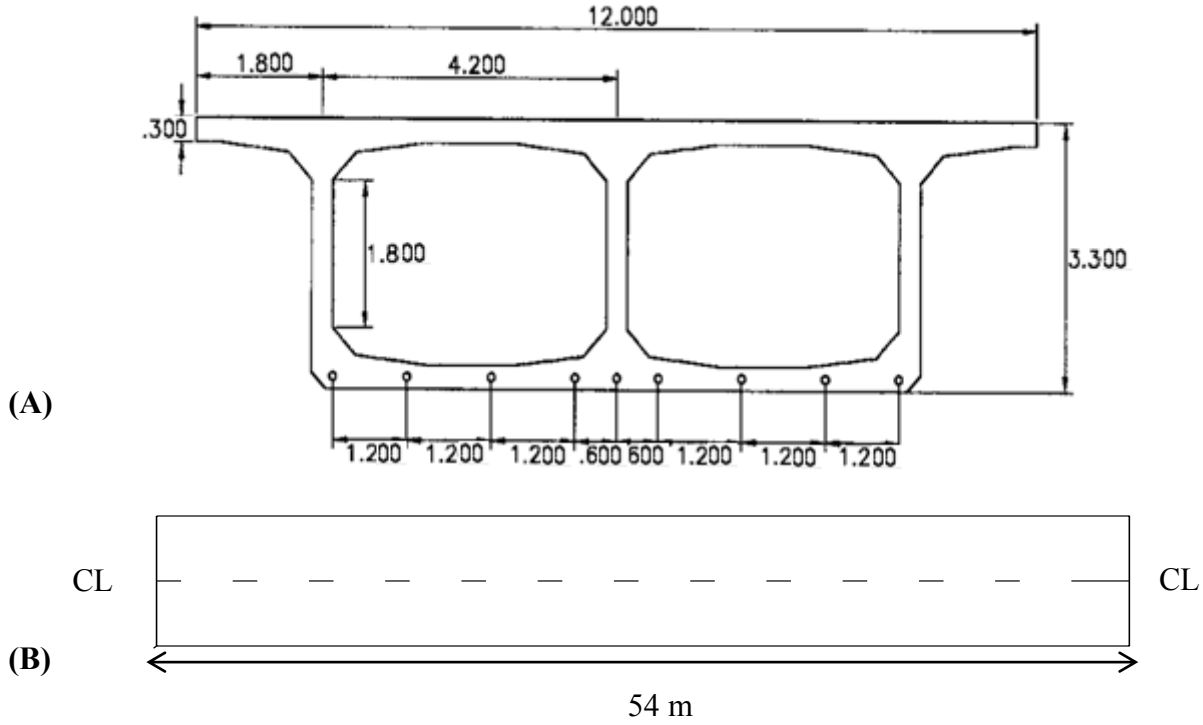

Figure (3.1) Geometry of curved bridge: (A) cross section and tendon position (B) plan view (all dimensions are in metres).

3.3 Box girder bridge calculations

In order to create the model, firstly some analytical calculations should be carried out. These calculations will serve as verification of the section properties for the FE, stresses ranges, and correct representation of the prestress (applied by means of an initial strain). These calculations are presented in, figure 3.2:

3.3.1- Calculation for Area and I for the section (FE model)

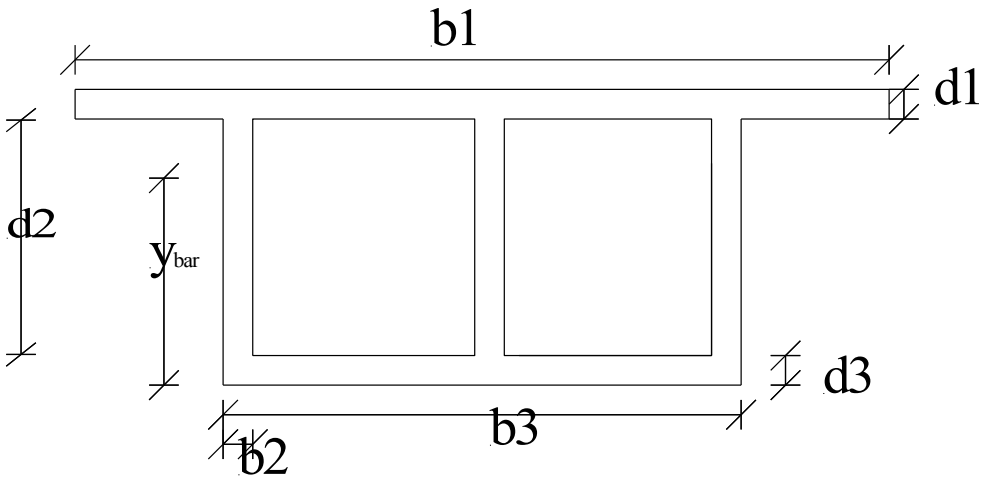

Figure (3.2) Cross-section of deck

Deck	b_1=12 m	d_1=0.3 m
Ribs	b_2= 0.3 m	d_2= 2.7 m
Soffit	b_3= 8.7 m	d_3 = 0.3 m

Calculate Area $A = b_1 \times d_1 + 3 \times (b_2 \times d_2) + b_3 \times d_3$ $A = 8.64\ m^2$

Calculate Y_{Bar}

Y_{Bar}

$$= \frac{\mathbf{b_1 \times d_1 \times \left(d_2 + \frac{d_1}{2} + d_3\right) + 3 \times (b_2 \times d_2 \times (0.5 \times d_2 + d_3)) + b_3 \times d_3 \times 0.5 \times d_3}}{\mathbf{A}}$$

Y_{Bar}= 1.822 m

Calculate second moment of area I

I =

$$\frac{b_1 \times d_1^{\,3}}{12} + \frac{3 \times b_2 \times d_2^{\,3}}{12} + \frac{b_3 \times d_3^{\,3}}{12} + b_1 \times d_1 \times \left(d_3 + d_2 + \frac{d_1}{2} \right)^2 + 3 \times b_2 \times d_2 \times (0.5 \times d_2 + d_3)^2 + b_3 \times d_3 \times (0.5 \times d_3)^2$$

I = 15.24 m^4

3.3.2- Calculation of required prestressing parameters

Calculation of required prestressing strain for the FE model:

Ultmate tensile strength (assumed from typical values) $\sigma_{ult} = 1800\ N.mm^{-2}$

Service stress in tendons $\sigma_{ten} = 0.6 \times \sigma_{ult}$ $\sigma_{ten} = 1080\ N.mm^{-2}$

Desired tension force in each tendon p= 5000 kN

Number of tendons $N_t = 9$

Total prestressing force $P = N_t \times p$ P = 45000 kN

Area of each tendon $A = \frac{p}{\sigma_{ten}}$ $A = 4.63 \times 10^3\ mm^2$

Steel modulus of elasticity $E = 200 \times 10^9\ N.m^{-2}$

Strain in each tendon $\varepsilon = \frac{\sigma_{ten}}{E}$ $\varepsilon = 5.4 \times 10^{-3}$

3.3.3- Stresses in FE model

From the calculations in 3.3.1, the stresses for comparison with the FE model can be calculated for the various load cases as follows:

Second moment of area I = 15.24 m^4
Cross sectional area A = 8.64 m^2
Distance from soffit to centroid Y_{bar} =1.822 m
Concrete unit weight ρ = 2400 kg. m^{-3}
Depth of section D = 3.3 m
Width of deck B = 12 m
Length of deck L = 54 m
Acceleration g= 9.81 m.sec^{-2}
Self-weight (W) $W = A \times \rho \times g$ W =211.9 kN/ m

Moment at mid-span from gravity $\mathbf{M_g = \frac{W \times L^2}{8}}$ $M_g = 7.73\times10^4$ kN.m

Prestressing force from all tendons P= 45000 kN

Eccentricity ecc= 1.822 m

Moment at mid-span from prestress $M_p = P\times ecc$ $M_p = 8.2\times10^4$ kN.m

Gravity load stresses:

$$\sigma_{tg} = \frac{-\mathbf{M_g \times (D - Y_{Bar})}}{\mathbf{I}} \qquad \sigma_{tg} = \text{-7.7 N.mm}^{-2} \quad \text{(top)}$$

$$\sigma_{bg} = \frac{\mathbf{Mg \times Y_{Bar}}}{\mathbf{I}} \qquad \sigma_{bg} = 9.3 \text{ N.mm}^{-2} \quad \text{(bottom)}$$

Stress from prestressing:

$$\sigma_{tp} = \frac{\mathbf{P}}{\mathbf{A}} + \frac{\mathbf{M_p \times (D - Y_{Bar})}}{\mathbf{I}} \qquad \sigma_{tp} = 3.2 \text{ N.mm}^{-2} \quad \text{(top)}$$

$$\sigma_{bp} = \frac{\mathbf{P}}{\mathbf{A}} - \frac{\mathbf{M_p \times Y_{Bar}}}{\mathbf{I}} \qquad \sigma_{bp} = -14.8 \text{ N.mm}^2 \quad \text{(bottom)}$$

Total stresses:

$\sigma_{tg} + \sigma_{tp} = -4.5 \text{ N.mm}^{-2}$ (top)

$\sigma_{bg} + \sigma_{bp} = -5.5 \text{ N.mm}^{-2}$ (bottom)

These stresses indicate that the prestress and gravity loads are nearly balanced with an approximately even compressive stress (shown as negative stresses) across the section elevation.

Note: The published paper stresses (Khaloo & Kafimosavi (2007)) for the load cases has been calculated here

- Calculation for stresses

Second moment of area $I = 15.24 \text{ m}^4$

Cross sectional area $A = 8.64 \text{ m}^2$

Distance from soffit to centroid $Y_{bar} = 1.822$ m

concrete unit weight $\rho = 2400 \text{ kg. m}^{-3}$

Depth of section D = 3.3 m

Width of deck B = 12 m

Length of deck L = 54 m

Acceleration $g = 9.81 \text{ m.sec}^{-2}$

Applied load (including self-weight) $UDL = 25 \text{ kN.m}^{-2}$

Load per unit length W = UDL×B $W = 300 \text{ kN. m}^{-1}$

Moment at mid-span from loading $\mathbf{M_g = \frac{W \times L^2}{8}}$ $M_g = 1.093\times10^5$ kN.m

Prestressing force from all tendons P= 45000 kN

Eccentricity ecc= 1.822 m

Moment at mid-span from prestress $M_p = P\times ecc$ $M_p = 8.199\times10^4$ kN.m

Applied load stresses

$$\sigma_{tg} = \frac{-\mathbf{M_g \times (D - Y_{Bar})}}{\mathbf{I}} \qquad \sigma_{tg} = \text{- 10.605 N.mm}^{-2}$$

$$\sigma_{bg} = \frac{Mg \times Y_{Bar}}{I}$$ $\sigma_{bg} = 13.073$ N.mm^{-2}

Prestress stresses

$$\sigma_{tp} = \frac{P}{A} + \frac{M_p \times (D - Y_{Bar})}{I}$$ $\sigma_{tp} = 2.743$ N.mm^{-2}

$$\sigma_{bp} = \frac{P}{A} - \frac{M_p \times Y_{Bar}}{I}$$ $\sigma_{bp} = -15\ N.mm^{2}$

Total stresses:

$\sigma_{tg} + \sigma_{tp} = -7.86\ N.mm^{-2}$ (Top)

$\sigma_{bg} + \sigma_{bp} = 1.94\ N.mm^{-2}$ (Bottom)

From the published work by Khaloo & Kafimosavi (2007) it can be seen that the model has considered both gravity and additional applied load effects. This results in a section which exhibits tensile stresses at the soffit of the slab as expected, and as such would not fall under a class 1 (no tension) design at serviceability limit state.

3.4 The finite element method: ANSYS

The finite element modelling and analysis carried out in this study uses the finite element program, ANSYS. ANSYS is a commercial finite element program created in 1970 by John A. Swanson of Swanson Analysis Systems. ANSYS 12th edition has been used in this study. ANSYS has a comprehensive library of spar, beam, shell and solid elements. ANSYS had also been qualified for use in the nuclear industry and also verified for commercial use. It is also NAFEMS approved. Brief descriptions of the elements used in the current model are presented below:

1. Shell 63 (elastic shell): A four noded element that has both bending and membrane capabilities. The element has six degrees of freedom at each node, translations in the nodal X, Y, and Z directions and rotations about the nodal X, Y, and Z axes. Large deflection capabilities are included in the element. It is stated in the ANSYS manual that an assemblage of this flat shell elements can produce good results for a curved shell surface provided that each flat element does not extend and also the shell element is mesh sensitive. Material properties and all the cross-section dimensions and calculations have mentioned before where the concrete is represented by the Shell 63 element. Figure 3.3 shows shell 63 element from ANSYS.

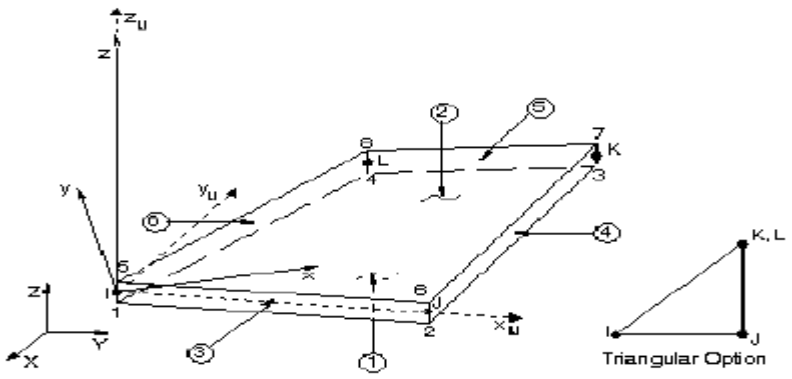

Figure (3.3) Shell63

2. Beam 188 (3-D Linear Finite Strain Beam): is a linear 2-node or quadratic beam element in 3-D. Beam 188 has six or seven degrees of freedom at each node. These include translations in the X, Y, and Z directions and rotations about the X, Y and Z directions. A seventh degree of freedom (warping magnitude) can also be considered. This element is well-suited for linear, large rotation, and/or large strain nonlinear applications. The beam elements are one-dimensional line elements in space. The cross-section details are breadth = 3m and height = 3m where Beam188 utilized for the rigid beam offsets used at the boundaries as shown in figure 3.4.

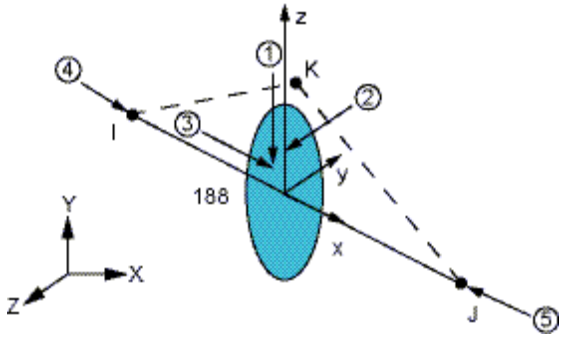

Figure (3.4) Beam188

3. Link 8 (3-D Spar): is a two-node, three-dimensional truss element. It is a uniaxial tension-compression element with three degrees of freedom at each node; translations in the nodal X, Y and Z directions. The element is a pin jointed structure with no bending capabilities. Material properties and the cross-section calculations have been mentioned before where Link8 represents the prestressing tendons, figure (3.5).

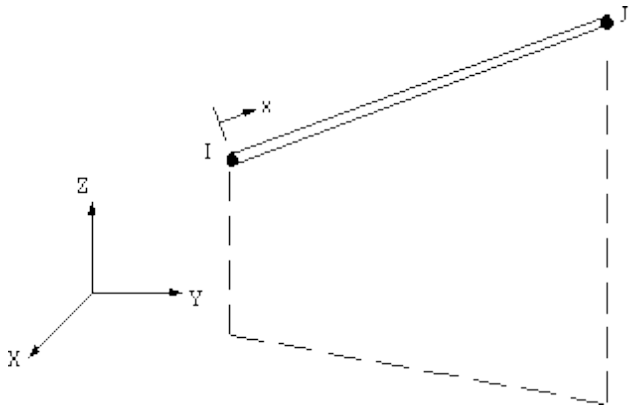

Figure (3.5) Link8

Creating any element using ANSYS can be carried out using one of two methods: the direct generation method by defining the nodes and elements for the section or use of the solid modelling method whereby the FE mesh is generated on the geometry of the model. The choice is governed by the fact that an easy and flexible parametric model was needed. In this study, after creating the models, applying loads and specifying the boundary condition using the ANSYS programme, stresses can be easily obtained after the model has been solved. In addition, it will be also used to compare the direct stresses between various models. Therefore, creating the same general box girder construction of straight and curved bridge models with the same boundary conditions is required. The direct generation method has been adopted for this research with a scripted approach using the ANSYS APDL (ANSYS Parametric Design Language), which allows the user to input the geometric parameters of the model whilst the file is read into the program therefore allowing automatic and rapid creation of the bridge deck. using the script file (APDL) allows the user to change the parameters such as span length, curvature, deck depth and width also changing the mesh.

3.5 Loading and boundary condition

The shell box bridge models were subjected to the gravity and uniform distributed load (25 kN/m^2) of the box first then prestressing forces are subsequently applied. Simple pinned support conditions were applied to a simple span with fixed torsional behaviour about the longitudinal axis. Horizontal movements were free at both ends along the curved axis, while the vertical displacements were completely constrained. The two ends of the bridges are closed by rigid

beam elements were joined at a node placed at the centroid of the section. This was done in order to reduce local effects, provide uniform distribution of the large support reactions and to make sure all nodes at the support ends are fully bonded with each other. A node at the centroid of the cross-section was created and connected to each node from the end support via the rigid beam elements. Figure (3.6) shows the box girder bridge. The complete model of the box girder comprises 5364 elements. The total number of nodes included in the model is 4927. The green bands with the boundary conditions figure represents the coupling coincident nodes which ensure that the various parts of the model are joined together in all degrees of freedom.

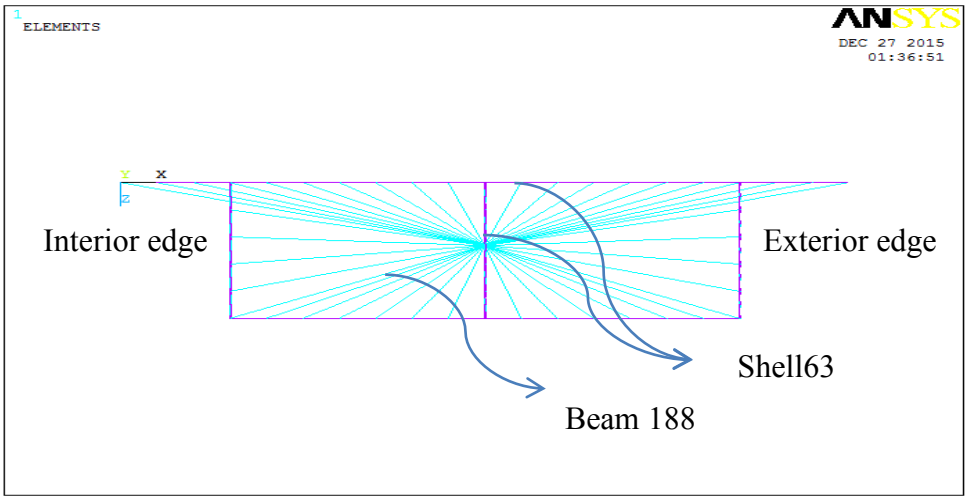

(A) Cross-section

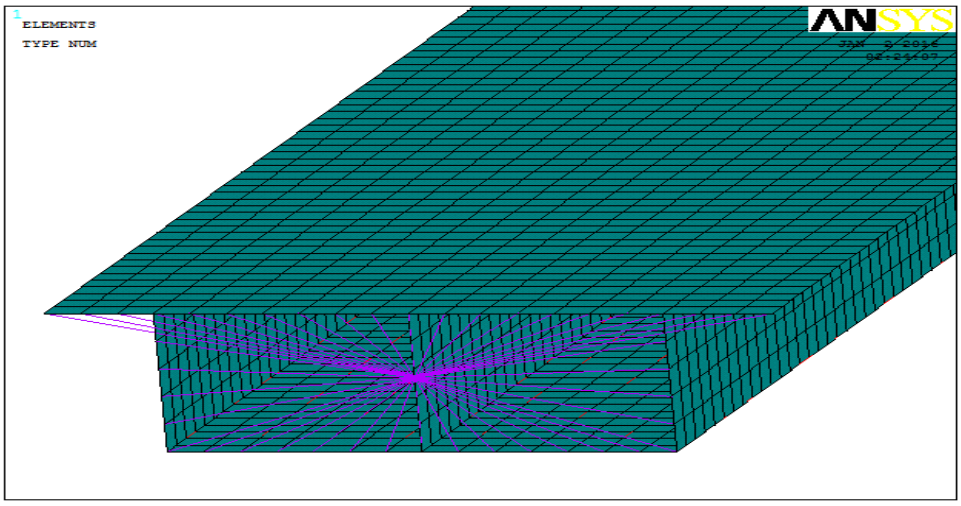

(B) Isometric view of model without prestress

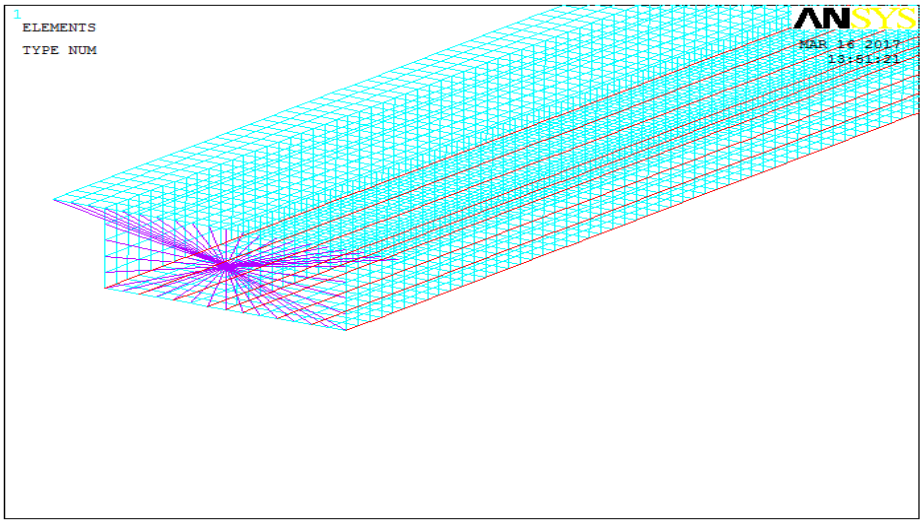

(C) Isometric view of model with prestress
Figure (3.6) Box girder bridge end restraint system.

3.6 Description of the bridge models

The box bridge models that are used in this chapter to study the behaviour of the straight and curved box girder are single-span multicell box girder bridges of total span length 54m. There are two types of bridges that are modelled in ANSYS for the current study.

1. Straight box shell model
2. Curved box shell model

For the straight box shell model, there is only one case used for verification purposes while for the curved box shell model there are 11 cases of curvature, each case has been investigated through three different types of loading and compared with the published work.

3.6.1 Straight box shell model

The straight box bridge model comprises shell 63 elements for the webs, top flange, and the bottom flange. The plate thicknesses and the material properties are required input for Shell 63. Boundary conditions have been represented by Beam 188 elements. Beam 188 connect each node at the edge end with a fixed node at the centroid of the cross-sectional face. The green bands in each boundary conditions diagrams represent coupling coincident nodes which ensure

that the various parts of the model are joined together in all degrees of freedom. Three different types of loading have been investigated for the straight box. These are:

1- Straight box model under gravity loading

The box girder in this case is straight and only subject to self-weight. A uniformly distributed load equal to 25 kN/m^2 represents the gravity load which acts vertically and downward on the top of the slab surface. The model was created using the APDL script which can be found in Appendix 2. The finite element model for this case is shown in figure (3.7). Figure (3.8) shows the straight box model under gravity and the boundary conditions (BC's). Deformed shape contours are shown in figure (3.9) and the stress contours and mid span stresses are shown in figure (3.10) & (3.11). The compression stresses and tension stresses at mid-span values are presented in tables (3.1) and (3.2).

1- Straight box model under gravity loading

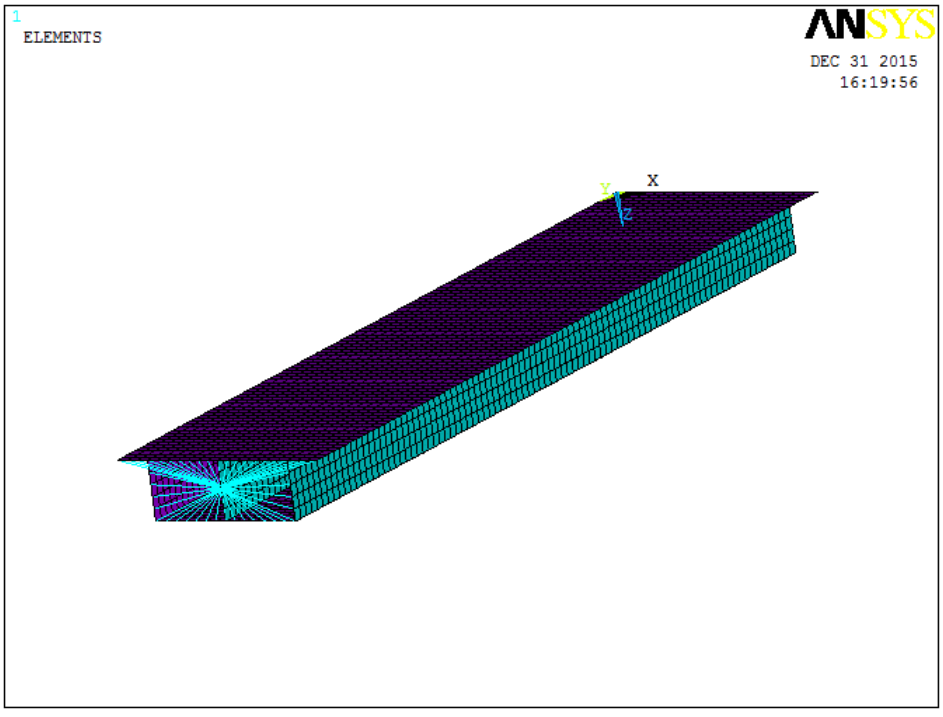

Figure (3.7) The finite element model for straight under gravity loading

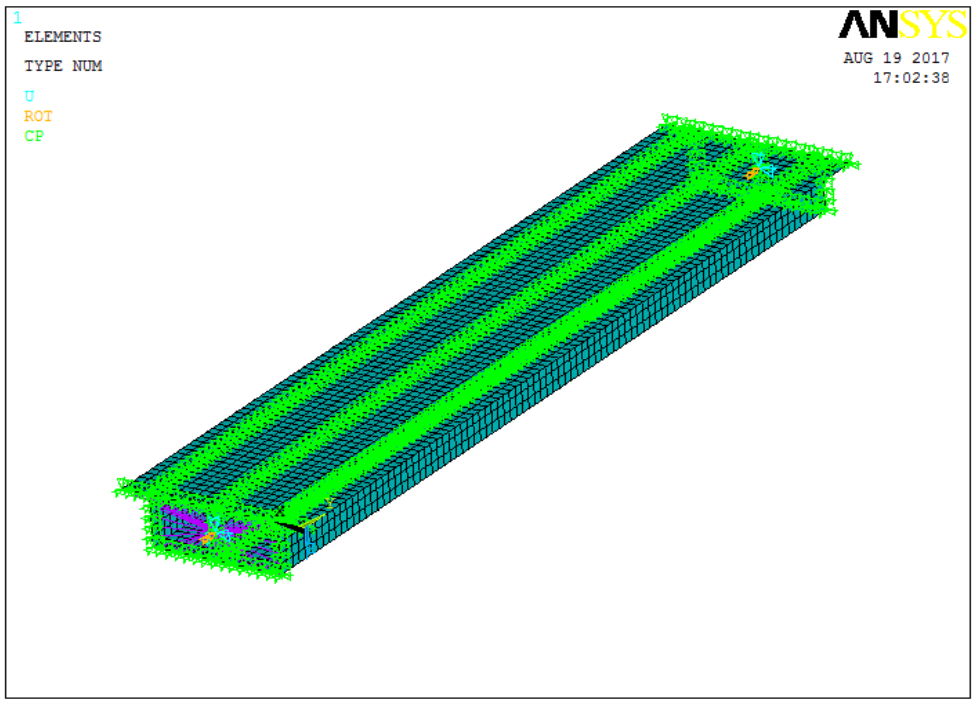

Figure (3.8) Boundary conditions including coupling for straight under gravity loading

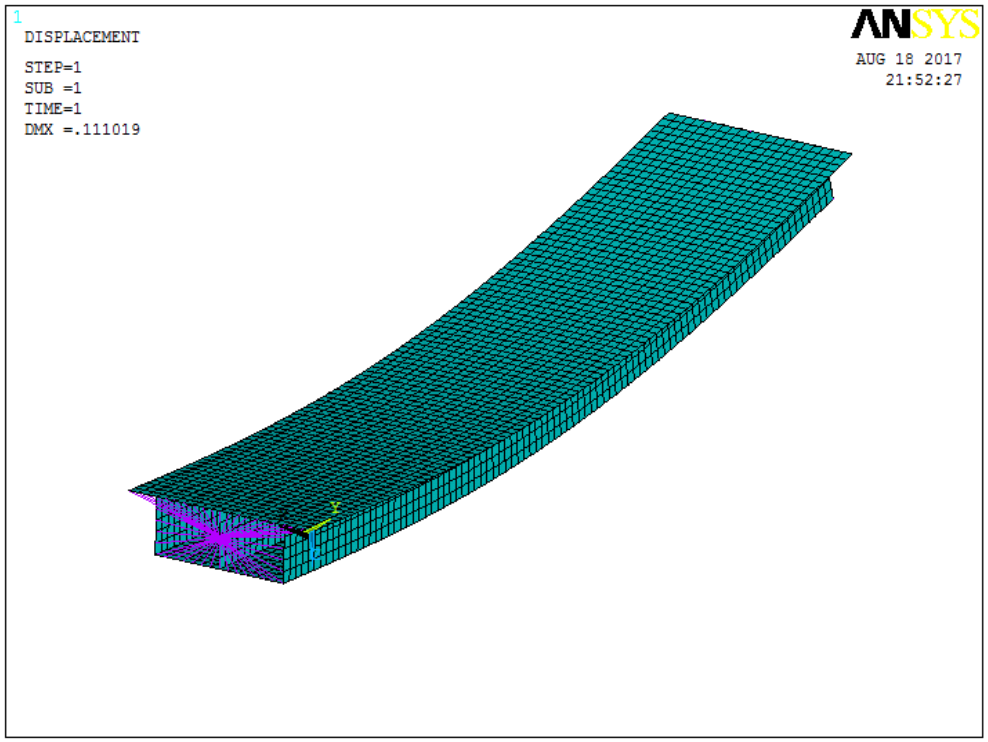

Figure (3.9) Deformed shape for straight under gravity loading

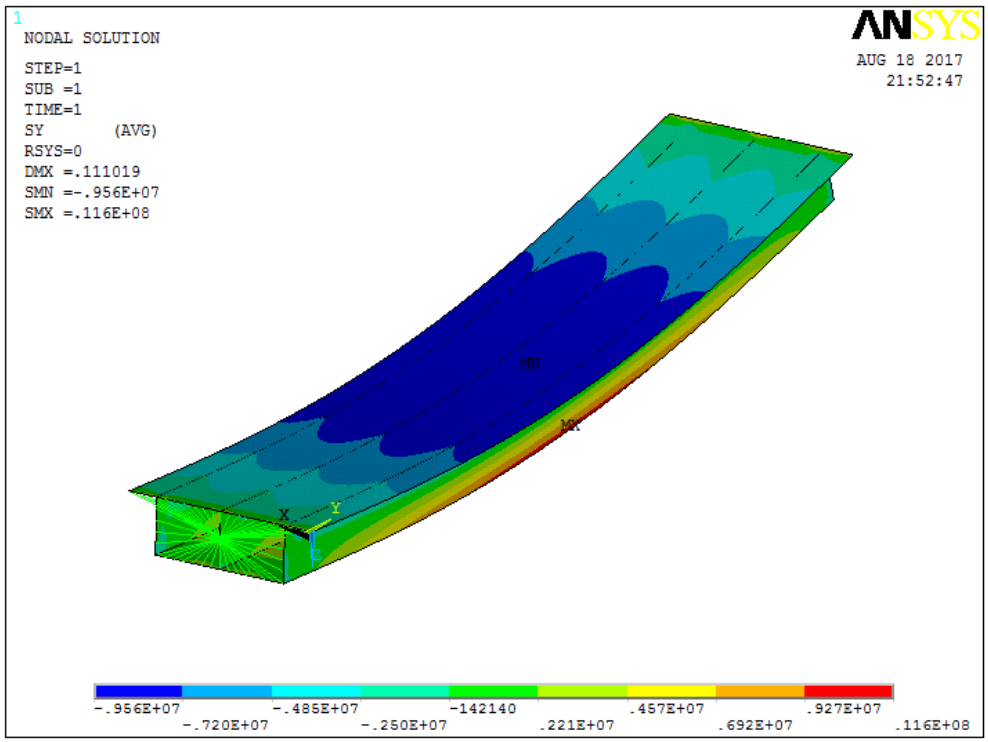

Figure (3.10) Longitudinal stresses for straight under gravity loading

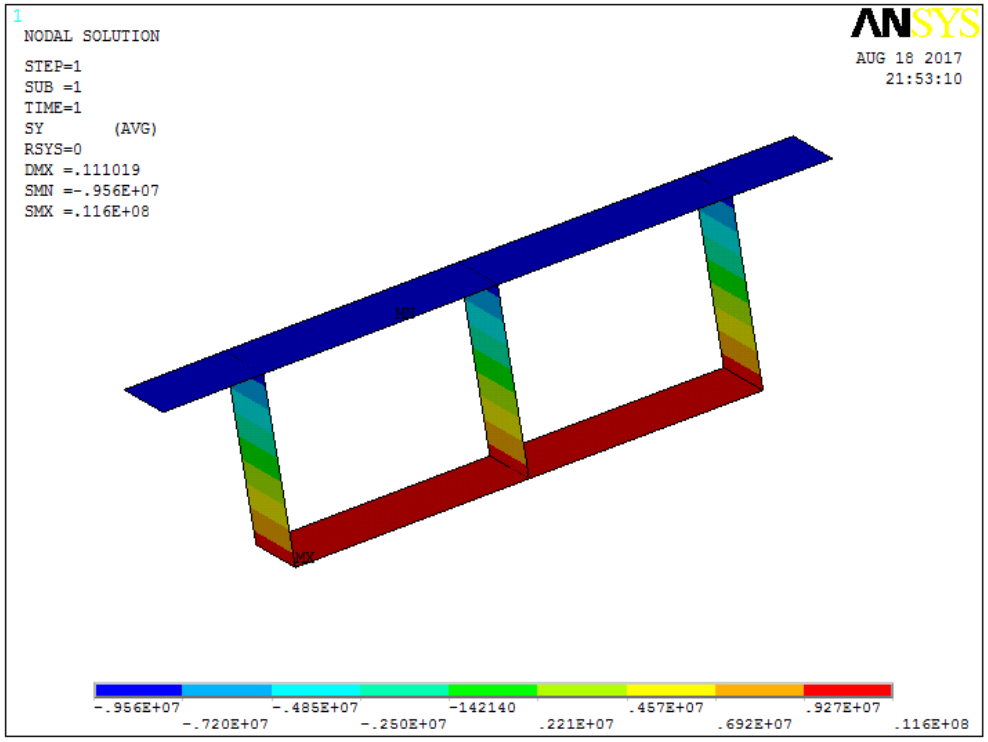

Figure (3.11) Longitudinal stresses at mid-span for straight under gravity loading

2- Prestressed straight box

The box girder in this case is straight and acting under the effects of prestress alone. The tendons are at the same elevation along the length of the member and are located at the soffit of the box girder. The full model is in Appendix 2 and the prestress is taken from section 3.3.2. The finite element model for this case is shown in figure (3.12). Figure (3.13) shows the prestressed straight box model and the boundary conditions. The deformed shape contour is shown in figure (3.14) and the stress contour and mid span stresses are shown in figures (3.15) & (3.16). The compression stresses and tension stresses for the mid-span values are given in table (3.1) and (3.2). The prestress is applied via initial strain in the link elements.

2- Prestressed straight box

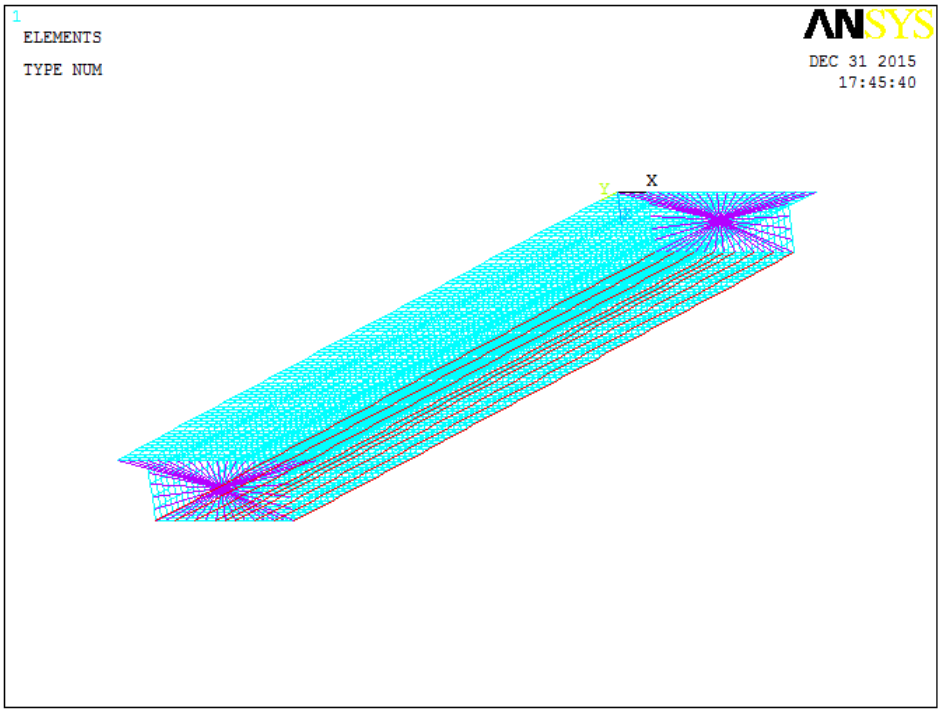

Figure (3.12) The finite element model for straight under prestress loading

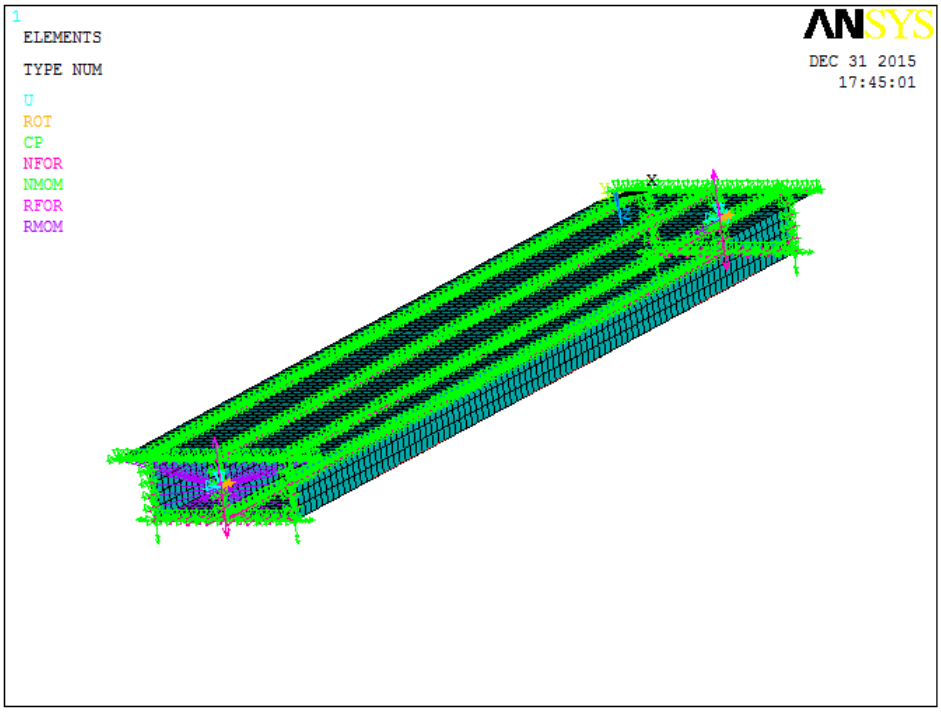

Figure (3.13) Boundary conditions for straight under prestress loading

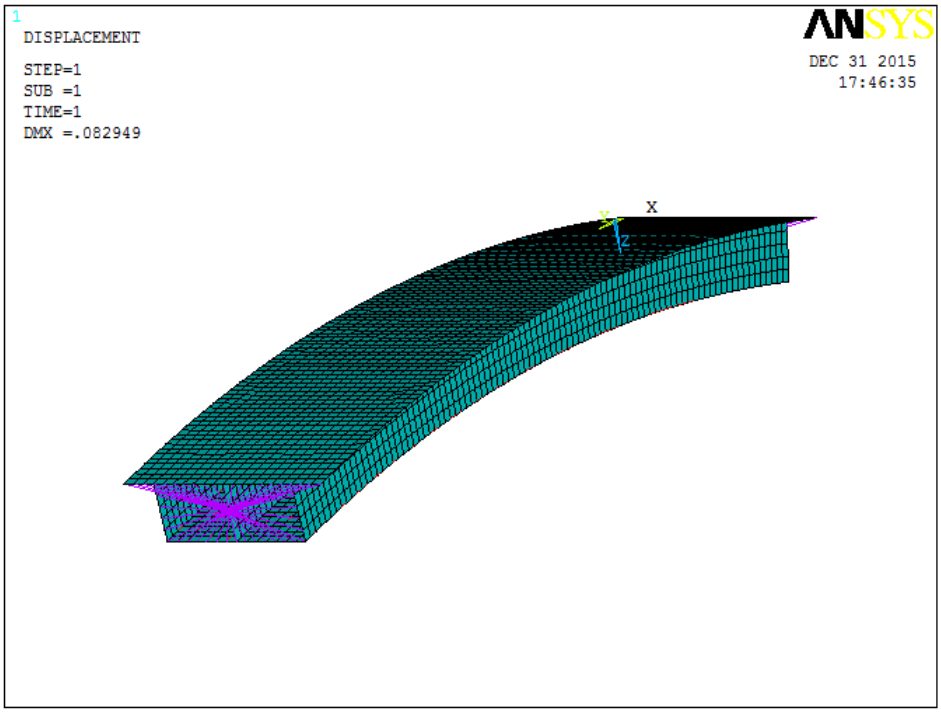

Figure (3.14) Deformed shape for straight under prestress loading

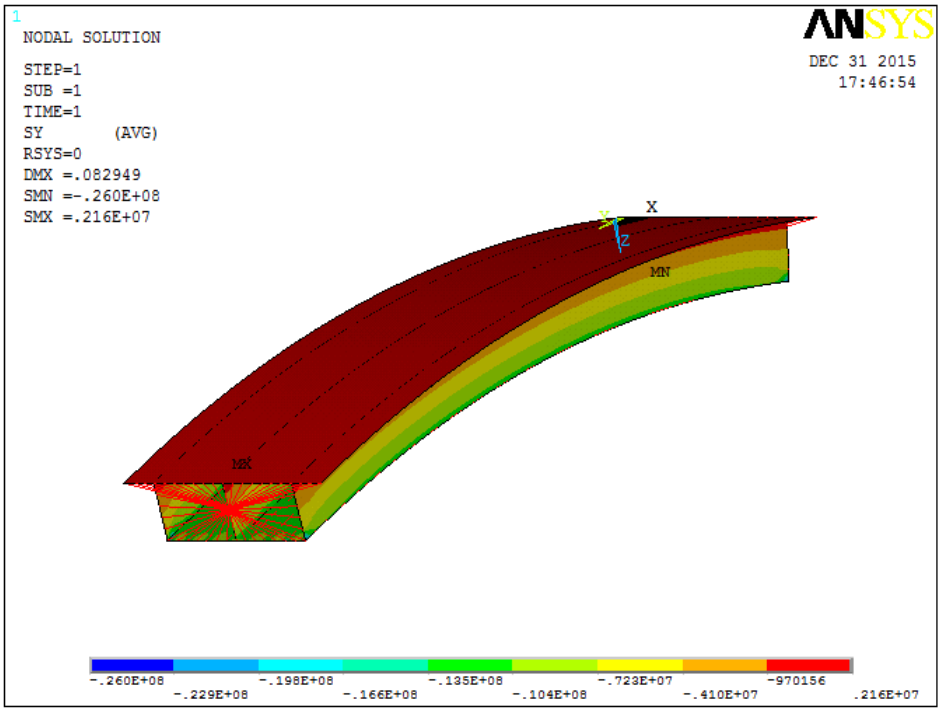

Figure (3.15) Longitudinal stresses for straight under prestress loading

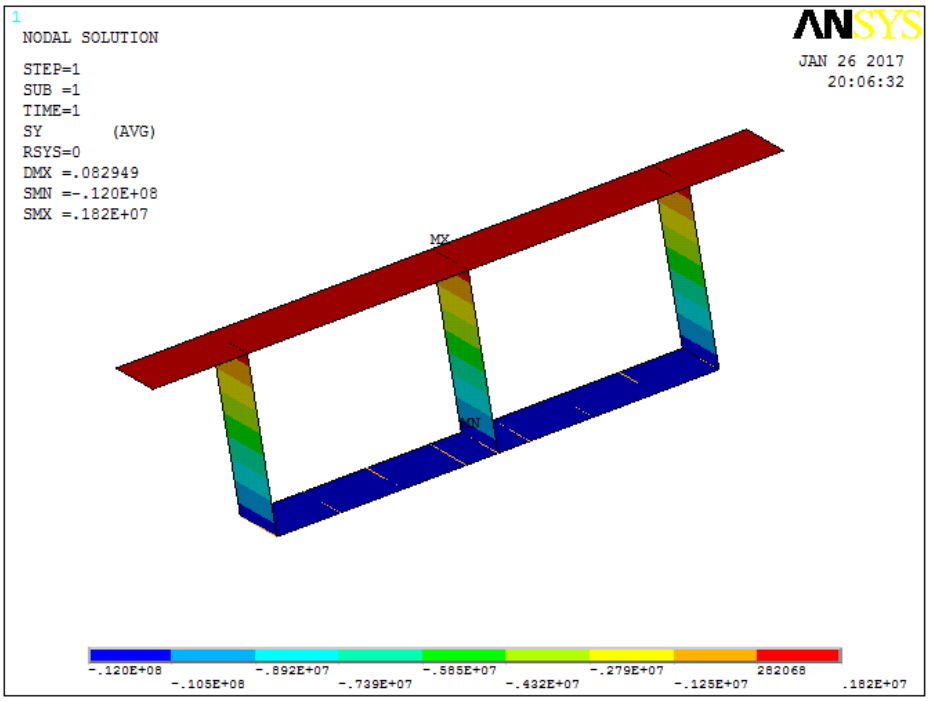

Figure (3.16) Longitudinal stresses at mid-span for straight under prestress loading

3- Gravity and prestress straight box model

The box girder in this case is straight and acting under both gravity (UDL =25 kN/m^2) and prestress, the details of the model are in Appendix 2 and the prestress has been calculated in section 3.3.2. The finite element model for this case is shown in figure (3.17). Figure (3.18) shows the prestressed straight box model under gravity and the BC's. The deformed shape is shown in figure (3.19) and the mid span stresses are shown in figures (3.20) & (3.21). Stresses and tension stresses for the mid-span values are presented in tables (3.1) and (3.2).

3- Gravity and prestressed straight box model

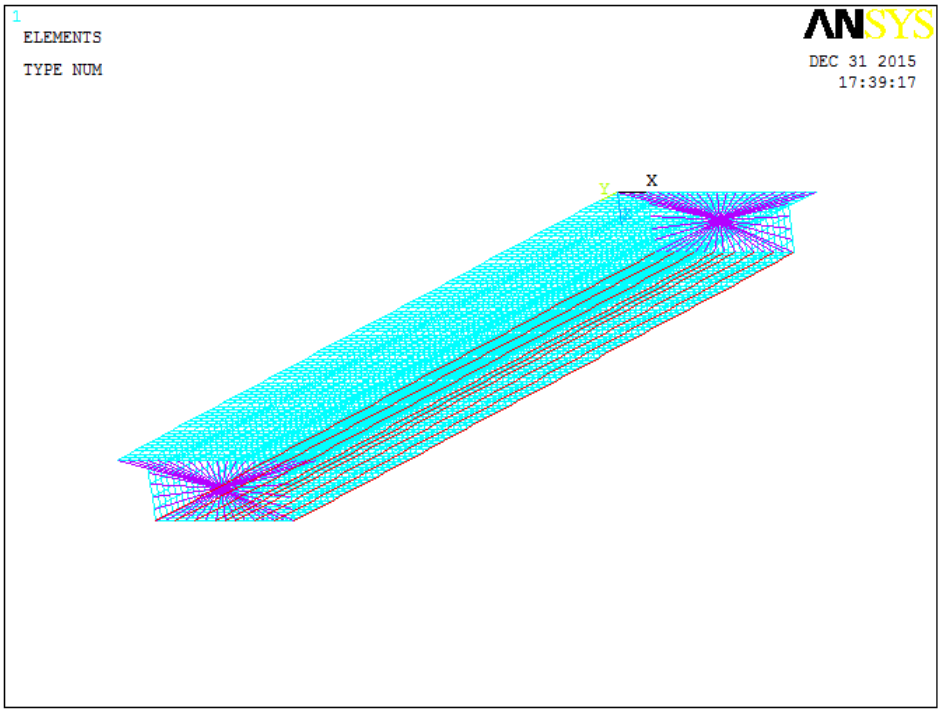

Figure (3.17) The finite element model for straight under gravity & prestress loadings

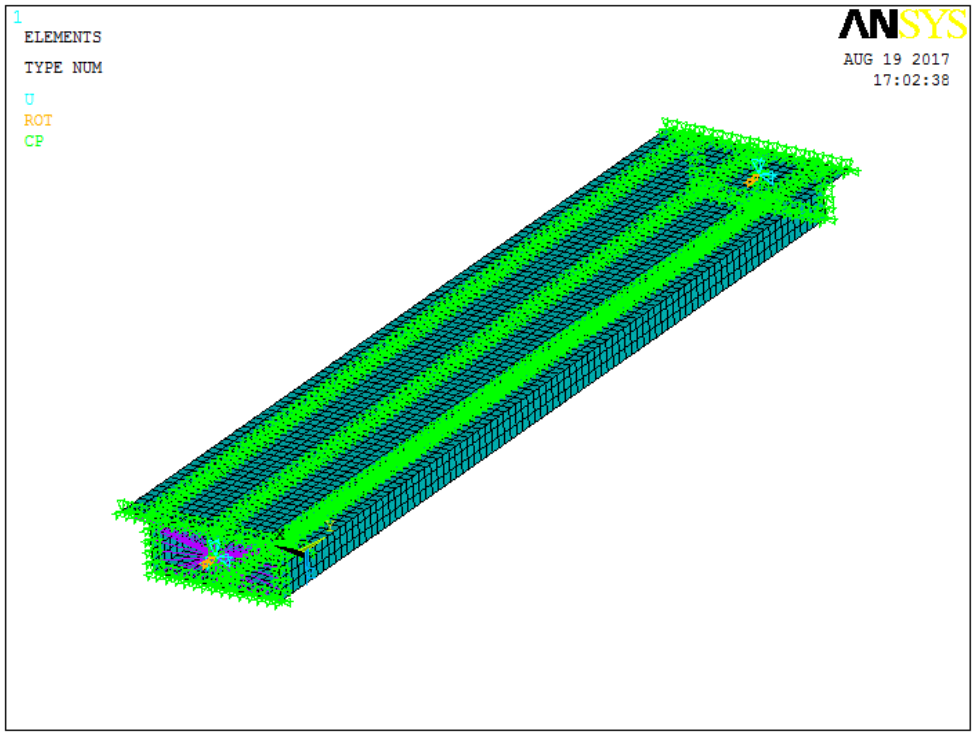

Figure (3.18) Boundary conditions for straight under gravity & prestress loadings

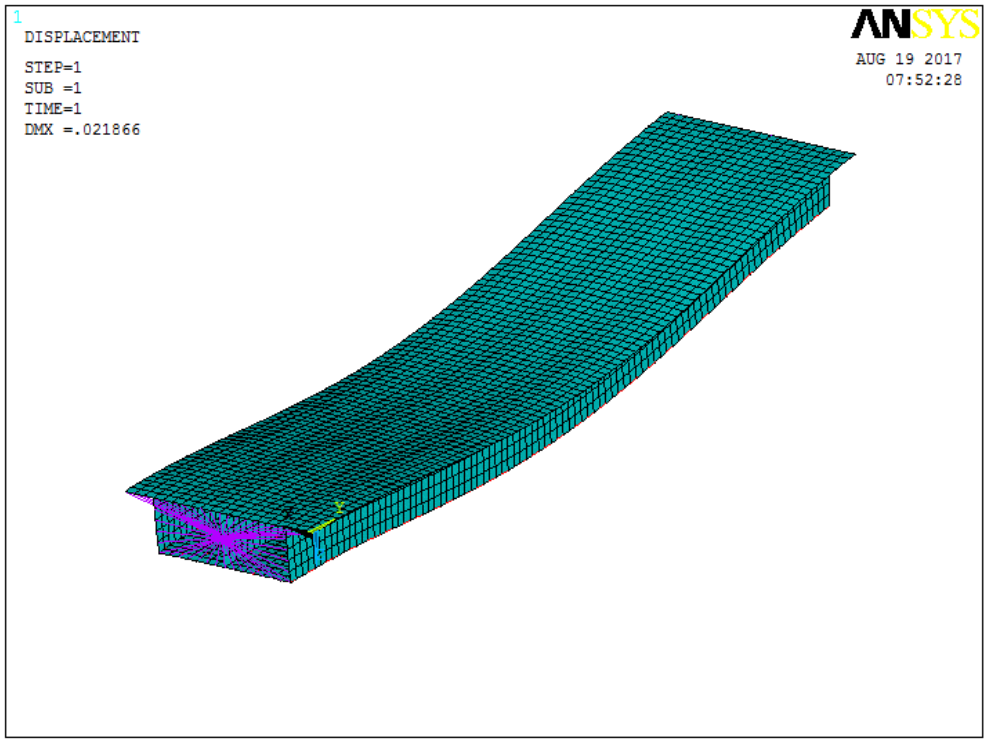

Figure (3.19) Deformed shape for straight under gravity & prestress loadings

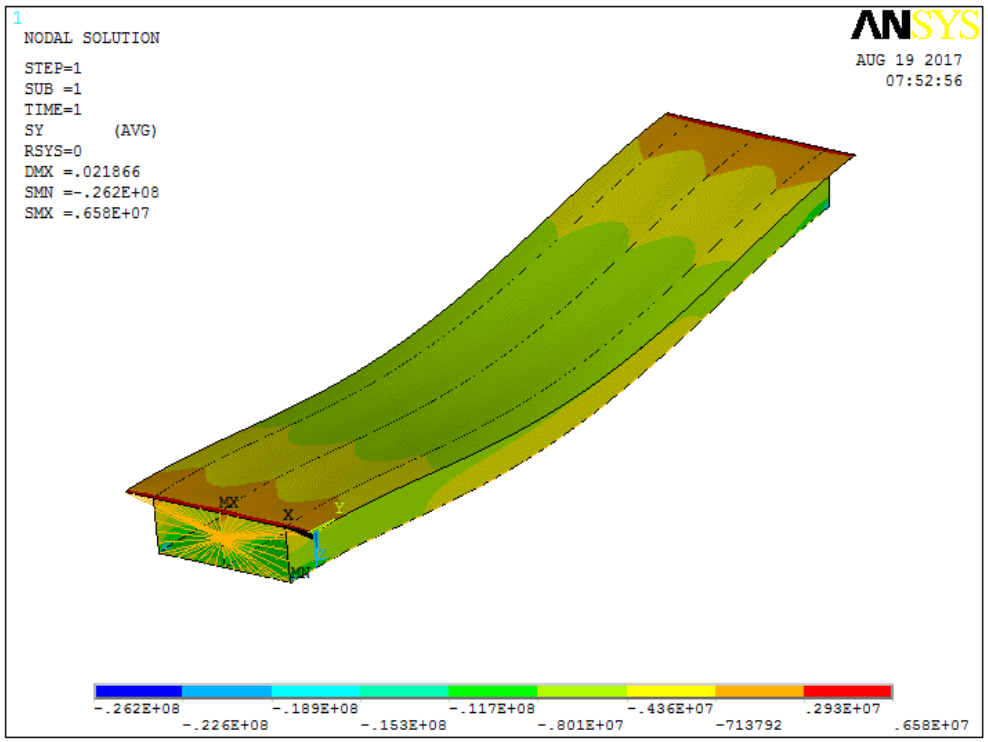

Figure (3.20) Longitudinal stresses for straight under gravity & prestress loadings

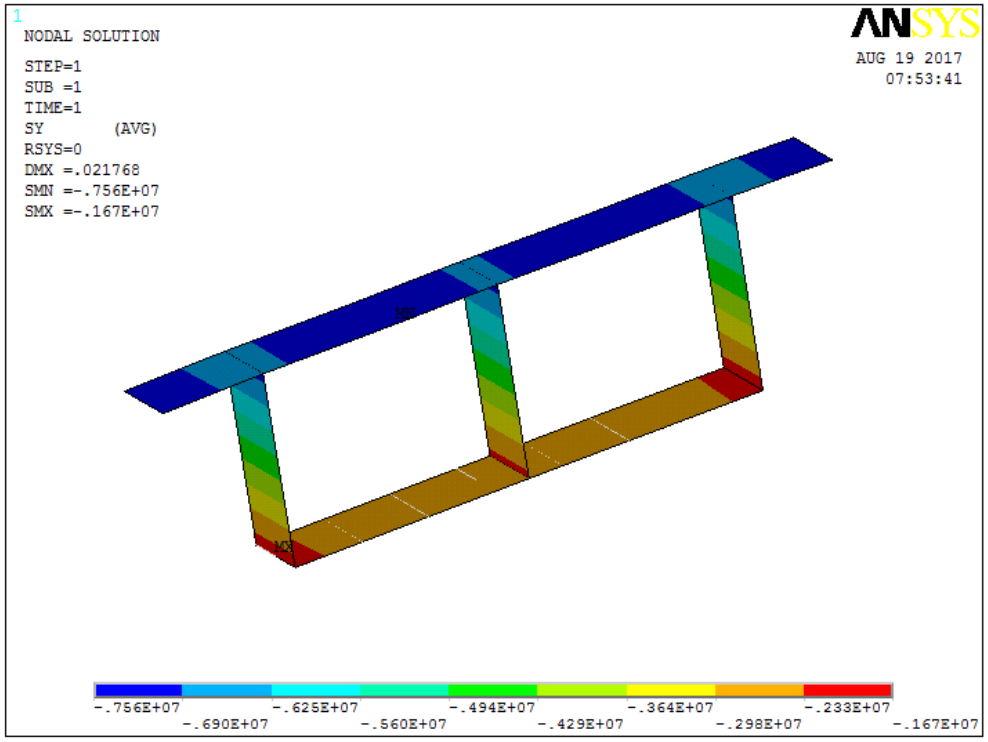

Figure (3.21) Longitudinal stresses at mid-span for straight under gravity & prestress loadings

3.6.2 Curved box shell model

The horizontally curved box bridge having a changeable radius of curvature is modelled using Shell 63 similar to that of the straight box shell model. Just like the straight shell models, for this single span multicell bridge, the support conditions are the same. The models are the same for model M1 in material properties and cross-section with the exception that they are curved in plan. The calculation of the various curvatures is shown below. Since the models are used for comparison purposes, both the models are of the same general construction as mentioned in the script file (Appendices 2 and 3). Eleven cases of curvature have been analysed with changing horizontal curvature, related to a step change in the width (δ) of the sector, which is presented here from 1 to 11m. Each single case has been examined under the effects individually of gravity and prestress and then both gravity and prestressing combined. This part of the analysis of the curved box shell model will illustrate the behaviour for 3 cases, delta (δ) will be equal to 1, 5 and 11m respectively to show the behaviour of the finite element models, deformed shapes and stress contours. The first case is when the span started to curve and second case when delta= 5m which is around the middle to show how changing curvature will affect box girder behaviour. The last case is when delta equal to 11 m and the box girder section has reached tension stresses.

1-Case 1 (δ=1m)

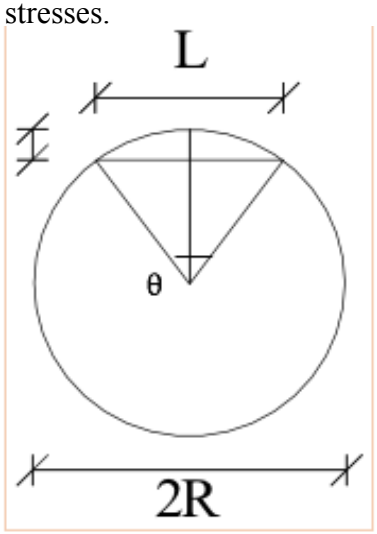

Span L =54 m

Delta $\delta_{step} = 1$ m

Radius of curvature $$R = \left[\frac{\delta_{step}^{\,2} + (0.5 \times L)^2}{2 \times \delta_{step}}\right]$$ R= 365 m

Subtended angle theta $$\theta = 2 \times \tan^{-1}\left[\frac{0.5 \times L}{\sqrt{R^2 - (0.5 \times L)^2}}\right]$$ θ = 8.848°

1-Curved box model under gravity effects

The curved box girder in this case is only subject to UDL (the gravity), the model is created by the APDL and it can be found in Appendices 1 & 2. The finite element model for this case is shown in figure (3.22). Figure (3.23) shows the curved box model under gravity and the applied BCs. The deformed shape is shown in figure (3.24) and the longitudinal stress contours and mid

span stresses are shown in figures (3.25) & (3.26). The longitudinal stresses at the mid-span section are presented in table (3.2).

1-Curved box model under gravity (δ=1m)

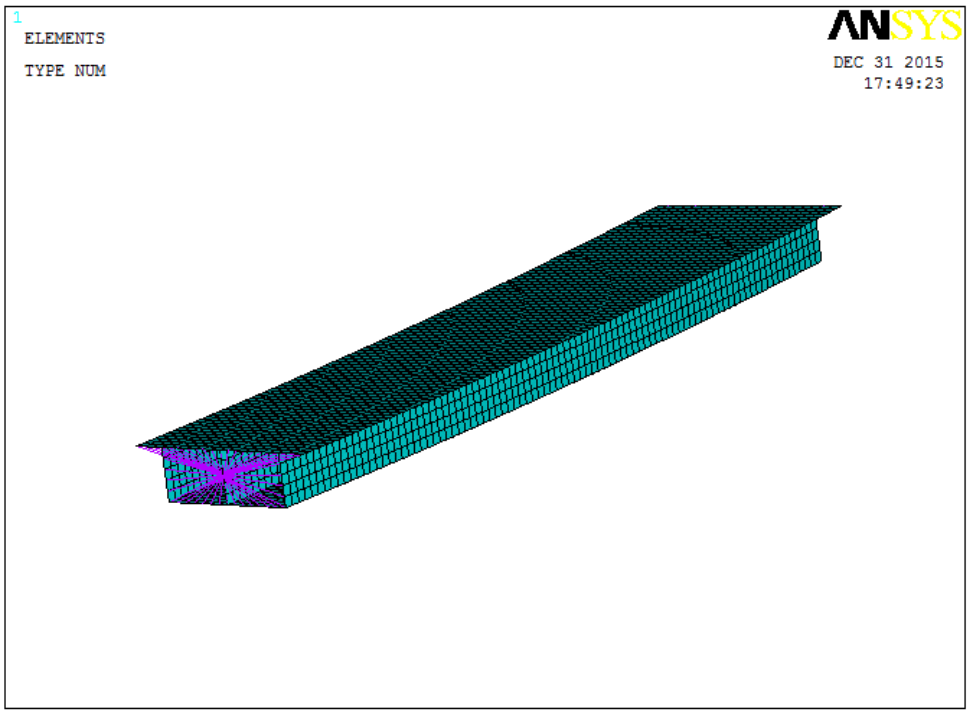

Figure (3.22) The finite element model under gravity (δ=1m)

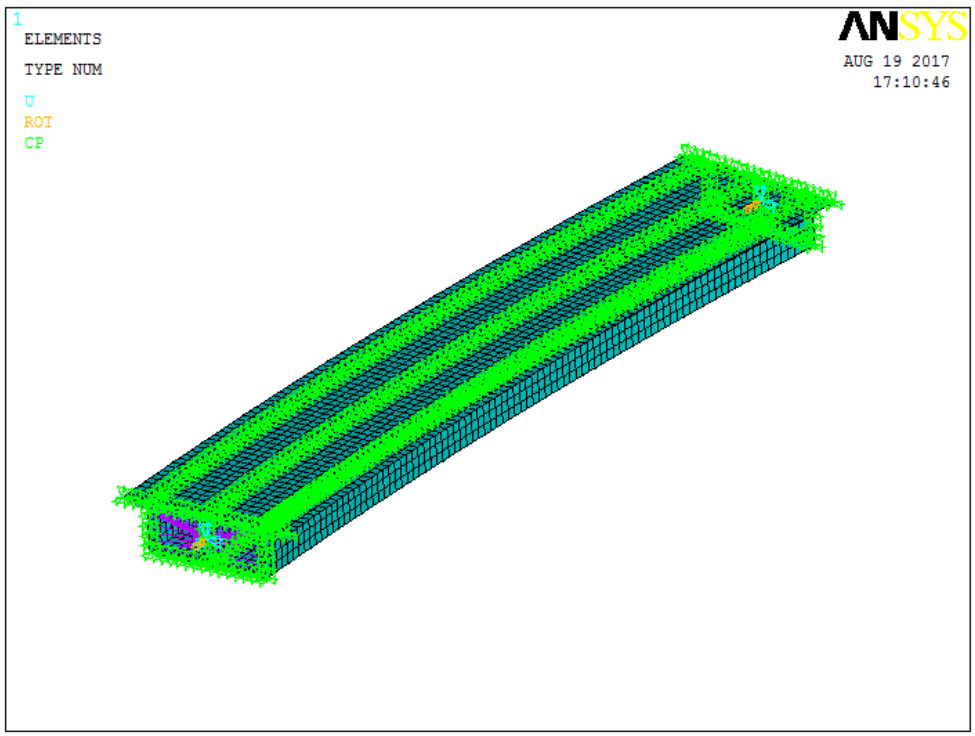

Figure (3.23) Applied boundary conditions including coupling under gravity (δ=1m)

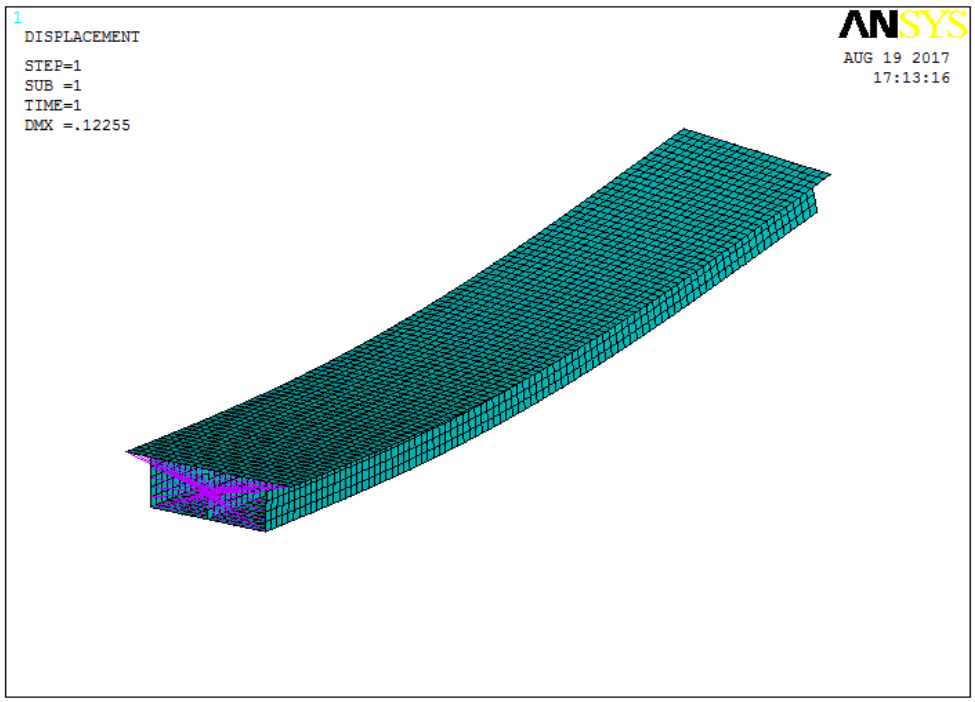

Figure (3.24) Deformed shape under gravity (δ=1m)

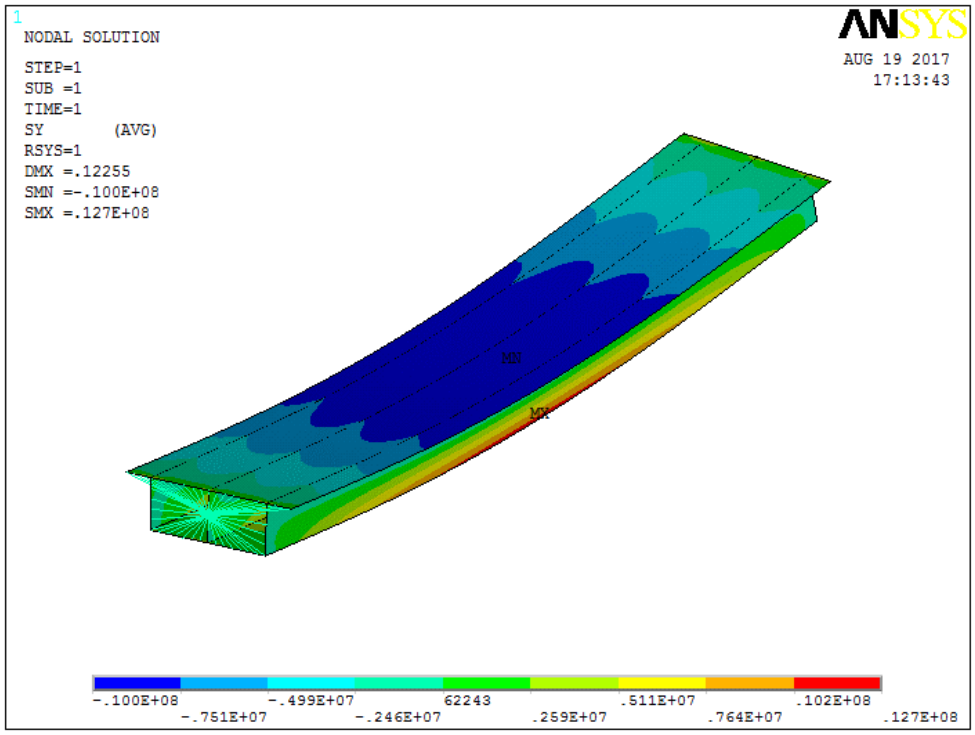

Figure (3.25) Longitudinal stresses under gravity (δ=1m)

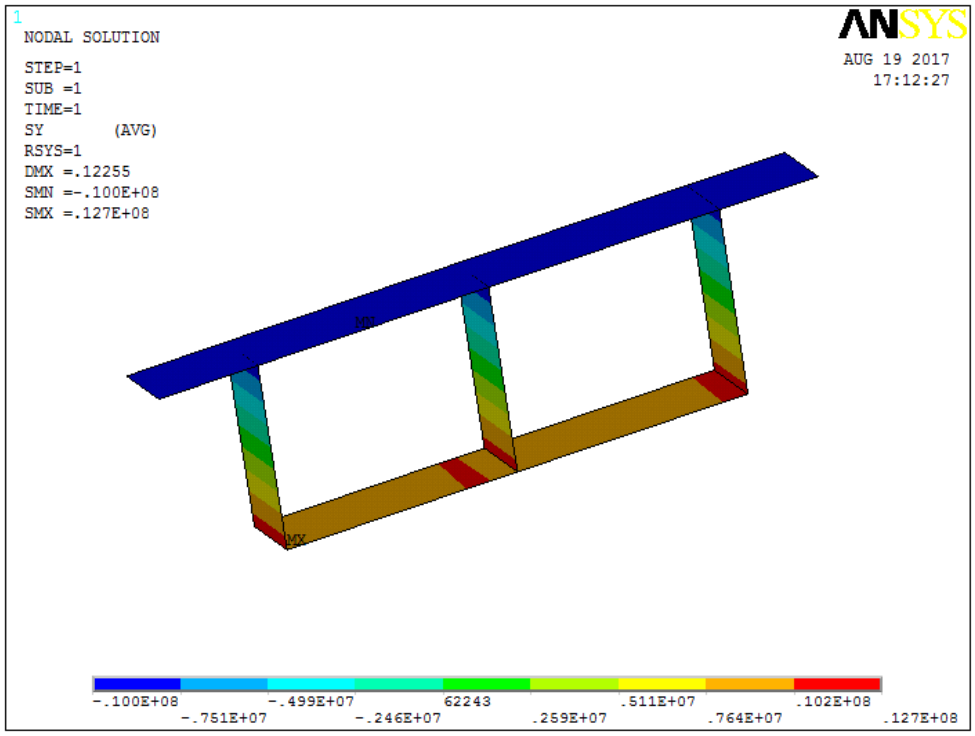

Figure (3.26) Longitudinal stresses at mid-span under gravity (δ=1m)

2-Prestressed curved box model

The curved box girder in this case is subject to the effects of prestress alone, the full model is provided in Appendices 2 & 3 and the prestress is taken from section 3.3.2. The finite element model for this case is shown in figure (3.27). Figure (3.28) shows the prestressed curved box model with the boundary conditions applied. The deformed shape is shown in figure (3.29) and the longitudinal stress contours and mid span stresses are shown in figures (3.30) & (3.31). Longitudinal stresses for the mid-span values are presented in table (3.2).

2-Prestressed curved box girder model (δ =1m)

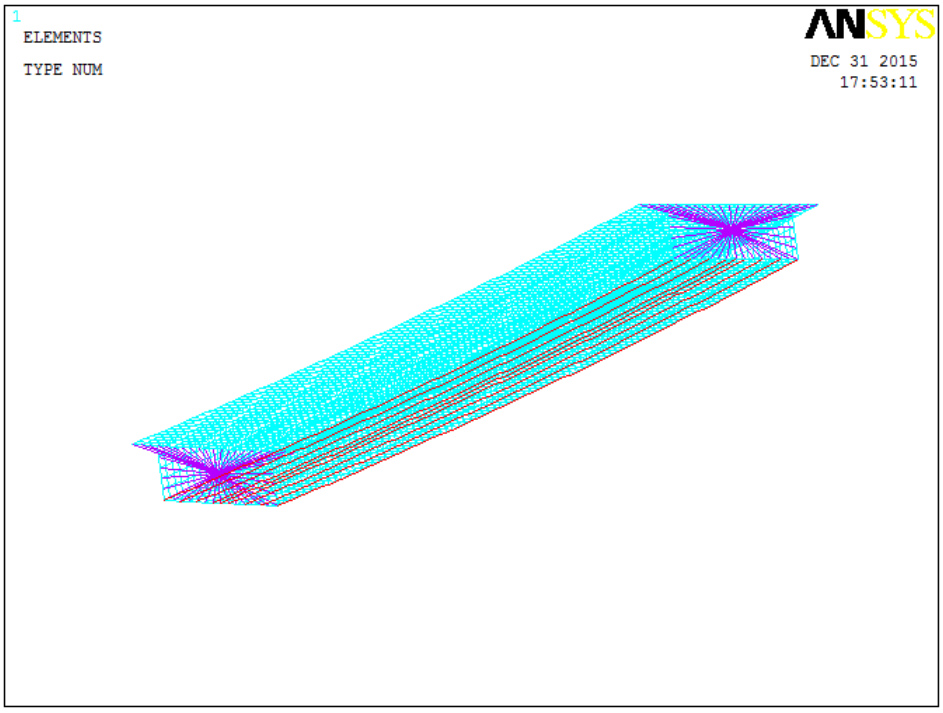

Figure (3.27) The finite element model under prestressed (δ=1m)

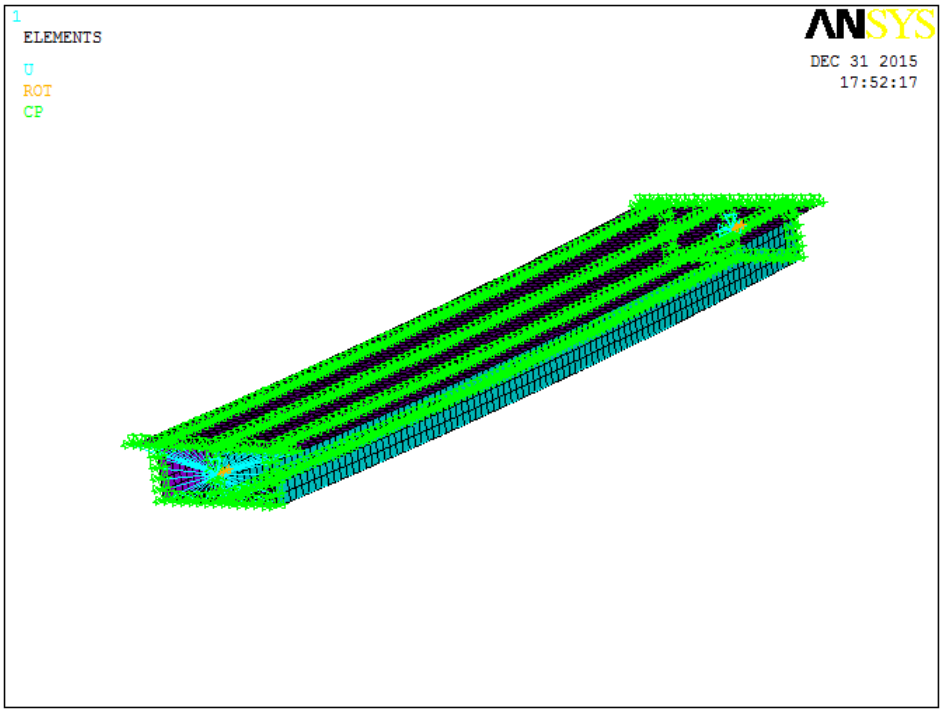

Figure (3.28) Boundary conditions under prestressed (δ=1m)

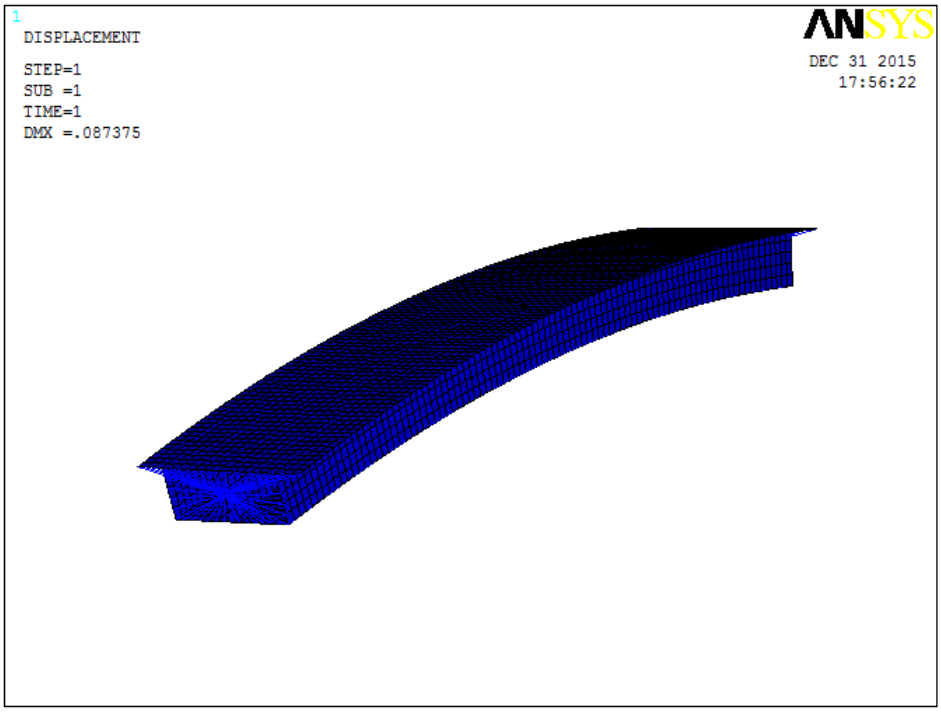

Figure (3.29) Deformed shape under prestressed (δ=1m)

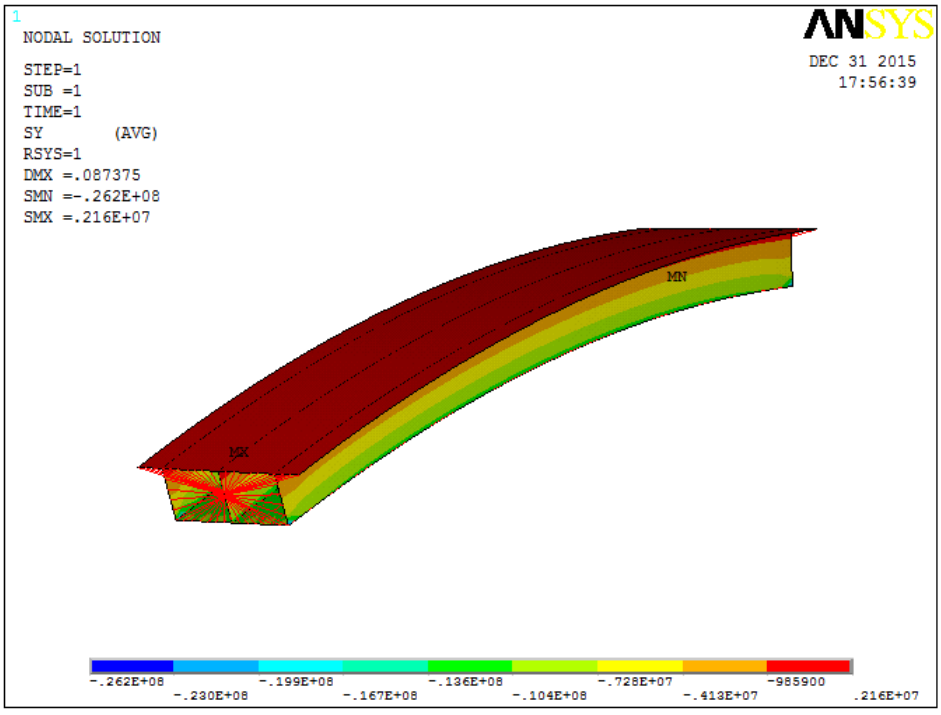

Figure (3.30) Longitudinal stresses under prestressed (δ=1m)

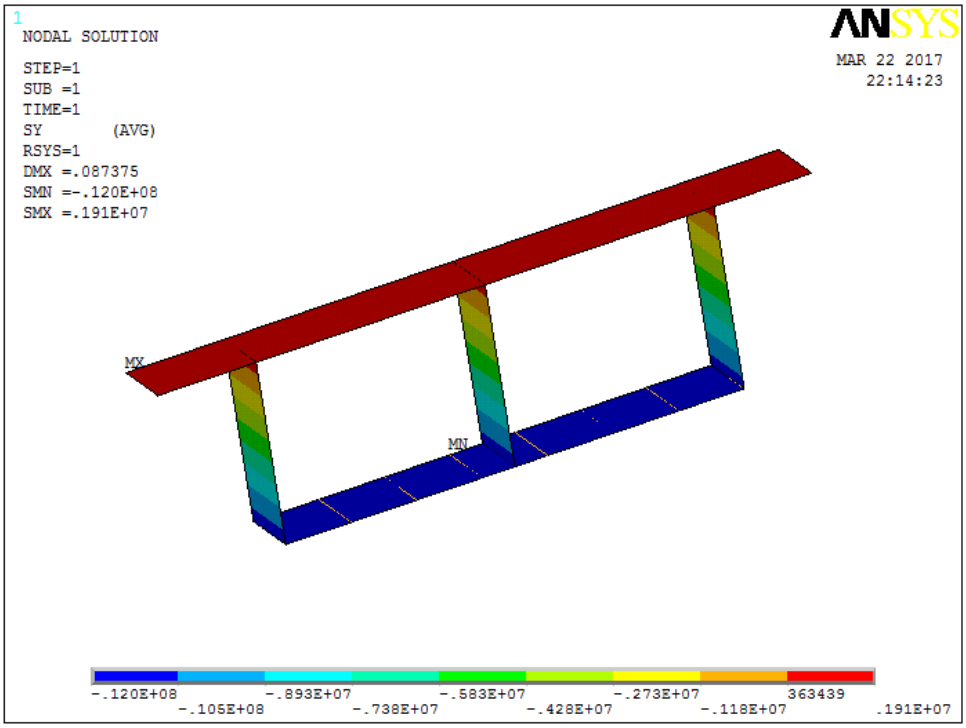

Figure (3.31) Longitudinal stresses at mid-span under prestressed (δ=1m)

3- Gravity and prestressed curved box model

The curved box girder in this case is subject to both self-weight and prestress, the model is shown in Appendices 2 &3 and the prestress has been calculated in section 3.3.2. The finite element model for this case is shown in figure (3.32). Figure (3.33) shows the prestressed curved box model subject to gravity and the applied BCs. The deformed shape is shown in figure (3.34) and the longitudinal stress is shown in figures (3.35) & (3.36). Stresses and tension stresses for the mid-span values are presented in table (3.2).

3-Gravity and prestressed curved box girder model (δ=1m)

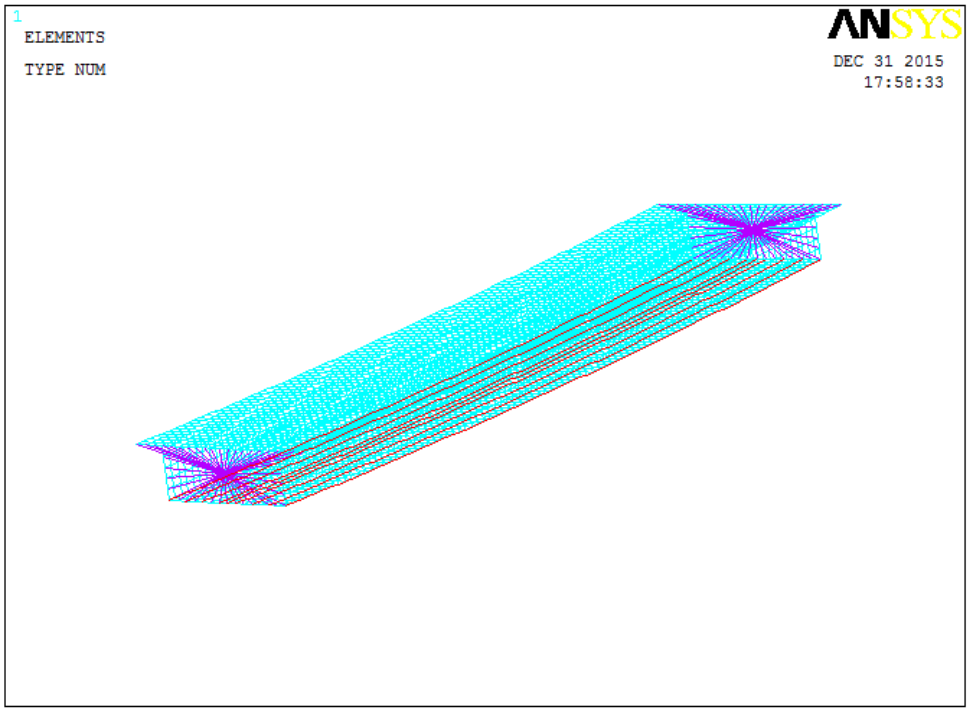

Figure (3.32) The finite element model under gravity & prestressed (δ=1m)

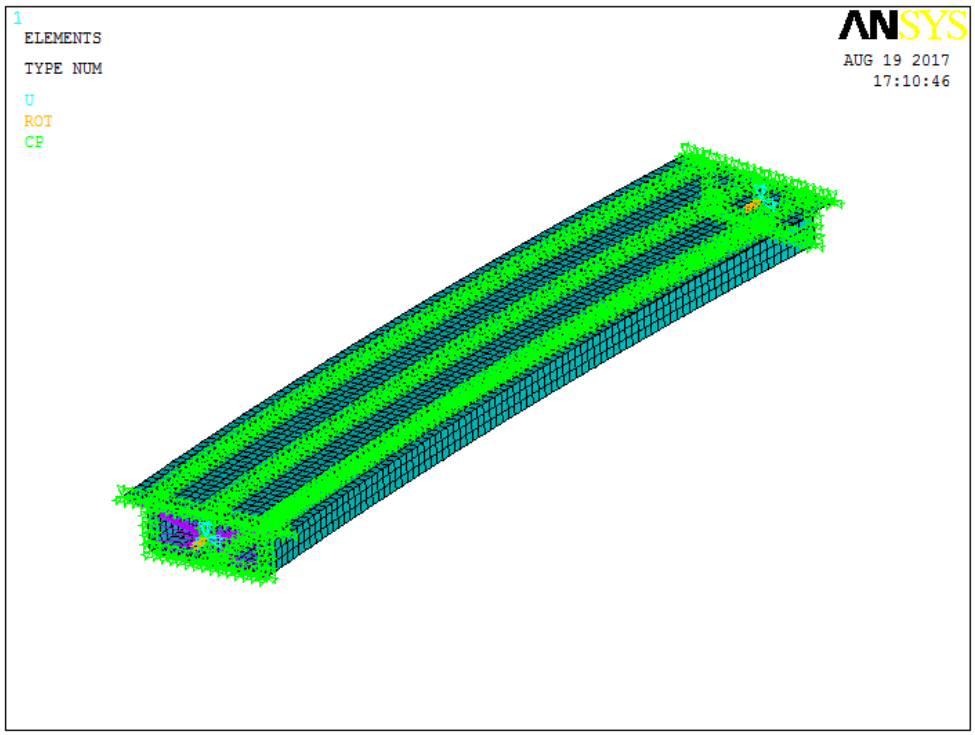

Figure (3.33) Boundary conditions under gravity & prestressed (δ=1m)

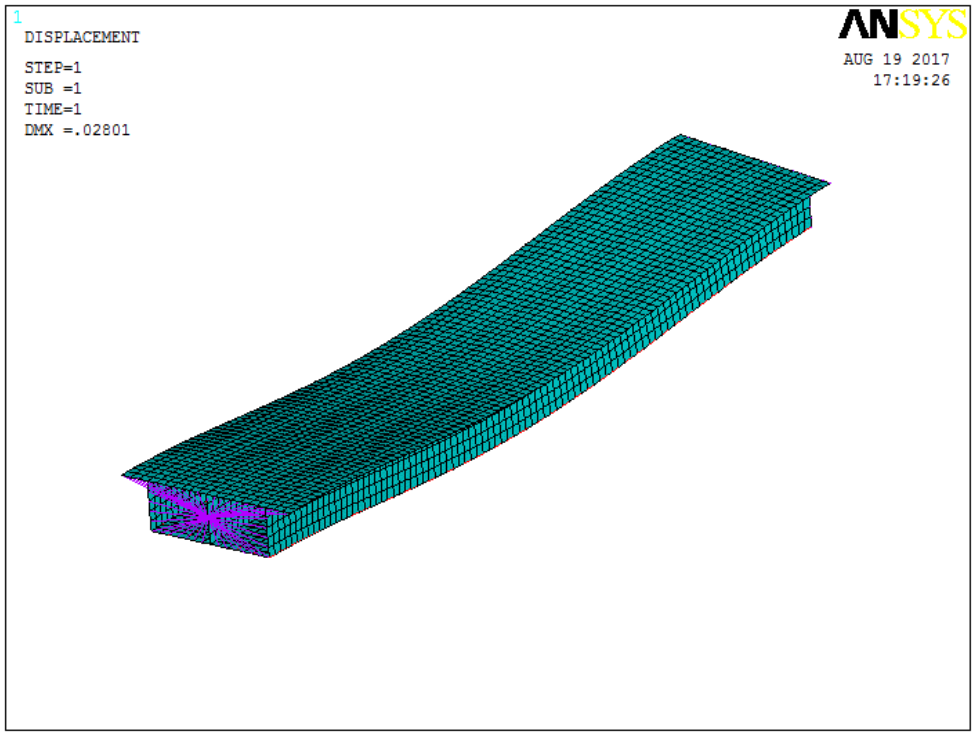

Figure (3.34) Deformed shape under gravity & prestressed (δ=1m)

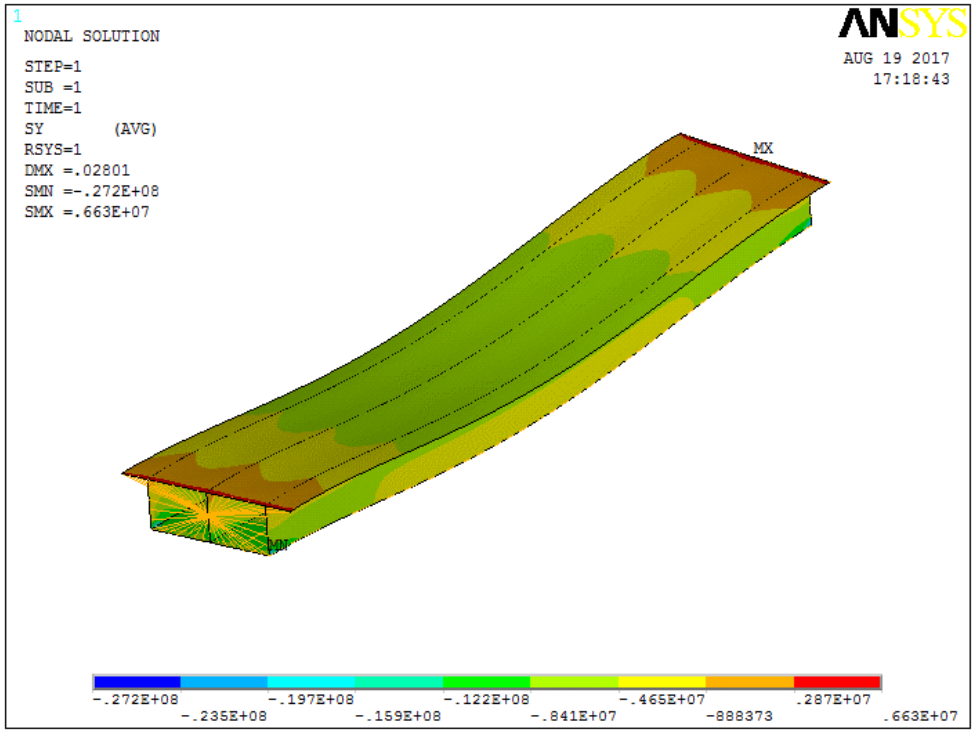

Figure (3.35) Longitudinal stresses under gravity & prestressed (δ=1m)

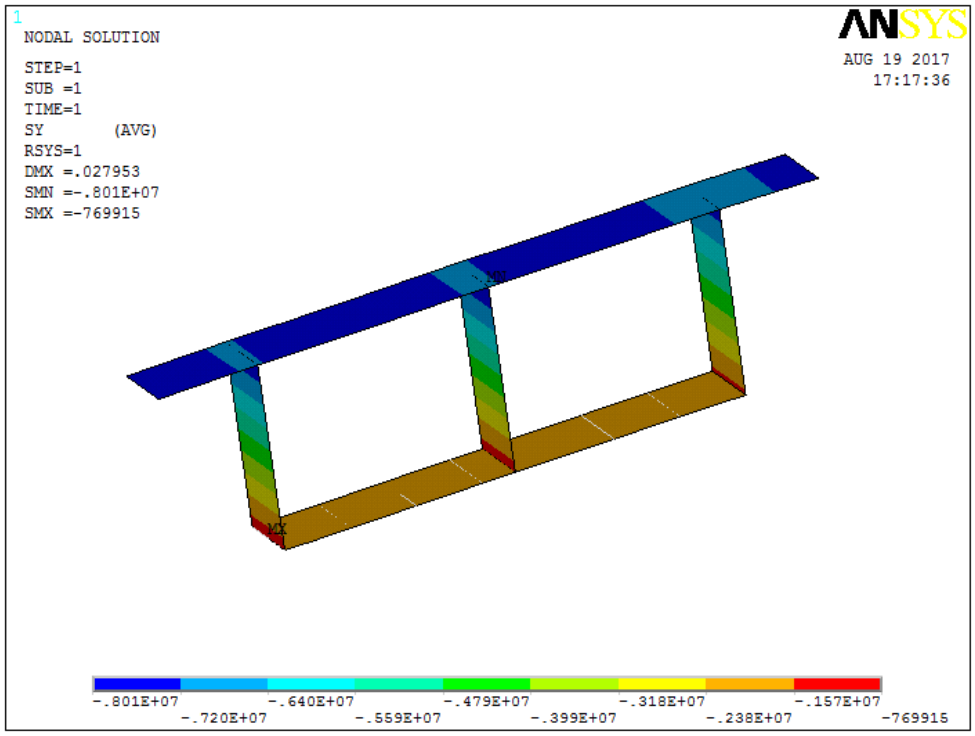

Figure (3.36) Longitudinal stresses at mid-span under gravity & prestressed (δ=1m)

2- Case 2 (δ=5m)

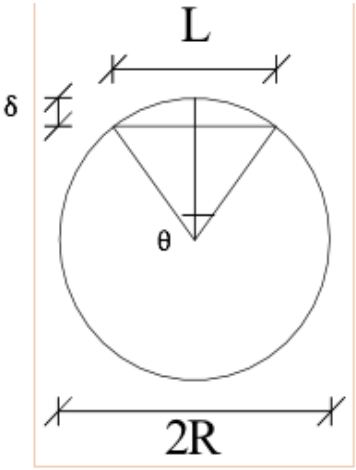

Span L =54 m

Delta $\delta_{step} = 5$ m

Radius of curvature $$R = \left[\frac{\delta_{step}^{2} + (0.5 \times L)^2}{2 \times \delta_{step}}\right]$$ R=75.4 m

Subtended angle Theta $$\theta = 2 \times \tan^{-1}\left[\frac{0.5 \times L}{\sqrt{R^2 - (0.5 \times L)^2}}\right]$$ $\theta = 41.966^{\circ}$

1-Curved box model under gravity

The curved box girder in this case is subjected only to self-weight. The model was created using the APDL which can be found in Appendices 2 & 3. The finite element model for this case is shown in figure (3.37). The deformed shape is shown in figure (3.38) and the longitudinal stress

contour and mid span stresses are shown in figures (3.39) & (3.40). Longitudinal stresses at the mid-span are presented in table (3.2).

1-Curved box model under gravity (δ =5m)

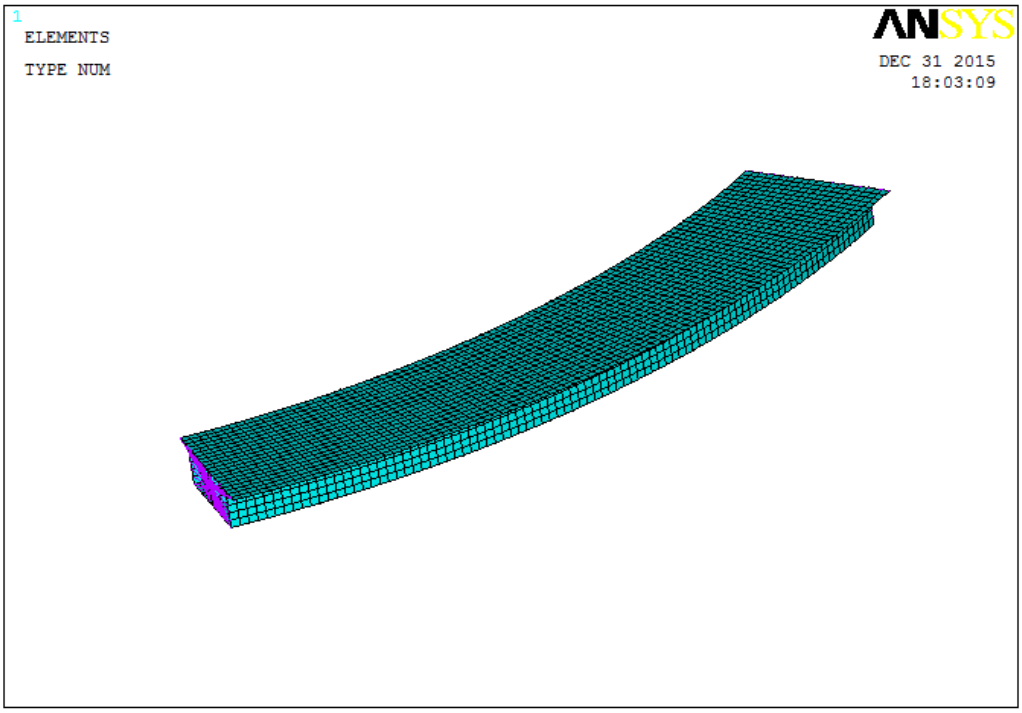

Figure (3.37) The finite element model under gravity (δ=5m)

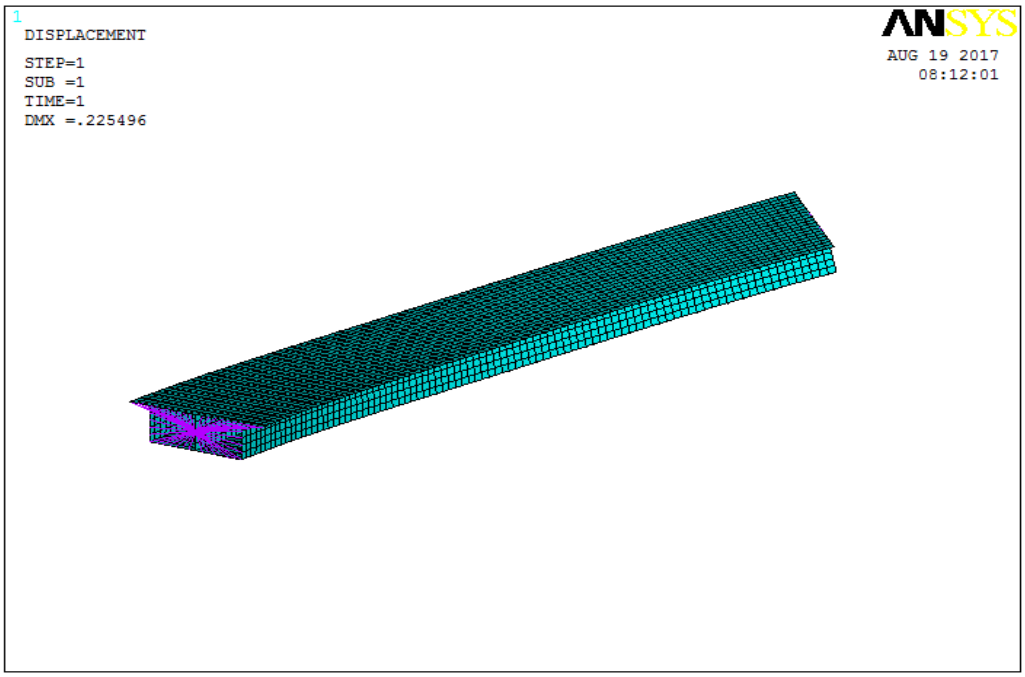

Figure (3.38) Deformed shape under gravity (δ=5m)

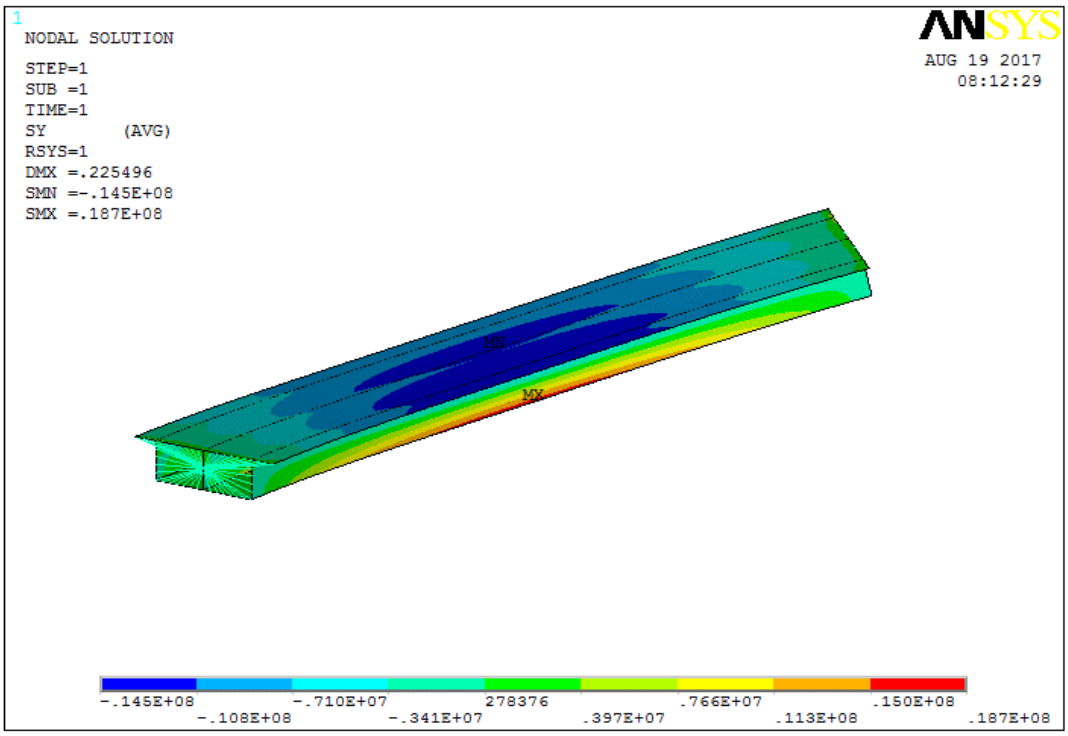

Figure (3.39) Longitudinal stresses under gravity (δ=5m)

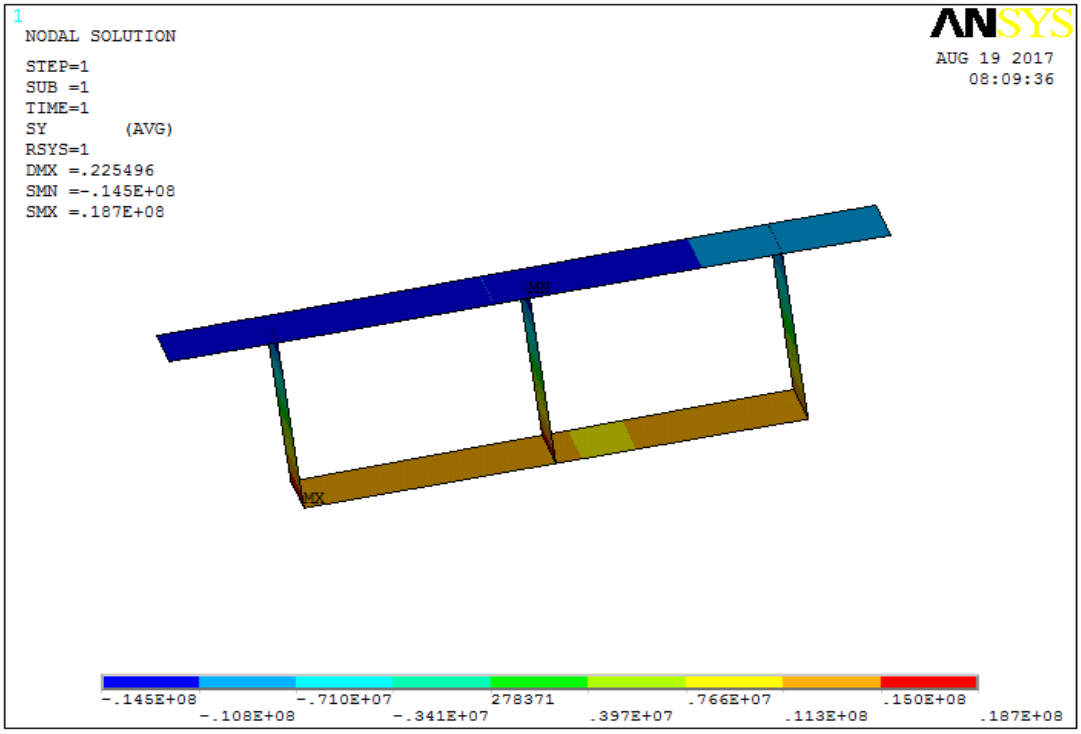

Figure (3.40) Longitudinal stresses at mid-span under gravity (δ=5m)

2-Prestressed curved box model

The curved box girder in this case is subject the effects of prestress alone, the full model is provided Appendices 2 & 3 and prestress is taken from section 3.3.2. The finite element for this case is shown in figure (3.41). The deformed shape is shown in figure (3.42) and the longitudinal stress contour and mid span stresses are shown in figures (3.43) & (3.44). Longitudinal stresses for the midspan values are presented in table (3.2).

2-Prestressed curved box model (δ=5m)

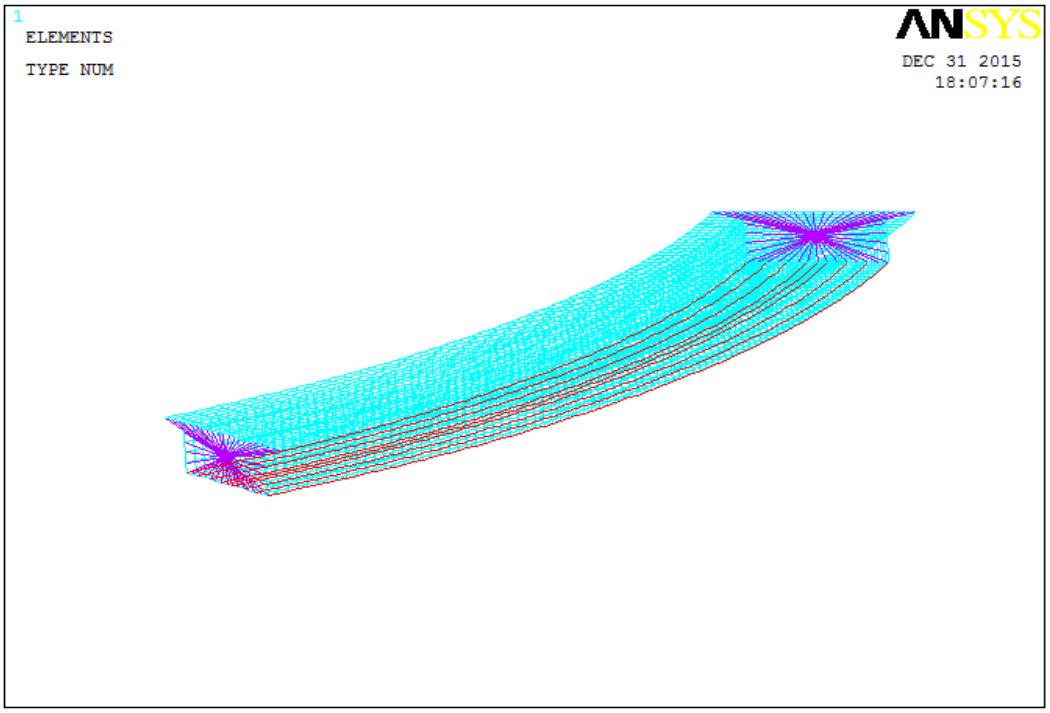

Figure (3.41) The finite element model under prestressed (δ=5m)

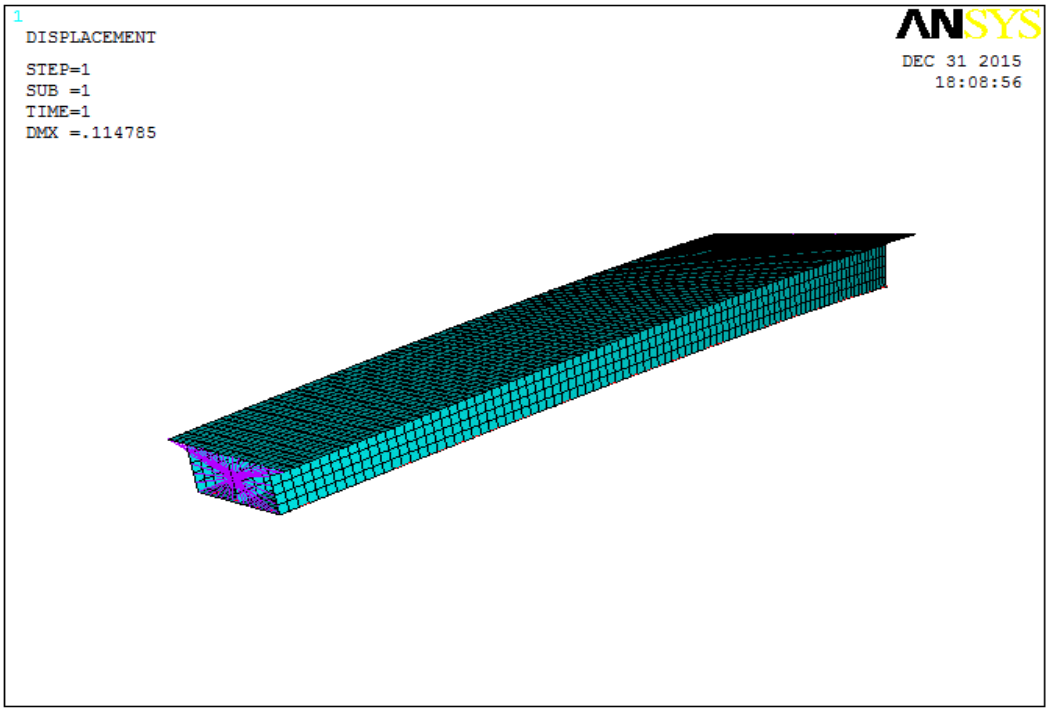

Figure (3.42) Deformed shape under prestressed (δ=5m)

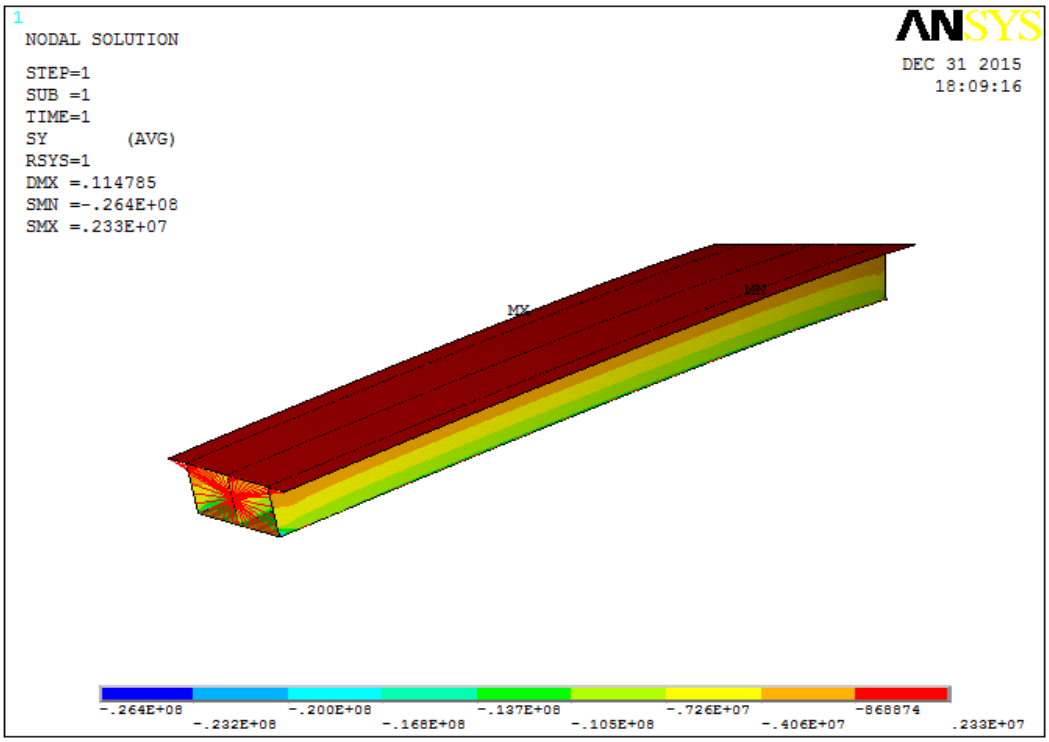

Figure (3.43) Longitudinal stresses under prestressed (δ=5m)

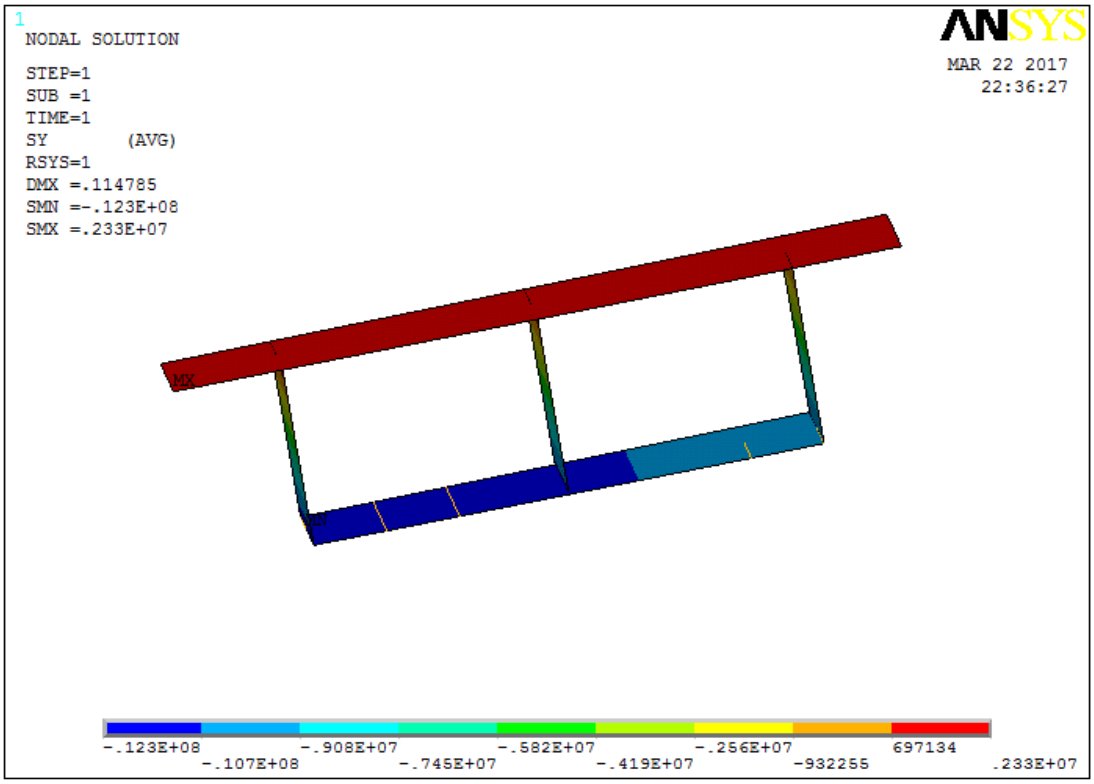

Figure (3.44) Longitudinal stresses at mid-span under prestressed (δ=5m)

3-Gravity and prestressed curved box model

The curved box girder in this case is subjected to both self-weight and prestressing, the model is provided Appendices 2 & 3 and the prestress has been calculated in section 3.3.2. The finite element model for this case is shown in figure (3.45). The deformed shape is shown in figure (3.46) and the longitudinal stress and mid span stresses are shown in figures (3.47) & (3.48). Longitudinal stresses for the mid-span values are presented in table (3.2).

3-Gravity and prestressed curved box model (δ= 5m)

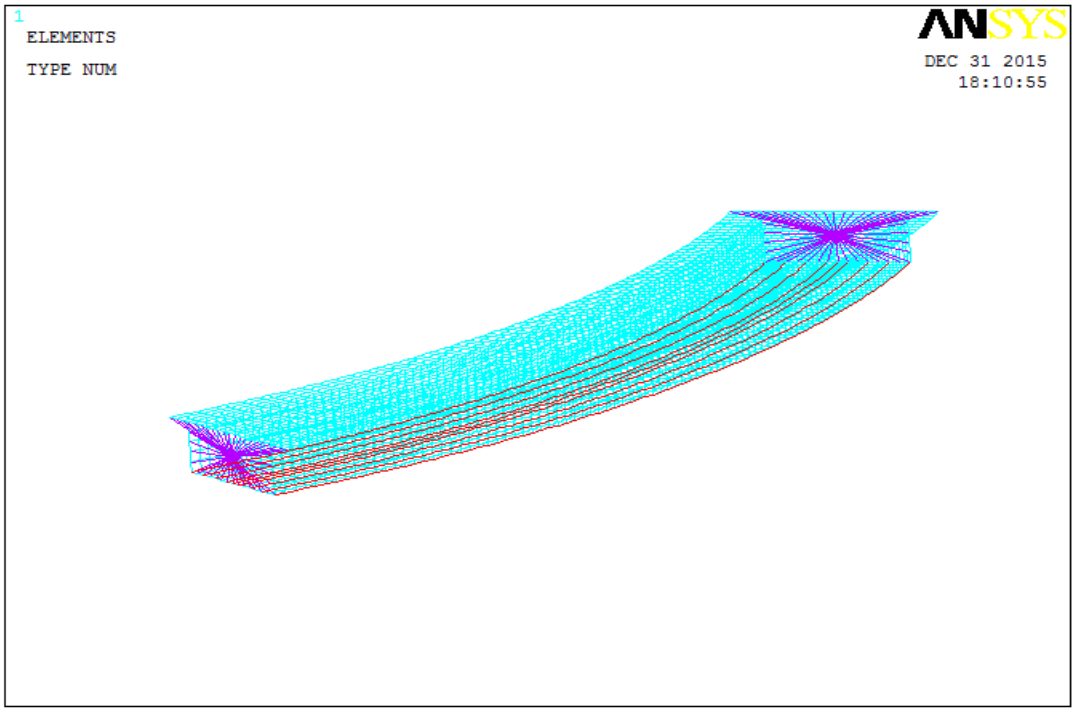

Figure (3.45) The finite element model under gravity & prestressed (δ=5m)

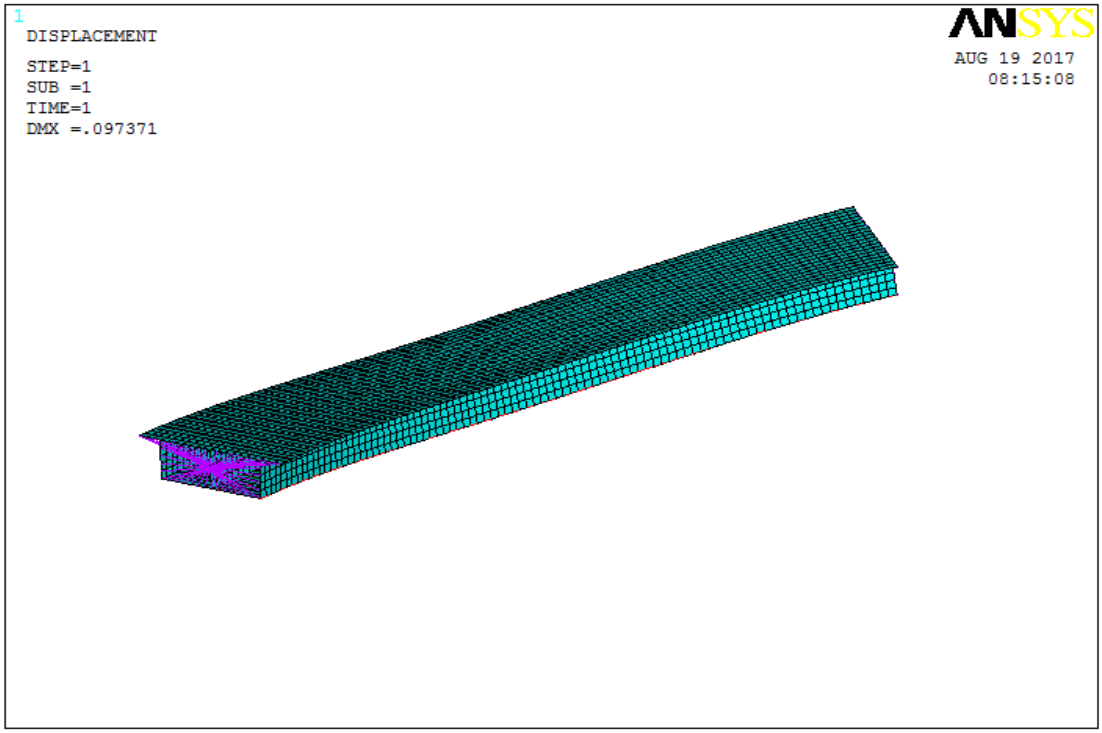

Figure (3.46) Deformed shape under gravity & prestressed (δ=5m)

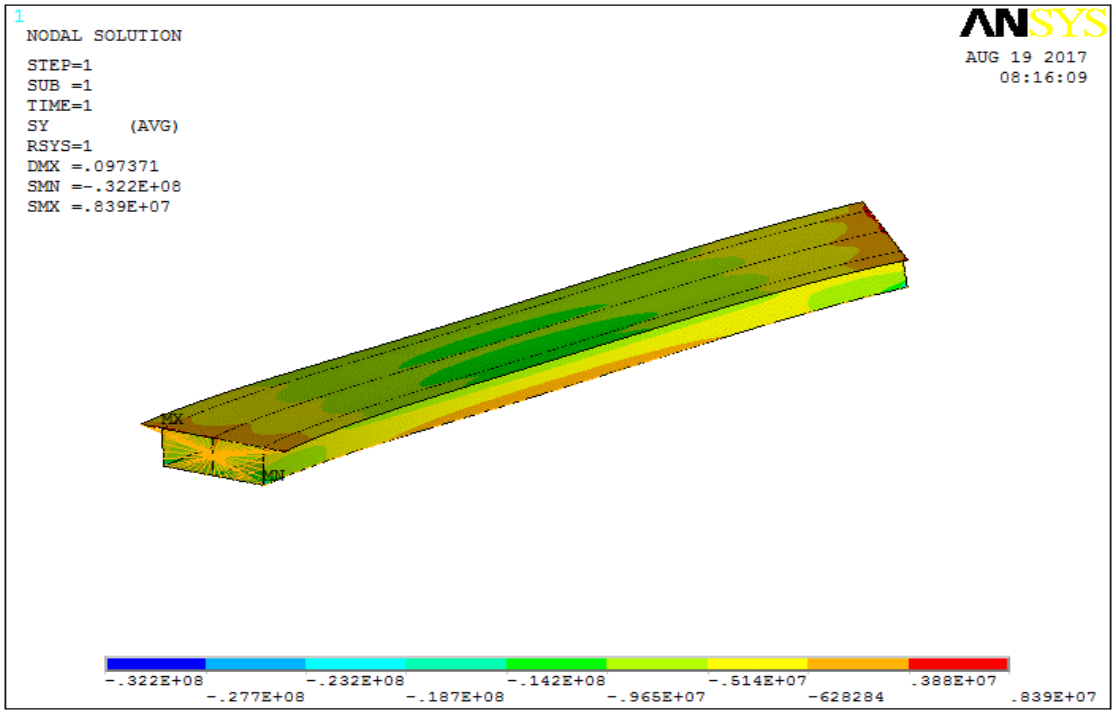

Figure (3.47) Longitudinal stresses under gravity & prestressed (δ=5m)

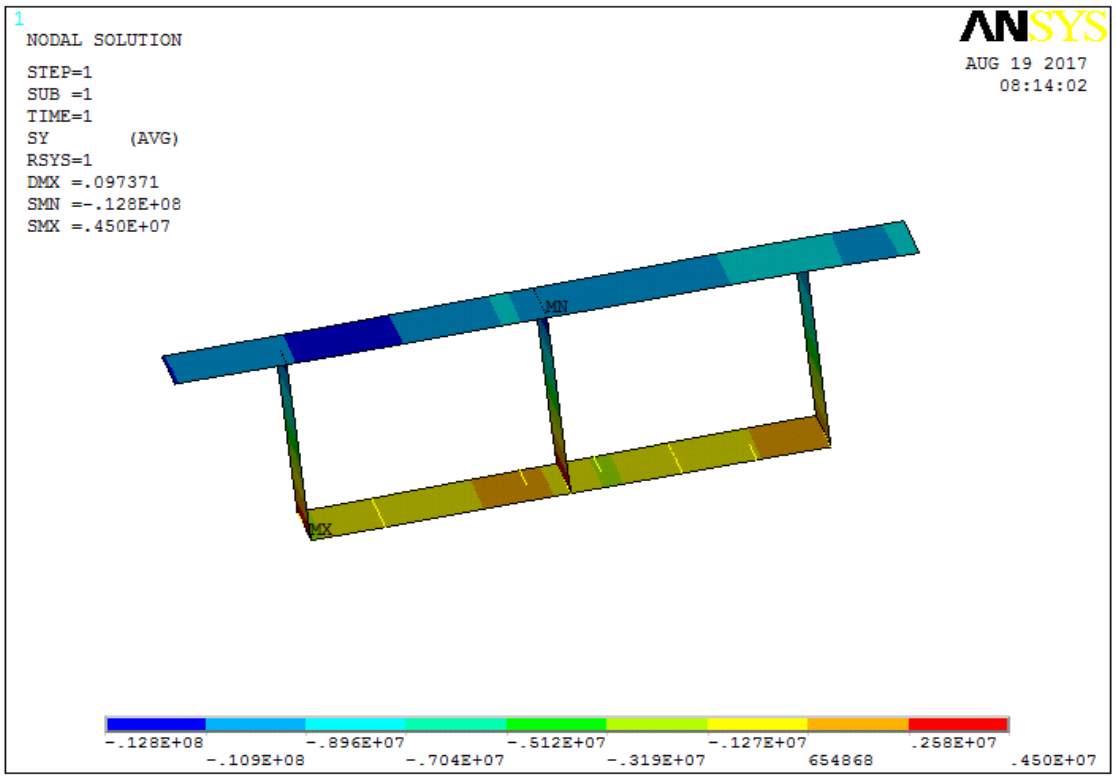

Figure (3.48) Longitudinal stresses at mid-span under gravity & prestressed (δ=5m)

3- Case 3 (δ=11)

Span L =54 m

Delta $\delta_{step} = 11\ m$

Radius of curvature $$R = \left[\frac{\delta_{step}^{\ 2} + (0.5 \times L)^2}{2 \times \delta_{step}}\right]$$ R= 38.63 m

Subtended angle Theta $$\theta = 2 \times \tan^{-1}\left[\frac{0.5 \times L}{\sqrt{R^2 - (0.5 \times L)^2}}\right]$$ θ = 88.66°

1-Curved box model under gravity

The curved box girder in this case is only subject self-weight, the model is created by the APDL and it can be found in Appendices 2 & 3. The finite element model for this case is shown in figure (3.49). The deformed shape is shown in figure (3.50) and the longitudinal stress contour and mid span stresses are shown in figures (3.51) & (3.52). Longitudinal stresses for the midspan section are presented in table (3.2).

1-Curved box model under gravity (δ =11m)

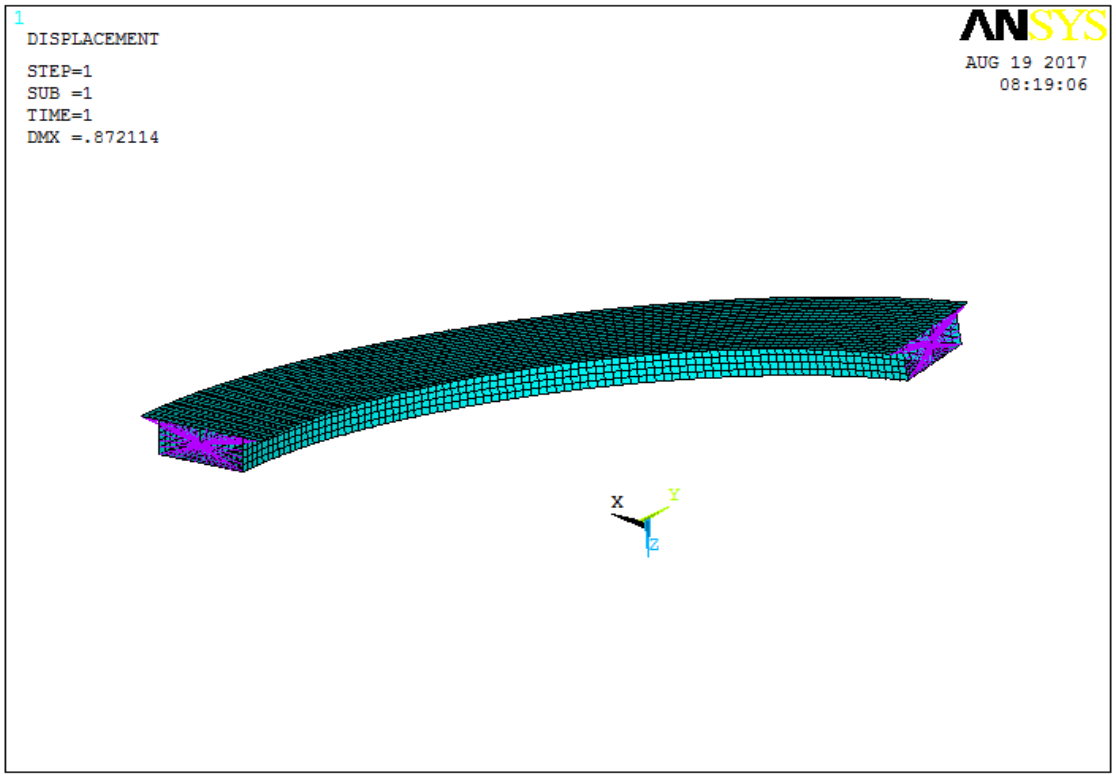

Figure (3.49) The finite element model under gravity (δ =11m)

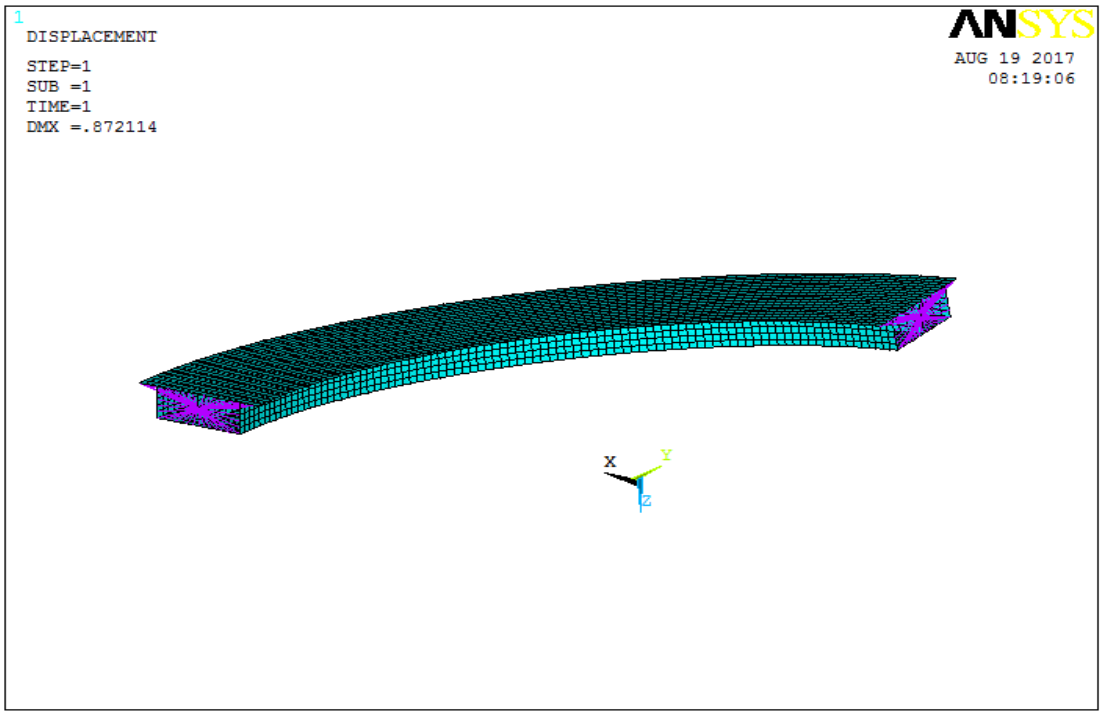

Figure (3.50) Deformed shape under gravity (δ =11m)

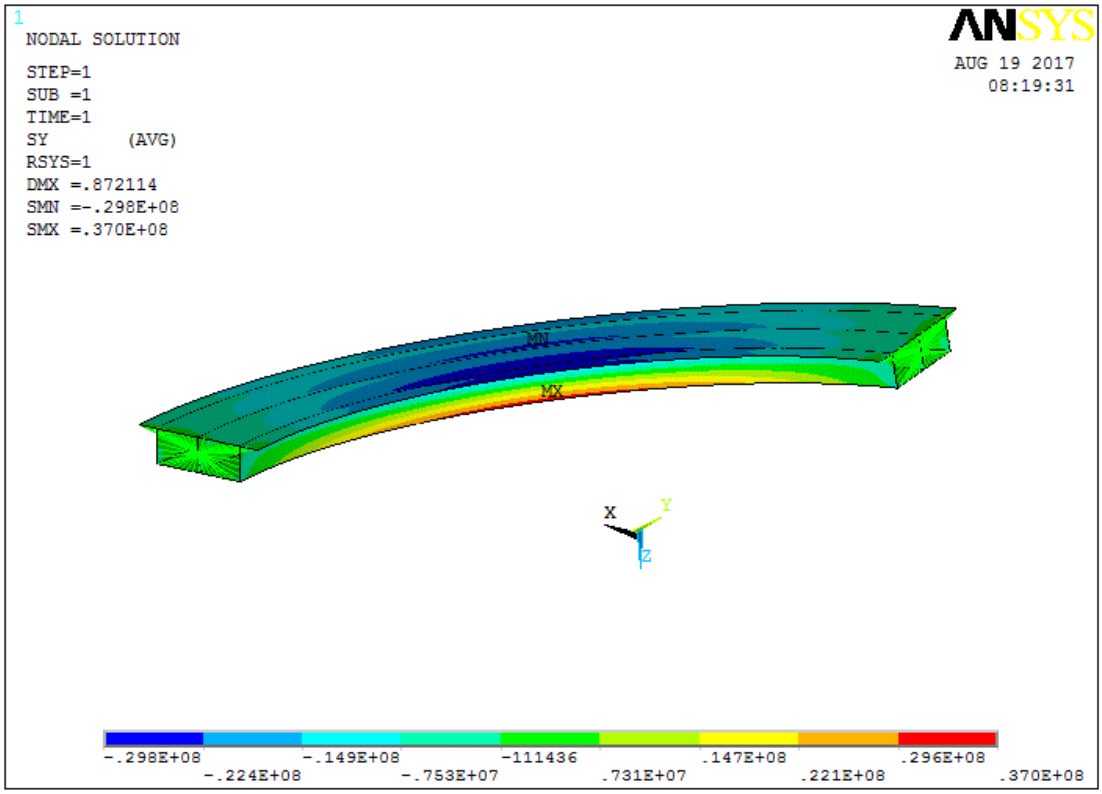

Figure (3.51) Longitudinal stresses under gravity (δ =11m)

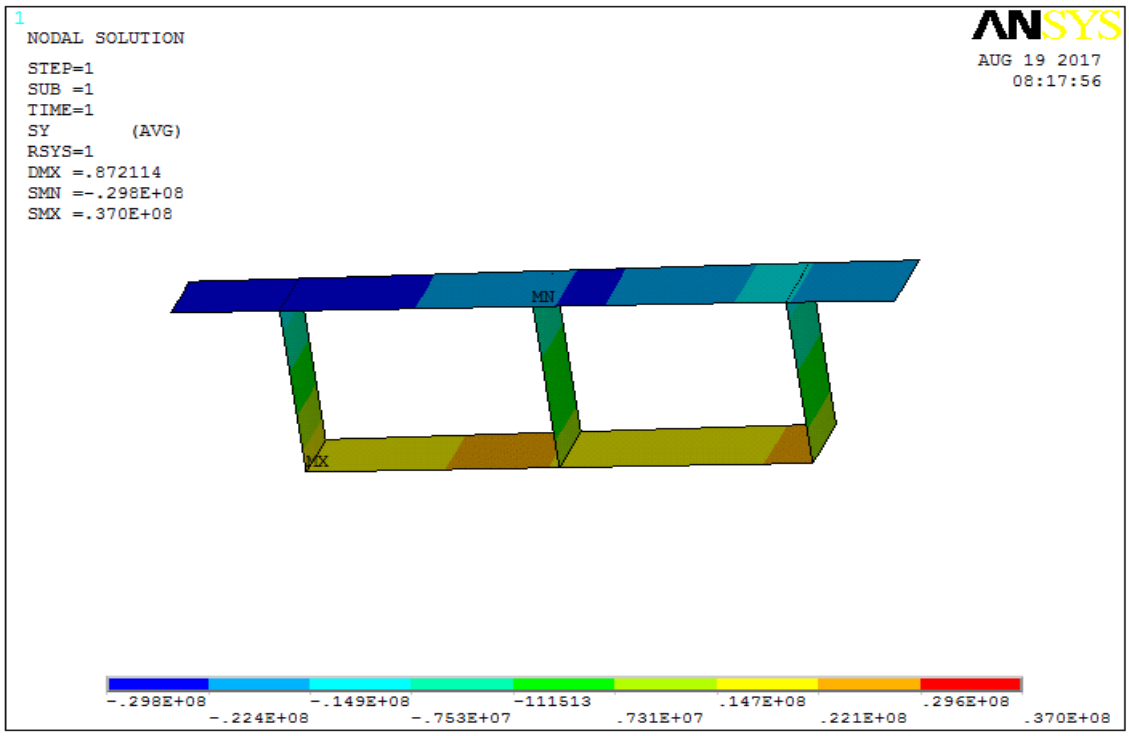

Figure (3.52) Longitudinal stresses at mid-span under gravity (δ =11m)

2-Prestressed curved box model

The curved box girder in this case is subject to prestress alone, the full model is provided in Appendix 2 & 3 and the prestress is taken from section 3.3.2. The finite element model for this case is shown in figure (3.53). The deformed shape is shown in figure (3.45) and the longitudinal stress contour and mid span stresses are shown in figures (3.55) & (3.56) respectively. Longitudinal stresses for the midspan section are presented in table (3.2).

2-Prestressed curved box model (δ =11m)

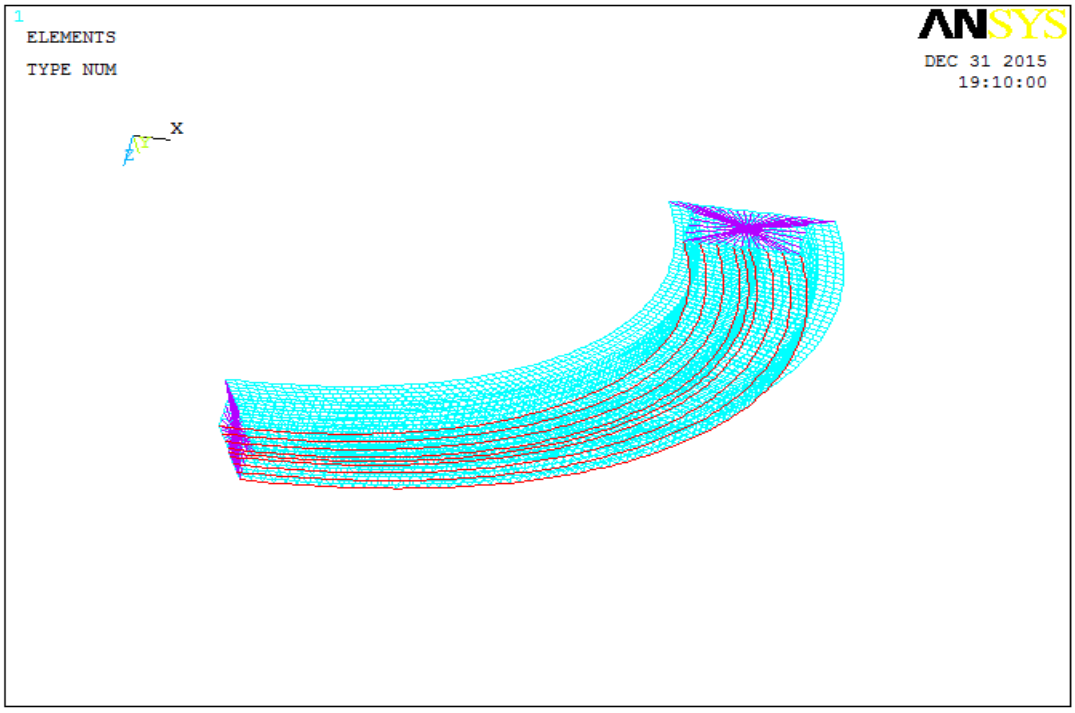

Figure (3.53) The finite element model under prestressed (δ =11m)

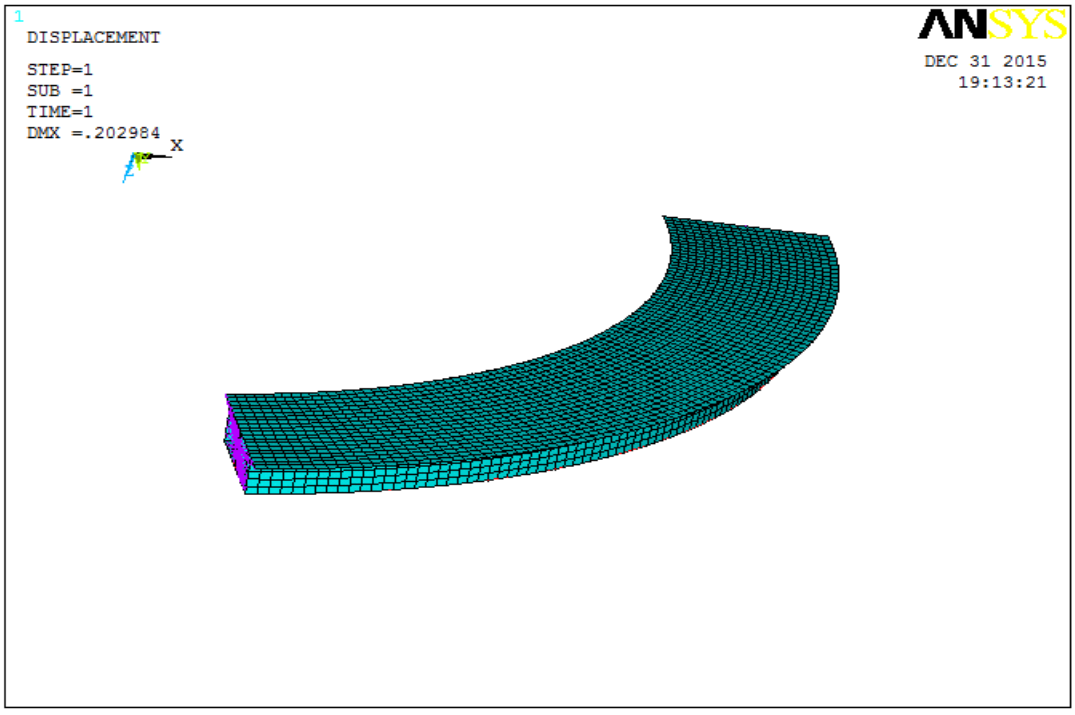

Figure (3.54) Deformed shape under prestressed (δ =11m)

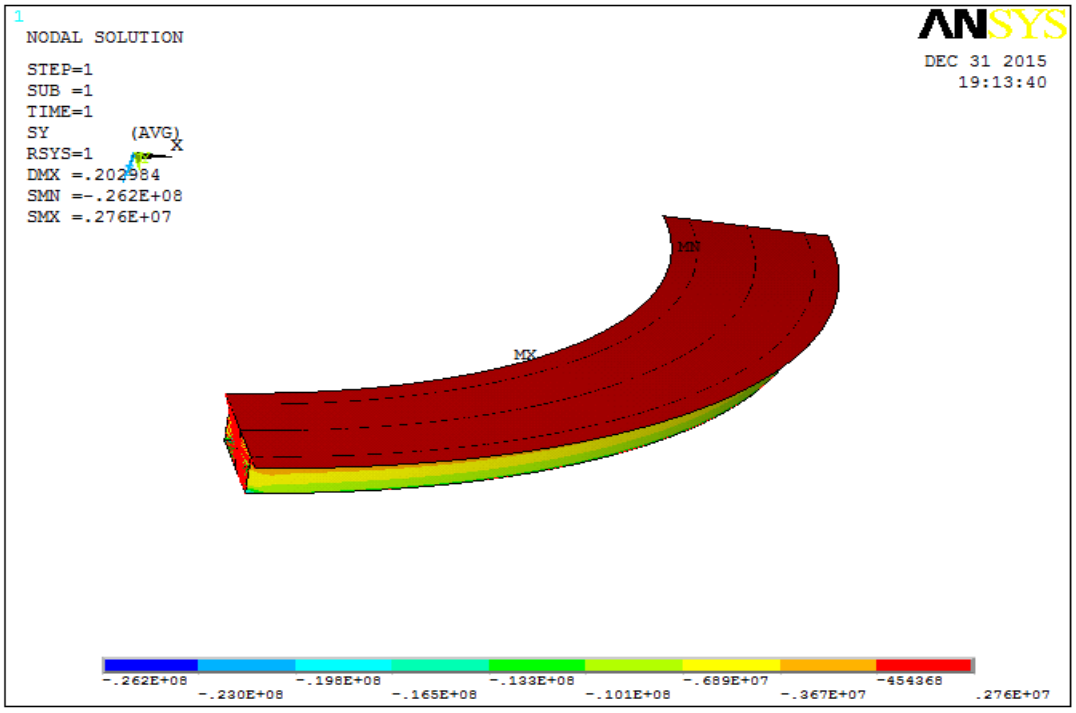

Figure (3.55) Longitudinal stresses under prestressed (δ =11m)

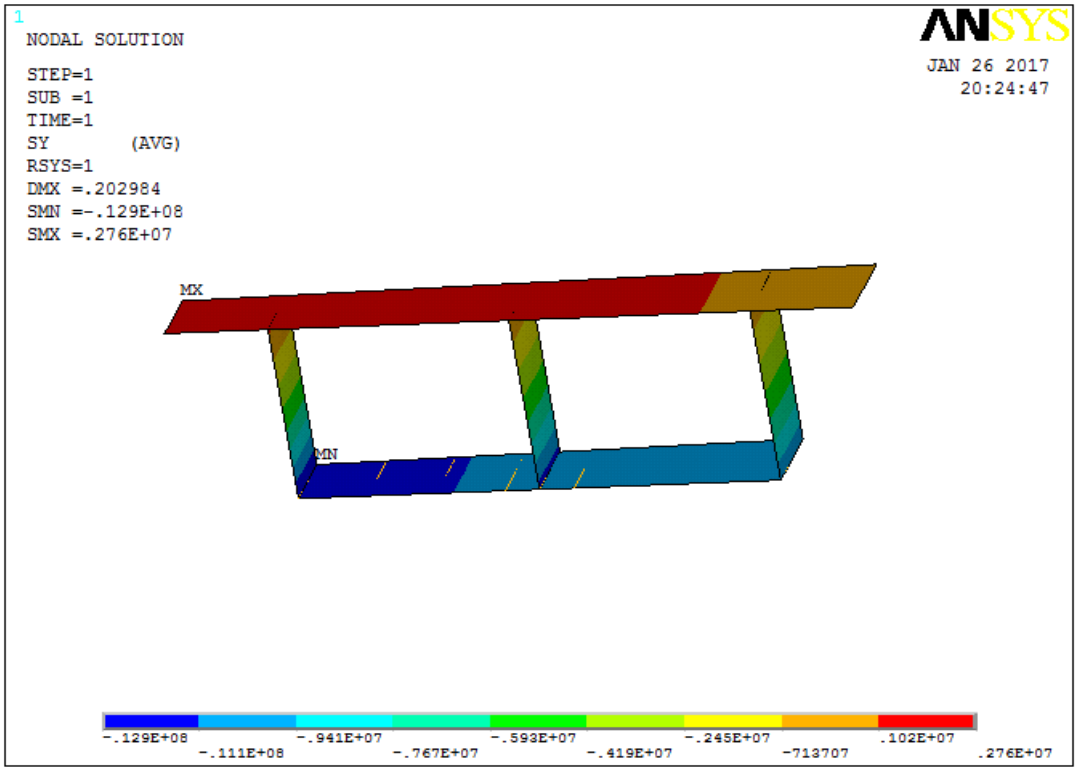

Figure (3.56) Longitudinal stresses at mid-span under prestressed (δ =11m)

3-Gravity and prestressed curved box model

The curved box girder in this case is subjected to both self-weight and prestressing, the model is provided in Appendices 2 & 3 and the prestress has been calculated in section 3.3.2. The finite element model for this case is shown in figure (3.57). The deformed shape is shown in figure (3.58) and the longitudinal stresses and mid span stresses are shown in figures (3.59) & (3.60) respectively. Longitudinal stresses for the mid-span section are presented in table (3.2).

3-Gravity and prestressed curved box model (δ =11m)

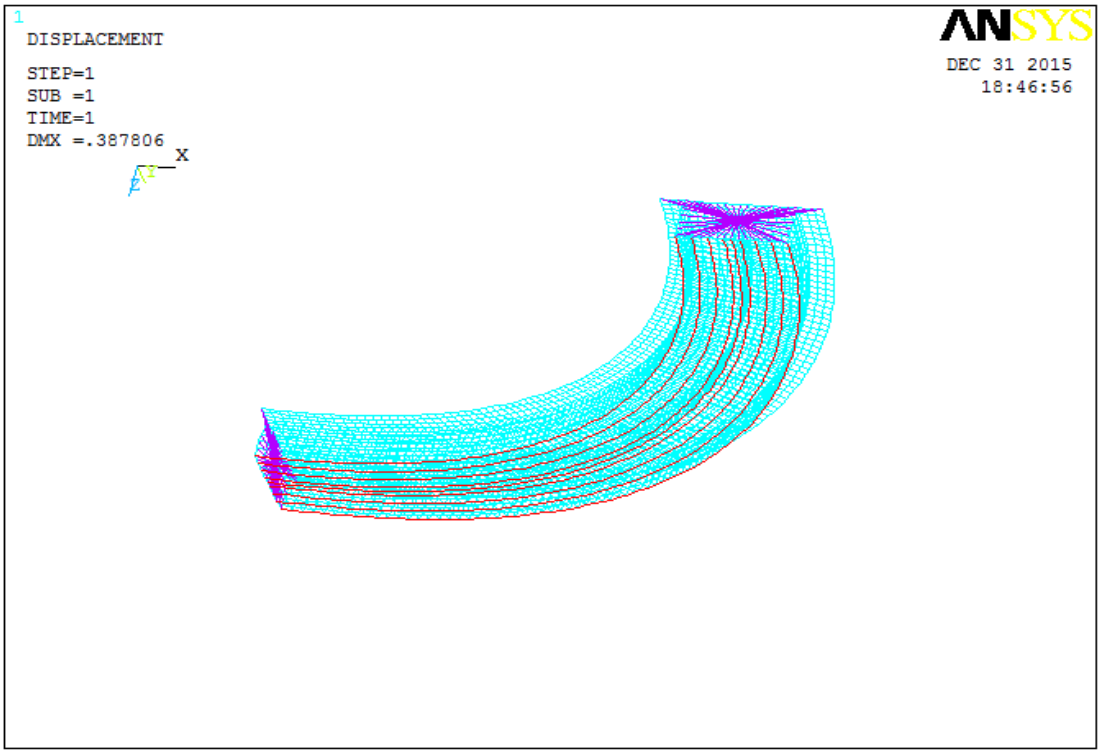

Figure (3.57) The finite element model under gravity and prestressed (δ =11m)

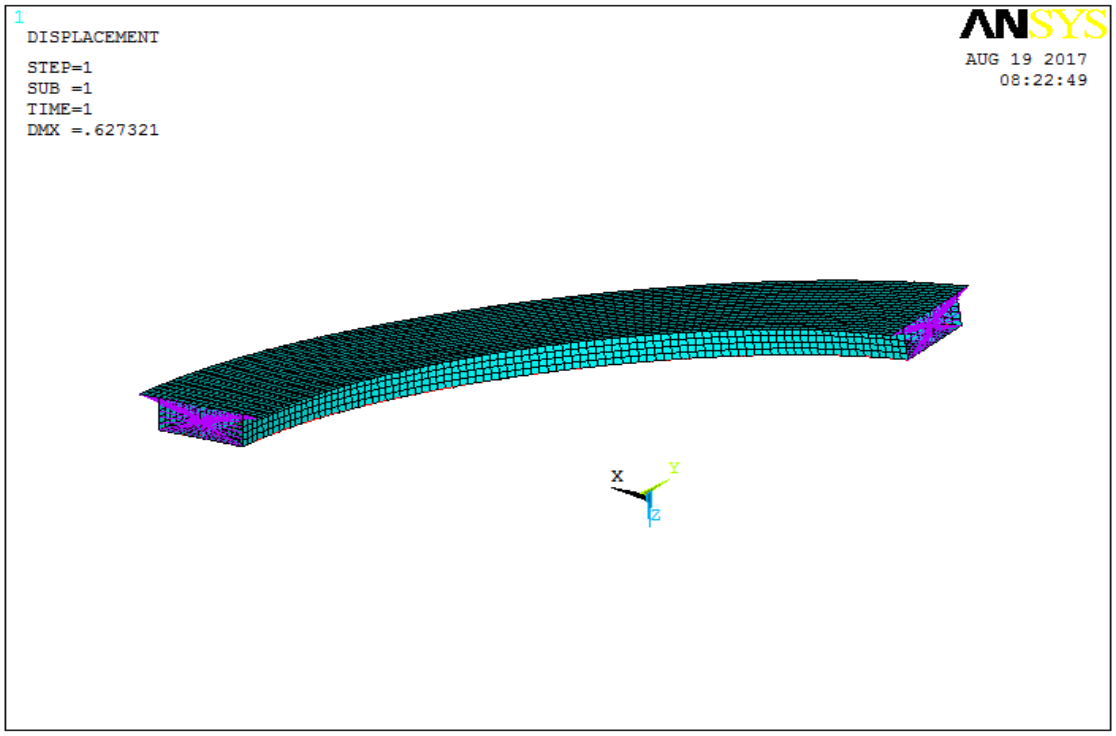

Figure (3.58) Deformed shape under gravity and prestressed (δ =11m)

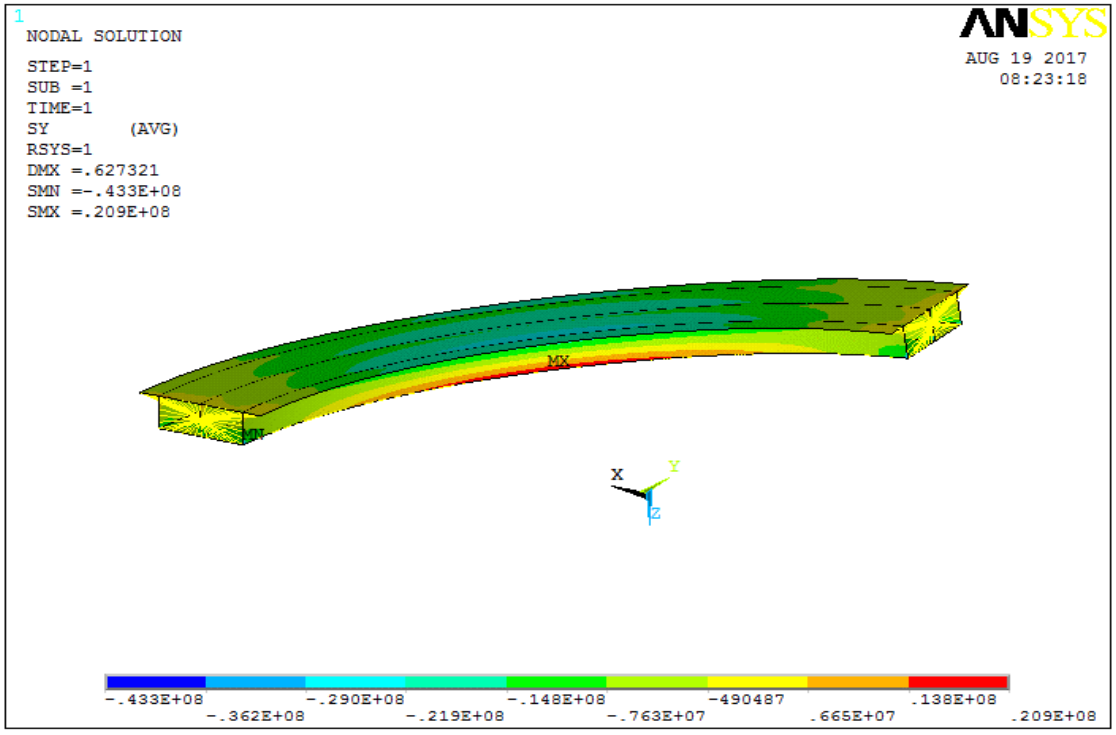

Figure (3.59) Longitudinal stresses under gravity and prestressed (δ =11m)

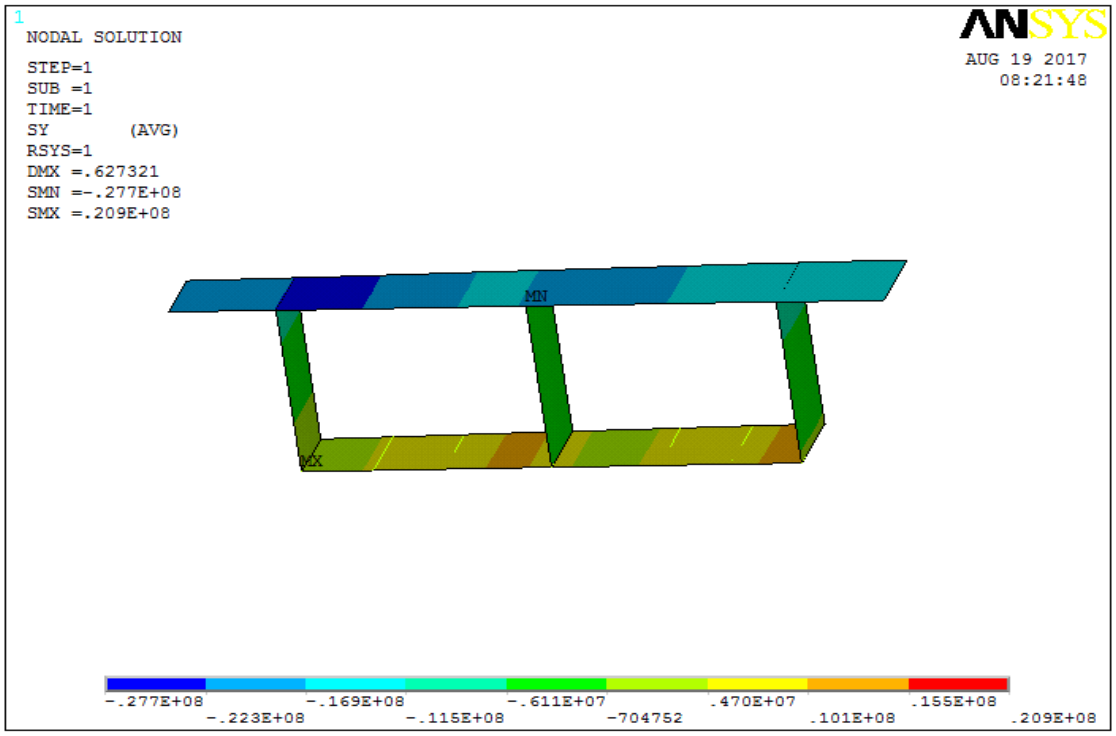

Figure (3.60) Longitudinal stresses at mid-span under gravity and prestressed (δ =11m)

3.7 Comparison of straight box girder and curved box girder behaviour

The objective of the study was to validate the FE model and study the behaviour of curved box girder bridges, the details of the bridge models of the curved and straight box have been presented previously. To compare the box bridges models, the same modelling techniques were employed for both the straight and curved bridge models except for changing the radius of curvature for each case of the curved box girder. Direct stresses at cross sections the cases of straight and curved were obtained. The midspan stresses as recorded in table (3.1) represent the highest value of stresses where the comparison is made based on the stresses to understand their behaviour under self-weight, prestressed effects and both. It can be noted that in the straight box girder the stress distribution is symmetric from one end to the other (in left and right top slab and soffit) whereas in the curved box girder the stress profile is not symmetric due to the effects of torsion and warping. Table (3.2) represents reactions, torsion moments and prestress losses.

Notes: All stresses in the tables are N/mm^2 and curvature angle in degrees.
Interior edge: near axes as shown in figure (3.6) (A).

Exterior edge: far from axes as shown in figure (3.6) (A).

Table (3.1) Stress distribution (A &B) for different load conditions under uniform prestressing and different angles of curvature (comparison between published results (Khaloo & Kafimosavi (2007)) and analysis results).

a) Published results, Khaloo & Kafimosavi (2007)

Location and curvature angle	Load type											
	Published results											
	Gravity				Prestressing				Gravity & prestressing			
	Slab		Soffit		Slab		Soffit		Slab		Soffit	
	Interior edge	Exterior edge	Interior edge	Exterior edge	Interior edge	Exterior edge	Interior edge	Exterior edge	Interior edge	Exterior edge	Interior edge	Exterior edge
0	-8.36	-8.36	9.85	9.85	1.17	1.17	-11.76	-11.76	-7.2	-7.2	-1.91	-1.91
30°	-10.24	-8.46	11.77	10.14	1.54	0.81	-12.2	-11.32	-7.65	-8.69	-0.44	-1.18
60°	-12.5	-8.56	14.78	10.99	1.94	0.48	-12.7	-10.96	-8.01	-10.5	1.24	-.059
90°	-16.5	-9.28	18.02	11.4	2.36	0.17	-13.25	-10.54	-9.1	-14.14	4.77	0.86

b) Analysis results

Location and curvature angle	Load type											
	Analysis results											
	Gravity				Prestressing				Gravity & prestressing			
	Slab		Soffit		Slab		Soffit		Slab		Soffit	
	Interior edge	Exterior edge	Interior edge	Exterior edge	Interior edge	Exterior edge	Interior edge	Exterior edge	Interior edge	Exterior edge	Interior edge	Exterior edge
0	-8.30	-8.30	10.75	10.75	1.22	1.22	-11.40	-11.40	-6.95	-6.95	-1.95	-1.95
30°	-10.34	-8.62	11.55	9.95	2.12	0.95	-12.80	-11.89	-8.45	-8.12	-0.60	-1.02
60°	-12.90	-9.01	15.33	11.21	2.21	1.33	-12.46	-10.75	-9.89	-10.12	1.03	0.88
90	-17.46	-12.68	18.80	13.60	1.98	0.53	-12.25	-10.04	-12.2	-14.72	5.04	1.15

The stresses distribution from the FE analysis for the straight box girder bridges show good agreement with the stresses from the published results. Table (3.2) shows the results for each curvature (from delta =0 to delta =11 m).

Table (3.2) Reactions, torsion moments, prestress, mass and stresses form the FE analysis (g: gravity, p: prestressed, g+p: gravity and prestress).

Delta (m)	Reaction (kN)	M_y (kN.m)	Prestress (kN)	Mass (Tonnes)	Mid-span stresses (N/mm^2)			
					Slab		Soffit	
					Interior	Exterior	Interior	Exterior
delta=0								
g	-16200	0		1180	-8.3	-8.3	10.8	10.8
p	0	0	4380	1180	1.22	1.22	-11.4	-11.4
g+p	-16200	0	4740	1180	-6.95	-6.95	-1.95	-1.95
delta =1								
g	-16400	1170	0	1200	-8.82	-7.2	9.95	8.3
p	0	0.00651	4380	1200	1.31	1.94	-11.5	-11.3
g+p	-16400	1170	4760	1200	-7.3	-6.2	-1.52	-1.95
delta= 2								
g	-16800	24400	0	1220	-9.61	-8.13	10.2	8.85
p	0	0.0137	4390	1220	1.39	1.05	-11.6	-11.2
g+p	-16800	24400	4780	1220	-8.86	-7.82	-1.2	-1.8
delta= 3								
g	-17100	38400	0	1250	-10.1	-8.45	10.5	8.55
p	0	0.0218	4400	1250	1.47	0.98	-11.8	-11.1
g+p	-17100	38400	4810	1250	-8.2	-8.02	-0.91	-1.43
delta =4								
g	-17500	54000	0	1270	-10.3	-8.62	11.6	9.95
P	0	0.0311	4400	1270	2.12	0.95	-12.8	-11.9
g+p	-17500	54000	4840	1270	-8.45	-8.12	-0.6	-1.02
delta =5								
G	-18000	71500	0	1300	-9.48	-8.78	13.3	10
P	0	0.0422	4410	1300	1.62	1.83	-12	-10.9
g+p	-18000	71500	4870	1300	-8.71	-8.25	0.15	-0.91
delta =6								
G	-18300	91500	0	1330	-11.9	-8.89	14.6	10.9
P	0	0.0554	4410	1330	2.36	0.77	-12.2	-9.59
g+p	-18300	91500	4920	1330	-9.35	-9.03	0.78	0.21
delta =7								
G	-18700	114000	0	1370	-12.9	-9.01	15.3	11.2
P	0	0.0714	4420	1370	2.21	1.33	-12.5	-10.8
g+p	-18700	114000	4970	1370	-9.89	-10.1	1.03	0.88
delta =8								
g	-19200	140000	0	1400	-13.8	-10.2	15.7	11.6

p	9.36E-09	0.091	4420	1400	2.37	0.84	-12.3	-10.2
g+p	-19200	140000	4920	1400	-10.1	-11.2	2.54	0.92
delta =9					0	0	0	0
g	-19700	172000	0	1430	-14.3	-11.8	16	12.1
p	0	0.115	4420	1430	2.45	0.92	-12.5	-9.56
g+p	-19700	172000	4900	1430	-11.3	-12.3	3.09	1.03
delta=10								
g	-14400	147000	0	1470	-15.2	-12	17.3	12.4
P	0	0.146	4430	1470	2.71	1.57	-12.6	10.8
g+p	-14400	147000	4980	1470	-12	-12.8	4.5	1.13
delta = 11								
g	-20700	250000	0	1510	-17.5	-12.7	18.8	13.6
P	0	0.185	4430	1510	1.98	0.53	-12.3	-10
g+p	-20700	250000	5000	1510	-12.2	-14.7	5.04	1.15

The following observations can be made from the tables as follows:

- Gravity: the stresses induced by the gravity load case showed differences between the published results and the analysis results. For the published results (Khaloo & Kafimosavi, 2007) the load was an applied UDL on the top deck which included self-weight and the same UDL has applied with this study. Self-weight case has checked which represented as density and gravity and it showed balanced compressive stresses class1 with zero tension represented.
- Prestress: prestress stresses showed similar results between the published results and the analysis results, losses are similar to prestensioning scenario i.e. (elastic shortening) Long term losses are not present. This shows that the representation of prestress using link elements with initial strain is valid.
- Gravity and Prestresses: the longitudinal stresses compared show a difference due to the application of a UDL which incorporates an applied load in addition to gravity case.

3.8 Design criteria as a class 1 prestressed concrete section

As is mentioned in the previous section, the design criteria adopted in this study is that the section will be designed as a class 1 prestressed concrete section, i.e. there will be no tensile stresses at serviceability limit state (SLS). This now provides the basis for further study to examine how much additional uniformly distributed load the section can carry before the SLS

class 1 criteria is violated at the midspan section. This will then provide a view on how the curvature may affect the load carrying capacity of the bridge deck. It should be noted that the tendons in this study will remain straight, and only the stresses at the midspan section will be taken as the governing criteria to be compared against the code requirement of no tension allowed. It should also be stated that prestressed concrete can be designed to take a minimum amount of tension as in class 2 or 3 partially prestressed sections, but their design is usually dependent on ultimate limit state criteria, so the FE modelling and comparisons will remain governed by class 1 design at SLS.

Different UDL's are applied to the deck of the box girder. This investigation is performed utilizing the previous three-dimensional FEM model of the box girder. The details for the box girder are the same as detailed in Appendices 2 & 3.

In this current study, four cases will be shown in the figures, these cases are

1- Straight box girder bridge with load intensity (9.3 kN/m^2) distributed on each node of the deck

The box girder in this case under both self-weight and prestressed, the model is in Appendix (2 and 3) prestressed has been calculated in section 3.3.2. Figure (3.61) shows the prestressed straight box model under gravity and the boundary conditions. Deformed shape contour shows in figure (3.62) and the stress and mid span stresses are shown in figures (3.63) & (3.64). Stresses and tension stresses for the mid-span values are mentioned in table (3.3).

2- Curved box girder bridge (δ =1 m) with a load intensity (7.5 kN/m^2) distributed on each node of the slab.

The curved box girder in this case under both self-weight and prestressed, the model is in Appendices (2 & 3) and prestressed has been calculated in section 3.3.2. Figure (3.65) shows the prestressed curved box model under gravity and the boundary conditions. Deformed shape contour shows in figure (3.66) and the stress is shown in figures (3.67) & (3.68). Stresses and tension stresses for the mid-span values are mentioned in table (3.3).

3- Curved box girder bridge (δ =3 m) with a load intensity (3.6 kN/m^2) distributed on each node of the slab.

The curved box girder in this case under both self-weight and prestressed, the model is in Appendices (2 & 3) and presstered has been calculated in section 3.3.2. Figure (3.69) shows the prestressed curved box model under gravity and the boundary conditions. Deformed shape

contour shows in figure (3.70) and the stress and mid span stresses are shown in figures (3.71) & (3.72).

Stresses and tension stresses for the mid-span values are mentioned in table (3.3).

4- Curved box girder bridge (δ =5 m) with a load intensity (0.5 kN/m^2) distributed on each node of the slab.

The curved box girder in this case under both its self-weight and prestressed, the model is in Appendices (2 & 3) and presstered has been calculated in section 3.3.2. Figure (3.73) shows the prestressed curved box model under gravity and the boundary conditions. Deformed shape contour shows in figure (3.74) and the stress and mid span stresses are shown in figures (3.75) and (3.76).

Stresses and Tension stresses for the midspan values are mentioned in table (3.3).

Table (3.3) & figure (3.77) show the results for all case studies.

As a result, the non-compliance is governed by the bridge going into tension (class 1 section). These stresses are essentially the superposition of normal bending plus warping torsion.

1- Straight box girder bridge

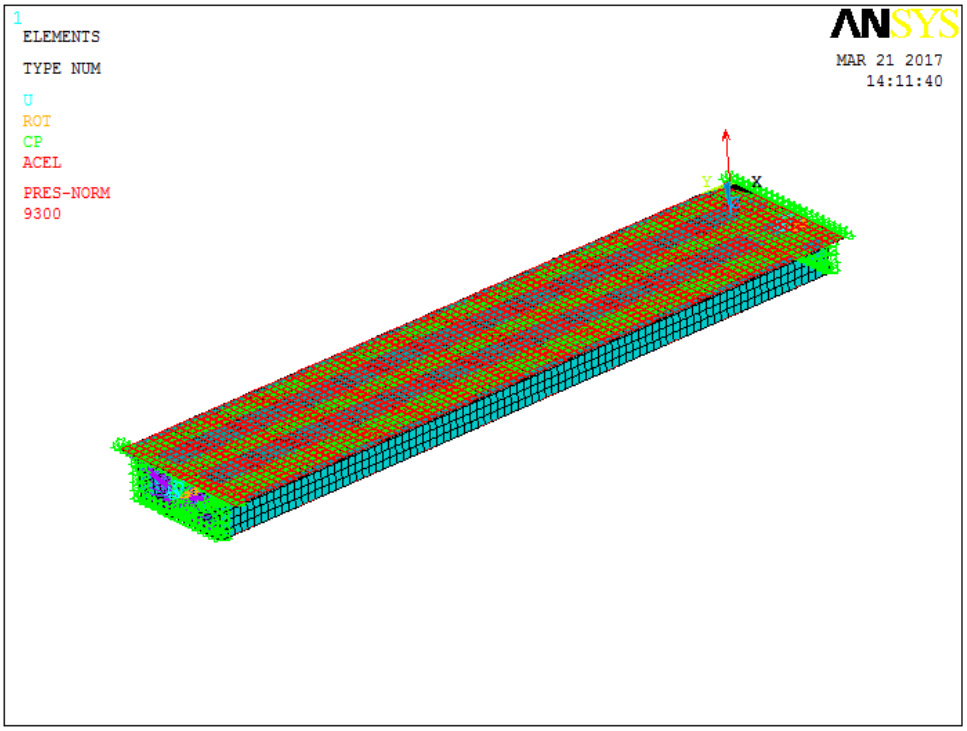

Figure (3.61) Boundary conditions for straight box girder bridge under loadings.

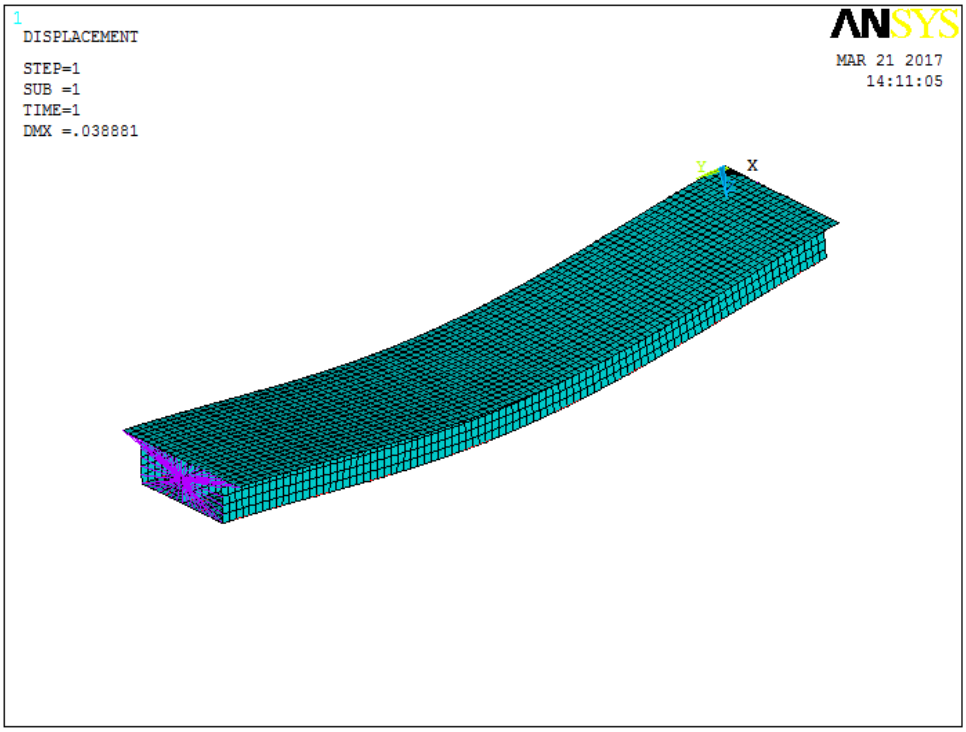

Figure (3.62) Deformed shape for straight box girder bridge under loadings.

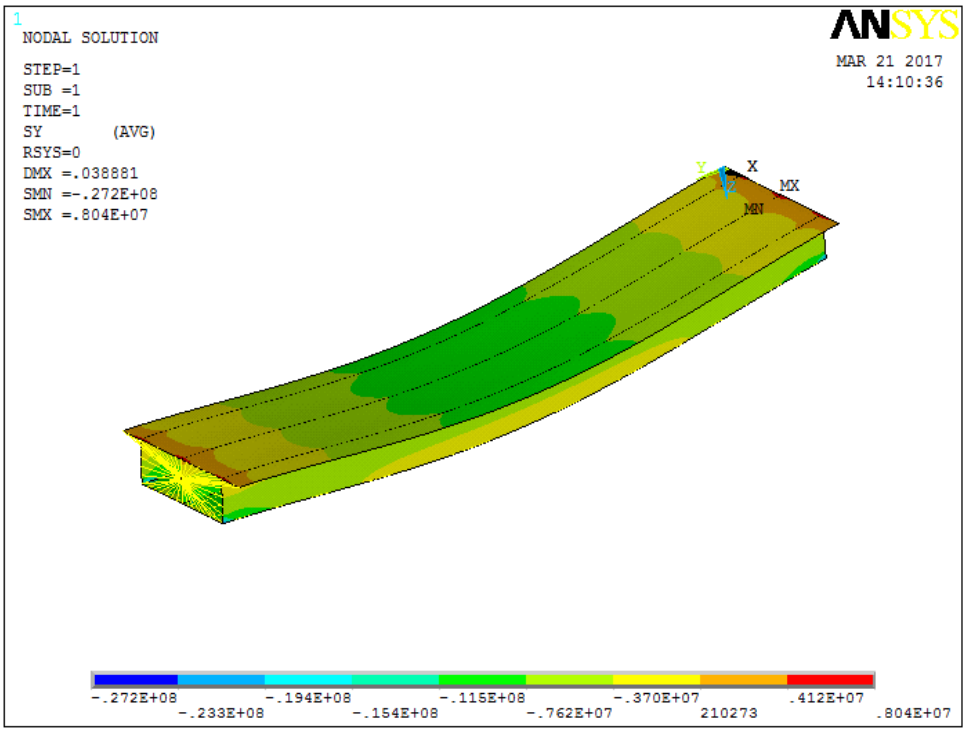

Figure (3.63) Longitudinal stresses (N/m^2) for straight box girder bridge under loadings

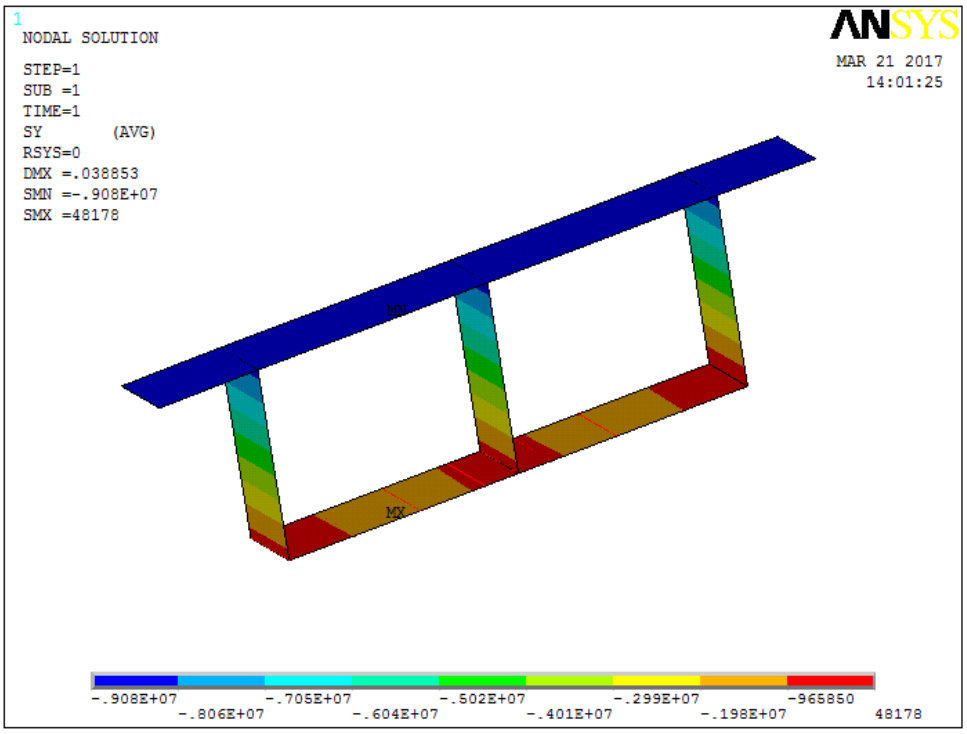

Figure (3.64) Longitudinal stresses (N/m^2) at mid-span for straight box girder bridge under loadings

2-Curved box girder bridge (δ =1 m)

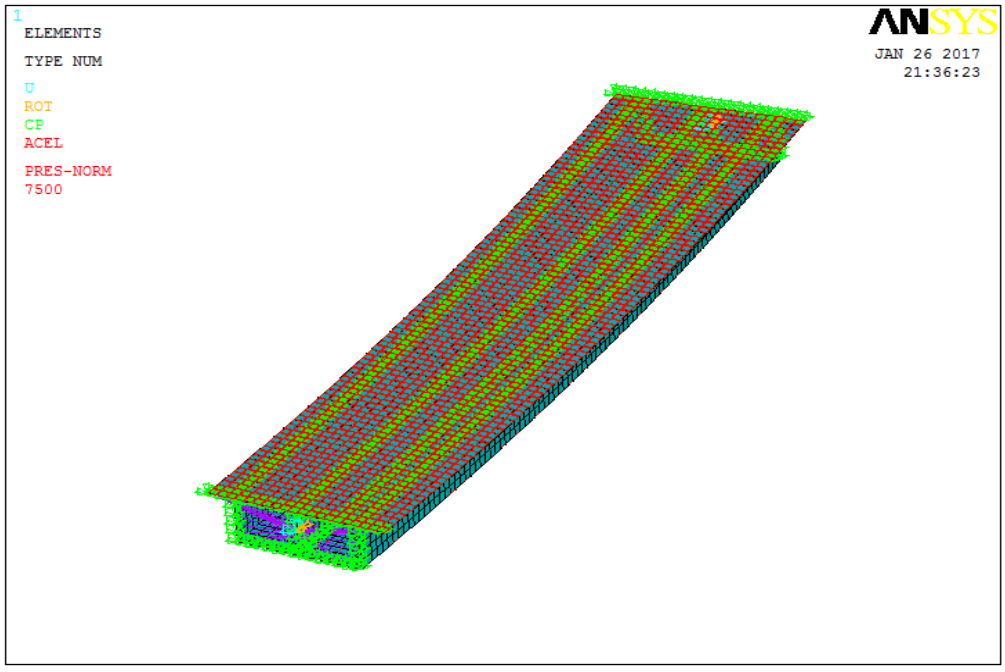

Figure (3.65) Boundary conditions for curved box girder bridge (δ =1 m) under loadings

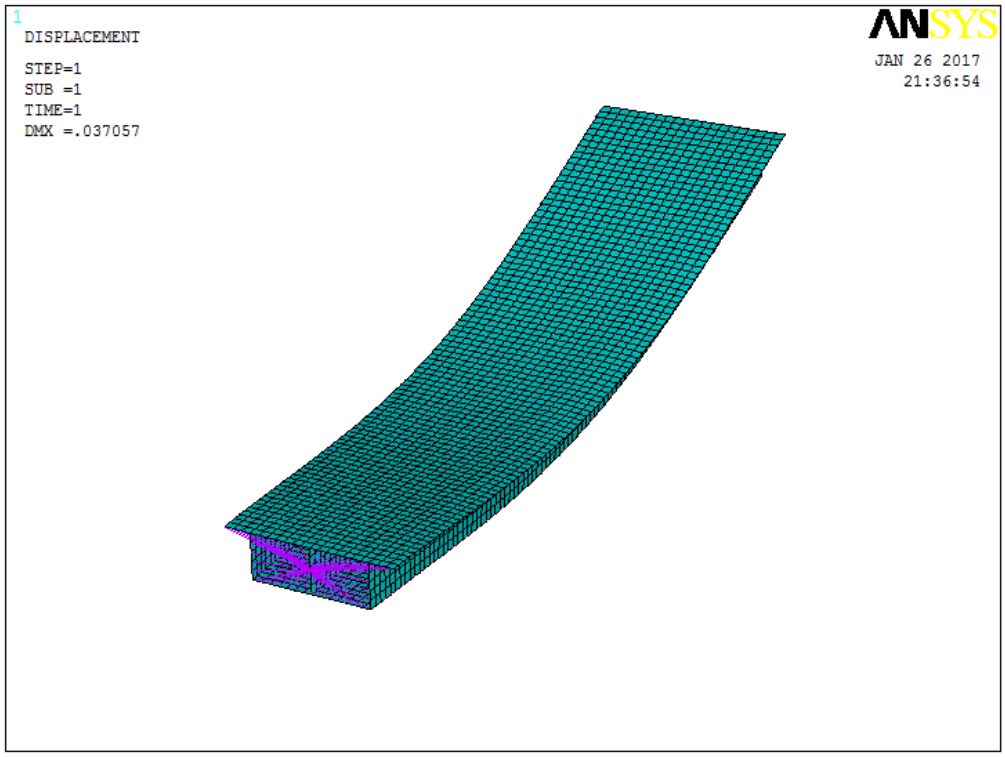

Figure (3.66) Deformed shape for curved box girder bridge (δ =1 m) under loadings

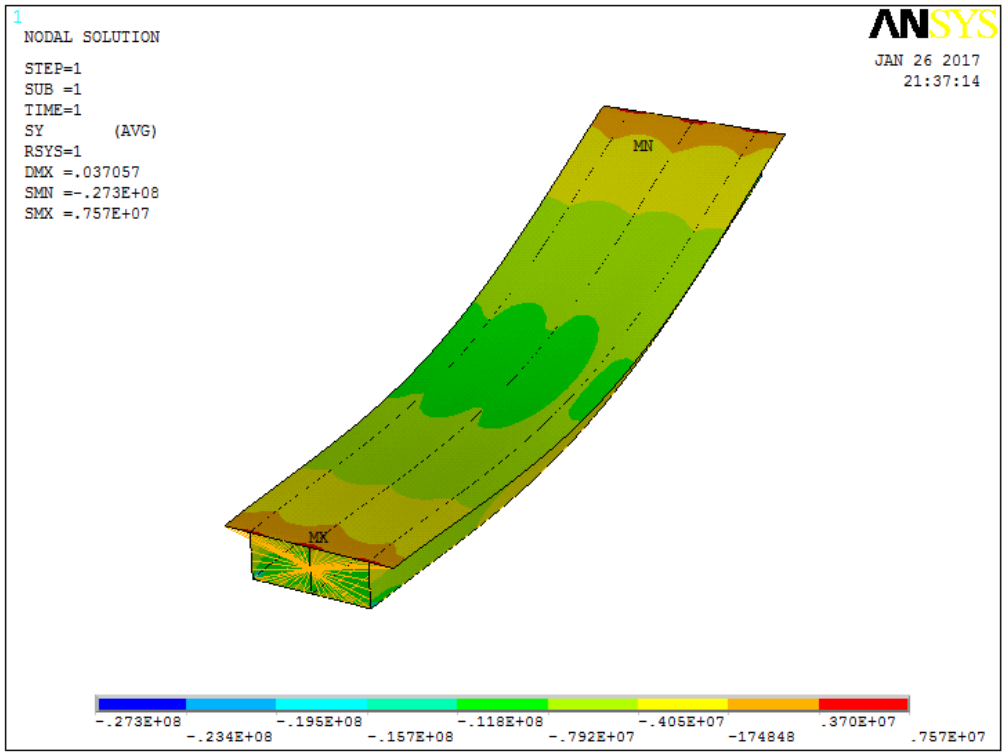

Figure (3.67) Longitudinal stresses for curved box girder bridge (δ =1 m) under loadings

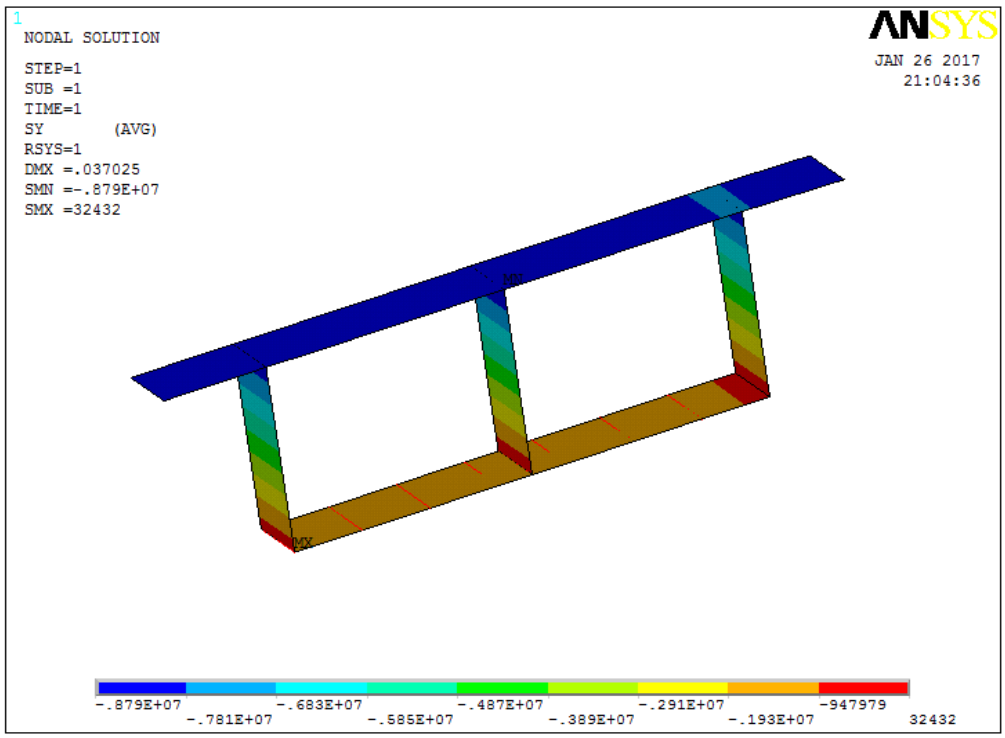

Figure (3.68) Longitudinal stresses at mid-span for curved box girder bridge (δ =1 m) under loadings

3-Curved box girder bridge (δ =3 m)

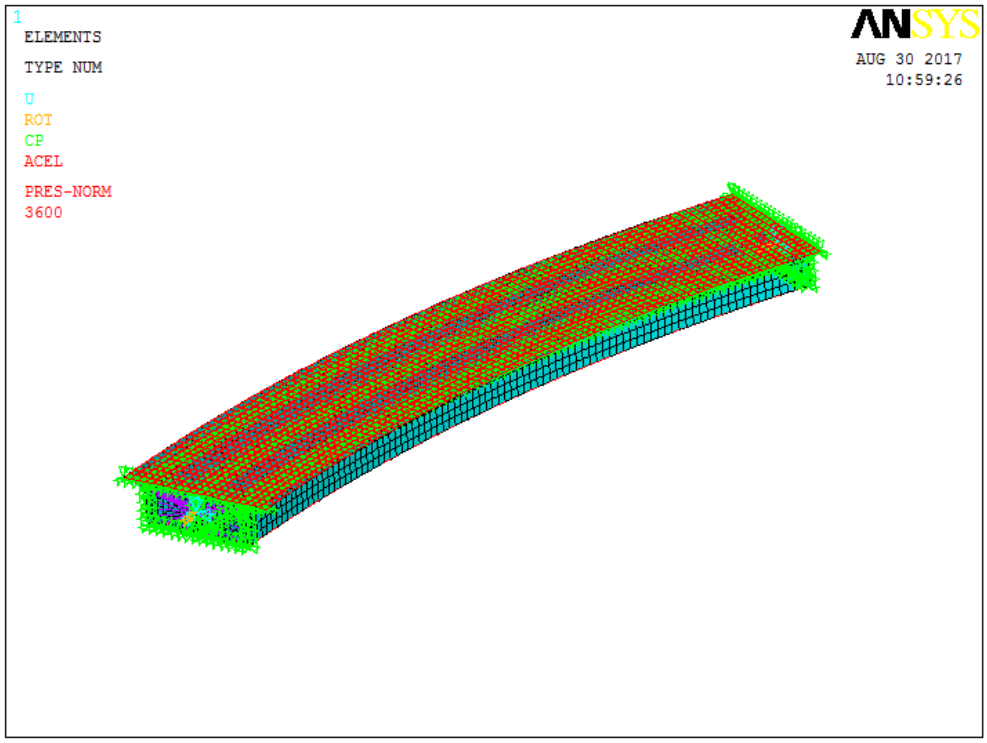

Figure (3.69) Boundary conditions for curved box girder bridge (δ =3 m) under loadings

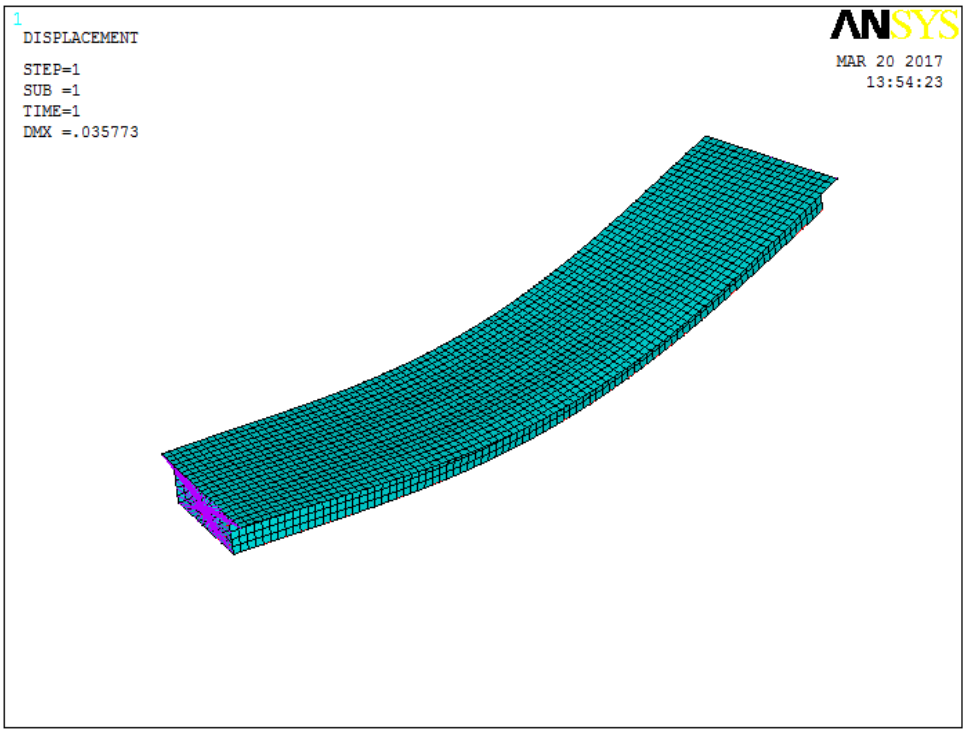

Figure (3.70) Deformed shape for curved box girder bridge (δ =3 m) under loadings

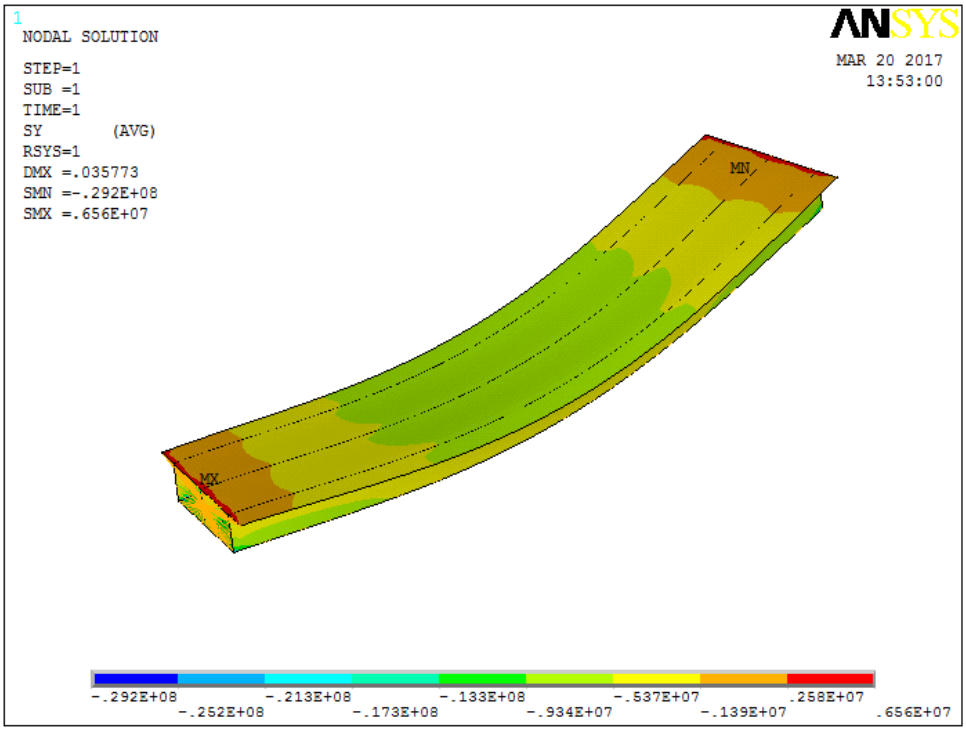

Figure (3.71) Longitudinal stresses for curved box girder bridge (δ =3 m) under loadings

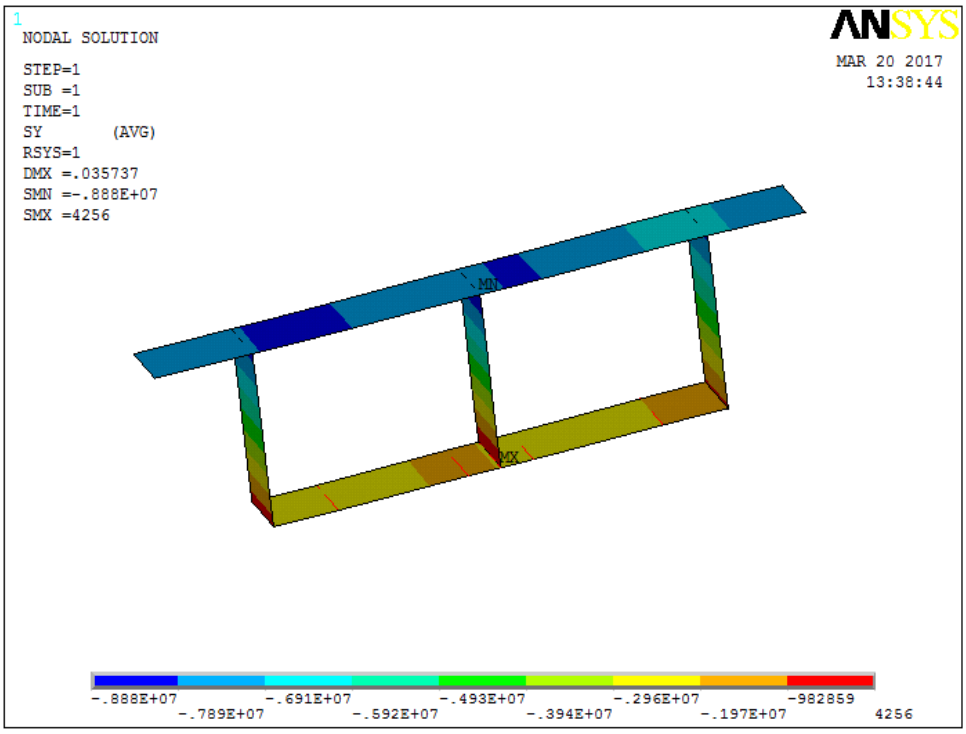

Figure (3.72) Longitudinal stresses at mid-span for curved box girder bridge (δ =3 m) under loadings

4-Curved box girder bridge (δ =5 m)

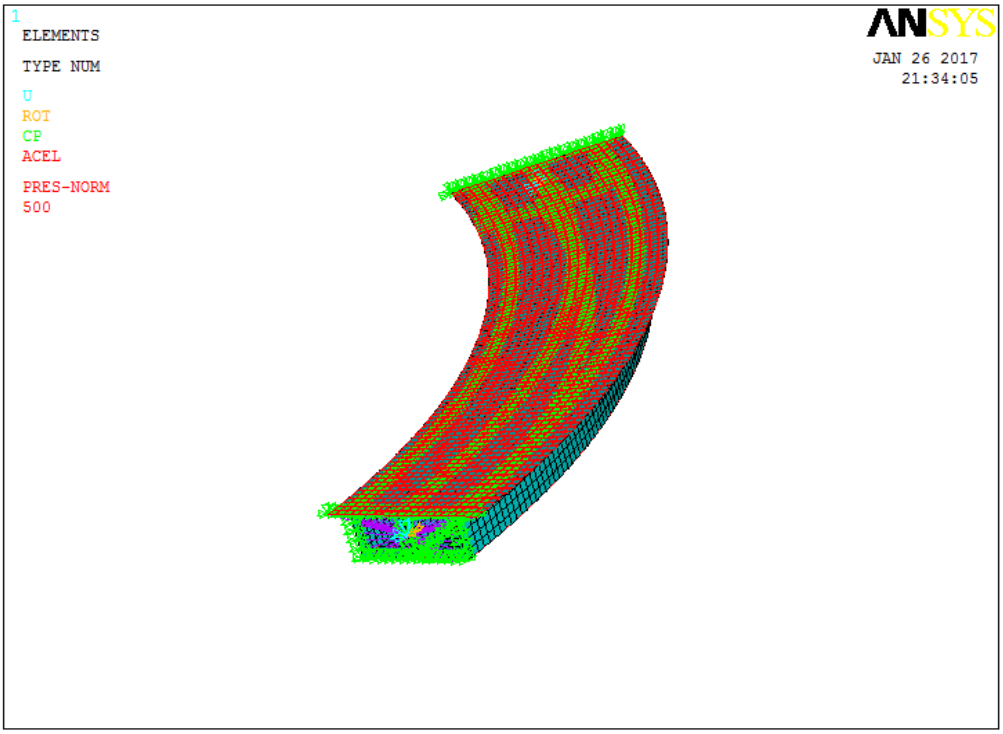

Figure (3.73) Boundary conditions for curved box girder bridge (δ =5 m) under loadings

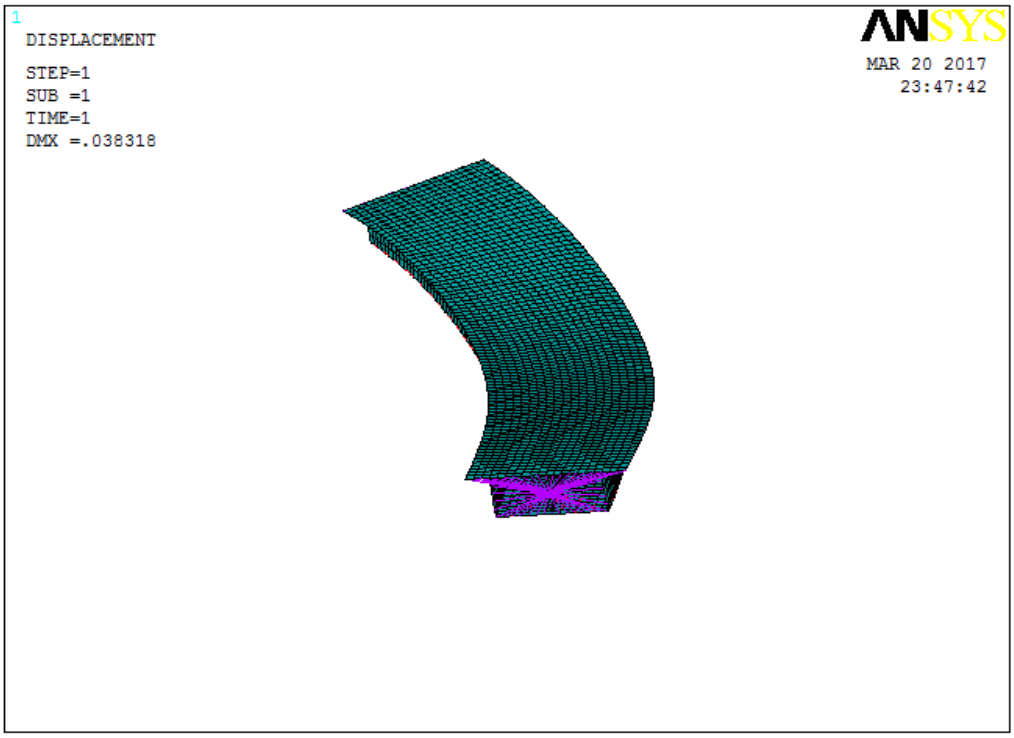

Figure (3.74) Deformed shape for curved box girder bridge (δ =5 m) under loadings

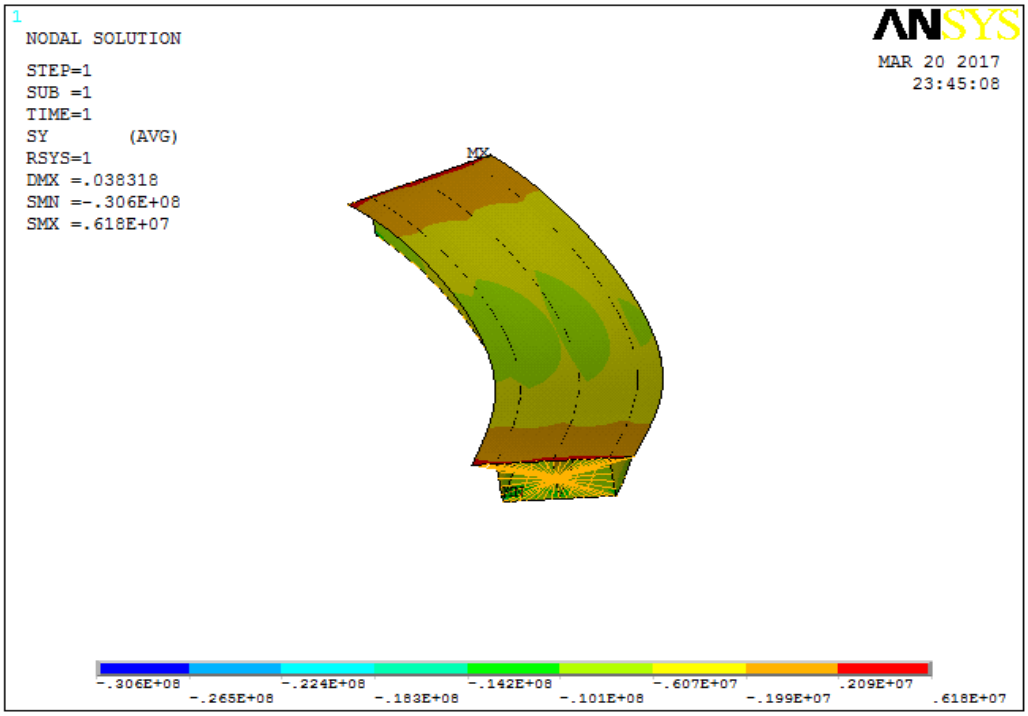

Figure (3.75) Longitudinal stresses for curved box girder bridge (δ =5 m) under loadings

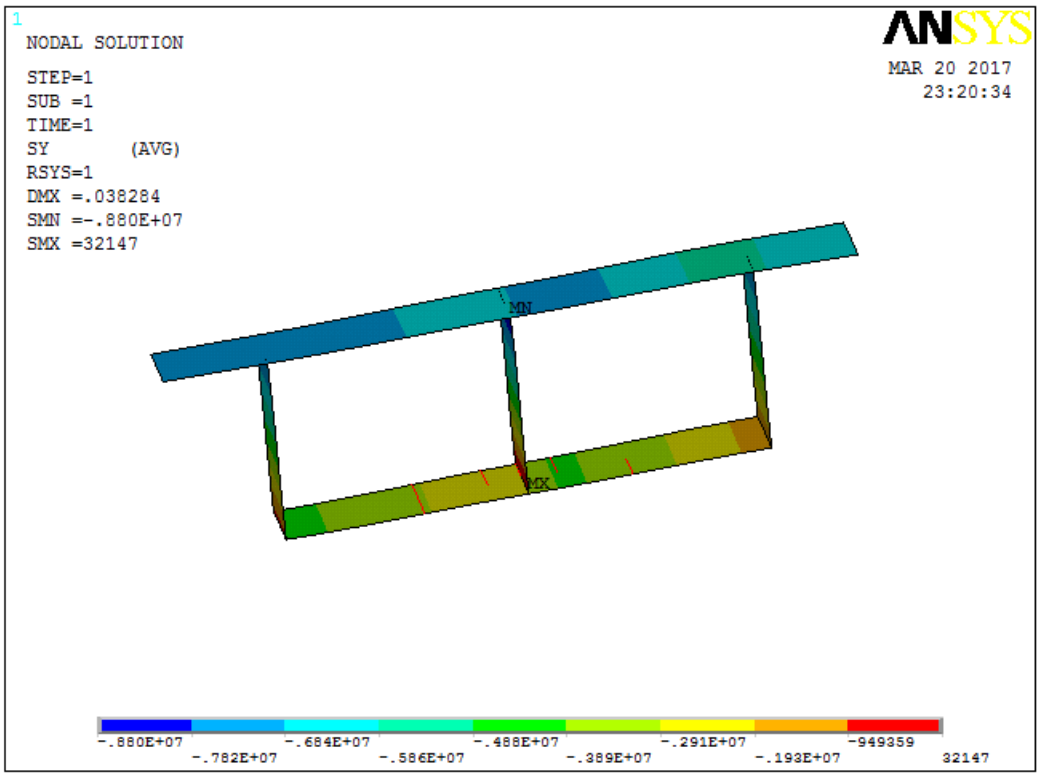

Figure (3.76) Longitudinal stresses at mid-span for curved box girder bridge (δ =5 m) under loadings

Table (3.3) Loads on straight and curved models.

Delta (m) and load (kN/m^2)	Mass (Tonnes)	Reaction (kN)	M_y (kN.m)	Prestress (kN)	Mid-span stresses (N/mm^2)			
					Slab		Soffit	
delta=0					Interior	Exterior	Interior	Exterior
Load=9.3	1180	-19100	0	4980	-9	-8.26	0.0482	0.0396
delta=1								
load =7.5	1200	-17900	12700	4960	-8.79	-8.12	0.0324	0.15
delta=2								
load 5.6	1220	-16700	24200	4940	-8.67	-6.5	0.0187	0.559
delta=3								
Load= 6.3	1250	-15400	34300	4920	-8.88	-7.99	0.00426	0.146
delta= 4								
load=1.85	1270	-14100	43300	4910	-8.22	-6.57	0.025	0.0197
delta=5								
Load=0.5	1300	-12900	51300	4880	-8.75	-7.63	0.0321	0.82

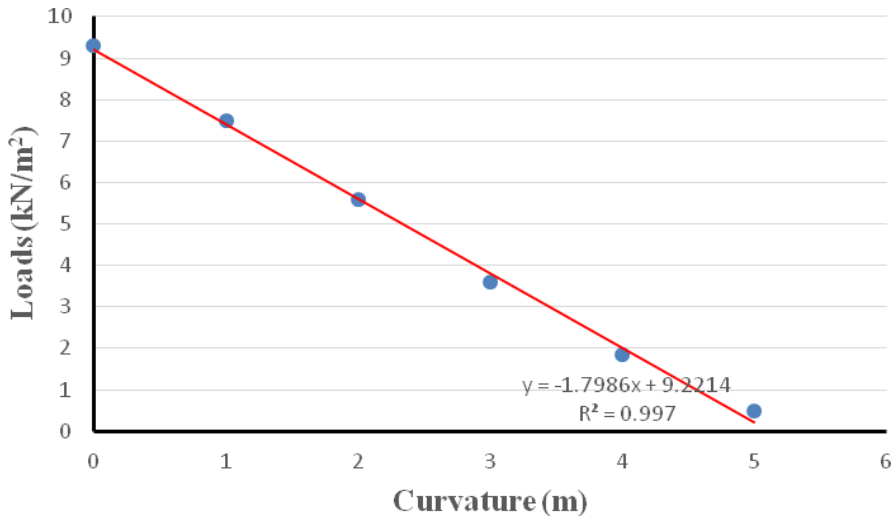

Figure (3.77) Relationship between load intensity and curvature

Straight box girder bridges carried the highest loads intensity from all the cases (straight and curved), and as the box girder curvature increased, the load capacity reduced in a near linear relationship until delta reached 5m when the curved box girder carried the lowest load capacity, equal to 0.5kN/m^2. The results for prestress losses resulting from the addition of applied loads, gravity and prestressing were all lower than 20%. The allowable curvature as measured by the sector dimension delta for the cases with applied loads (δ = 5m) when tension stresses started to show, being around half of the delta obtainable with gravity and prestressing (δ = 11m). The last value of tensile stress occurred at a value of delta (δ = 5m) with a load equal to 0.5kN/m^2 (class 1 design SLS); whilst with gravity and prestressing alone, the tensile stresses developed when delta was equal to 11m.

Figure (3.77) shows as the loads increased curvatures decreases to maintain a class 1 section design, as expected.

Chapter Four
Parametric Analysis

4.1 Introduction

The previous chapter presented the validation of the finite element box girder model by comparing with the results of Khaloo & Kafimosavi (2007). This has resulted in a modelling philosophy which will be taken forward to a parametric study of different bridge curvatures, levels of prestressing and the effects of traffic loading and patterning. These parameters are set out in the following sections.

4.2 Parametric models

1. Varying the level of prestress (4 values)
2. Varying the level of horizontal curvature
3. Varying the applied loads (self-weight, prestress, both and uniformly distributed load)

The various combinations of parameters which will be studied are shown in table 4.1.

The table shows each case with different applied loads, gravity – which consists as density and acceleration, prestress by applying the prestress profile alone and the combination of both gravity and prestress. All were applied due to changing curvature.

Table (4.1) The parametric study

Delta (m)	Curv. 1/R (m^{-1})	Case 1			Case 2			Case 3			Case 4		
		g	p	g+p	g	p	g+p	g	p	g+p	g	p	g+p
0	0	✓	✓	✓	✓	✓	✓	✓	✓	✓	✓	✓	✓
1	0.0027	✓	✓	✓	✓	✓	✓	✓	✓	✓	✓	✓	✓
2	0.0055	✓	✓	✓	✓	✓	✓	✓	✓	✓	✓	✓	✓
3	0.0081	✓	✓	✓	✓	✓	✓	✓	✓	✓	✓	✓	✓
4	0.0107	✓	✓	✓	✓	✓	✓	✓	✓	✓	✓	✓	✓
5	0.0133	✓	✓	✓	✓	✓	✓	✓	✓	✓	✓	✓	✓
6	0.157				✓	✓	✓	✓	✓	✓	✓	✓	✓
7	0.0180							✓	✓	✓	✓	✓	✓
8	0.0202										✓	✓	✓

There are some variations and developments in the modelling as explained in the following sections:

4.3 Tendon profile

In the previous chapter the finite element model incorporated a straight tendon profile which was displaced downward from the section centroid with a constant eccentricity. The dead loads at mid-span were balanced by the prestressing, however elsewhere along the beam profile, the prestressing would create hogging moments which are especially critical at the ends of the beam. Ideally a parabolic tendon profile would provide a full balanced uniformly distributed load along the length of the beam, hence it would be desirable to reproduce this effect. By the nature of the FE model, any curvature in the tendon profile is usually achieved in a piecewise linear fashion. To follow a curve faithfully at mutual nodes in the beam web would require shallow web elements and aspect ratios outside of the acceptable range. Hence it was decided to incline the tendon at a third of the way along the beam to provide a profile which can approximately balance the applied load bending moment. The equivalent load will be in the form of upward point loading at the third points of the beam.

Figure (4.1) shows the details of the single cell box girder bridge model used for the parametric study. For the purpose of accuracy and to reduce the error, only two tendons will be adopted in the study each will be inclined along with web on both sides. The boundary conditions at the ends of the beam are such that they represent pinned ends with torsional restraint about the longitudinal/tangential axis.

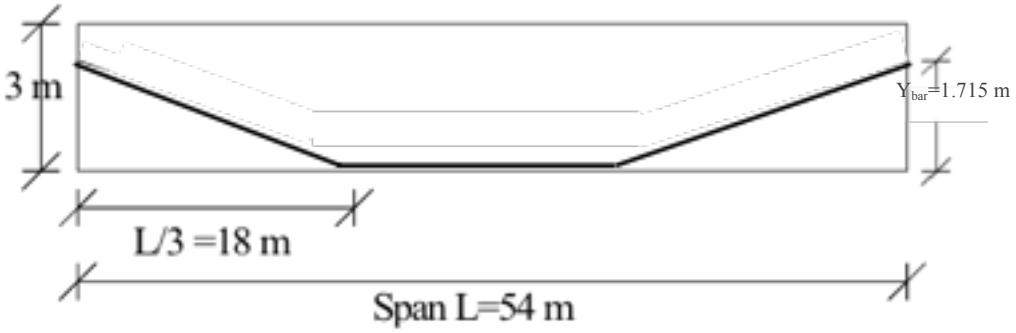

A - Tendon Profile

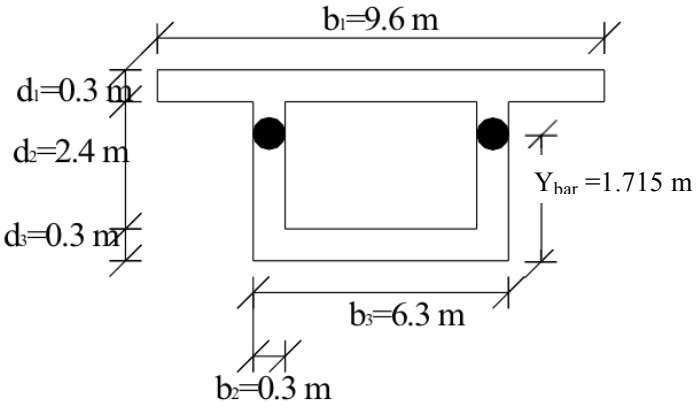

B - End span cross-section

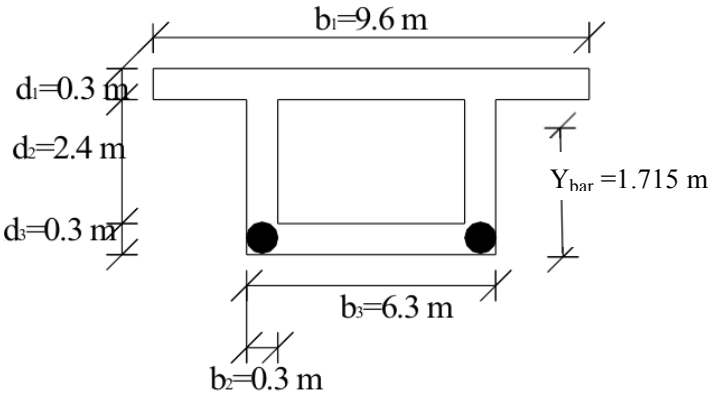

C - Midspan cross-section

Figure (4.1) Box girder bridge tendon profile and cross-sections.

Model details:

Length of span = 54m

Depth of deck = 3m

Deck width = 9.6m.

Two prestressed tendons located at the soffit.

The material properties are as follows:

Modulus of elasticity of the concrete $E_c = 17\times10^9$ N/m^2

Density of the concrete ρ = 2400kg/m^3

Modulus of elasticity of the tendons $E_s = 200\times10^9$ N/m^2.

The rectangular single cell box girder has been modelled with Shell 63 elements, with rigid beam elements at the ends and simply supported boundary conditions at the centroid of the section as described in the previous chapter. A series of static analyses were then conducted with the model. The load cases were as follows:

1. Gravity only
2. Prestress only
3. Prestressing + gravity
4. Prestress + gravity + UDL
5. Prestress + gravity + UDL + traffic loading (chapter five)

The reason for adopting different prestressing forces (different prestress values case1, case2, case3 and case4) is to examine the basic design principle for class 1 prestressed sections (i.e. that there should be no tension in the concrete at serviceability limit state). The bridge at different curvatures will have a loading capacity (UDL) at which the class 1 design becomes invalid as the direct stresses will go into tension.

Hence the parametric study will examine different levels of prestressing and different UDL's to determine the load capacity for various ranges of curvature using the finite element programme ANSYS12.

The objectives of this parametric work are:

- To compare the behaviour of a prestressed horizontally curved box girder bridge to a straight bridge and study the effects of using different levels of prestressing.
- To investigate the impact of changing the radius of curvature on the behaviour of the box girder bridge.
- To determine the most appropriate radius of curvature for different spans based on their stress patterns.
- To examine the effects of load patterning from typical vehicle loading.

Throughout the parametric study, the cross-sectional properties of the box girder bridge remain constant.

4.4 Box girder bridge section properties

The first part of the calculation determines the section properties (area and second moment of area) based on the geometry shown in figure (4.1)

Deck b_1=9.6 m d_1=0.3 m

Ribs b_2= 0.3 m d_2= 2.4 m

Soffit b_3= 6.3 m d_3 = 0.3 m

Calculate Area $A = b_1 \times d_1 + 2 \times (b_2 \times d_2) + b_3 \times d_3$ $A = 6.21\ m^2$

Calculate Y_{Bar},

$$Y_{Bar} = \frac{b_1 \times d_1 \times (0.5 \times d_1 + d_2 + d_3) + 2 \times \left(b_2 \times d_2 \times \left(0.5 \times d_2 + d_3\right)\right) + b_3 \times d_3 \times 0.5 \times d_3}{A}$$

Y_{Bar}= 1.715 m

Caclulate I,

$$I = \frac{b_1 \times {d_1}^3}{12} + \frac{2 \times b_2 \times {d_2}^3}{12} + \frac{b_3 \times {d_3}^3}{12} + b_1 \times d_1 \times (0.5 \times d_1 + d_2 + d_3 - Y_{Bar})^2 + 2 \times b_2 \times d_2 \times (0.5 \times d_2 + d_3 - Y_{Bar})^2 + b_3 \times d_3 \times \left(Y_{Bar} - \frac{d_3}{2}\right)^2$$

$I = 9.133\ m^4$

4.5 Loading and boundary conditions

The model is similar to the previous model with regards the loading conditions. The shell box girder bridge models are subjected to the self-weight of the box first, then prestressing forces are subsequently applied. A combination of self-weight and prestress loading have then been analysed. Subsequently different loading conditions (UDL's) are applied for each curvature, and finally, different traffic patterns are applied to the top surface of the deck. The complete FE model of the box girder bridge is shown in figure (4.2).

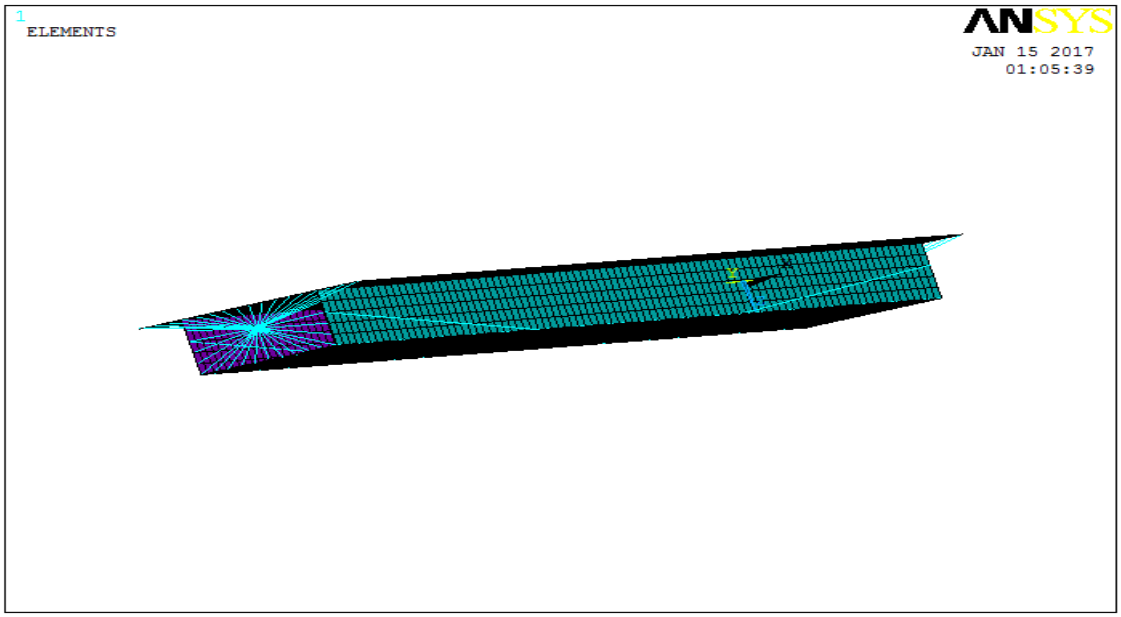

A) Isometric view

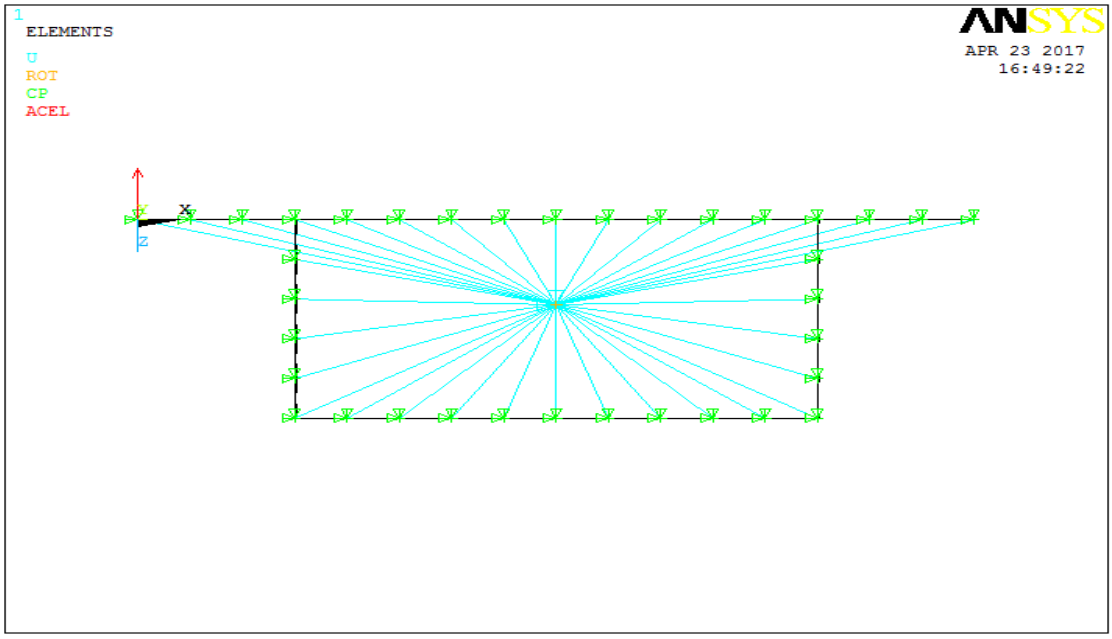

(B) Cross-section showing boundary conditions

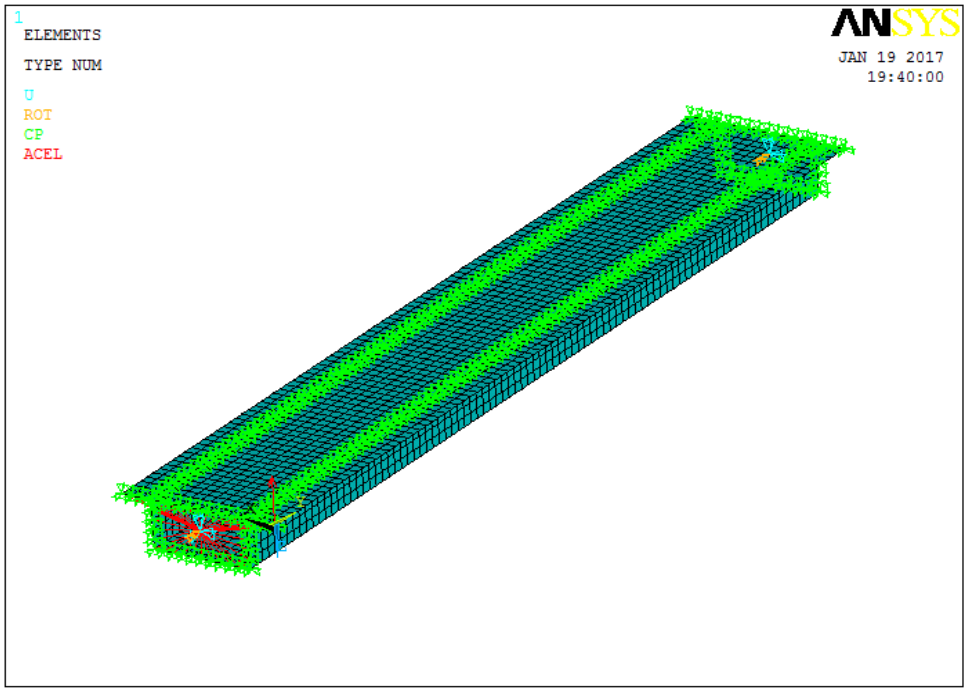

(C)Boundary conditions for single cell box girder bridge

Figure (4.2) Views of the FE model for the parametric study

4.6 Parametric study

4.6.1 Prestressing force

4.6.1.1 Applied prestress = 31000 kN

4.6.1.1.1 Prestress calculation

For each scenario of prestressing force, the tendon prestrain requires calculation for input to the ANSYS model.
Ultmate tensile strength (assumed from typical values)

σ_{ult} = 1800 N.mm^{-2}

Service stress in tendons taken as 60% of the ultimate stress

$\sigma_{ten} = 0.6 \times \sigma_{ult}$ σ_{ten} = 1080 N.mm^{-2}

Desired tension force in tendons (2 tendons):

P = 31000 kN

Tension force in each tendon $p = \frac{P}{2}$
p =15500 kN

Area of each tendon:

$$\mathbf{A} = \frac{\mathbf{p}}{\boldsymbol{\sigma}_{\mathbf{ten}}} \qquad A = 1.435\times10^{4}\ mm^{2}$$

Steel modulus of elasticity:

$E_s = 200\times10^{9}\ N.m^{-2}$

Strain in tendons:

$$\varepsilon = \frac{\sigma_{ten}}{E} \qquad \varepsilon = 5.4\times10^{-3}$$

4.6.1.1.2 Calculation of direct stresses due to gravity, prestress, and combination of gravity and prestress

Second moment of area	$I = 9.133\ m^4$	
Cross sectional area	$A = 6.21\ m^2$	
Distance from soffit to centroid	$Y_{bar} = 1.715$ m	
Concrete unit weight	$\rho = 2400\ kg.\ m^{-3}$	
Depth of section	$D = 3$ m	
Width of deck	$B = 9.6$ m	
Length of deck	$L = 54$ m	
Acceleration	$g = 9.81\ m.sec^{-2}$	
Moment at mid-span from gravity:		
Self-weight	$W = A\times\rho\times g$	$W = 146.158$ kN/m
Total mass	$M = A\times\rho\times L$	$M = 8.048\times10^{5}$ kg
Bending moment at mid-span from gravity	$M_g = \frac{W\times L^2}{8}$	$M_g = 5.327\times10^{4}$ kN.m
Prestressing force from all tendons	$P = 31000$ kN	
Eccentricity for straight tendon	$ecc = 1.715$ m	
Moment at midspan from prestress	$M_p = P\times ecc$	$M_p = 5.316\times10^{4}$kN.m

Gravity load stresses

$$\sigma_{tg} = \frac{-M_g\times(D - Y_{Bar})}{I} \qquad \sigma_{tg} = -7.496 N.mm^{-2}$$

$$\sigma_{bg} = \frac{Mg\times Y_{Bar}}{I} \qquad \sigma_{bg} = 10.004 N.mm^{-2}$$

Prestress stresses

$$\sigma_{tp} = \frac{P}{A} + \frac{M_p\times(D - Y_{Bar})}{I} \qquad \sigma_{tp} = 2.488 N.mm^{-2}$$

$$\sigma_{bp} = \frac{P}{A} - \frac{M_p\times Y_{Bar}}{I} \qquad \sigma_{bp} = -14.975 N.mm^{2}$$

Total stresses:

Total stresses at top $\sigma_{tg} + \sigma_{tp} = -5.007\ N.mm^{-2}$

Total stresses at bottom $\sigma_{bg} + \sigma_{bp} = -4.971\ N.mm^{-2}$

It can be seen that these stresses are compressive across the section so this level of prestress is approximately balanced and the stresses are compressive.

4.6.1.1.3 Description of the bridge models

The box bridge models that are used in this chapter to study the behaviour of the straight and curved box girder are single-span single cell box girder bridges of total span length 54m. There are two types of bridges that are modelled in ANSYS for the current study:

1. Straight box shell model
2. Curved box shell model

For the straight box shell model, there is only one case while for the curved box shell model there are five cases of curvature.

Straight box shell model

The straight box girder has been modelled similarly to the straight box shell model presented in chapter three. The box girder cross-section in this chapter has been modified as a single cell cross section with different cross sectional dimensions. Three different types of loading have been investigated for the straight box. These are:

1- Straight box model under gravity

The box girder in this case is straight and only subject to self-weight, the model is created using the APDL which can be found in Appendix 4. The finite element model for this case is shown in figure (4.3). Figure (4.4) shows the straight box model under gravity and the boundary conditions. The deformed shape is shown in figure (4.5), and the stress contours are shown in figure (4.6) with the elements at mid-span extracted so that the stresses at mid-span are clearer, as shown in figure (4.7). The stresses are summarised in table (4.2).

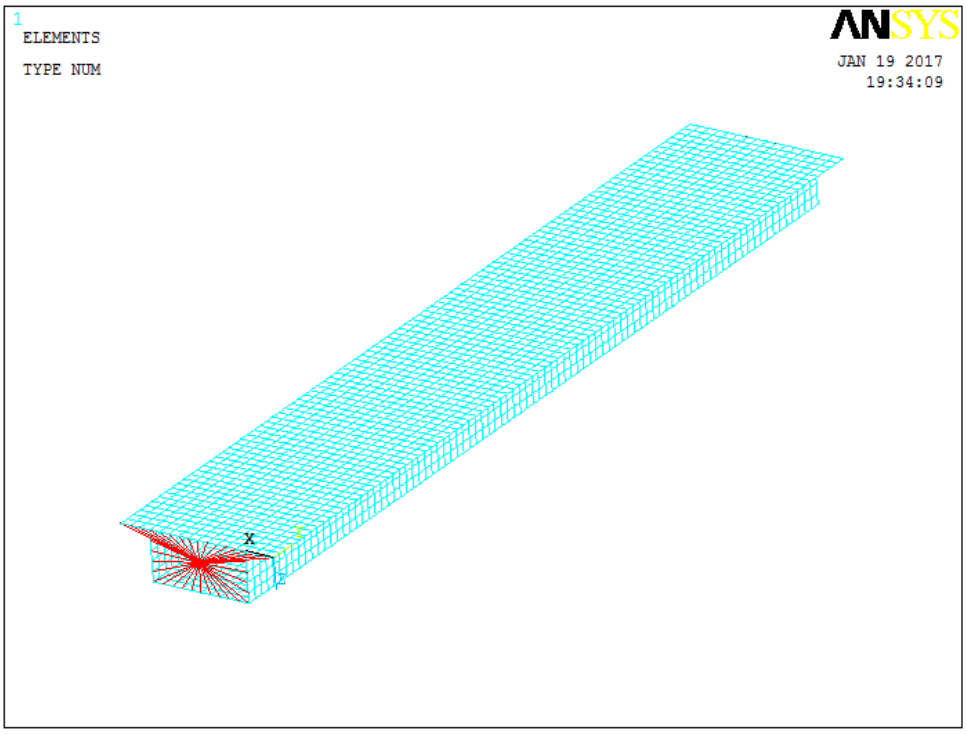

Figure (4.3) The finite element model for straight box girder bridge under gravity case1

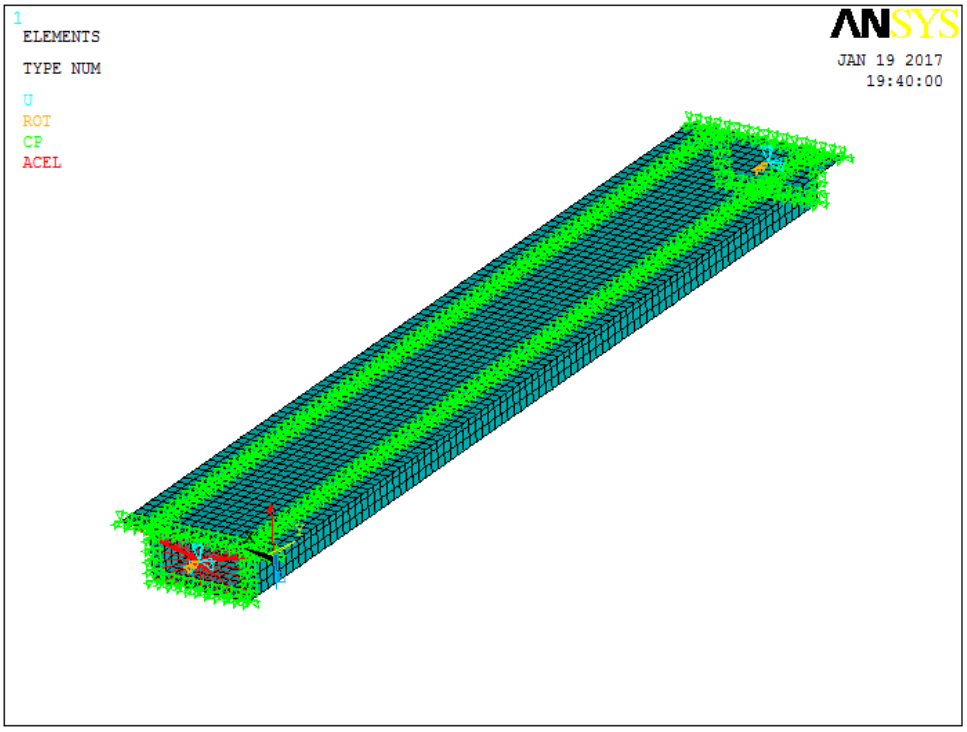

Figure (4.4) Boundary conditions for straight box girder bridge under gravity case1

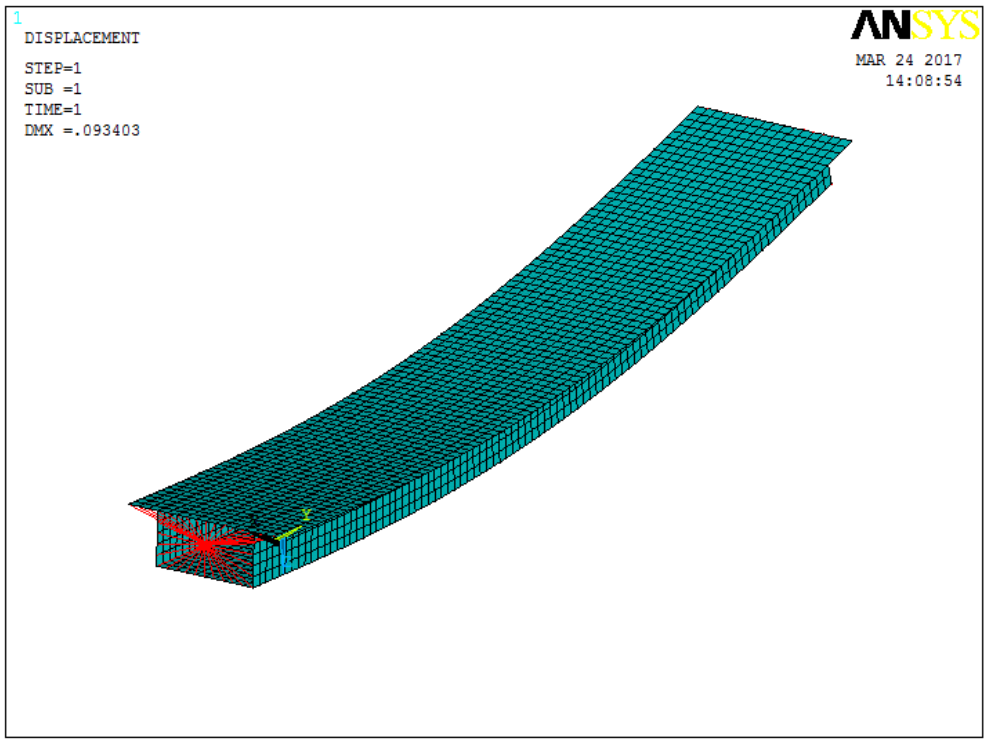

Figure (4.5) Deformed shape for straight box girder bridge under gravity case1

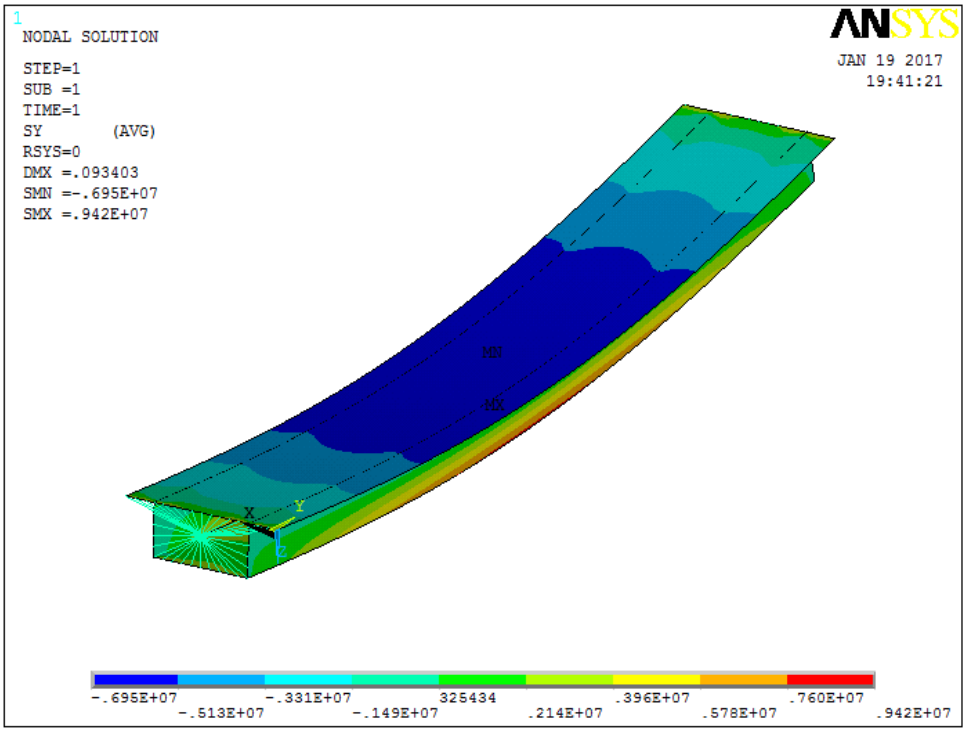

Figure (4.6) Longitudinal stress distribution for straight box girder bridge case1 (N/m^2)

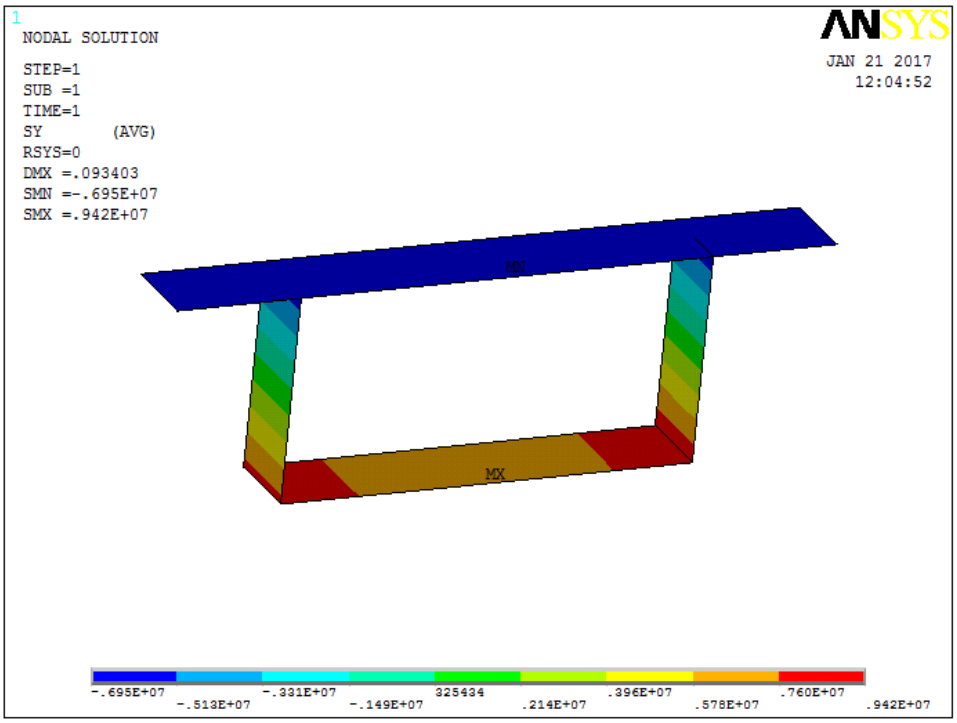

Figure (4.7) Longitudinal stresses at mid-span for straight box girder bridge case1

2-Prestressed straight box model

The box girder in this case is straight in plan, and subject to the effect of prestress alone. The APDL for the full model is provided in Appendix 4 and prestress is applied using the initial strain calculated in previous section. The finite element model for this case is shown in figure (4.8), clearly showing the modified tendon profile. The deformed shape is shown in figure (4.9) and the stress contour is shown in figure (4.10). The stresses at midspan are shown in figure (4.11). Stresses for the midspan section are summarized in table (4.2).

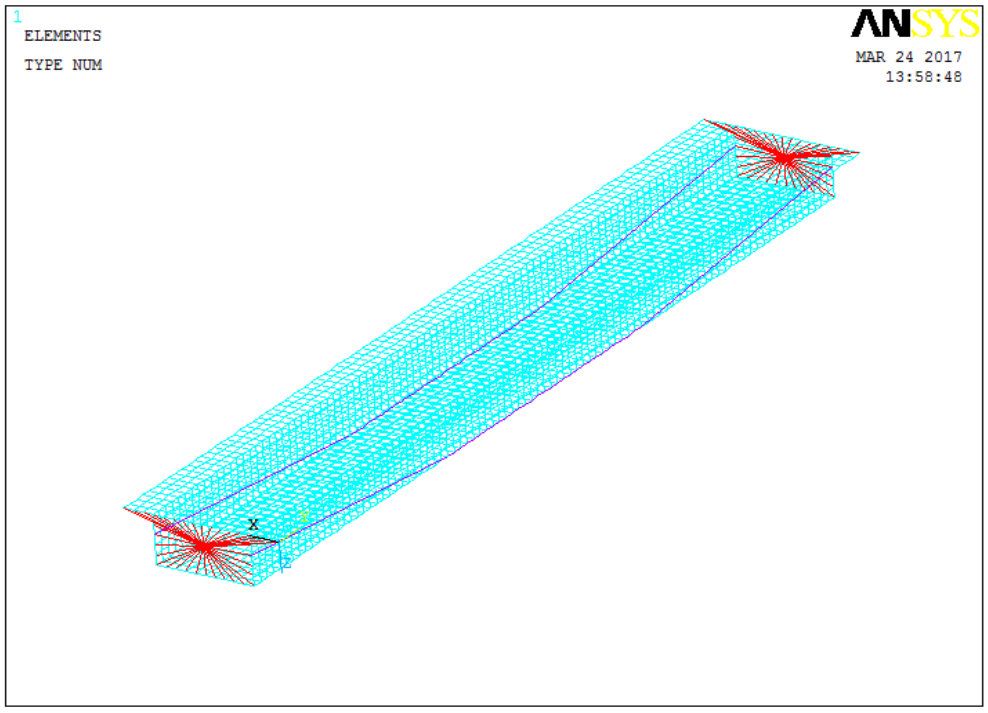

Figure (4.8) The finite element model for straight box girder bridge for prestress, case1

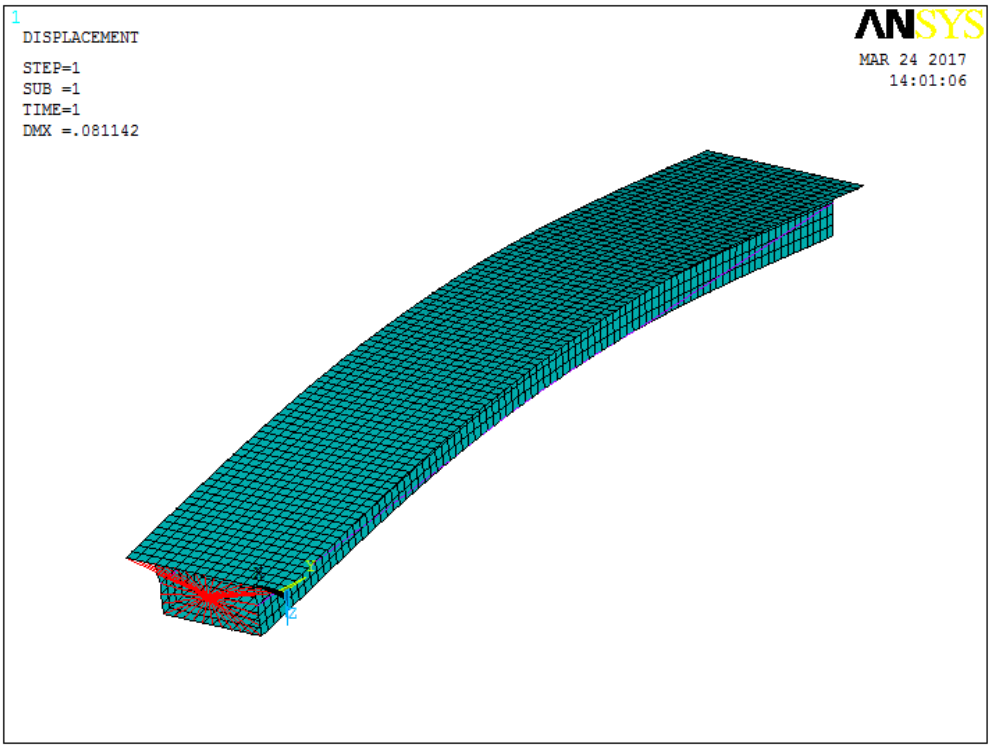

Figure (4.9) Deformed shape for straight box girder bridge for prestress, case1

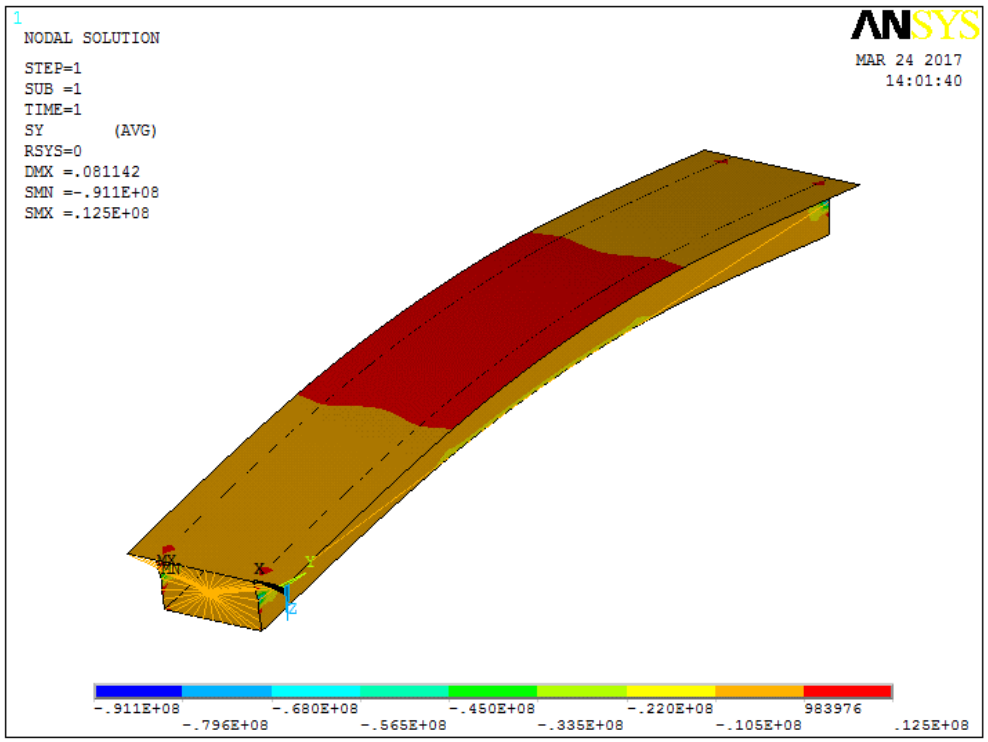

Figure (4.10) Longitudinal stresses distribution for straight box girder bridge for prestress, case1

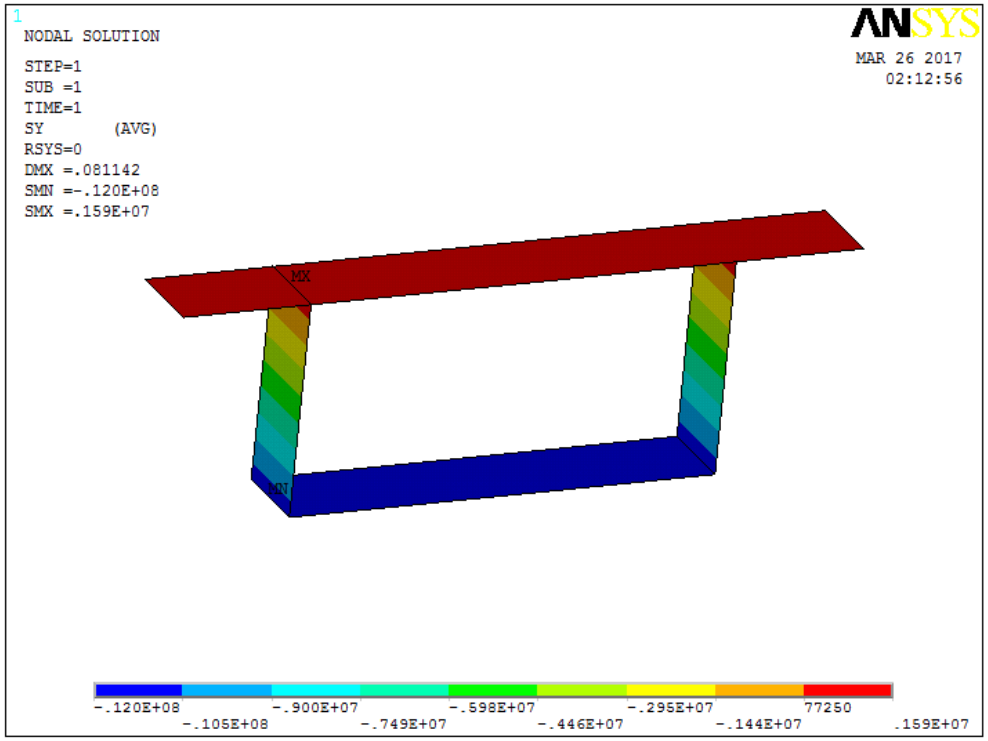

Figure (4.11) Longitudinal stresses at mid-span for straight box girder bridge for prestress, case1

3- Gravity and prestressed straight box model

Under the combined action of prestressing and gravity loading, the deformed shape is shown in figure (4.12) and the longitudinal stress contours are shown in figure (4.13). The elements at the midspan section have been extracted so that the stress contours at midspan are clearer, as shown in figure (4.14). Longitudinal stresses for the midspan section are summarized in table (4.2).

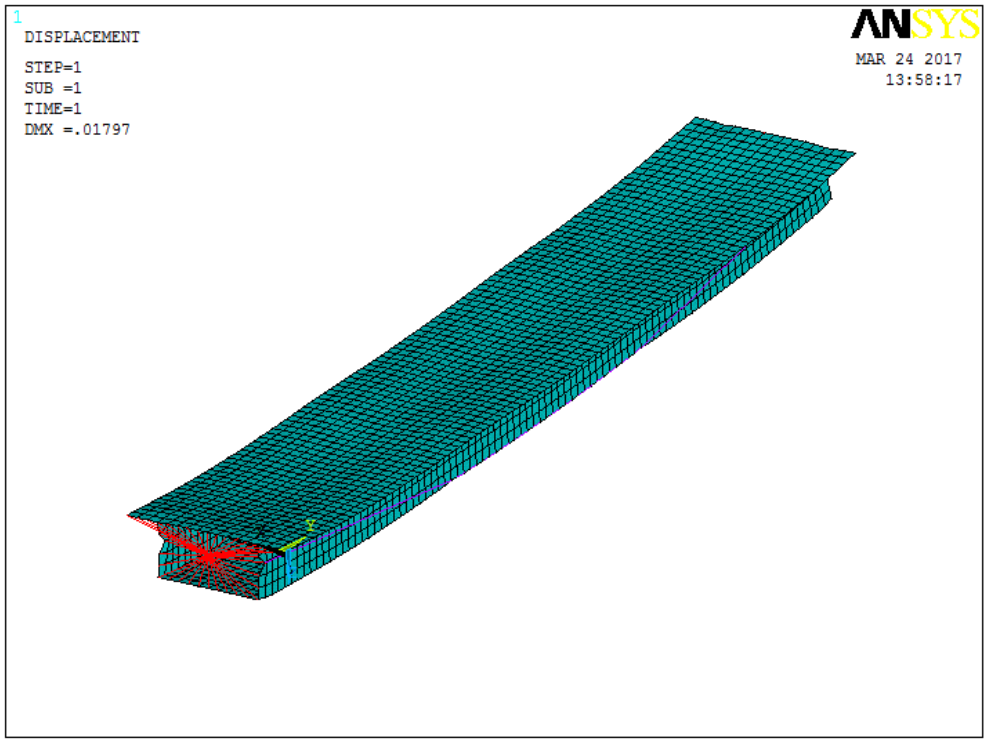

Figure (4.12) Deformed shape for straight box girder bridge (prestress plus gravity), case1

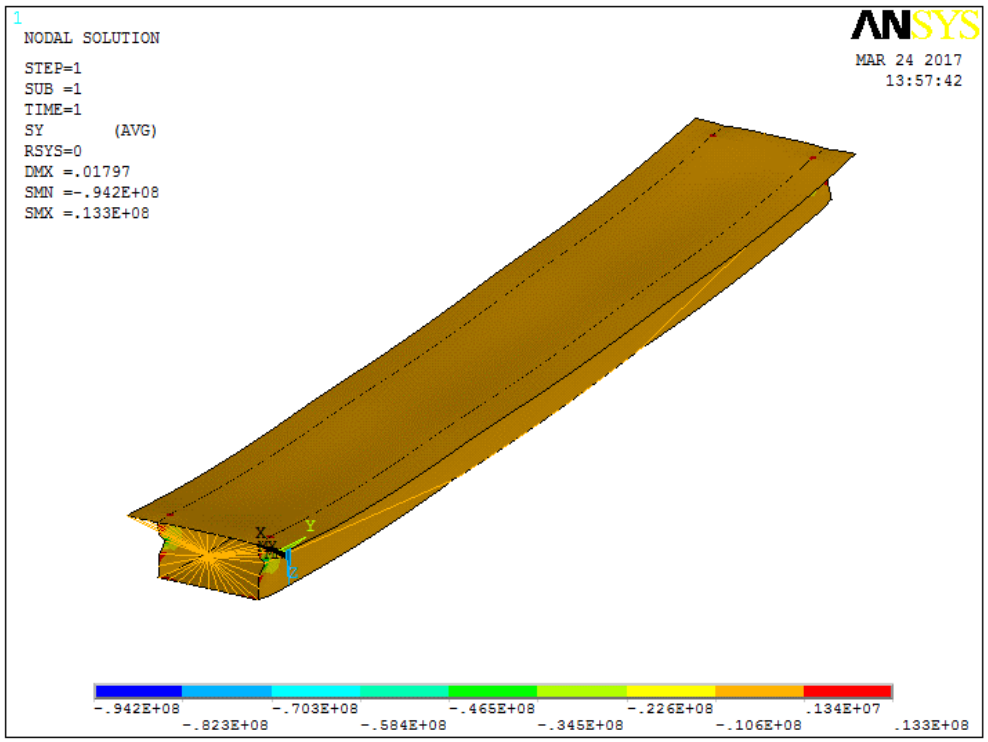

Figure (4.13) Longitudinal stresses distribution for straight box girder bridge (prestress plus gravity), case1

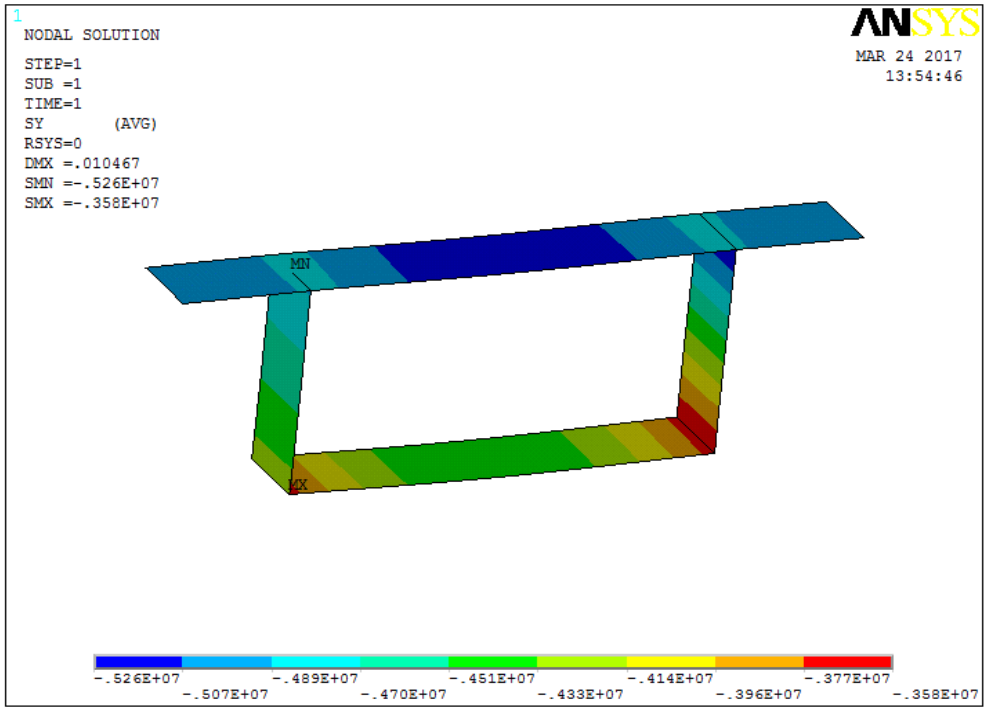

Figure (4.14) Longitudinal stresses at mid-span for straight box girder bridge (prestress plus gravity), case1

It can be seen that the global structural behaviour and longitudinal stress distributions for the various load cases are as expected when compared to the predictions from the hand calculations. Compression stress on top and bottom which was as expected from hand calculations a class 1 design SLS with no tension stress.

Curved box shell model

The horizontally curved box bridge is represented as a model with a changeable radius of curvature. The same modelling philosophy from the previous chapter has been utilized. Six cases of curvature have been analysed changing the horizontal sector dimension delta (δ) in 1m increments from 1m to 5m. For each case, the effects of gravity, prestressing and combined gravity and prestressing have been investigated. Only the modelling of the last case (δ = 5 m) has been shown in detail here which is considered as the worst case where the section is close to developing tensile stresses. The finite element model details, deformed shapes and stress contours will be shown.

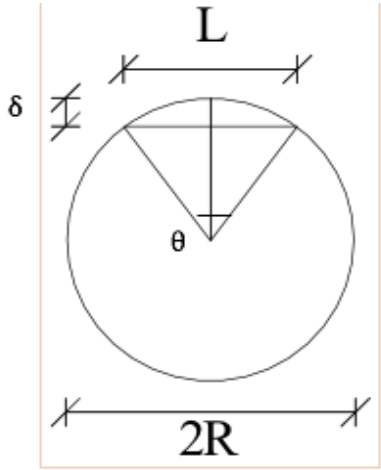

Delta (δ = 5m)

Span L = 54 m

Delta $\delta_{step} = 5$ m

Radius $$R = \left[\frac{\delta_{step}^{\,2} + (0.5 \times L)^2}{2 \times \delta_{step}}\right]$$ R= 75.4 m

Theta $$\theta = 2 \times \tan^{-1}\left[\frac{0.5 \times L}{\sqrt{R^2 - (0.5 \times L)^2}}\right]$$ θ = 41.966°

Curved box model under load cases of gravity, prestress and combination.

As for the previous case, the box girder model is subject to gravity only, prestress only then a combination of these loads. The following figures show these load cases as follows:

Gravity only: Figures 4.15 to 4.19

Prestress only: Figures: 4.20 to 4.23

Gravity and prestress combined: Figures 4.24 to 4.26, Table 4.2 summarises the results.

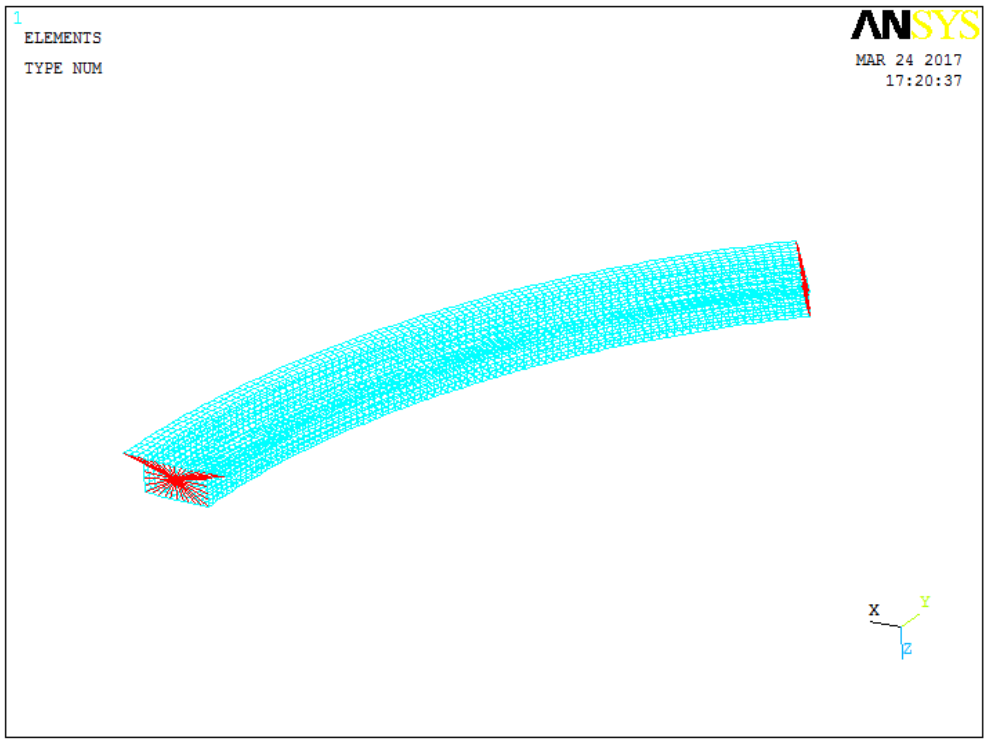

Figure (4.15) The finite element model for curved box girder bridge under gravity, δ=5 m, case1

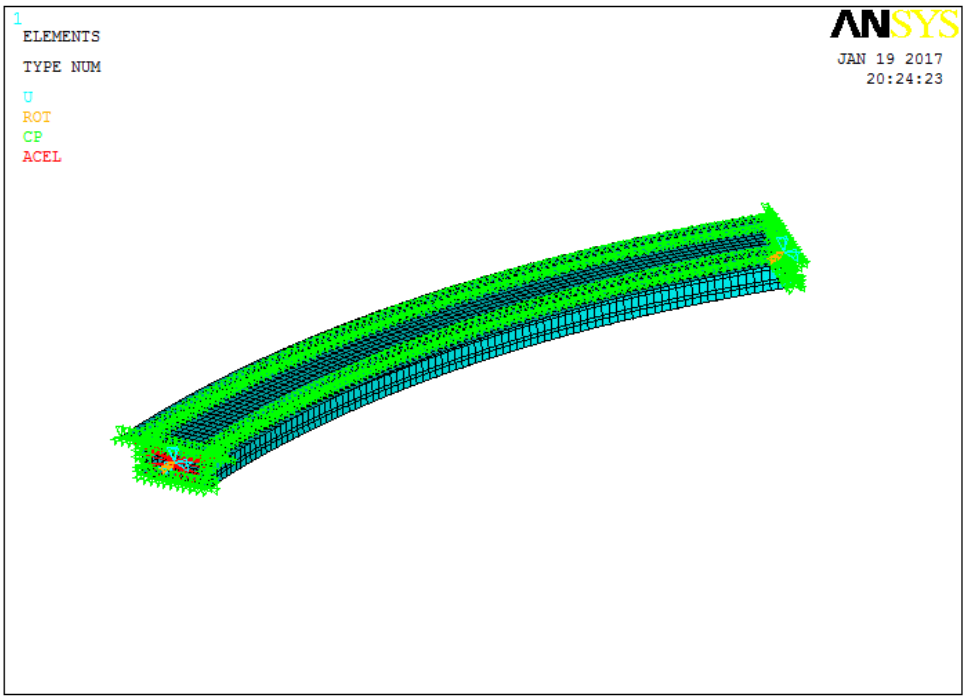

Figure (4.16) Boundary conditions for curved box girder bridge under gravity, δ=5m, case1

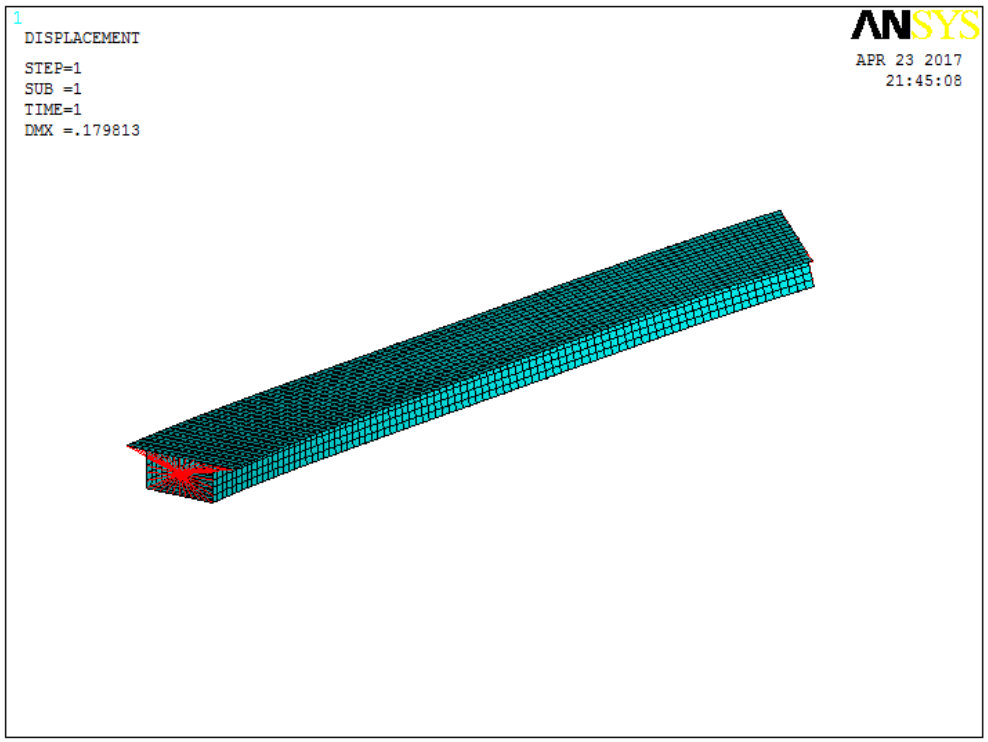

Figure (4.17) Deformed shape (Gravity) for curved box girder bridge, δ=5m, case1

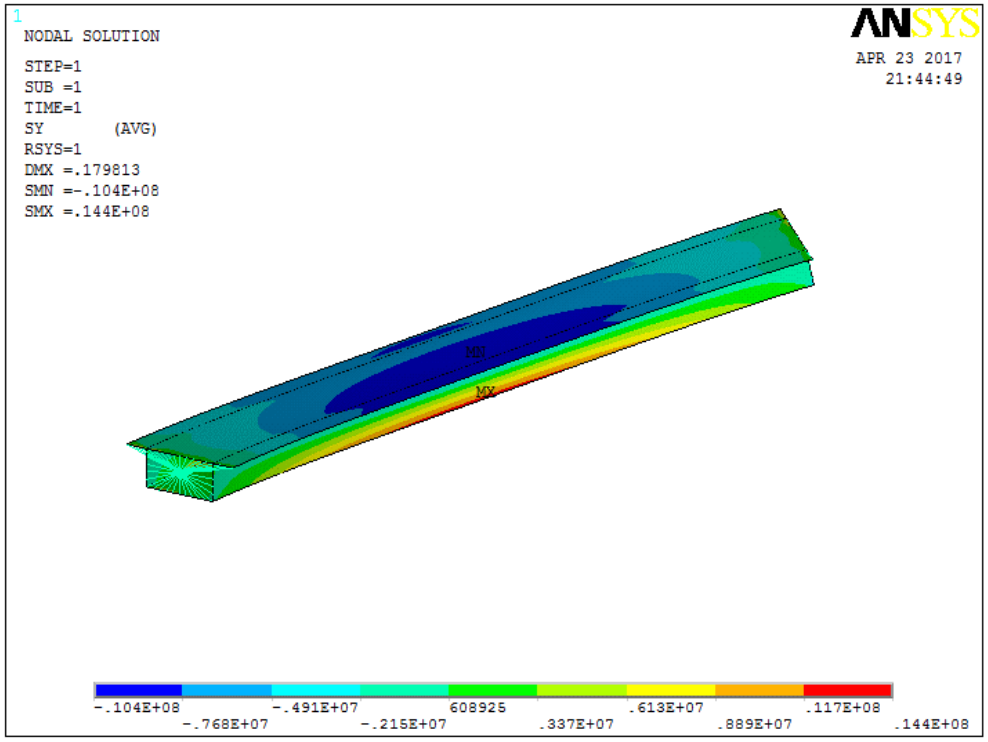

Figure (4.18) Longitudinal stresses (Gravity) for curved box girder bridge, δ=5m, case1

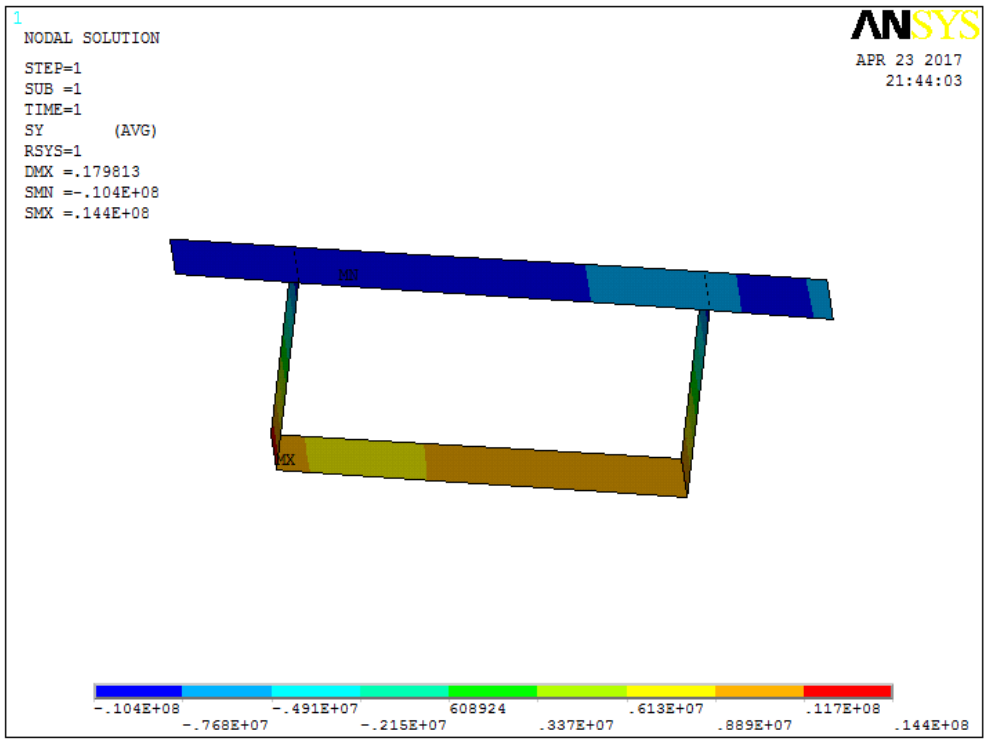

Figure (4.19) Longitudinal stresses at mid-span (Gravity) for curved box girder bridge, δ=5m, case1

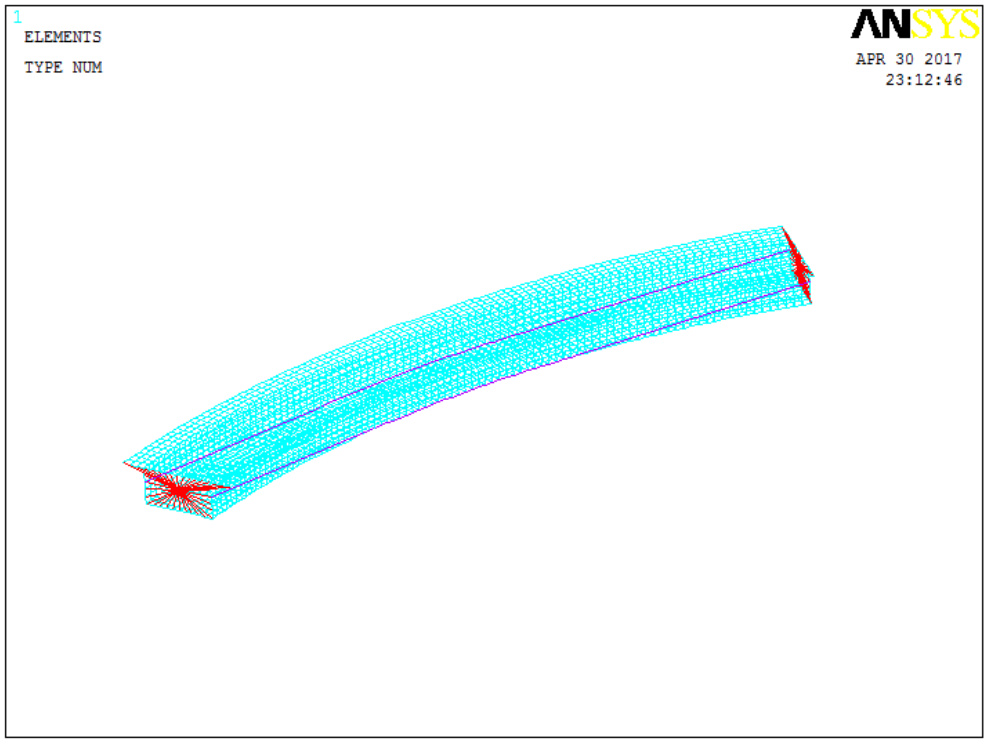

Figure (4.20) The finite element model (prestress only) for curved box girder bridge, δ=5m, case1

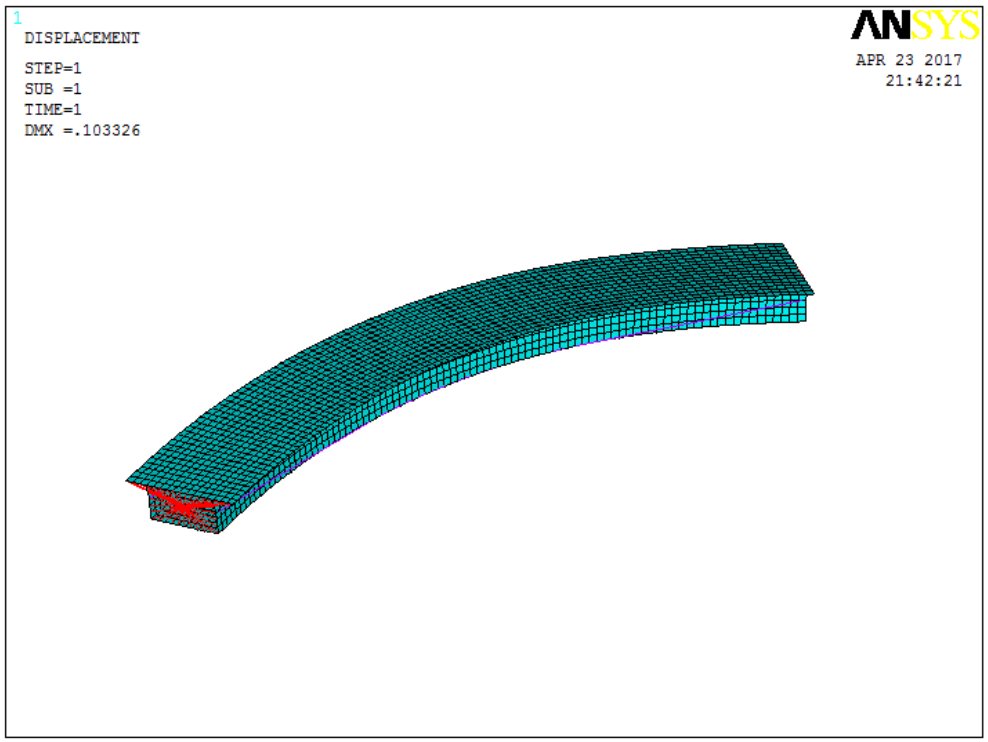

Figure (4.21) Deformed shape (prestress only) for curved box girder bridge, δ=5m, case1

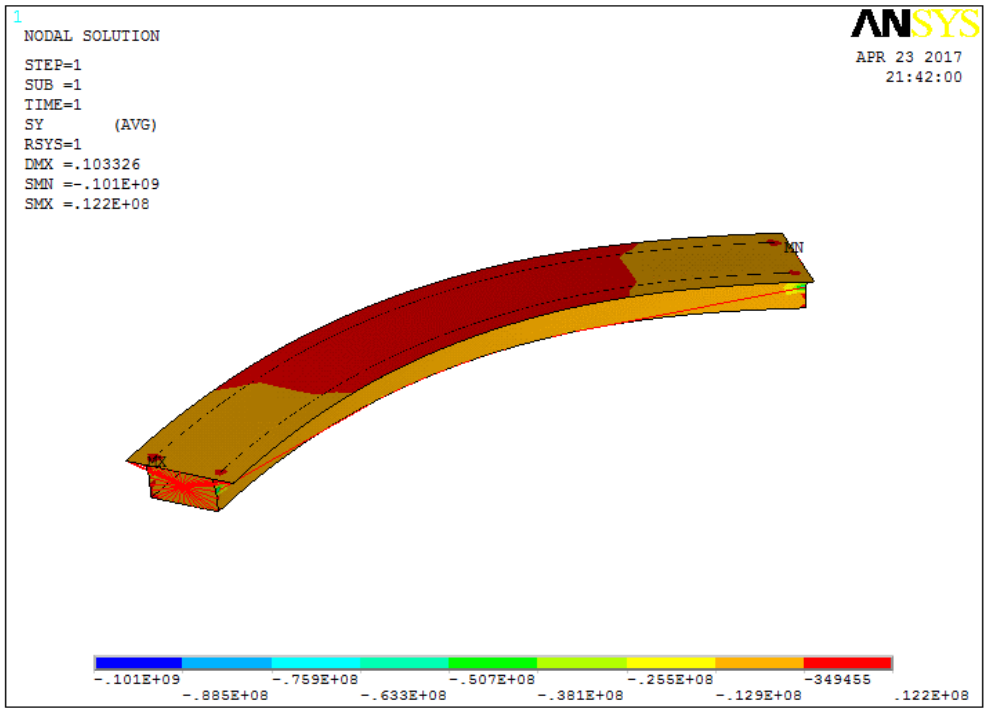

Figure (4.22) Longitudinal stresses (prestress only) for curved box girder bridge, δ=5m, case1

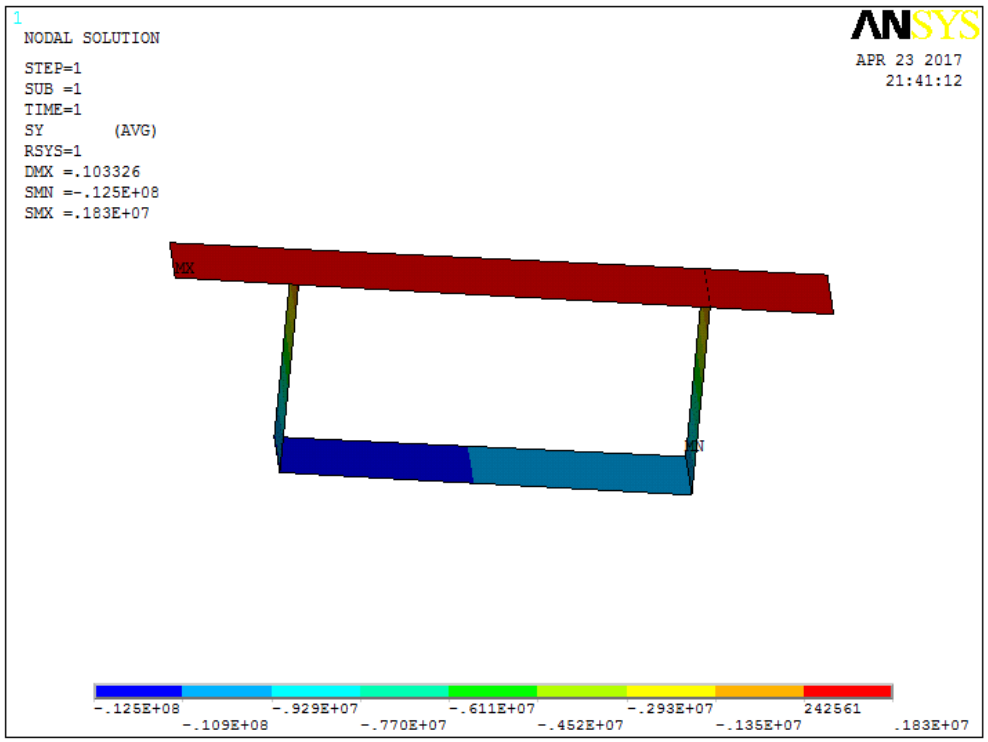

Figure (4.23) Longitudinal stresses at mid-span (prestress only) for curved box girder bridge, δ=5m, case1

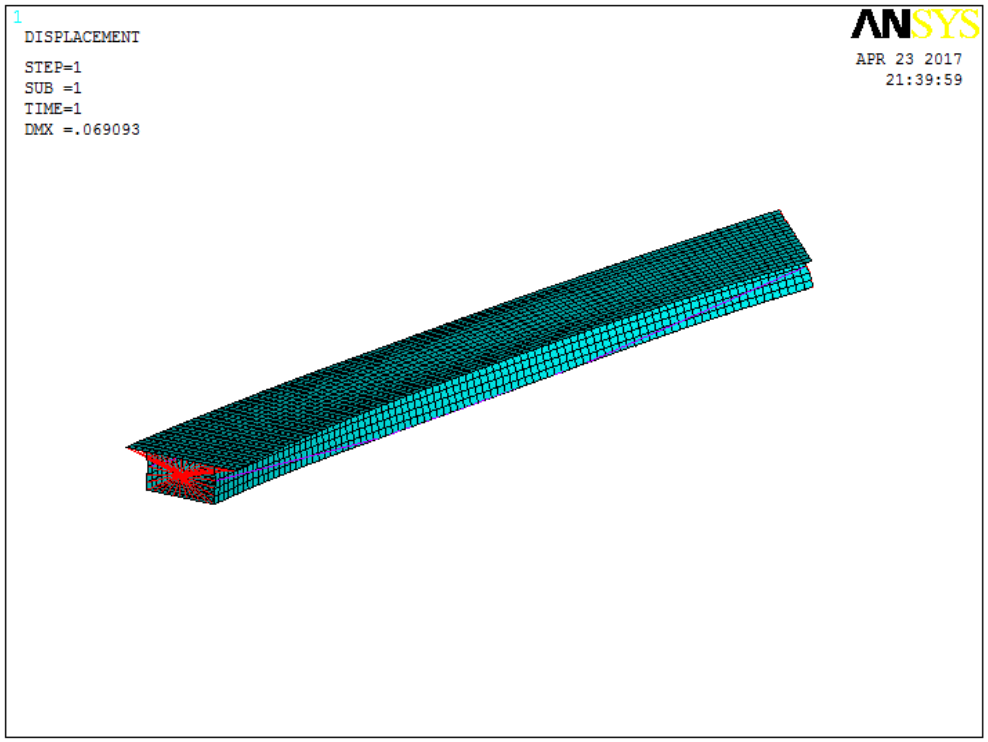

Figure (4.24) Deformed shape (gravity plus prestress), delta = 5m, case1

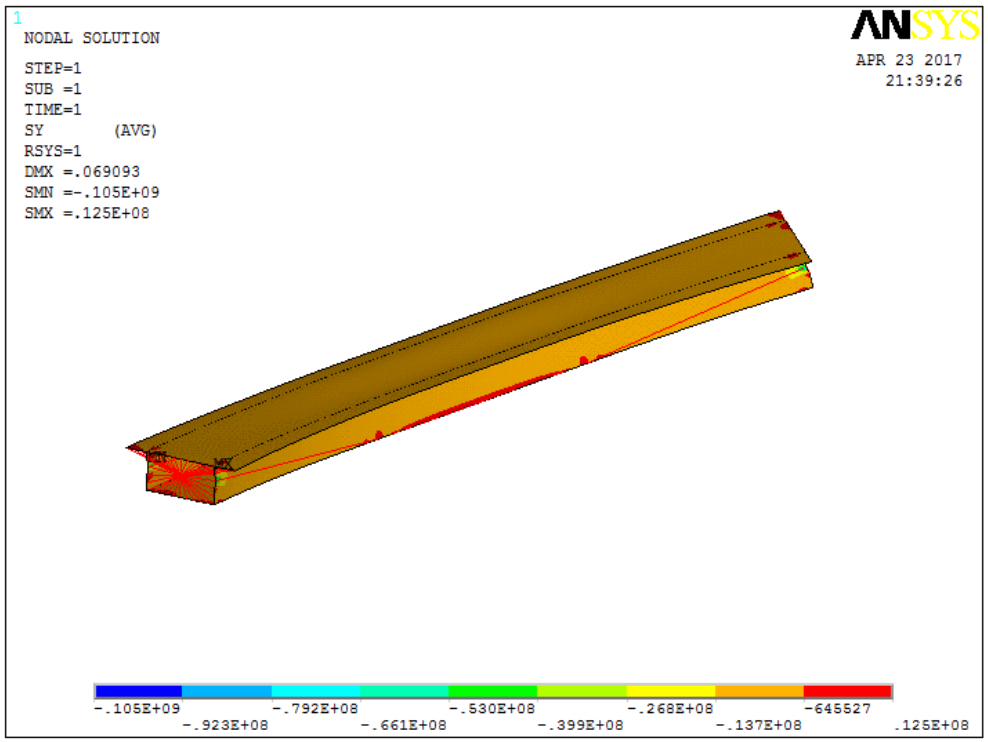

Figure (4.25) Longitudinal stresses (gravity plus prestress, delta = 5m), case1

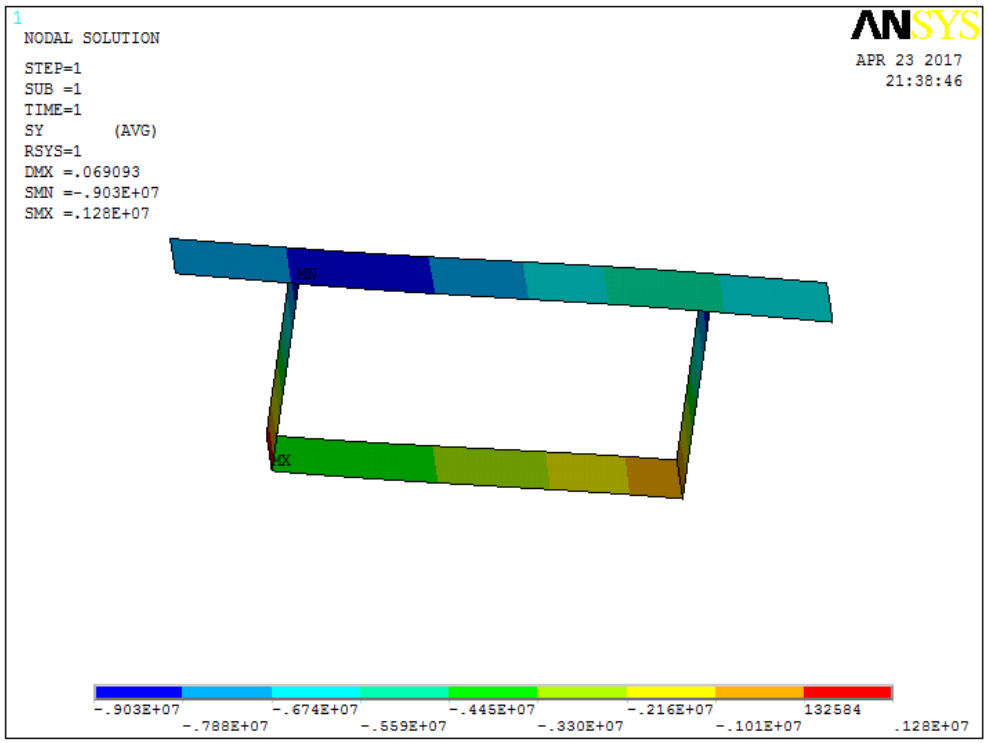

Figure (4.26) Longitudinal stresses at mid-span (gravity plus prestress, delta = 5m), case1

Table (4.2) Reactions, torsion moments, prestress, mass and stresses form the FE analysis, case1.

Delta (m)	Reaction (kN)	M_y (kN.m)	Prestress (kN)	Mass (Tonnes)	Stresses (N/mm^2)			
					Slab		Soffit	
					Interior	Exterior	Interior	Exterior
Delta =0								
g	-8240	0		840	-6.06	-6.06	8.57	8.57
p	0	0	13600	840	0.97	0.97	-11.4	-11.4
g+p	-8230	0	14800	840	-5.00	-5.00	-3.91	-3.91
Delta =1								
g	-8350	5800		851	-7.68	-6.82	9.95	8.55
p	0	0.00358	13600	851	1.14	1.00	-11.40	-10.70
g+p	-8350	5800	14900	851	-6.52	-5.96	-2.89	-2.64
Delta= 2								
g	-8490	12000		865	-7.67	-6.54	10.60	8.60
p	0	0.00746	13600	865	1.63	1.08	-12.40	-10.7
g+p	-8490	12000	15000	865	-6.25	-5.78	-2.75	-2.19
Delta 3								
g	-8630	21600		880	-8.65	-7.71	11.9	9.75
p	0	0.0117	13600	880	1.55	1.09	-12.00	-11.00
g+p	-8630	21600	15000	880	-7.11	-6.95	-1.86	-1.40
Delta = 4								
g	-8790	26300		860	-9.35	-7.87	11.30	10.90
p	0	0.0165	13600	896	1.14	0.54	-12.50	-11.00
g+p	-8790	26300	15100	896	-7.83	-6.97	-1.20	-0.09
Delta =5								
g	-8960	34700		914	-10.40	-8.66	13.00	12.10
p	0	0.0221	13600	914	1.78	0.25	-11.50	-11.40
g+p	-8960	34700	15300	914	-9.19	-7.85	1.52	0.65

4.6.1.2 Prestressing force = 35000 kN

4.6.1.2.1 Prestress calculation

Service stress in tendons

$\sigma_{ten} = 1080\ N.mm^{-2}$

Desired tension force in tendons

P = 35000 kN

Tension force in each tendon

$p = \frac{P}{2}$ $\quad p = 17500\ kN$

Area of tendon

$A = \frac{p}{\sigma_{ten}}$ $\quad A = 1.62\times10^{4}\ mm^{2}$

Steel modulus of elasticity

$E_s = 200\times10^{9}\ N.m^{-2}$

Strain in each tendon

$\varepsilon = \frac{\sigma_{ten}}{E}$ $\quad \varepsilon = 5.4\times10^{-3}$

4.6.1.2.2 Calculation of direct stresses due to (gravity, prestress and combination of stresses)

Second moment of area	I = 9.133 m^4	
Cross sectional area	A = 6.21 m^2	
Distance from soffit to centroid	Y_{bar} =1.715 m	
Concrete unit weight	ρ = 2400 kg. m^{-3}	
Depth of section	D = 3 m	
Width of deck	B = 9.6 m	
Length of deck	L = 54 m	
Acceleration	g= 9.81 m.sec^{-2}	
Moment at mid-span from gravity:		
Self-weight	W = A×ρ×g	W = 146.158 kN/m
Total mass	M = A×ρ×L	M = 8.048×10^5 kg
BM at mid-span from gravity	$M_g = \frac{W \times L^2}{8}$	M_g =5.327×10^4 kN.m
Prestressing force from all tendons	P= 35000 kN	
Eccentricity for straight tendon	ecc= 1.715 m	
Moment at midspan from prestress	M_p= P×ecc	M_p= 6.003×10^4kN.m

Gravity load stresses

$\sigma_{tg} = \frac{-M_g \times (D - Y_{Bar})}{I}$ $\quad \sigma_{tg} =$ -7.496N.mm^{-2}

$\sigma_{bg} = \frac{Mg \times Y_{Bar}}{I}$ $\quad \sigma_{bg}$ = 10.004N.mm^{-2}

Prestress stresses

$$\sigma_{tp} = \frac{P}{A} + \frac{M_p \times (D - Y_{Bar})}{I} \qquad \sigma_{tp} = 2.809 N.mm^{-2}$$

$$\sigma_{bp} = \frac{P}{A} - \frac{M_p \times Y_{Bar}}{I} \qquad \sigma_{bp} = -16.908 N.mm^{2}$$

Total stresses:

Total stresses at top $\sigma_{tg} + \sigma_{tp} = -4.686\ N.mm^{-2}$

Total stresses at bottom $\sigma_{bg} + \sigma_{bp} = -6.904\ N.mm^{-2}$

4.6.1.2.3 Description of the bridge models

The prestressing will now be taken as 35000 kN and the results will be illustrated as for the previous section i.e.

1- Straight box shell model
2- Curved box shell model

Straight box model

For the straight box shell model, there is only one case while for the curved box shell model there are six cases of curvature. The investigation carried out until δ= 6 m where tension stress started to occur. As the gravity case is the same as for the previous model refer to figures 4.15 to 4.19 for this load case.

The following figures show the load cases as follows: Prestress only Figures 4.27 to 4.29

Gravity plus prestress Figures 4.30 to 4.32

The results are summarised in table 4.3

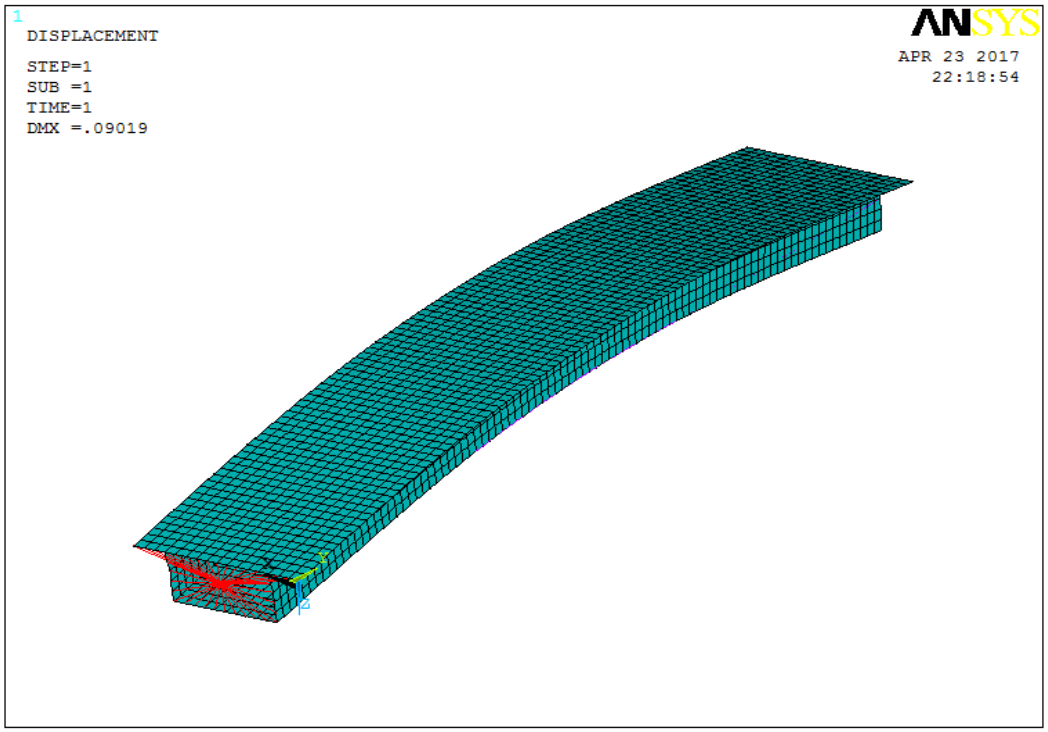

Figure (4.27) Deformed shape (straight, prestress case2)

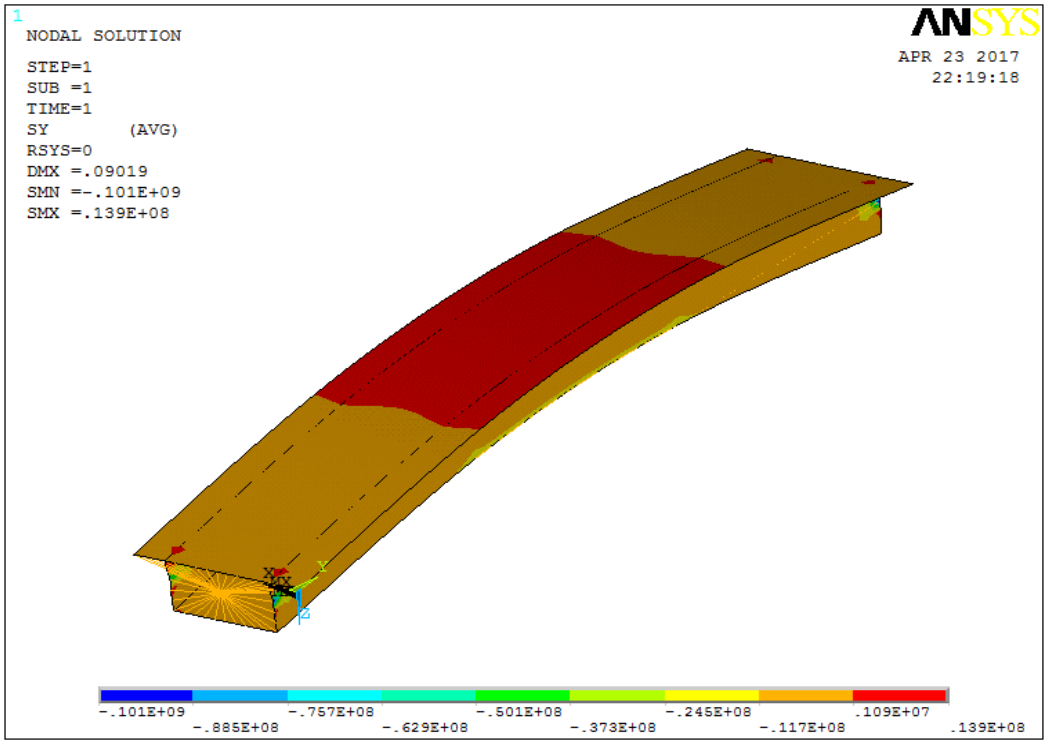

Figure (4.28) Longitudinal stresses (straight, prestress case2)

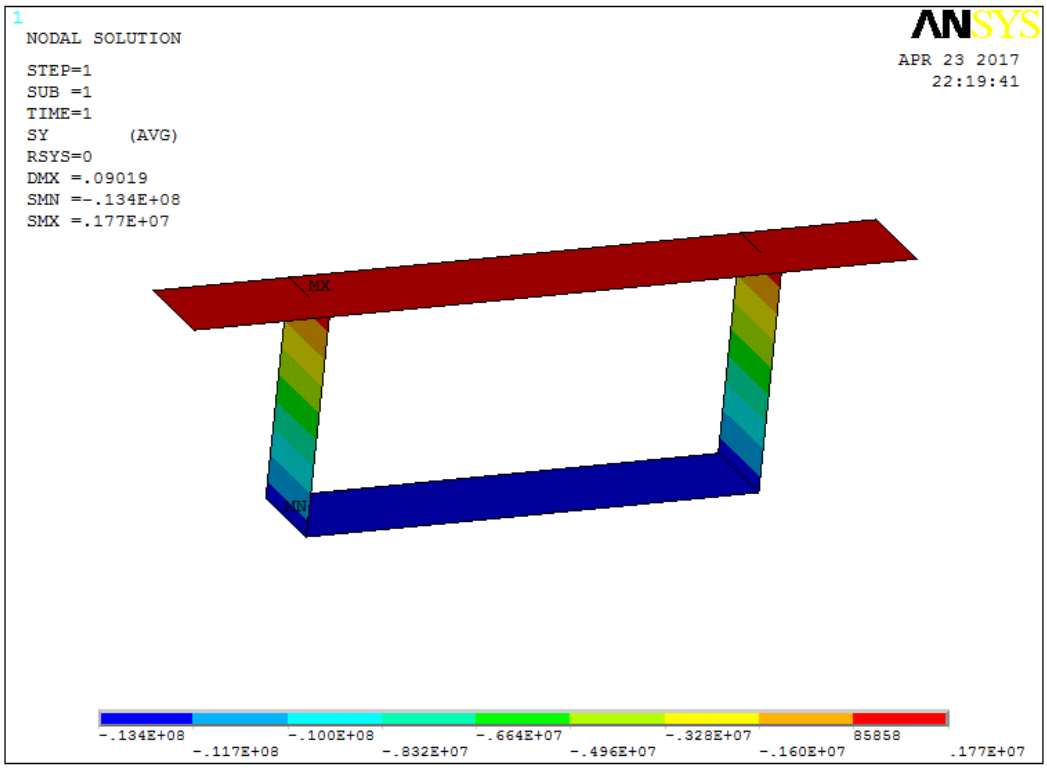

Figure (4.29) Longitudinal stresses at mid-span (straight, prestress case2)

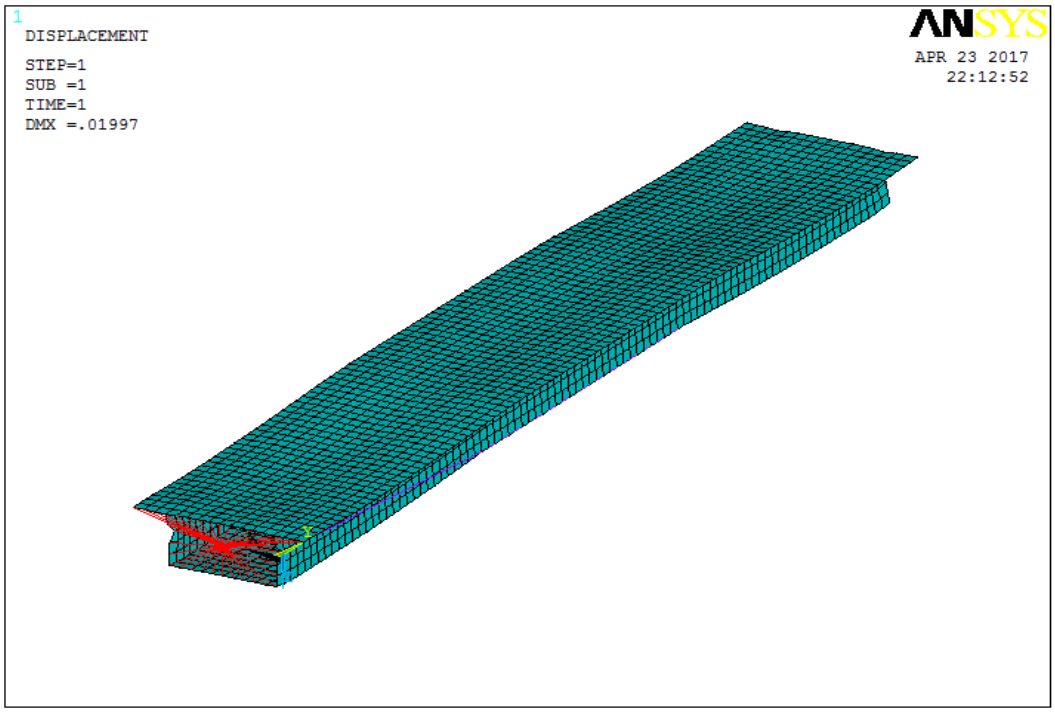

Figure (4.30) Deformed shape (straight, gravity plus prestress case2)

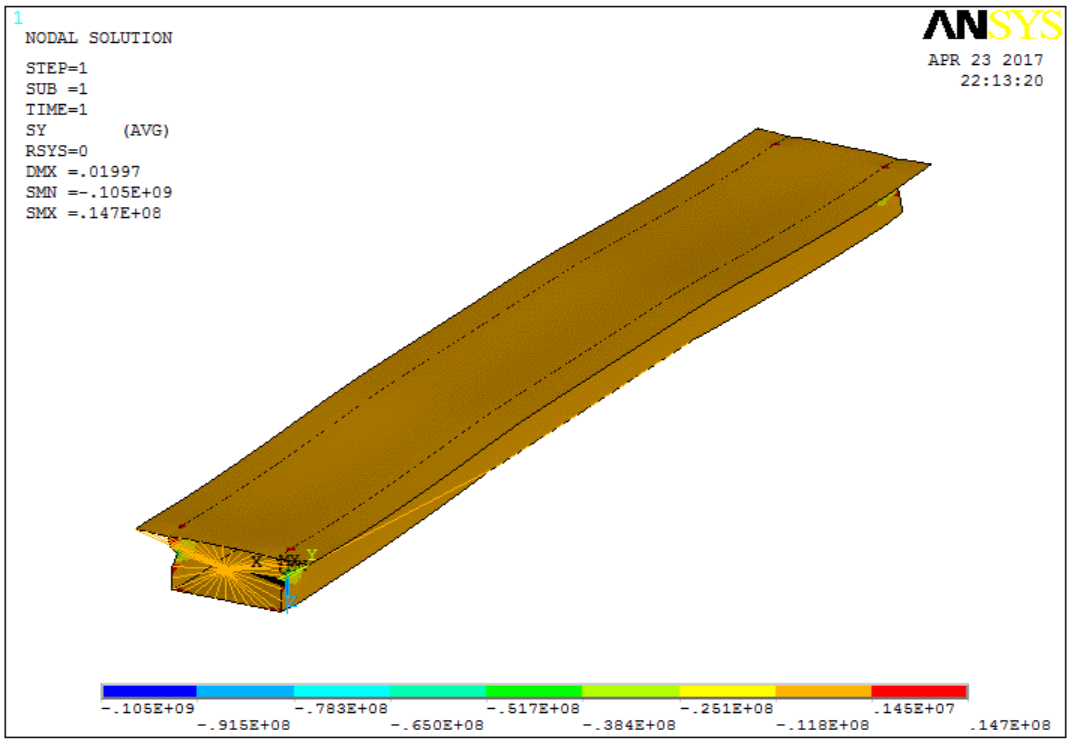

Figure (4.31) Longitudinal stresses (straight, gravity plus prestress, case 2)

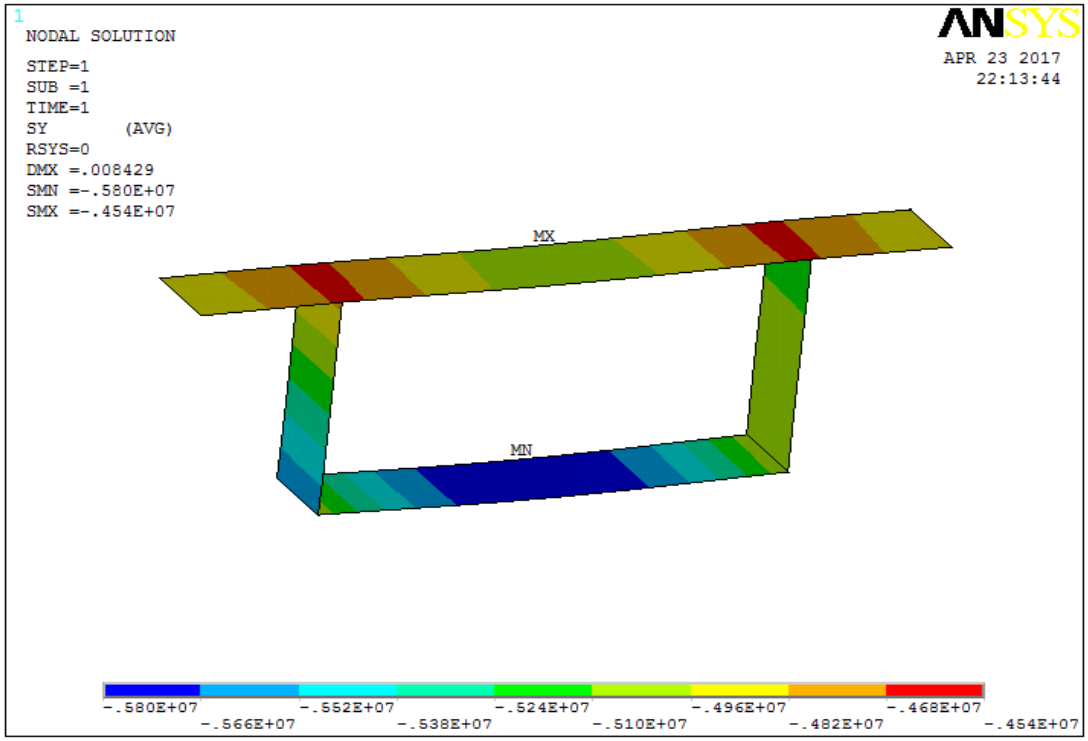

Figure (4.32) Longitudinal stresses at mid-span (straight, gravity plus prestress, case2)

Curved box shell model

As before, the results for the curved box model under the various load conditions will only be shown for the single case of curvature for the sector dimension delta = 6 m.

The following figures show these load cases as follows:

Gravity only Figures 4.33 to 4.36

Prestress only Figures 4.37 to 4.40

Gravity plus prestress Figures 4.41 to 4.43

The results are summarised in table 4.3

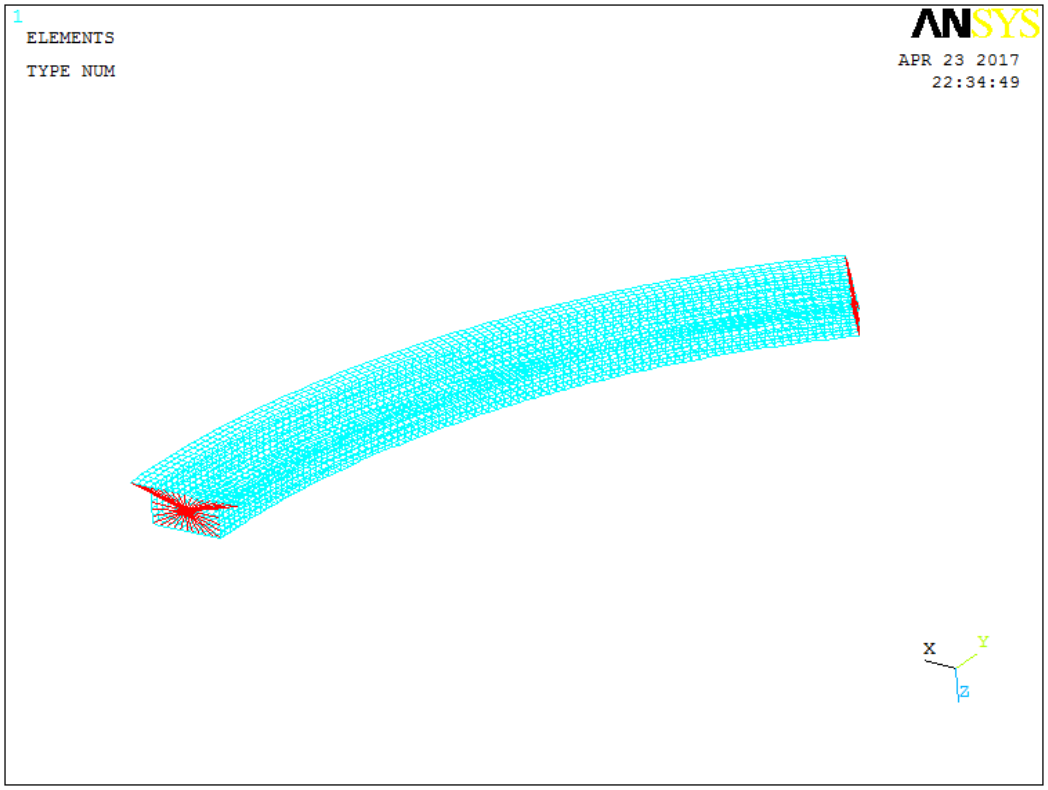

Figure (4.33) The finite element model (curved, gravity only, delta = 6m, case2)

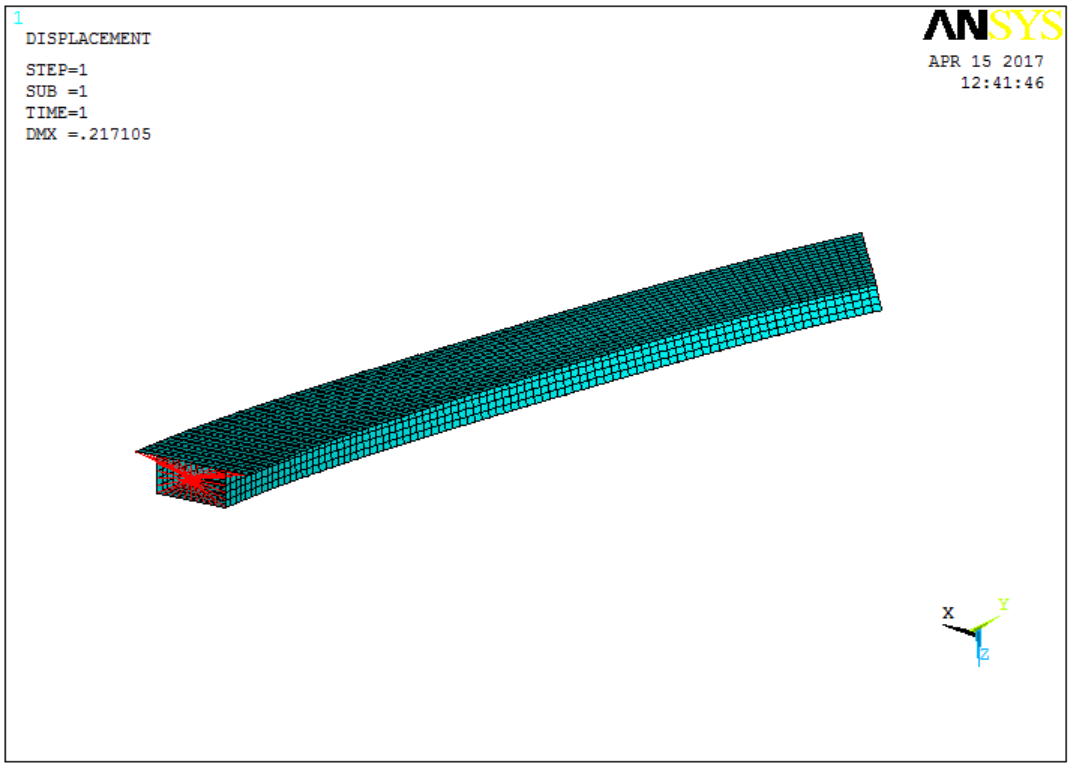

Figure (4.34) Deformed shape (curved, gravity only, delta = 6m, case2)

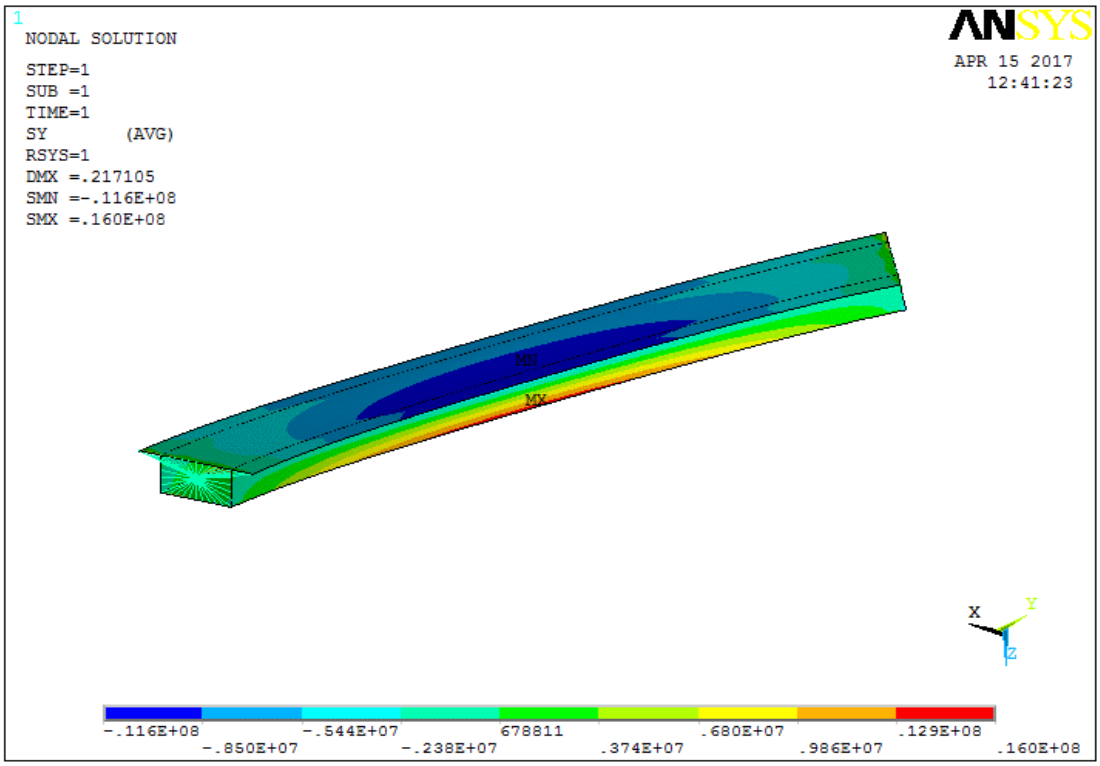

Figure (4.35) Longitudinal stresses (curved, gravity only, delta = 6m, case2)

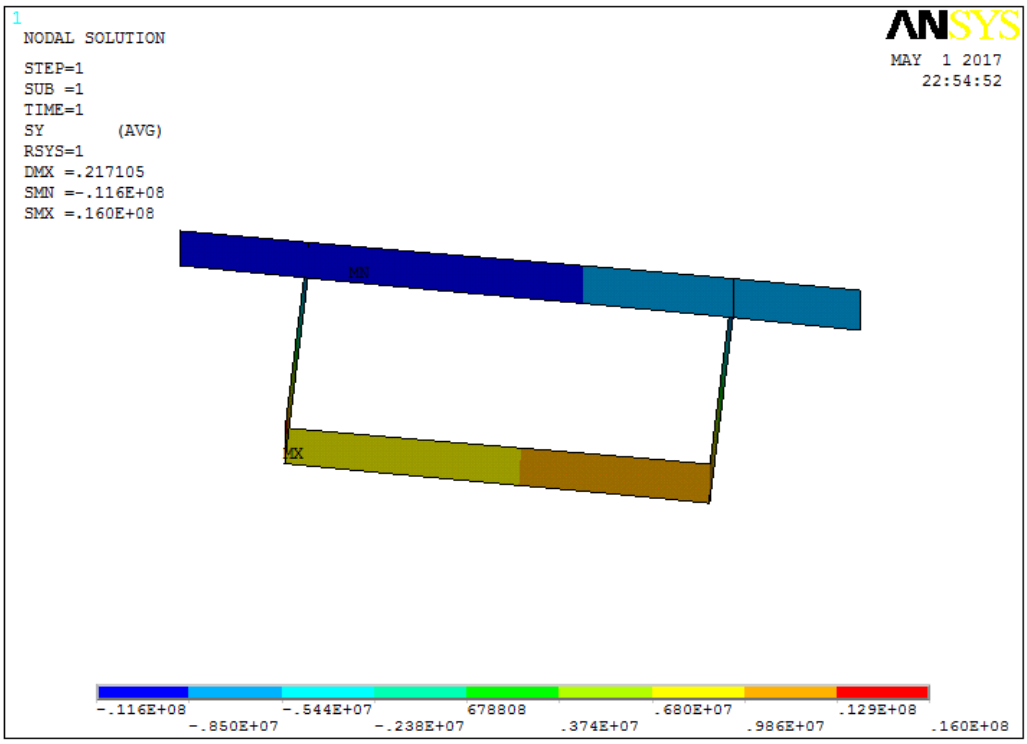

Figure (4.36) Longitudinal stresses at mid-span (curved, gravity only, delta = 6 m, case2)

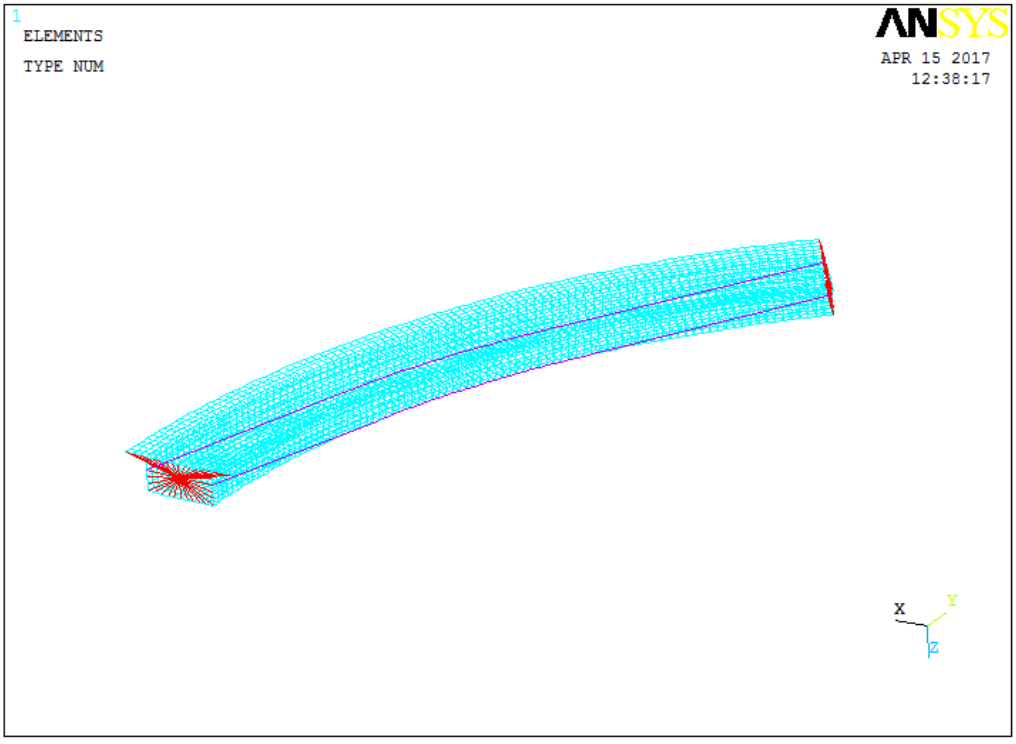

Figure (4.37) The finite element model (prestress only, curved, delta = 6 m, case2)

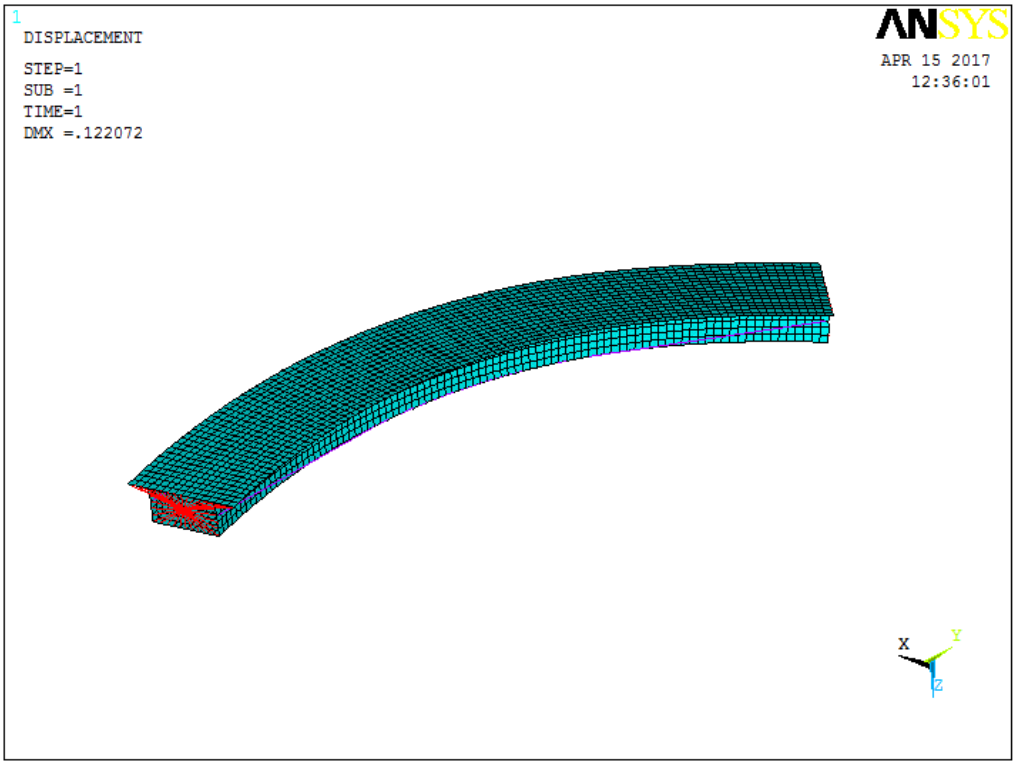

Figure (4.38) Deformed shape (prestress only, curved, delta = 6m, case2)

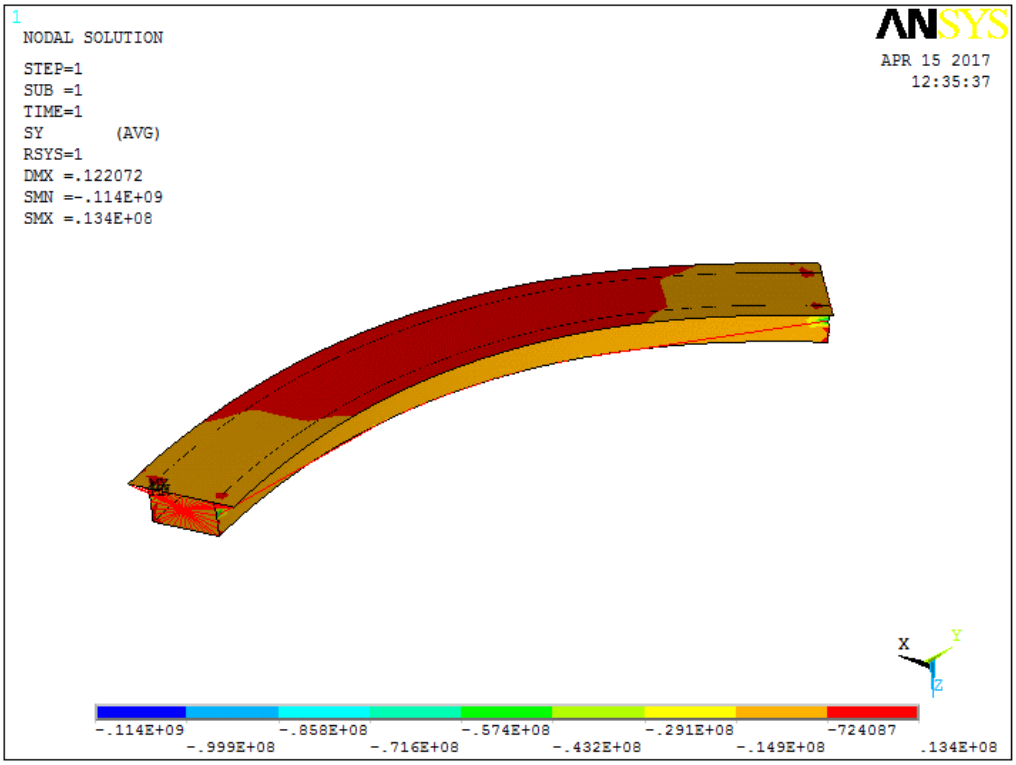

Figure (4.39) Longitudinal stresses (prestress only, curved, delta = 6 m, case2)

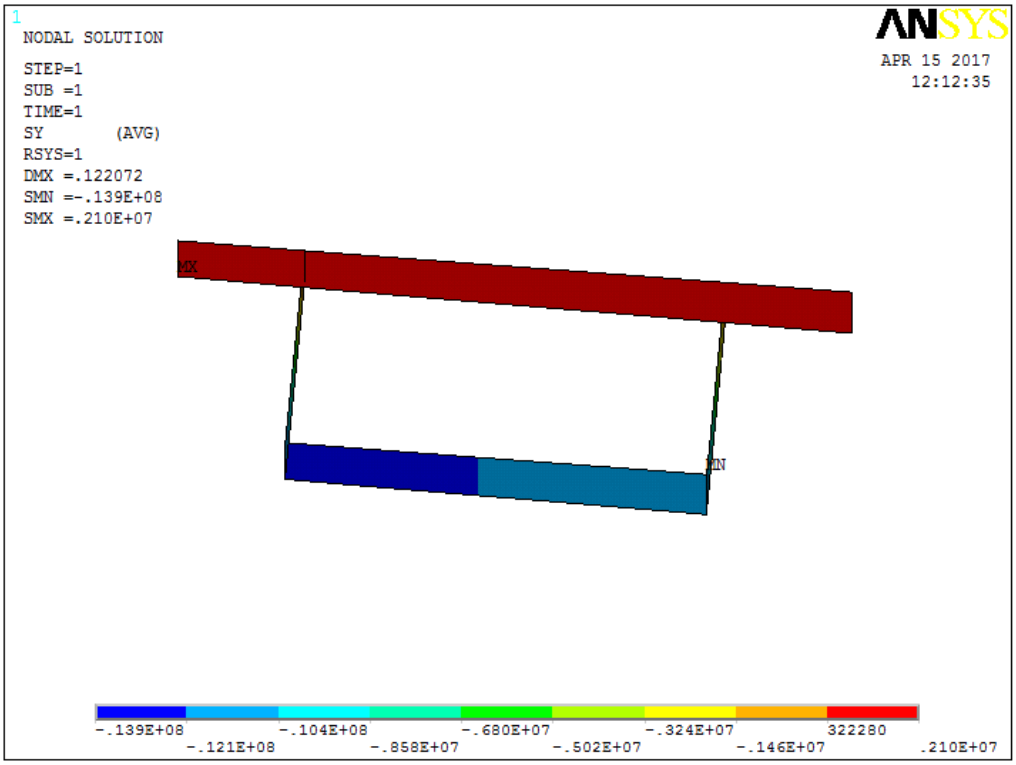

Figure (4.40) Longitudinal stresses at mid-span (prestress only, curved, delta = 6 m, case2)

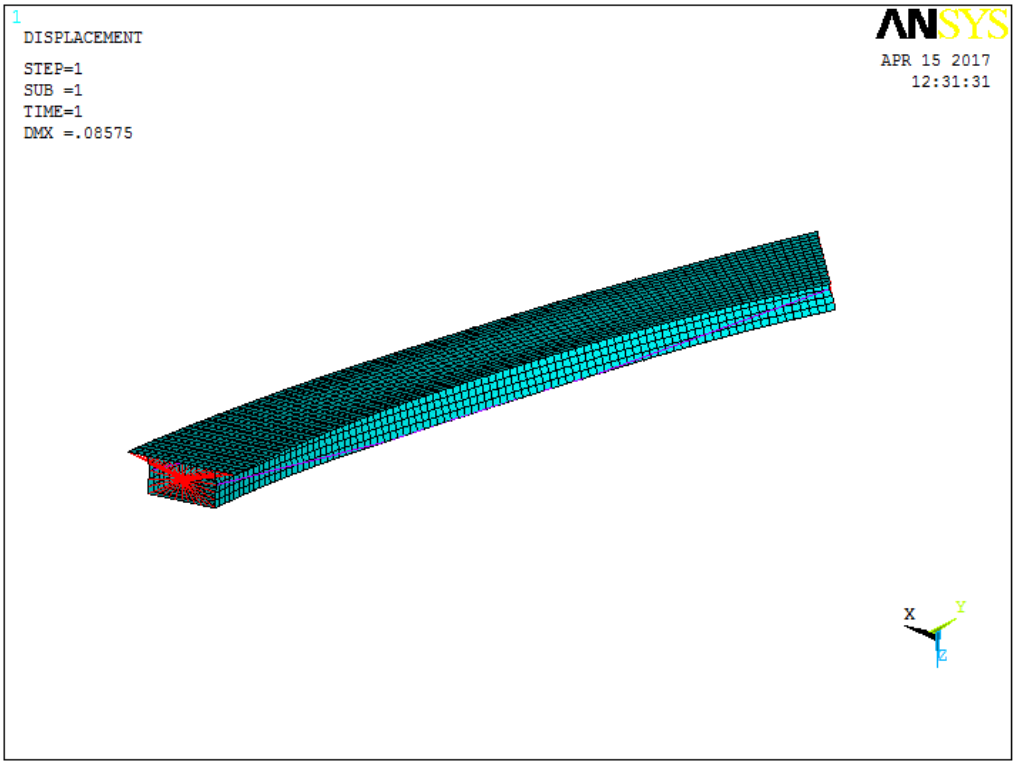

Figure (4.41) Deformed shape (prestress plus gravity, curved, delta =6 m, case2)

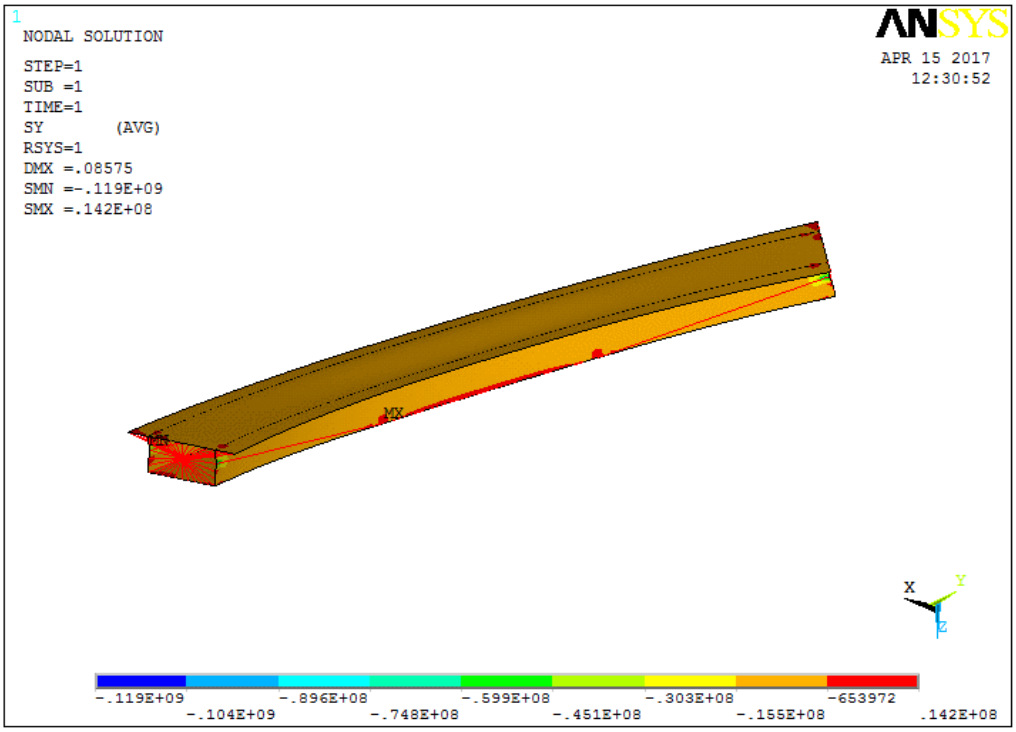

Figure (4.42) Longitudinal stresses (prestress plus gravity, curved, delta =6 m, case2)

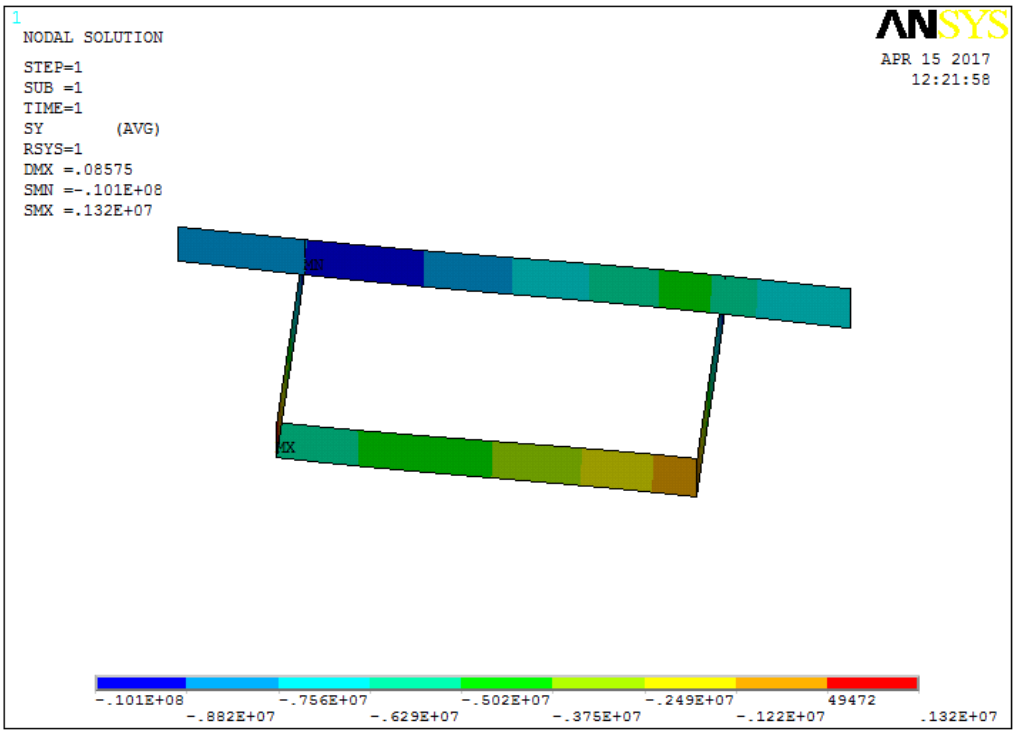

Figure (4.43) Longitudinal stresses at mid-span (prestress plus gravity, curved, delta = 6 m, case2)

Table (4.3) Reactions, torsion moments, prestress, mass and stresses form the FE analysis, case2.

Delta (m)	Reaction (kN)	M_y (kN.m)	Prestress (kN)	Mass (Tonnes)	Stresses (N/mm^2)			
					Slab		Soffit	
					Interior	Exterior	Interior	Exterior
delta =0								
g	-8240	0		840	-6.06	-6.06	8.57	8.57
p	0	0	15100	840	0.97	0.97	-11.4	-11.4
g+p	-8230	0	16500	840	-5.00	-5.00	-3.91	-3.91
delta =1								
g	-8350	5800		851	-7.68	-6.82	9.95	8.55
p	0	0.00398	15100	851	1.01	0.85	-13.44	-12.50
g+p	-8350	5800	16500	851	-6.03	-5.76	-4.87	-4.15
delta= 2								
g	-8490	12000		865	-7.67	-6.54	10.56	8.60
p	0	0.0083	15100	865	1.42	0.75	-13.67	-10.72
g+p	-8490	12000	16600	865	-6.31	-5.84	-3.85	-3.61
delta 3								
g	-8630	21600		880	-8.65	-7.71	11.88	9.75
p	0	0.013	15100	880	1.73	0.98	-13.76	-13.10
g+p	-8630	21600	16700	880	-7.03	-6.78	-3.01	-2.59
delta = 4								
g	-8790	26300		860	-9.35	-7.87	11.25	10.88
p	0	0.0184	15100	896	1.60	1.04	-13.56	-12.90
g+p	-8790	26300	16800	896	-7.88	-6.73	-2.22	-1.98
delta =5								
g	-8960	34700		914	-10.35	-8.66	13.0	12.07
p	0	0.0245	15100	914	1.62	0.53	-13.63	-12.32
g+p	-8960	34700	16900	914	-8.81	-8.20	-0.65	-0.202
delta =6								
g	-9150	44300		932	-11.78	-9.46	15.18	13.20
p	0	0.0317	15100	932	1.85	0.52	-13.80	-12.61
g+p	-9150	44300	17100	932	-9.95	-8.98	1.31	0.53

4.6.1.3 Prestressing force = 39000 kN

4.6.1.3.1 Prestress calculation

Service stress in tendons

$\sigma_{ten} = 1080\ N.mm^{-2}$

Desired tension force in each tendon
P = 39000 kN
Tension force in each tendon

$$p = \frac{P}{2} \qquad p = 19500\ kN$$

Area of tendon

$$A = \frac{p}{\sigma_{ten}} \qquad A = 1.806\times10^{4}\ mm^{2}$$

Steel modulus of elasticity

$E_s = 200\times10^{9}\ N.m^{-2}$

Strain in each tendon

$$\varepsilon = \frac{\sigma_{ten}}{E} \qquad \varepsilon = 5.4\times10^{-3}$$

4.6.1.3.2 Calculation of direct stress due to (gravity, prestress and combination of stresses)

Second moment of area	$I = 9.133\ m^4$	
Cross sectional area	$A = 6.21\ m^2$	
Distance from soffit to centroid	$Y_{bar} = 1.715$ m	
Concrete unit weight	$\rho = 2400\ kg.\ m^{-3}$	
Depth of section	D = 3 m	
Width of deck	B = 9.6 m	
Length of deck	L = 54 m	
Acceleration	$g = 9.81\ m.sec^{-2}$	

Moment at mid-span from gravity:

Self-weight	$W = A\times\rho\times g$	$W = 146.158$ kN/m
Total mass	$M = A\times\rho\times L$	$M = 8.048\times10^{5}$ kg
BM at mid-span from gravity	$M_g = \frac{W \times L^2}{8}$	$M_g = 5.327\times10^{4}$ kN.m
Prestressing force from all tendons	P= 39000 kN	
Eccentricity for straight tendon	ecc= 1.715 m	
Moment at mid-span from prestress	$M_p = P\times ecc$	$M_p = 6.689\times10^{4}$kN.m

Gravity load stresses

$$\sigma_{tg} = \frac{-M_g \times (D - Y_{Bar})}{I} \qquad \sigma_{tg} = -7.496 N.mm^{-2}$$

$$\sigma_{bg} = \frac{Mg \times Y_{Bar}}{I} \qquad \sigma_{bg} = 10.004 N.mm^{-2}$$

Prestress stresses

$$\sigma_{tp} = \frac{P}{A} + \frac{M_p \times (D - Y_{Bar})}{I} \qquad \sigma_{tp} = 3.13 N.mm^{-2}$$

$$\sigma_{bp} = \frac{P}{A} - \frac{M_p \times Y_{Bar}}{I} \qquad \sigma_{bp} = -18.84 N.mm^{2}$$

Total stresses:

Total stresses at top $\sigma_{tg} + \sigma_{tp} = -4.365 N.mm^{-2}$

Total stresses at bottom $\sigma_{bg} + \sigma_{bp} = -8.836\ N.mm^{-2}$

4.6.1.3.3 Description of the bridge models

The prestressed will be taken as 39000 kN and the results will show at the same way as in previous section which can be illustrated as:

1- Straight box shell model
2- Curved box shell model

Straight box model

For the straight box shell model, there is only one case while for the curved box shell model there are seven cases of curvature. As the gravity case is the same as for the previous model refer to figures 4.15 to 4.19 for this load case.

The following figures show the load cases as follows: Prestress only Figures 4.44 to 4.46. Gravity plus prestress Figures 4.47 to 4.49. The results are summarised in table 4.4.

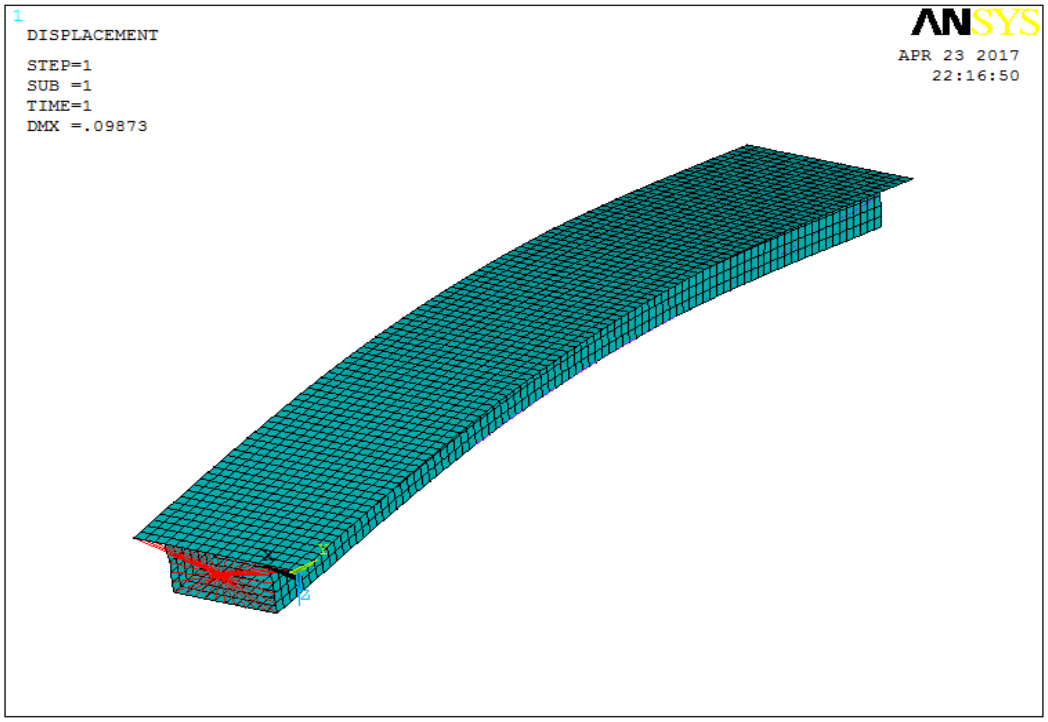

Figure (4.44) Deformed shape (straight, prestress, case3)

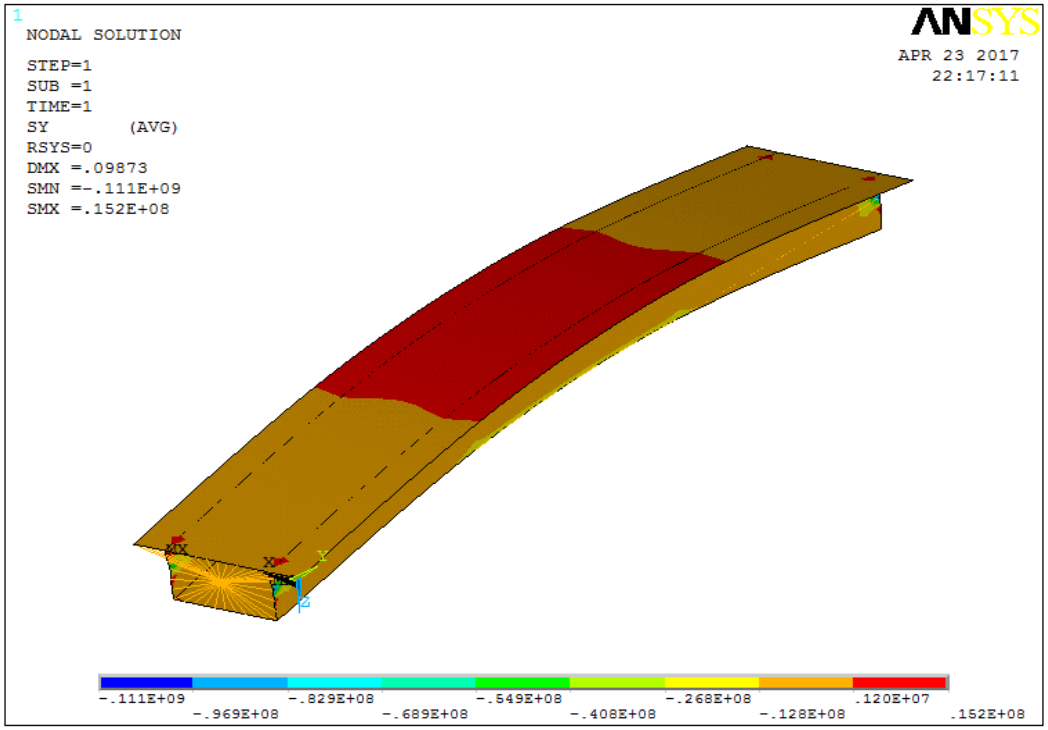

Figure (4.45) Longitudinal stresses (straight, prestress, case3)

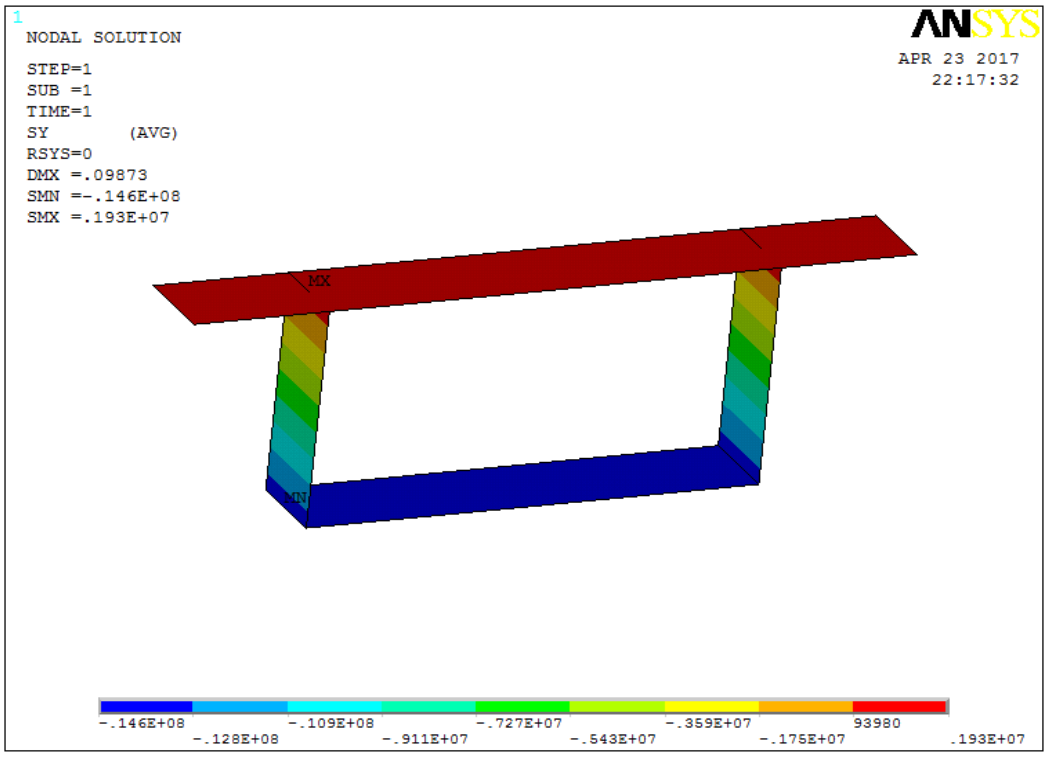

Figure (4.46) Longitudinal stresses at mid-span (straight, prestress case3)

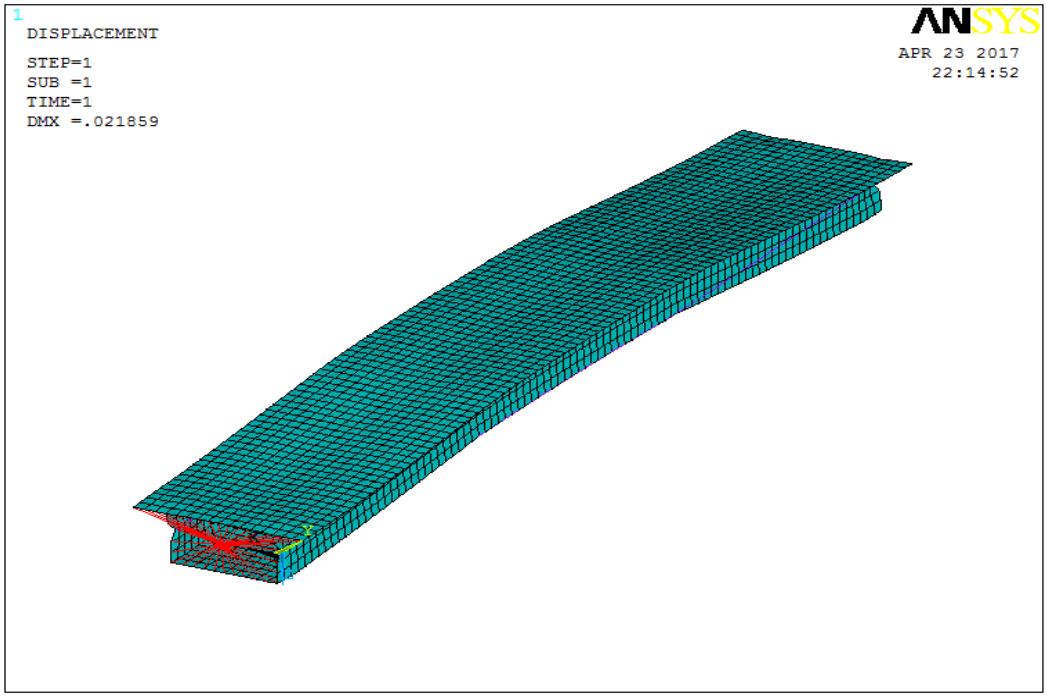

Figure (4.47) Deformed shape (straight, gravity plus prestress, case3)

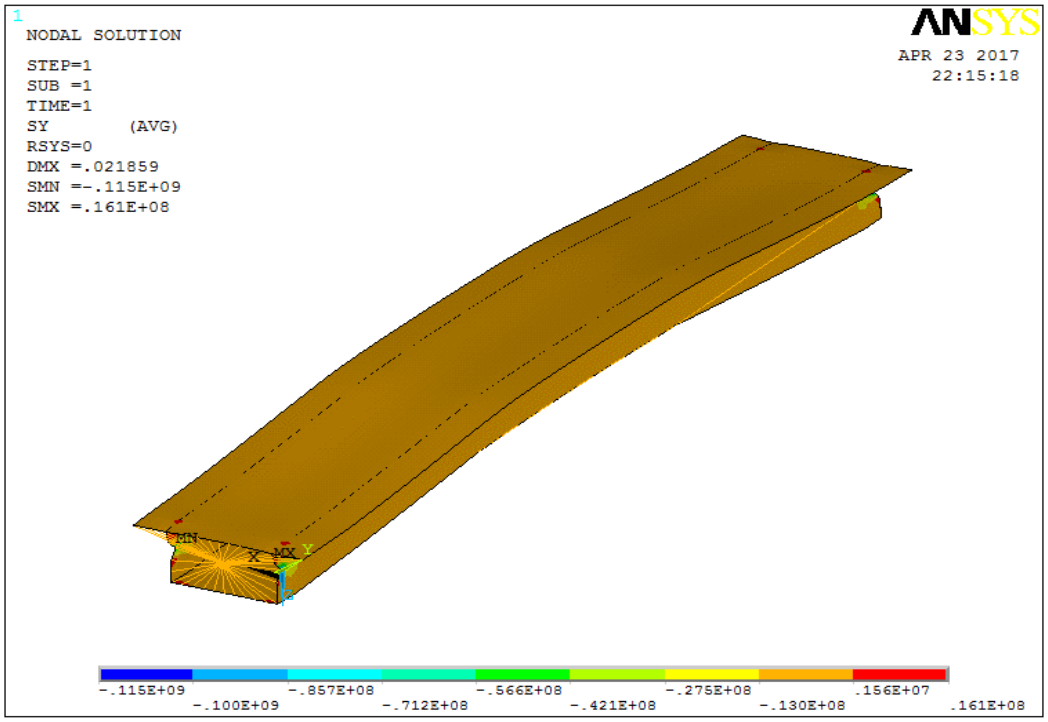

Figure (4.48) Longitudinal stresses (straight, gravity plus prestress, case3)

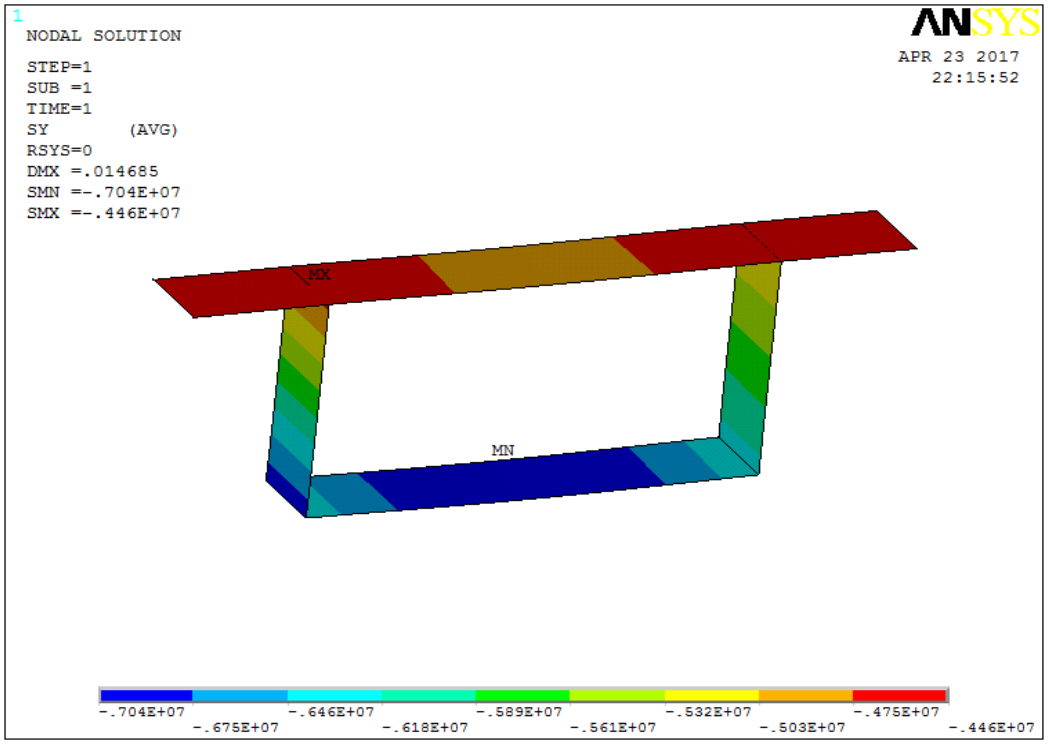

Figure (4.49) Longitudinal stresses at mid-span (straight, gravity plus prestress, case3)

Curved box shell model

As before, the results for the curved box model under the various load conditions will only be shown for the single case of curvature where the sector dimension delta = 7 m.

The following figures show these load cases as follows:

Gravity only Figures 4.50 to 4.53

Prestress only Figures 4.54 to 4.57

Gravity plus prestress Figures 4.58 to 4.60

The results are summarised in table 4.4.

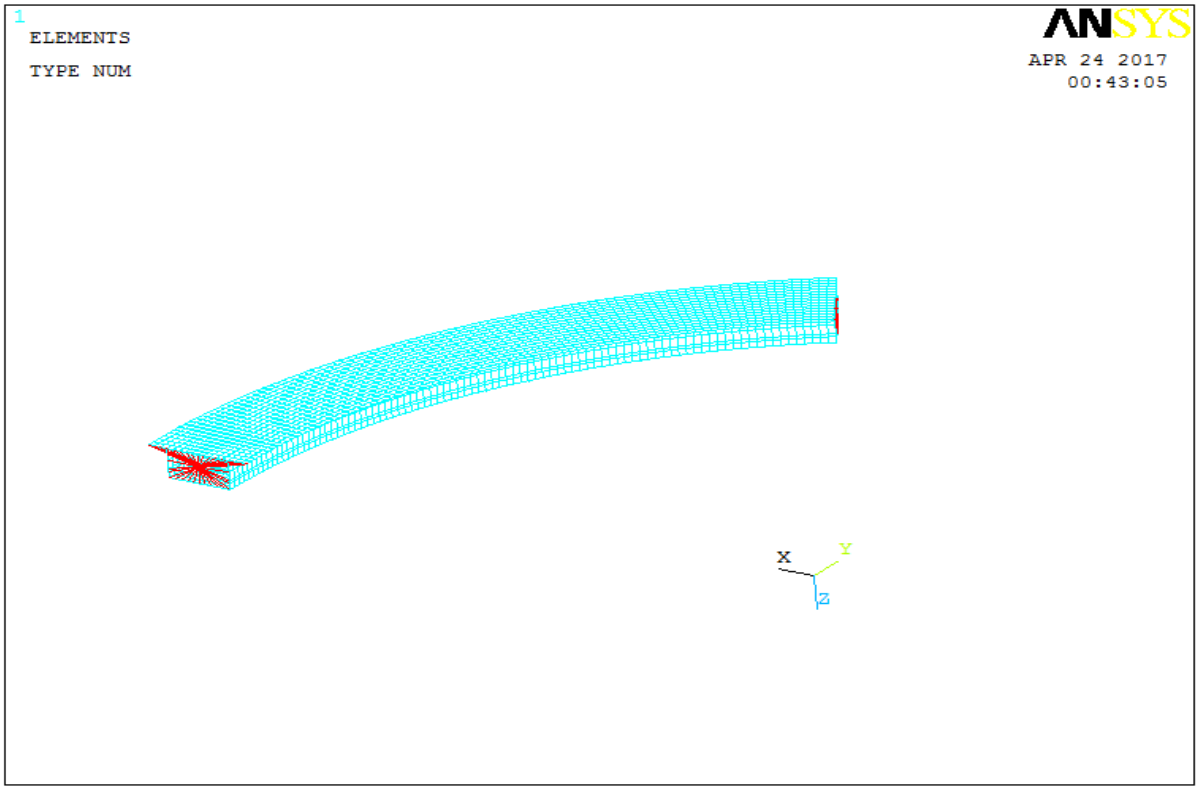

Figure (4.50) The finite element model (curved, gravity only, delta = 7m, case3)

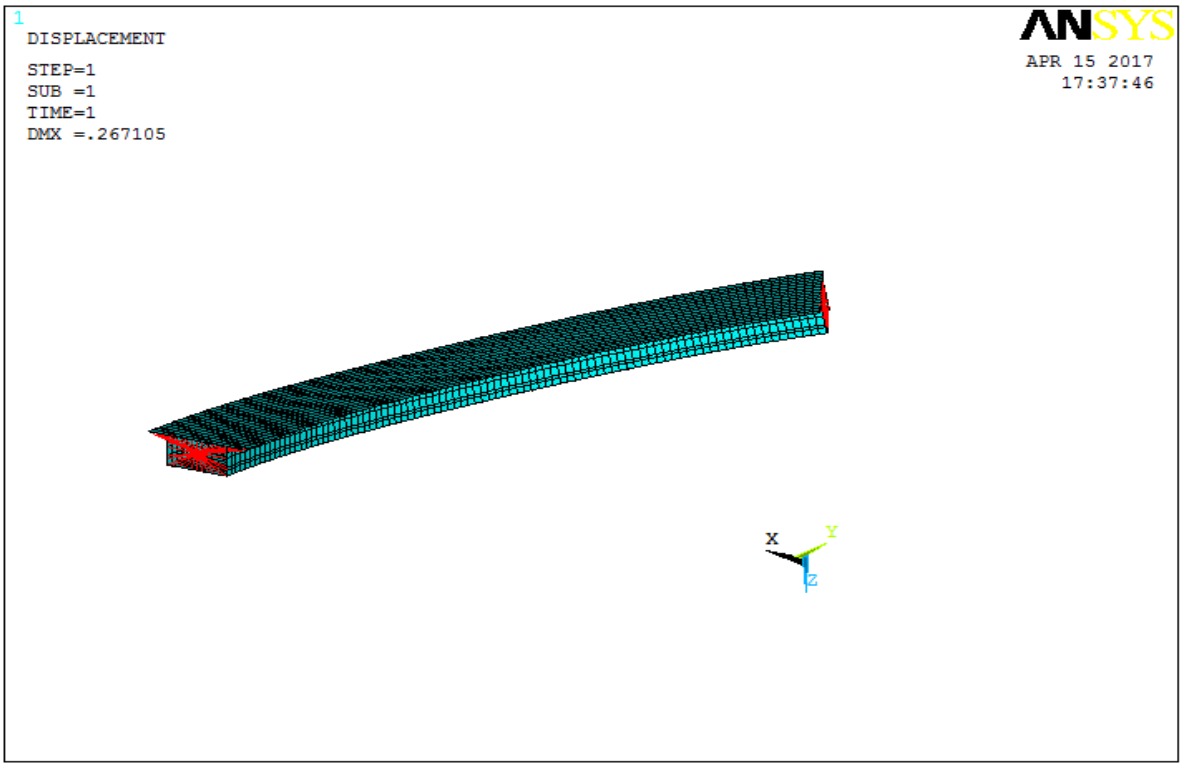

Figure (4.51) Deformed shape (curved, gravity only, delta = 7m, case3)

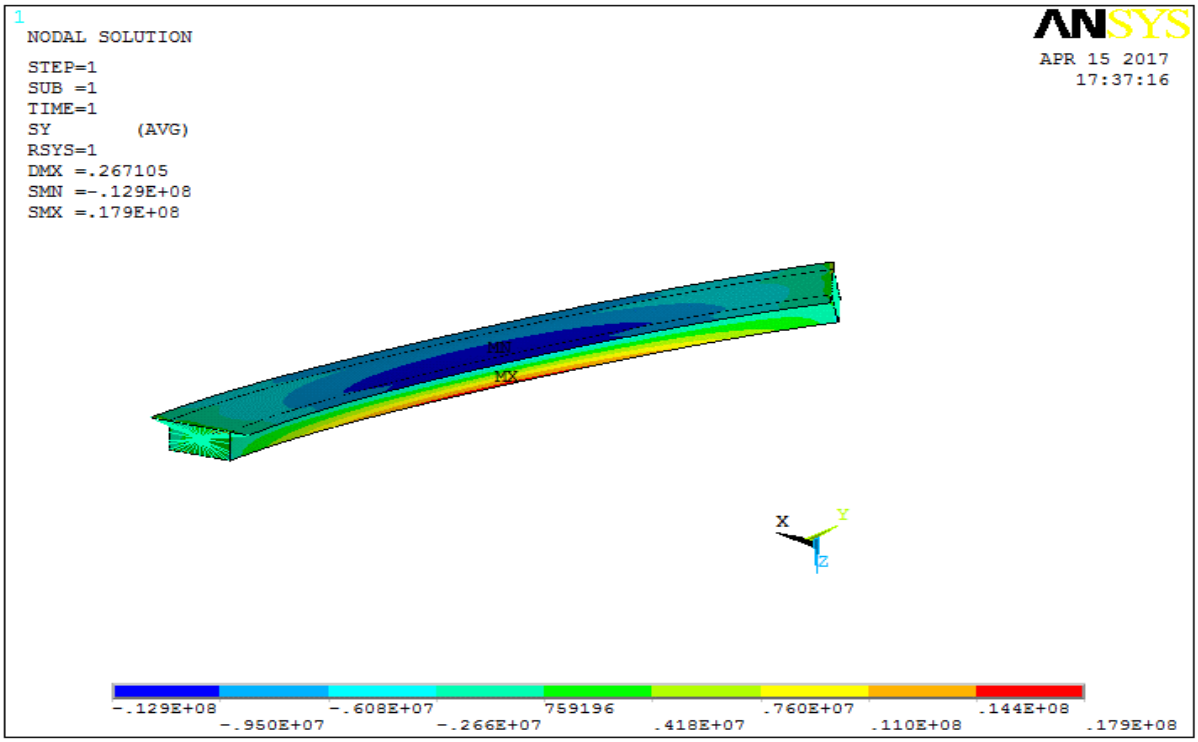

Figure (4.52) Longitudinal stresses (curved, gravity only, delta = 7m,

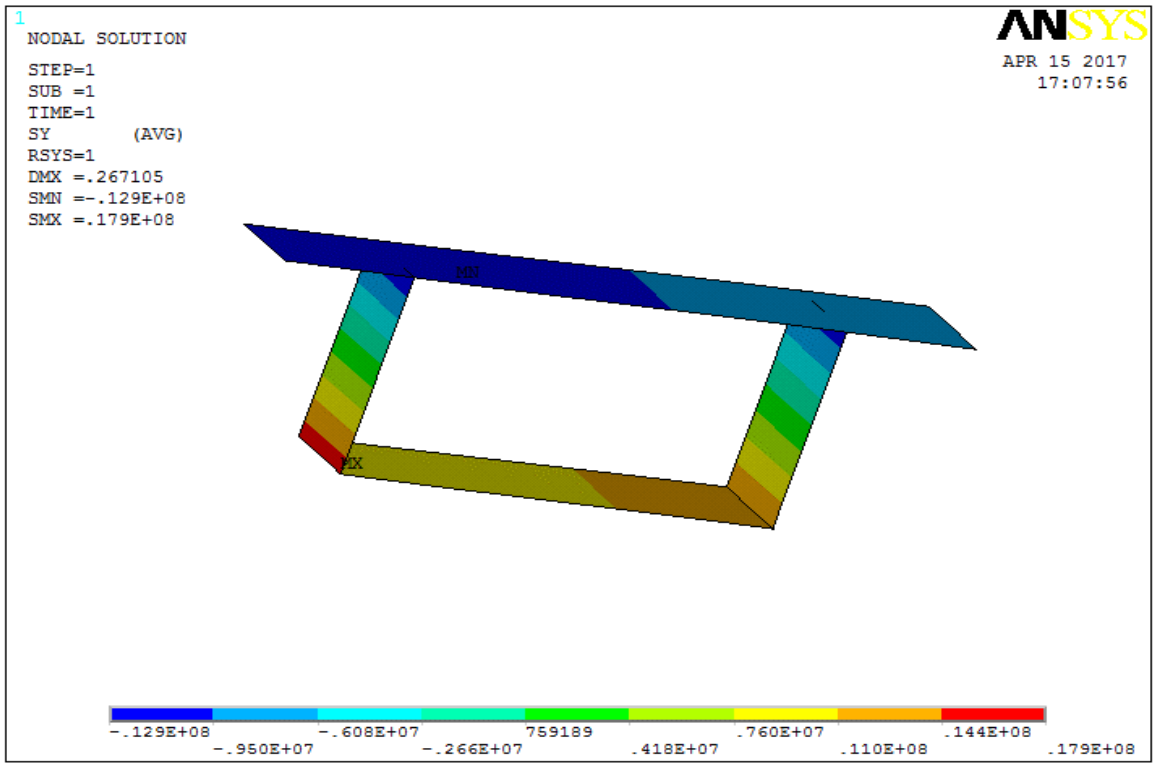

Figure (4.53) Longitudinal stresses at mid-span (curved, gravity only, delta = 7m, case3)

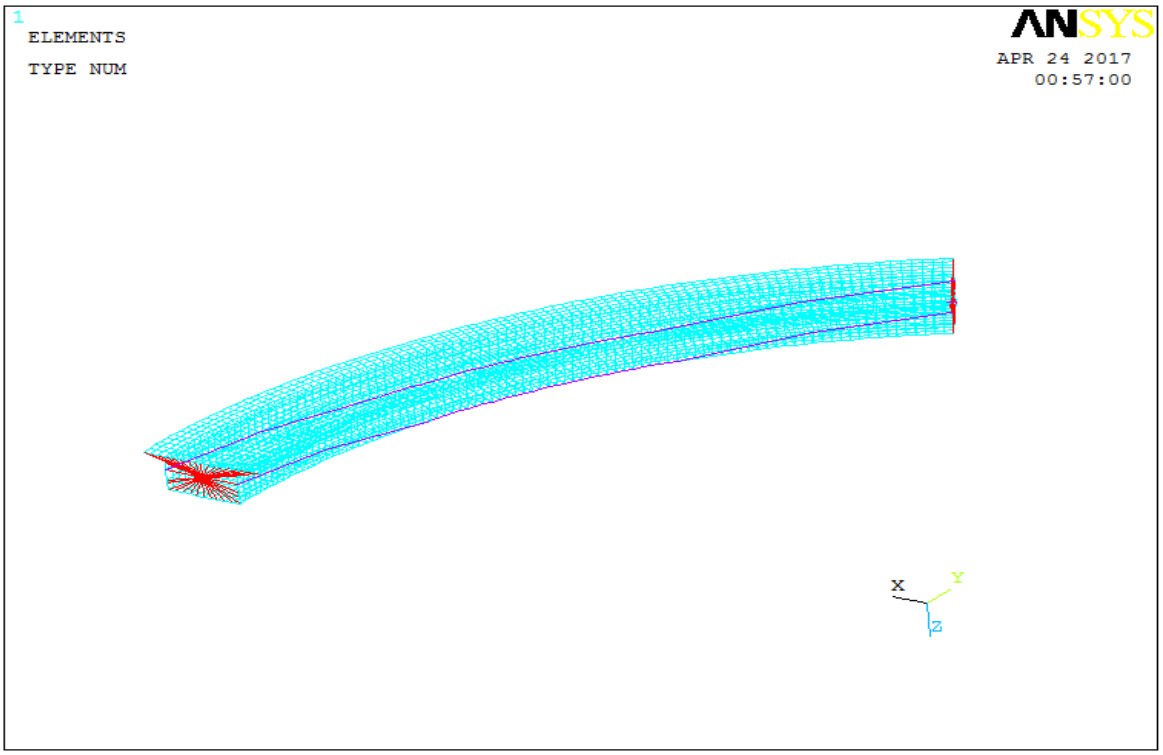

Figure (4.54) The finite element model (prestress only, curved, delta = 7 m, case3)

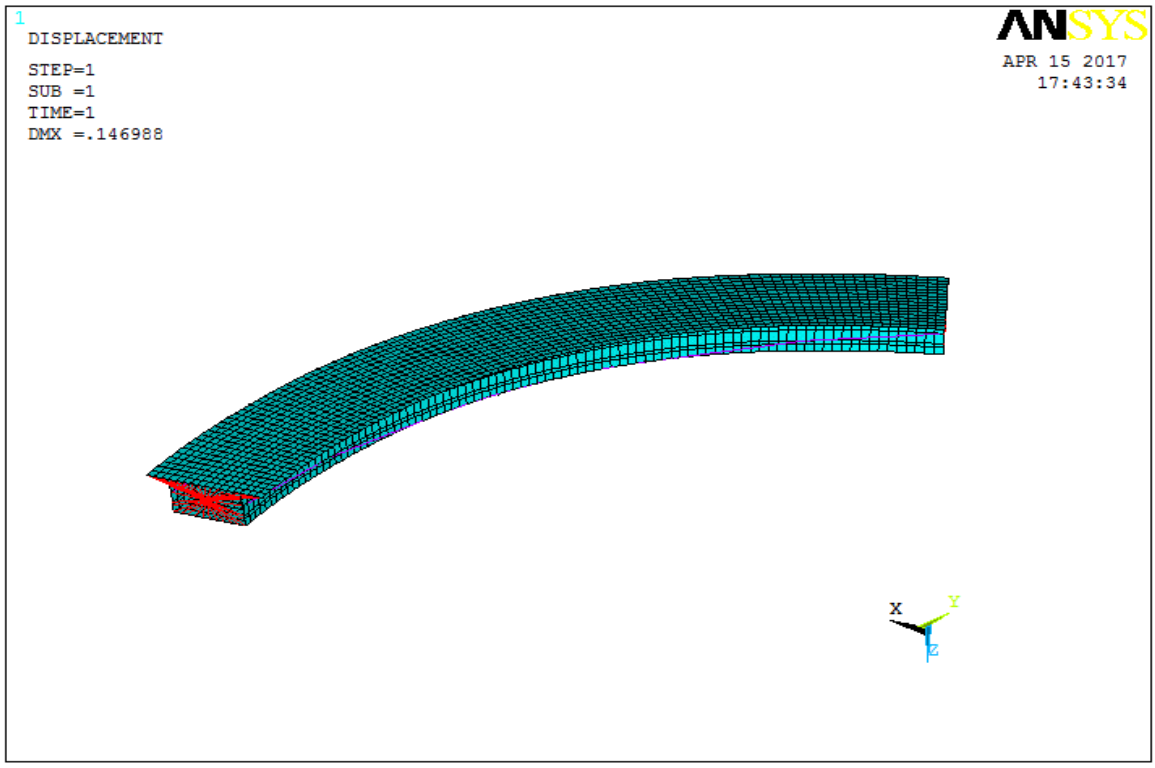

Figure (4.55) Deformed shape (prestress only, curved, delta = 7 m, case3)

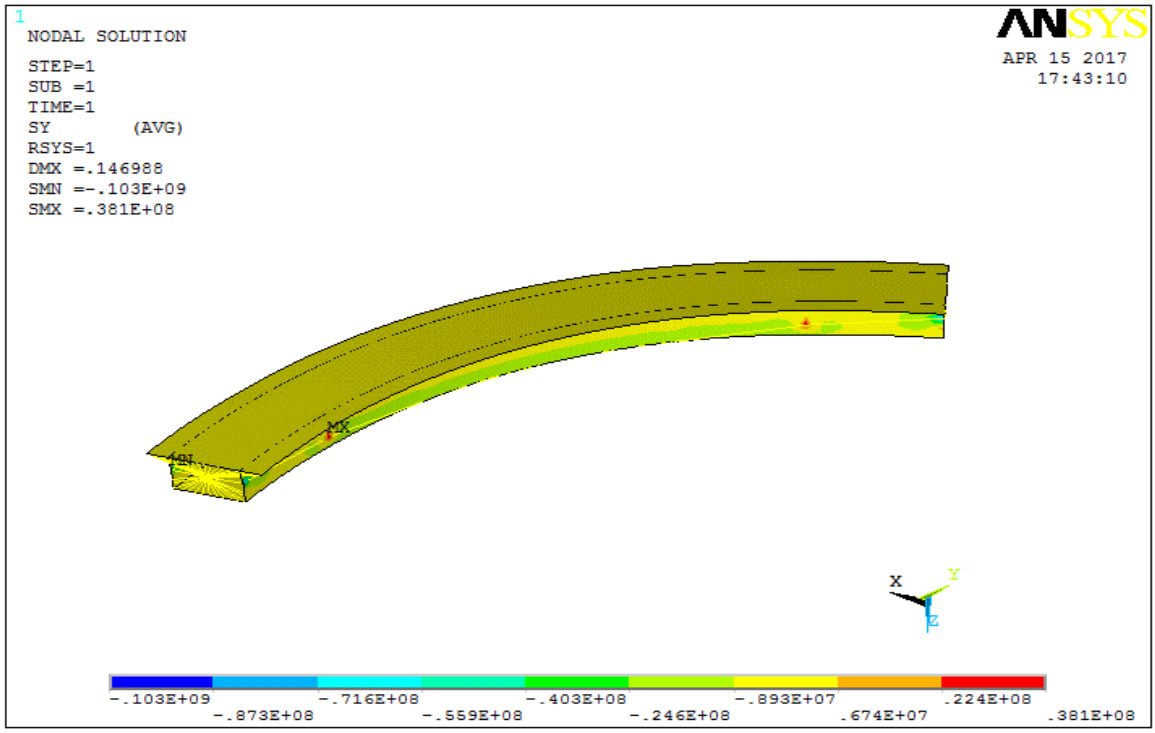

Figure (4.56) Longitudinal stresses (prestress only, curved, delta = 7 m, case3)

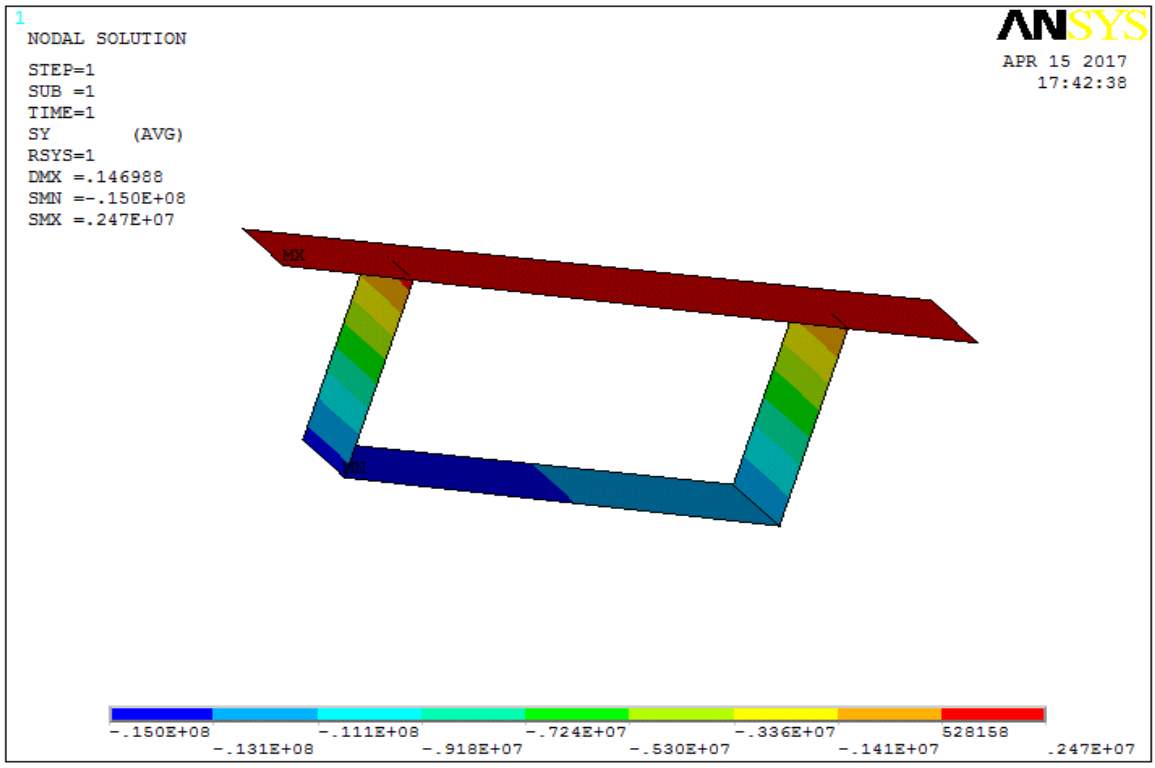

Figure (4.57) Longitudinal stresses at mid-span (prestress only, curved, delta = 7 m, case3)

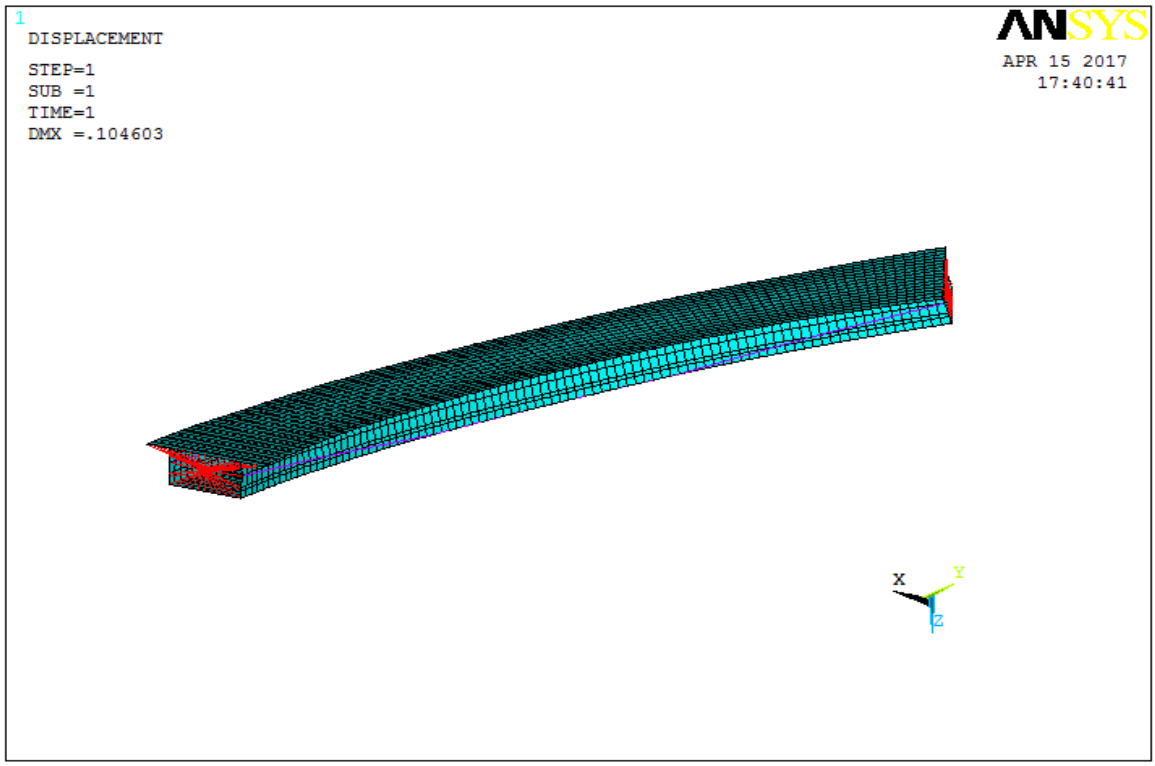

Figure (4.58) Deformed shape (prestress plus gravity, curved, delta =7 m, case3)

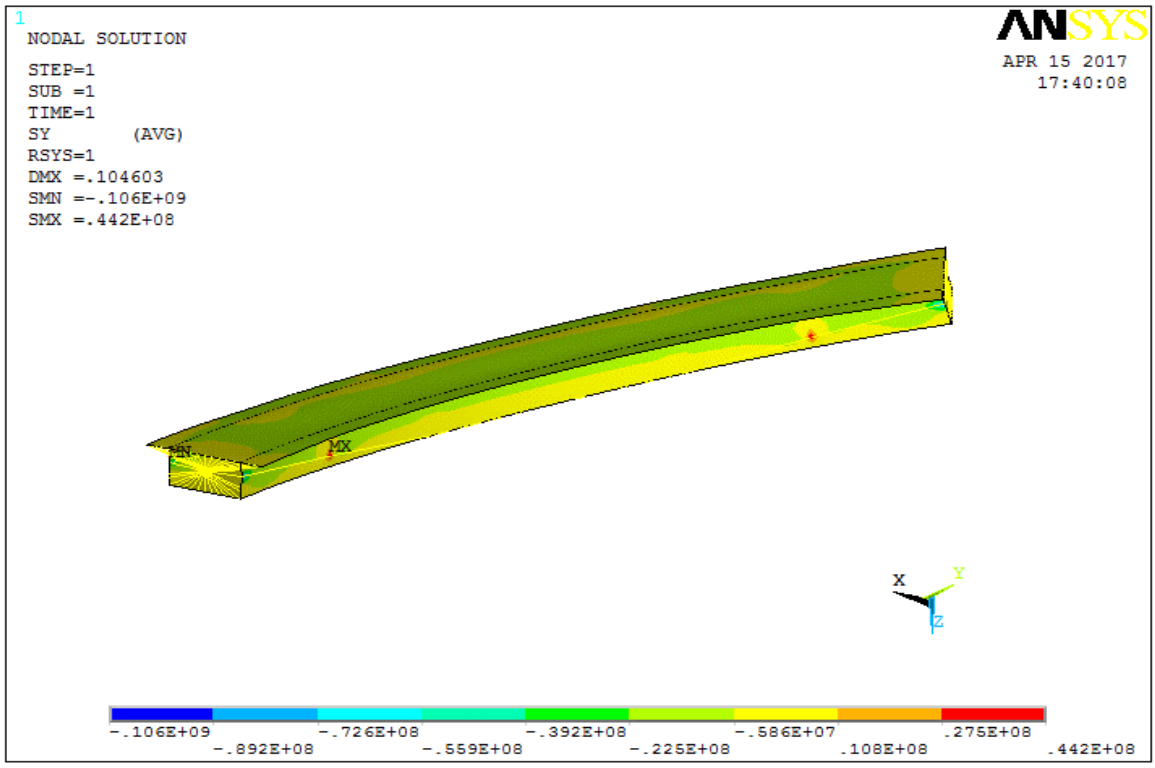

Figure (4.59) Longitudinal stresses (prestress plus gravity, curved, delta =7 m, case3)

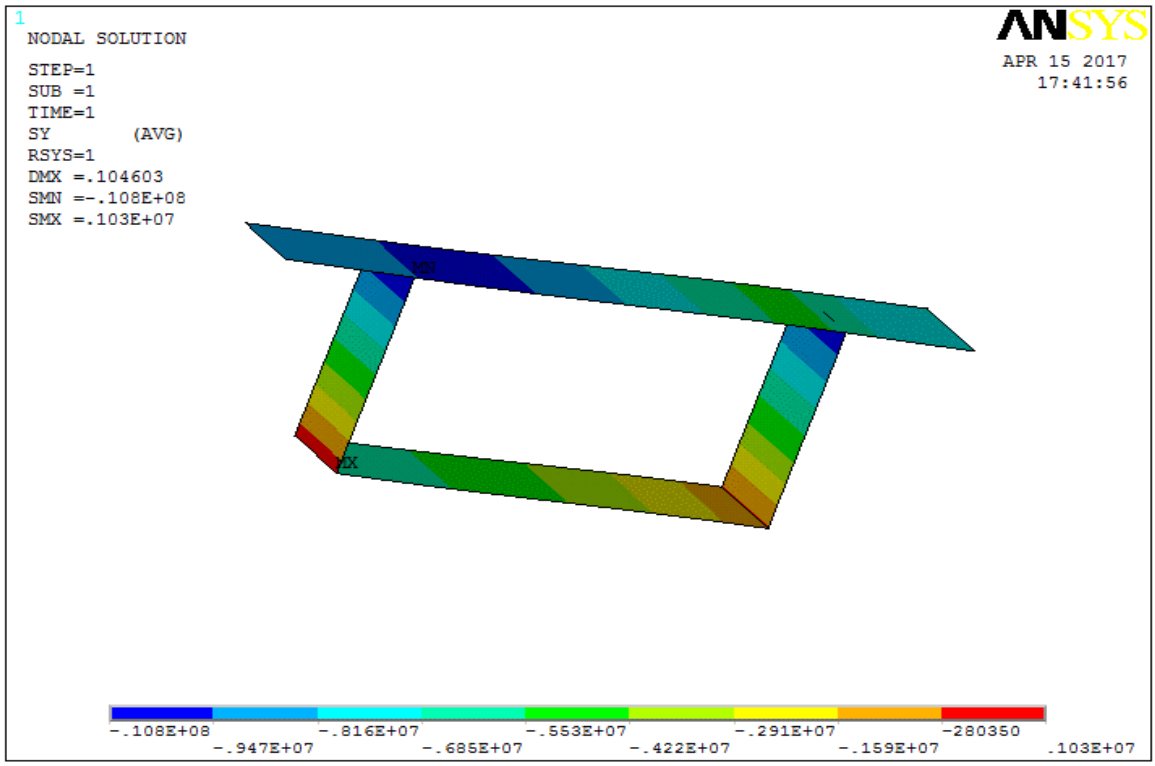

Figure (4.60) Longitudinal stresses at mid-span (prestress plus gravity, curved, delta = 7 m, case3)

Table (4.4) Reactions, torsion moments, prestress, mass and stresses form the FE analysis, case3.

Delta (m)	Reaction (kN)	M_y (kN.m)	Prestress (kN)	Mass (Tonnes)	Stresses (N/mm^2)			
					Slab		Soffit	
					Interior	Exterior	Interior	Exterior
delta =0								
g	-8240	0		840	-6.06	-6.06	8.57	8.57
p	0	0	16500	840	0.97	0.97	-11.4	-11.4
g+p	-8240	0	18000	840	-5.00	-5.00	-3.91	-3.91
delta =1								
g	-8350	5800		851	-7.68	-6.82	9.95	8.55
p	0	0.00436	16500	851	2.05	1.71	-16.55	-14.90
g+p	-8350	5800	18100	851	-5.52	-4.80	-6.71	-6.63
delta= 2								
g	-8490	12000		865	-7.67	-6.54	10.56	8.60
p	0	0.00908	16500	865	2.10	1.88	-16.83	-13.95
g+p	-8490	12000	18200	865	-5.48	-4.71	-6.40	-5.31
delta 3								
g	-8630	21600		880	-8.65	-7.71	11.88	9.75
p	0	0.0143	16500	880	2.13	1.79	-15.93	-13.83
g+p	-8630	21600	18300	880	-6.43	-6.12	-4.11	-4.02
delta = 4								
g	-8790	26300		860	-9.35	-7.87	11.25	10.88
p	0	0.0202	16600	896	1.40	0.92	-14.51	-13.19
g+p	-8790	26300	18400	896	-8.07	-6.98	-3.22	-2.37
delta =5								
g	-8960	34700		914	-10.35	-8.66	13.00	12.07
p	0	0.0269	16600	914	2.24	1.35	-15.18	-13.75
g+p	-8960	34700	18500	914	-8.20	-7.28	-2.16	-1.74
delta =6								
g	-9150	44400		932	-11.78	-9.46	15.18	13.20
p	0	0.0347	16600	932	2.21	0.96	-16.30	-13.76
g+p	-9150	44400	18700	932	-9.75	-8.59	-1.17	-0.45
delta =7								
g	-9380	55300		953	-12.85	-10.60	15.42	13.53
p	-36.8	218	16600	953	2.45	1.82	-14.35	-13.08
g+p	-9380	55300	18900	953	-10.31	-8.75	1.02	0.39

4.6.1.4 Prestressing force = 45000 kN

4.6.1.4.1 Prestress calculation

Service stress in tendons

$\sigma_{ten} = 1080\ N.mm^{-2}$

Desired tension force in tendons

P = 45000 kN

Tension force in each tendon

$p = \frac{P}{2}$ p =22500 kN

Area of tendon

$A = \frac{P}{\sigma_{ten}}$ $A = 2.083\times10^{4}\ mm^{2}$

Steel modulus of elasticity

$E_s = 200\times10^{9}\ N.m^{-2}$

Strain in each tendon

$\varepsilon = \frac{\sigma_{ten}}{E}$ $\varepsilon = 5.4\times10^{-3}$

4.6.1.4.2 Calculation of direct stress due to (gravity, prestress and combination of stresses)

Second moment of area	$I = 9.133\ m^4$	
Cross sectional area	$A = 6.21\ m^2$	
Distance from soffit to centroid	Y_{bar} =1.715 m	
Concrete unit weight	$\rho = 2400\ kg.\ m^{-3}$	
Depth of section	D = 3 m	
Width of deck	B = 9.6 m	
Length of deck	L = 54 m	
Acceleration	$g = 9.81\ m.sec^{-2}$	
Moment at mid-span from gravity:		
Self-weight	$W = A\times\rho\times g$	W = 146.158 kN/m
Total mass	$M = A\times\rho\times L$	$M = 8.048\times10^{5}$ kg
BM at mid-span from gravity	$M_g = \frac{W \times L^2}{8}$	$M_g = 5.327\times10^{4}$ kN.m
Prestressing force from all tendons	P= 45000 kN	
Eccentricity for straight tendon	ecc= 1.715 m	
Moment at mid-span from prestress	$M_p = P\times ecc$	$M_p = 7.718\times10^{4}$kN.m

Gravity load stresses

$\sigma_{tg} = \frac{-M_g \times (D - Y_{Bar})}{I}$ $\sigma_{tg} =$ -7.496N.mm^{-2}

$$\sigma_{bg} = \frac{\mathbf{Mg} \times \mathbf{Y_{Bar}}}{\mathbf{I}}$$ σ_{bg}= 10.004N.mm^{-2}

Prestress stresses

$$\sigma_{tp} = \frac{\mathbf{P}}{\mathbf{A}} + \frac{\mathbf{M_p} \times (\mathbf{D} - \mathbf{Y_{Bar}})}{\mathbf{I}}$$ σ_{tp} = 3.612N.mm^{-2}

$$\sigma_{bp} = \frac{\mathbf{P}}{\mathbf{A}} - \frac{\mathbf{M_p} \times \mathbf{Y_{Bar}}}{\mathbf{I}}$$ $\sigma_{bp} = -21.738\mathbf{N.mm^2}$

Total stresses:

Total stresses at top $\sigma_{tg} + \sigma_{tp} = -3.884\ \mathbf{N.mm^{-2}}$

Total stresses at bottom $\sigma_{bg} + \sigma_{bp} = -11.734\mathbf{N.mm^{-2}}$

4.6.1.4.3 Description of the bridge models

The last prestress was taken as 45000 kN and the results are shown in the same way as in previous section i.e.:

1- Straight box shell model
2- Curved box shell model

Straight box model

For the straight box shell model, there is only one case while for the curved box shell model there are eight cases of curvature where tension stresses started to show. As the gravity case is the same as for the previous model refer to figures 4.15 to 4.19 for this load case.

The following figures show the load cases as follows: Prestress only Figures 4.61 to 4.63.

Gravity plus prestress Figures 4.64 to 4.66.

The results are summarised in table 4.5.

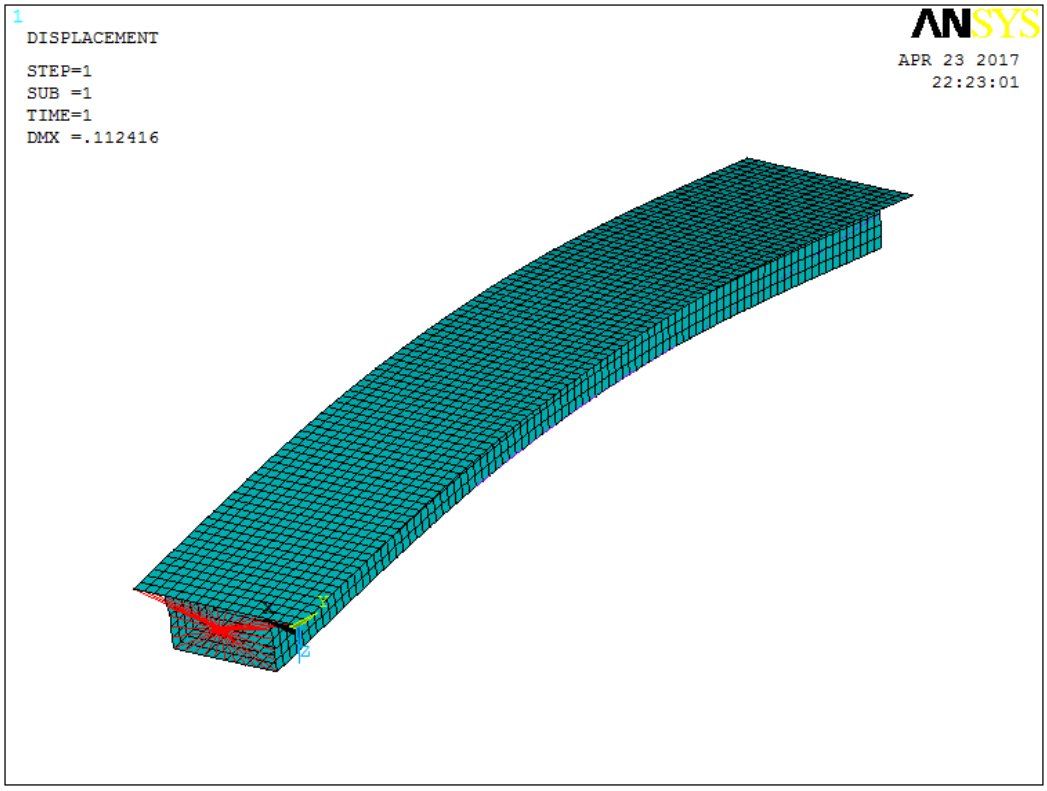

Figure (4.61) Deformed shape (straight, prestress, case4)

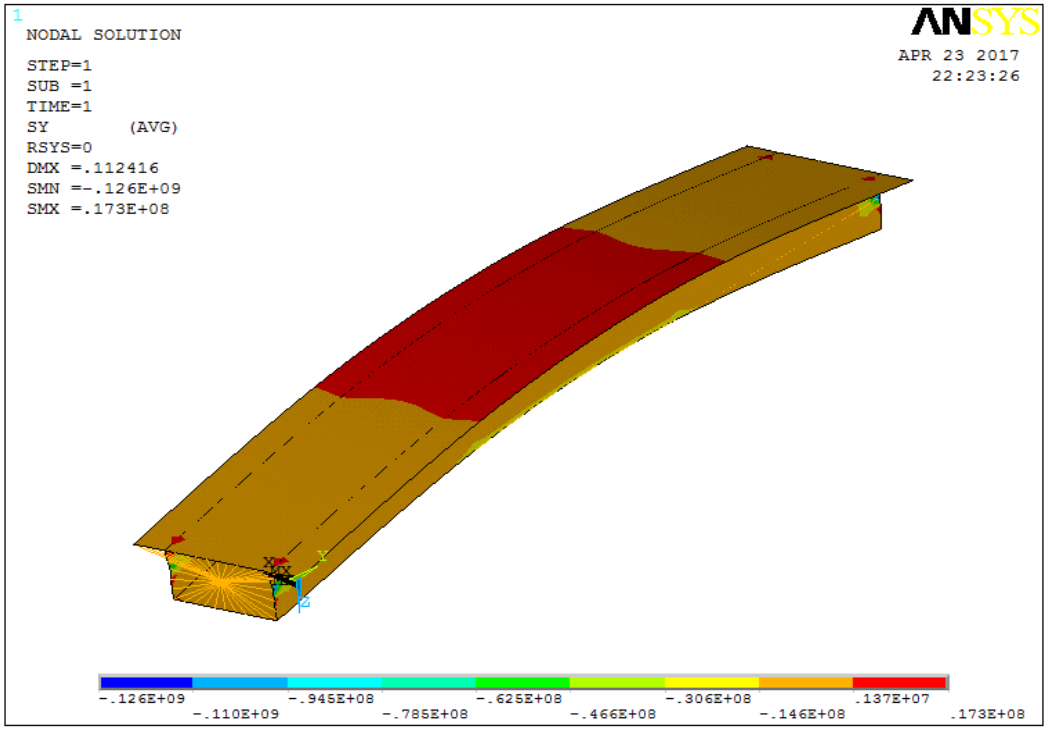

Figure (4.62) Longitudinal stresses (straight, prestress, case4)

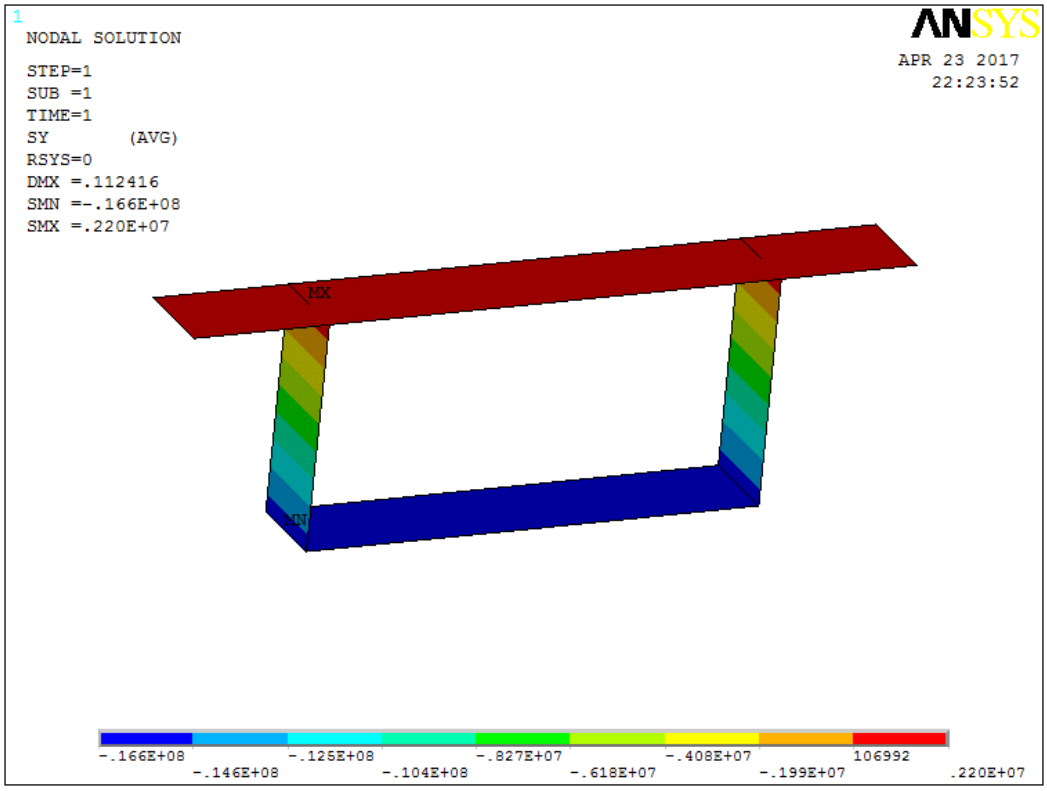

Figure (4.63) Longitudinal stresses at midspan (straight, prestress, case4)

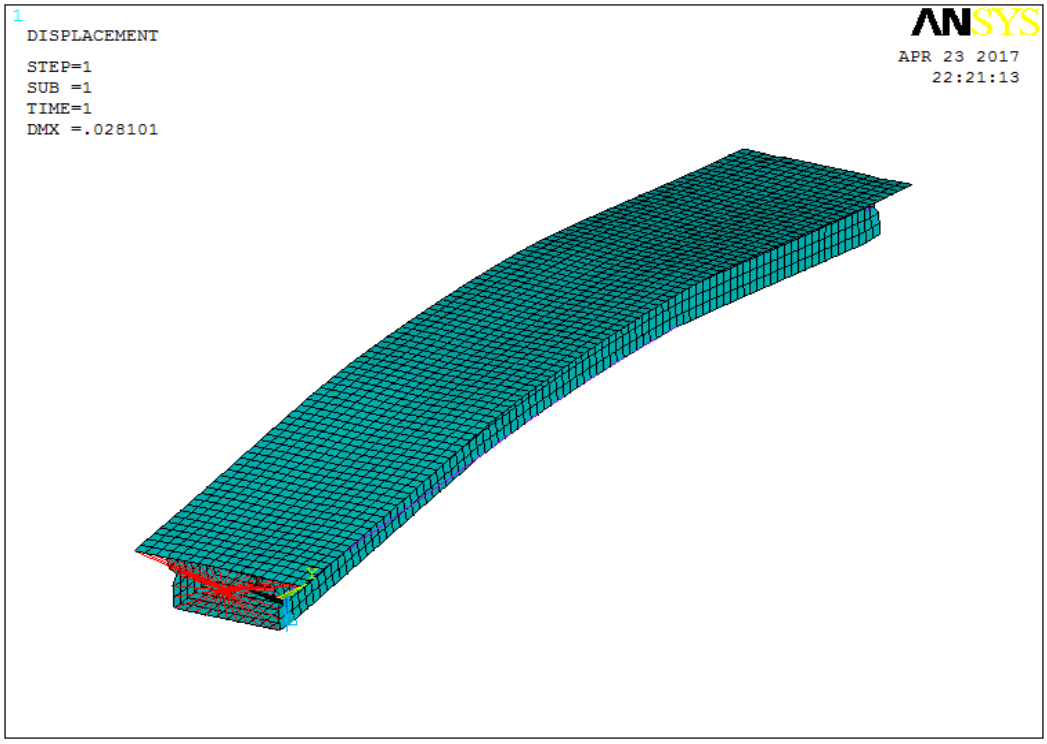

Figure (4.64) Deformed shape (straight, gravity plus prestress, case4)

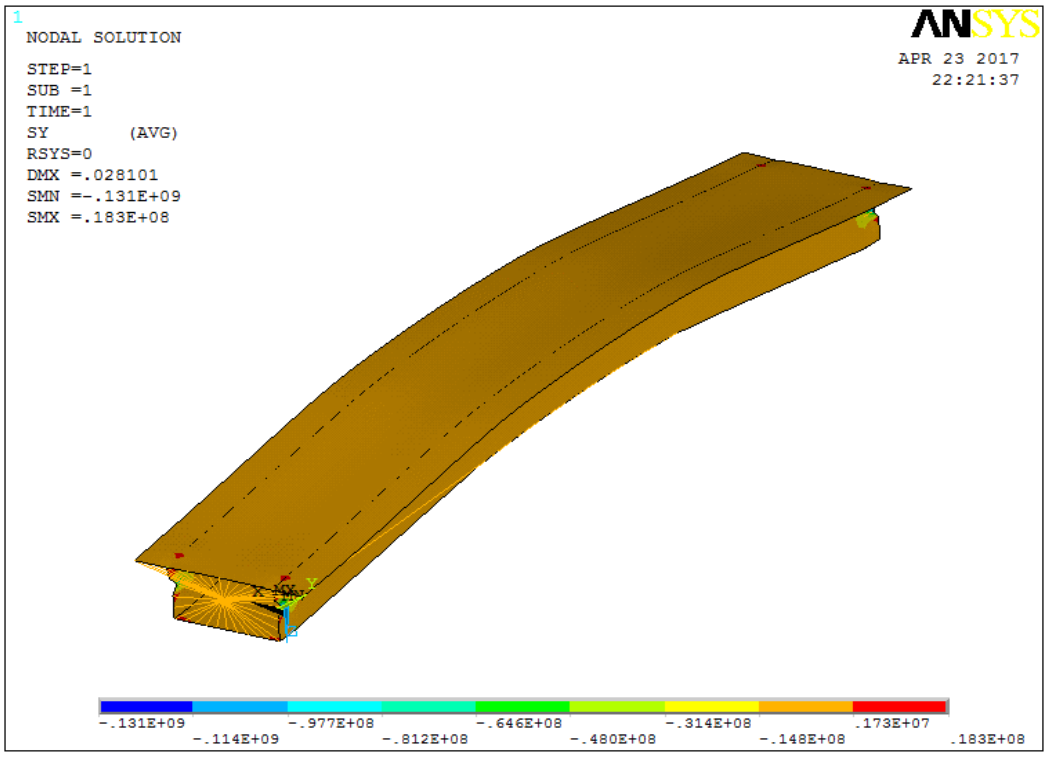

Figure (4.65) Longitudinal stresses (straight, gravity plus prestress, case4)

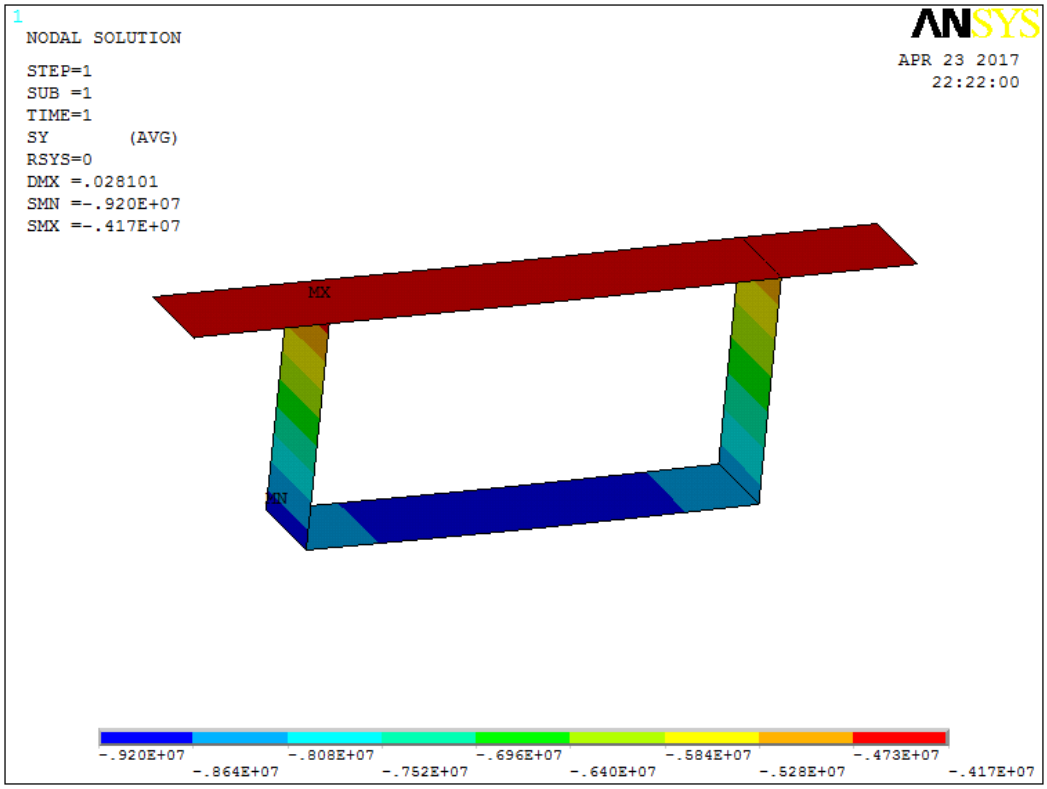

Figure (4.66) Longitudinal stresses at mid-span (straight, gravity plus prestress, case4)

Curved box shell model

As before, the results for the curved box model under the various load conditions will only be shown for the single case of curvature where the sector dimension delta = 8 m.

The following figures show these load cases as follows:

Gravity only Figures 4.67 to 4.70

Prestress only Figures 4.71 to 4.74

Gravity plus prestress Figures 4.75 to 4.77

The results are summarised in table 4.5

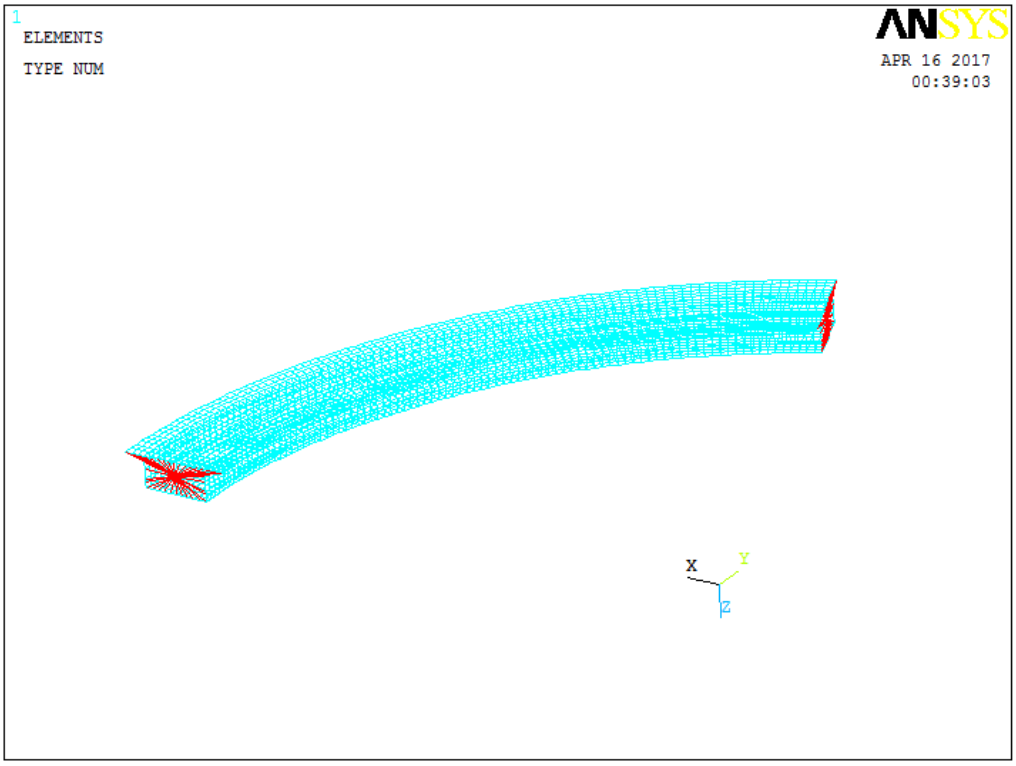

Figure (4.67) The finite element model (curved, gravity only, delta = 8m, case4)

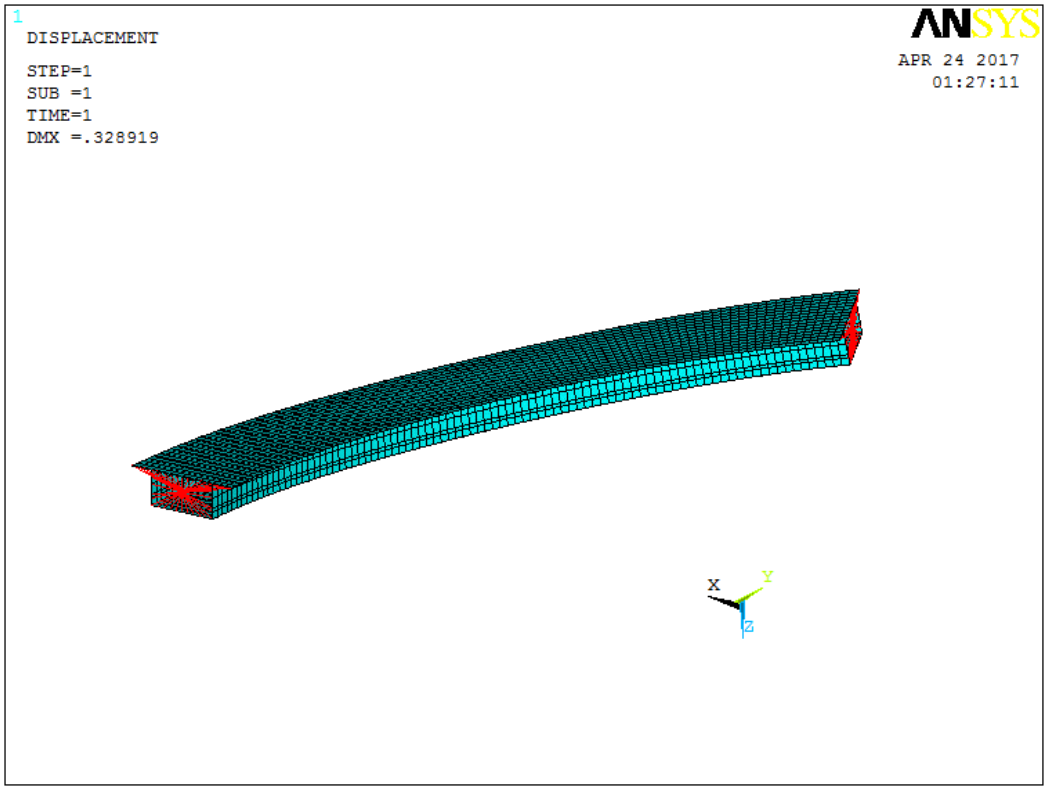

Figure (4.68) Deformed shape (curved, gravity only, delta = 8m, case4)

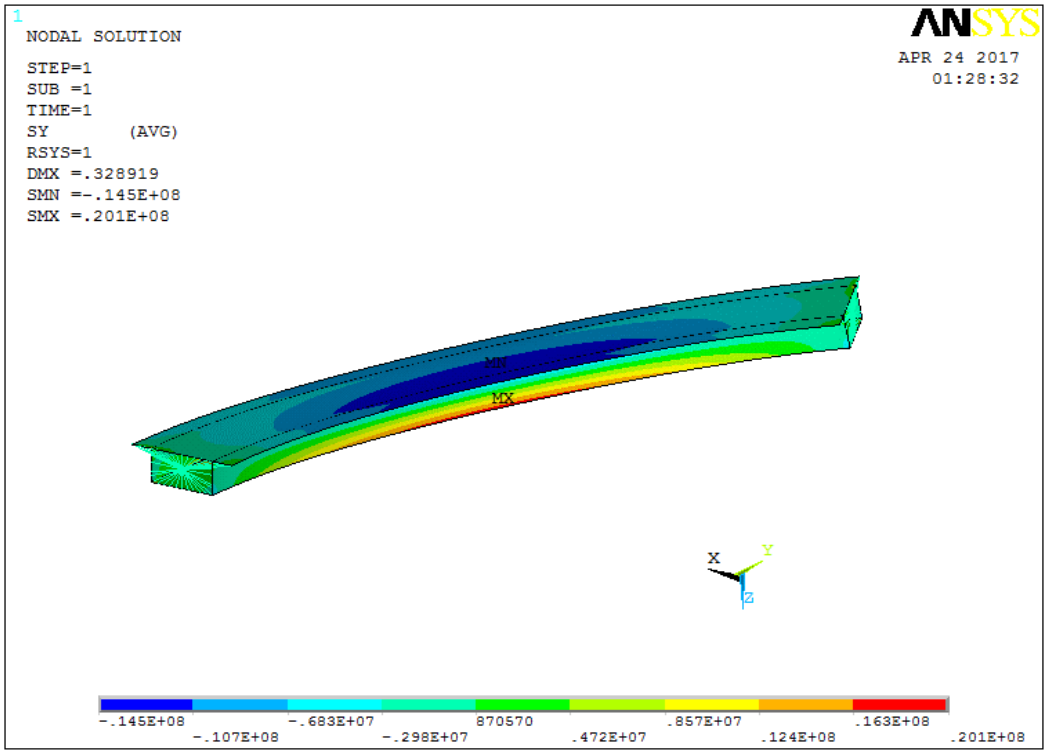

Figure (4.69) Longitudinal stresses (curved, gravity only, delta = 8m, case4)

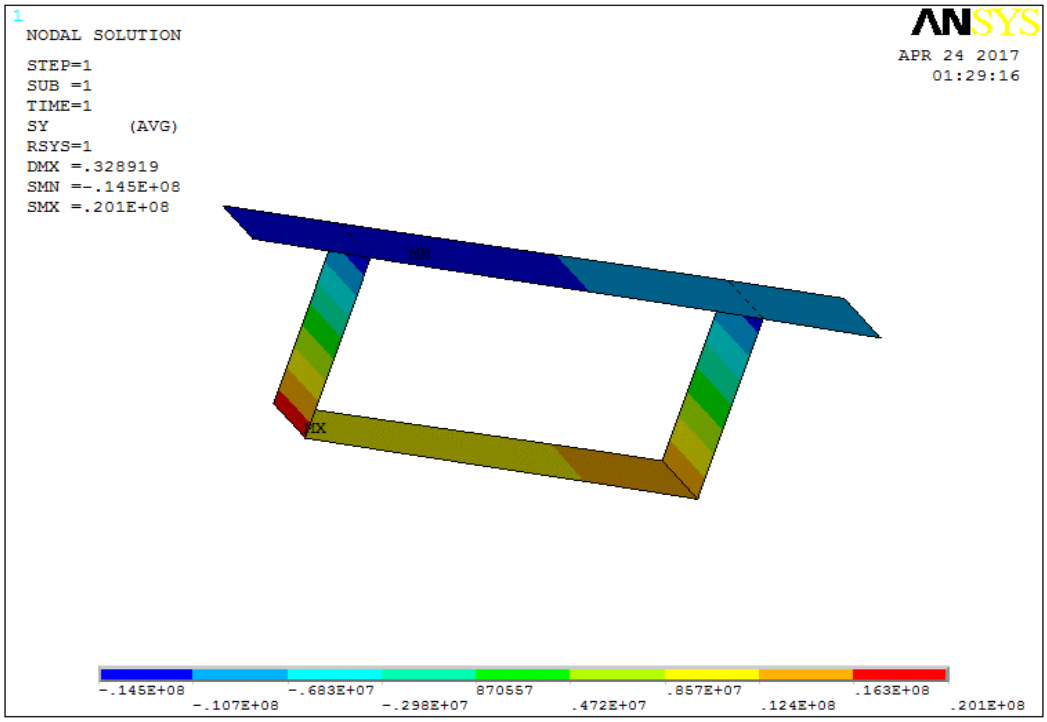

Figure (4.70) Longitudinal stresses at mid-span (curved, gravity plus prestress, case4)

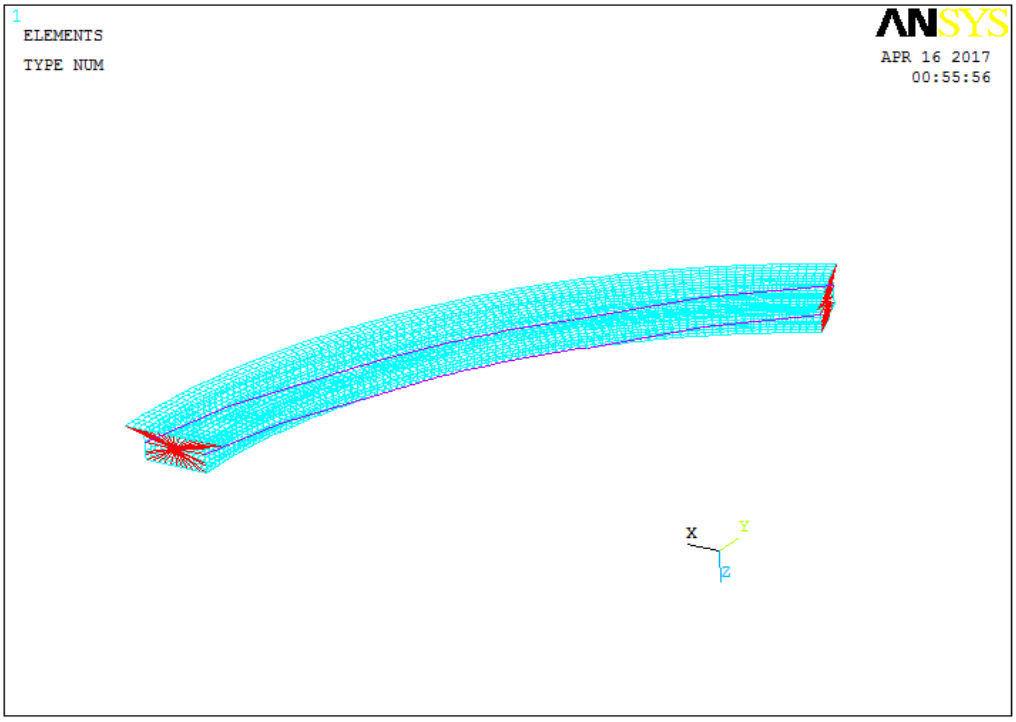

Figure (4.71) The finite element model (prestress only, curved, delta = 8m, case4)

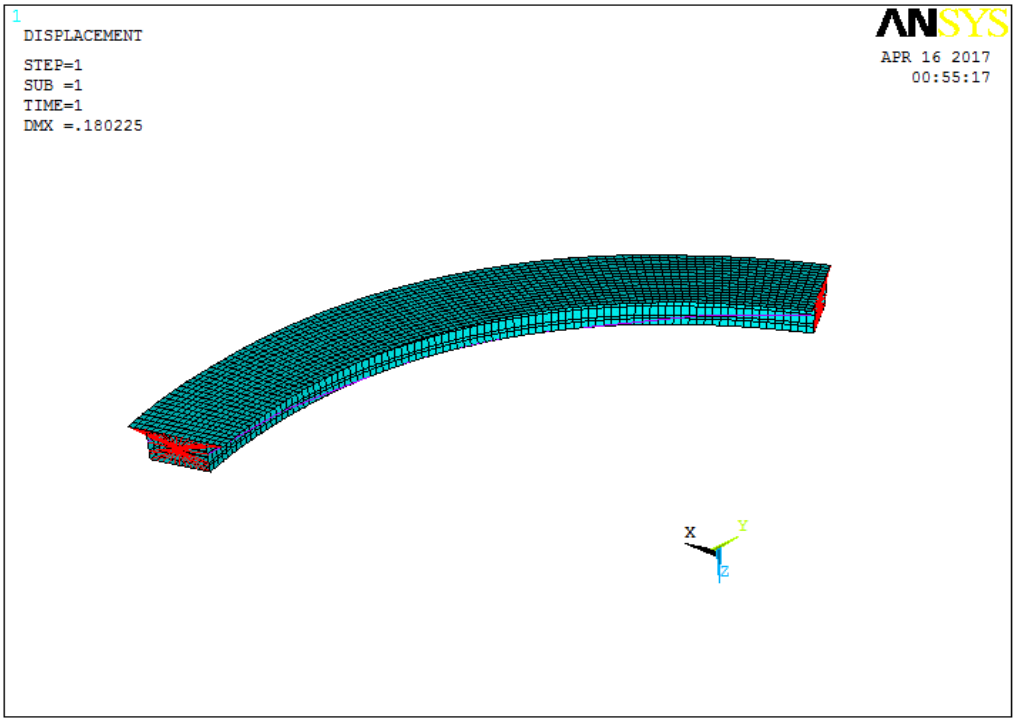

Figure (4.72) Deformed shape (prestress only, curved, delta = 8m, case4)

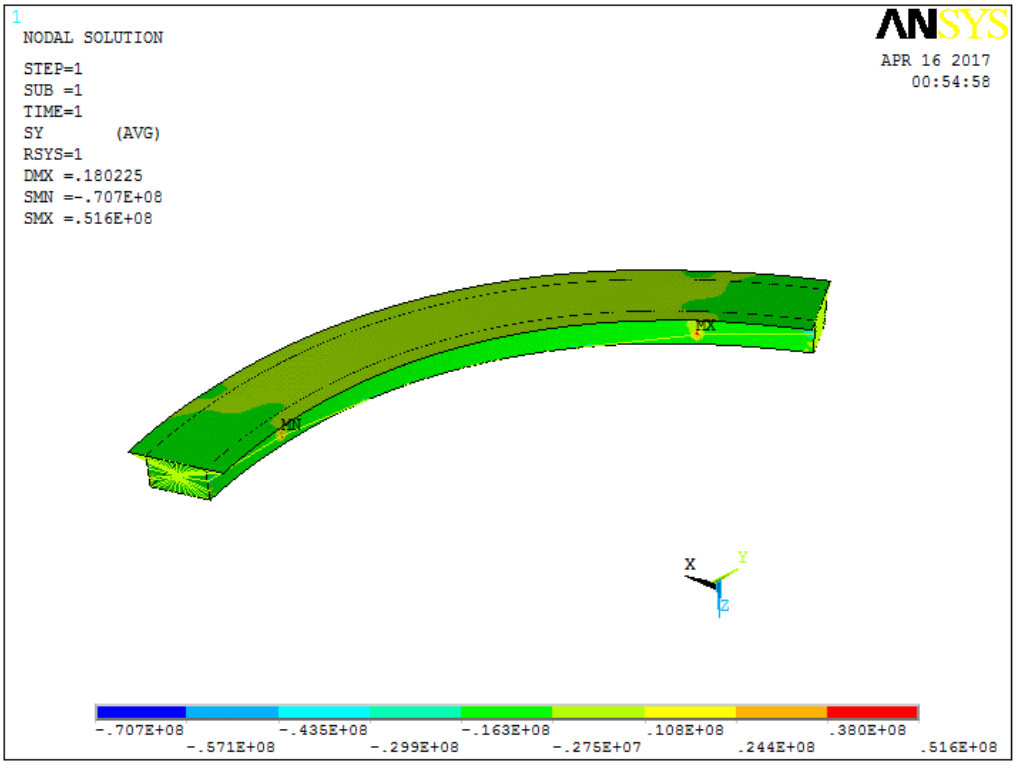

Figure (4.73) Longitudinal stresses (prestress only, curved, delta = 8m, case4)

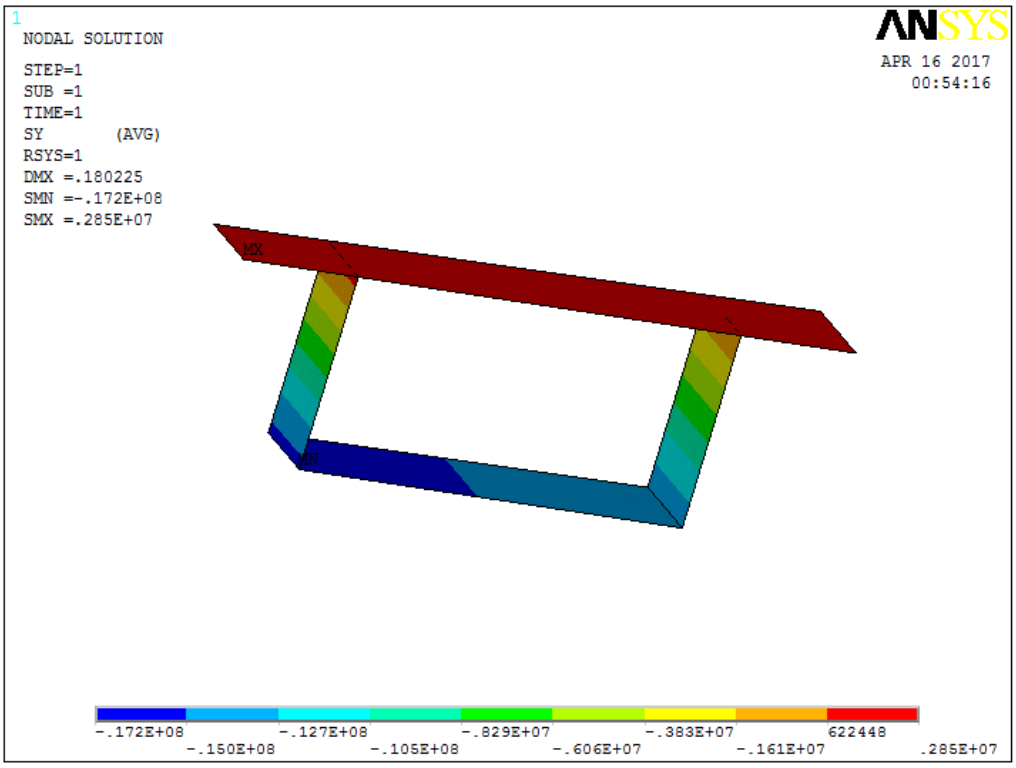

Figure (4.74) Longitudinal stresses at mid-span (prestress only, curved, delta = 8m, case4)

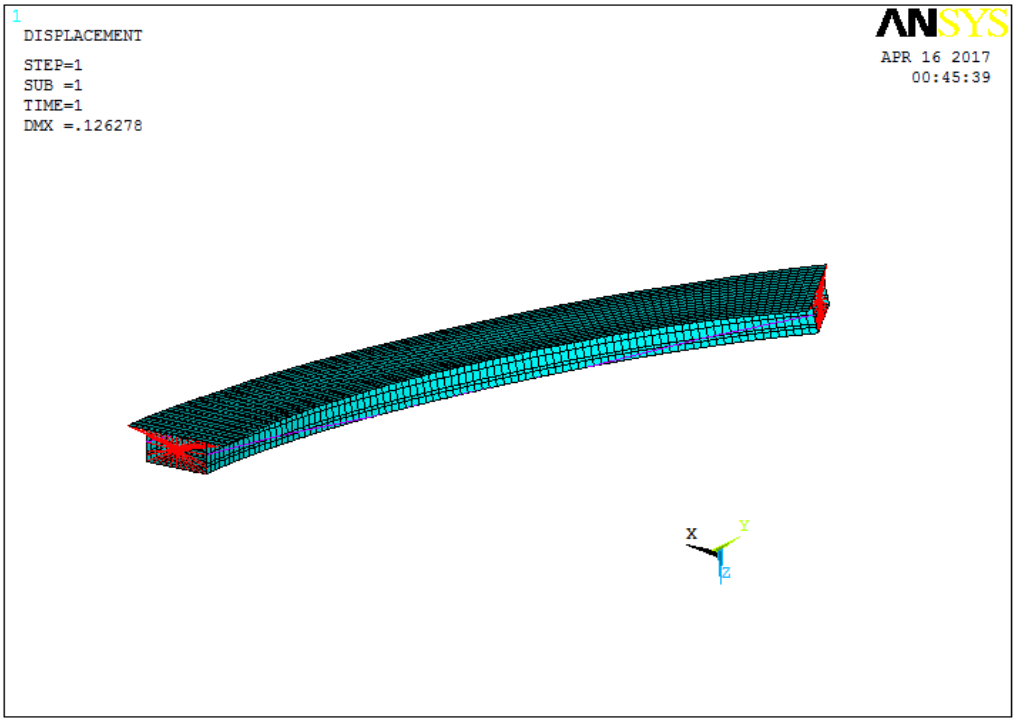

Figure (4.75) Deformed shape (prestress plus gravity, curved, delta =8m, case4)

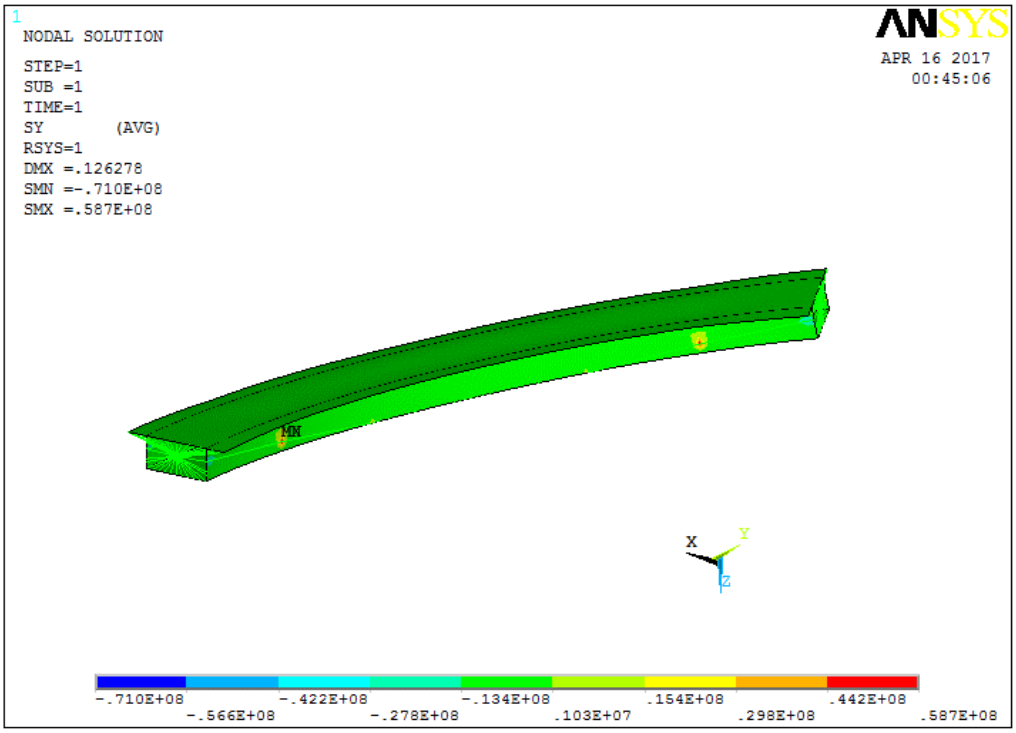

Figure (4.76) Longitudinal stresses (prestress plus gravity, curved, delta =8m, case4)

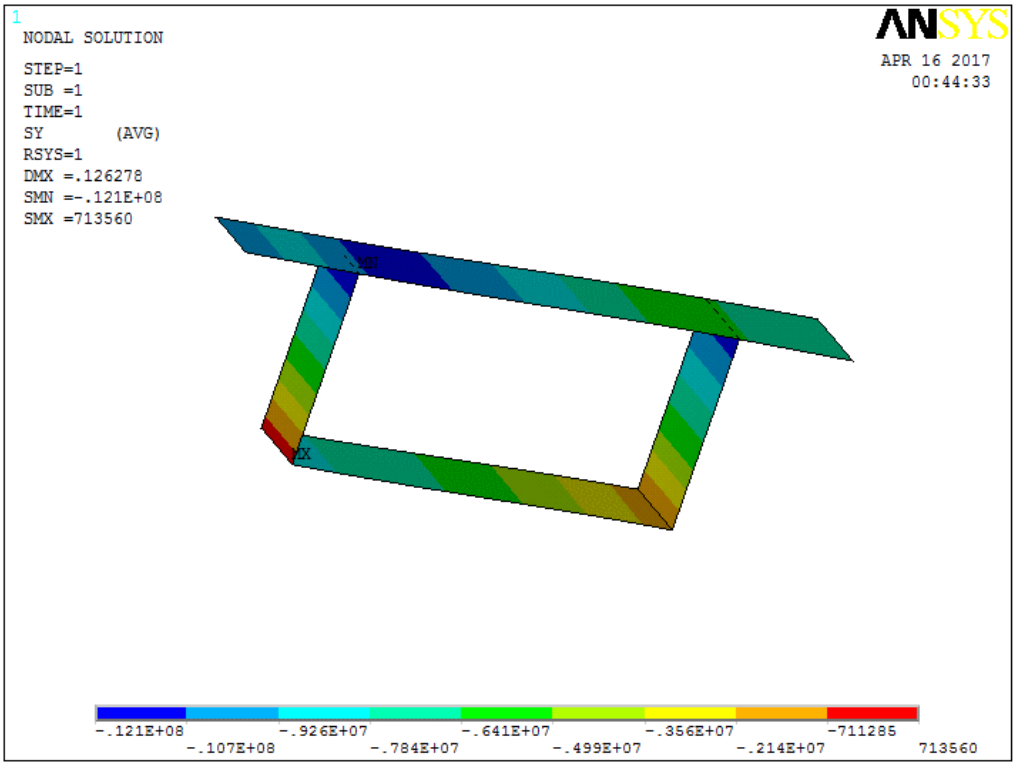

Figure (4.77) Longitudinal stresses at mid-span (prestress plus gravity, curved, delta = 8m, case4)

Table (4.5) Reactions, torsion moments, prestress, mass and stresses form the FE analysis, case4.

Delta (m)	Reaction (kN)	M_y (kN.m)	Prestress (kN)	Mass (Tonnes)	Stresses (N/mm^2)			
					Slab		Soffit	
					Interior	Exterior	Interior	Exterior
delta =0								
g	-8240	0		840	-6.06	-6.06	8.57	8.57
p	0	0	18800	840	0.97	0.97	-11.40	-11.4
g+p	-8240	0	20500	840	-5.00	-5.00	-3.91	-3.91
delta =1								
g	-8350	5800		851	-7.68	-6.82	9.95	8.55
p	0	0.00497	18800	851	2.25	1.92	-16.75	-15.69
g+p	-8350	5800	20600	851	-5.36	-4.85	-6.92	-7.26
delta= 2								
g	-8490	12000		865	-7.67	-6.54	10.56	8.60
p	0	0.0103	18800	865	2.23	2.08	-16.98	-15.05
g+p	-8490	12000	20700	865	-5.37	-4.45	-6.66	-6.41
delta 3								
g	-8630	21600		880	-8.65	-7.71	11.88	9.75
p	0	0.0163	18800	880	2.32	1.95	-17.30	-16.86
g+p	-8630	21600	20800	880	-6.16	-5.52	-6.65	-7.13
delta = 4								
g	-8790	26300		860	-9.35	-7.87	11.25	10.88
p	0	0.0229	18900	896	2.46	2.20	-17.18	-16.19
g+p	-8790	26300	20900	896	-6.75	-5.73	-6.02	-5.48
delta =5								
g	-8960	34700		914	-10.35	-8.66	13.00	12.07
p	0	0.0306	18900	914	1.06	0.85	-17.18	-15.60
g+p	-8960	34700	21100	914	-9.48	-7.74	-4.25	-3.40
delta =6								
g	-9150	44400		932	-11.78	-9.46	15.18	13.20
p	0	0.0395	18900	932	2.56	1.28	-17.60	-15.45
g+p	-9150	44400	21200	932	-9.40	-8.19	-2.54	-2.30
delta =7								
g	-9380	55300		953	-12.85	-10.60	15.42	13.53
p	-36.8	218	18900	953	2.70	2.32	-17.05	-15.12
g+p	-9380	55300	21400	953	-10.15	-8.49	-1.86	-1.45
delta =8								
g	-9640	68200		953	-14.50	-9.93	18.09	17.35
p	-36.8	218	16600	953	2.68	0.72	-17.30	-16.96
g+p	-9640	68200	21700	953	-11.95	-9.28	0.65	0.34

4.6.2 Design criteria as a class 1 prestressed concrete section

To examine the load capacity of the sections with different prestress forces (class 1, i.e. no tensile stress at service limit state) in relation to their curvature, all of the models were subject to distributed load to determine how much load each span could carry before tensile stress starts to show at the midspan section. Hence this provides an overview of the limit of curvature a particular prestress can achieve.

This investigation has been carried out using the previous three dimensional FEM model of the box girder with the four different levels of prestressing. The details for the box girder are the same as provided in Appendix 4.

Table (4.6) shows all cases of prestressing and curvature subjected to uniformly distributed loads which just cause tension in the section, however, only the values for cases 1 to 4 are shown here.

Table (4.6) Uniformly distributed loads at different curvatures (loads unit are kN/m^2).

Delta (m)	Curvature 1/R (m^{-1})	Case 1 P=31000kN	Case 2 P=35000kN	Case 3 P=39000kN	Case 4 P=45000kN
0	0	6.2	8.7	11.2	15.3
1	0.0027	4.85	7.1	9.3	12.9
2	0.0055	3.15	5.2	7.1	10.4
3	0.0081	1.6	3.4	5.1	8.0
4	0.0107	0.1	1.7	3.3	5.9
5	0.0133		0.2	1.6	4.0
6	0.0157			0.1	2.2
7	0.0178				1.15

Case 1 (prestressed force = 31000kN) Curved box girder bridge (δ =4 m) with an applied load (0.2 kN/m^2) distributed on each element of the slab.

The deformed shape contour is shown in figure (4.78) and the longitudinal stress contours and longitudinal mid-span stresses are shown in figures (4.79) & (4.80).

The longitudinal stresses for the mid-span location for case 1 are provided in table (4.7).

Figure (4.90) shows the relationship between load and curvature.

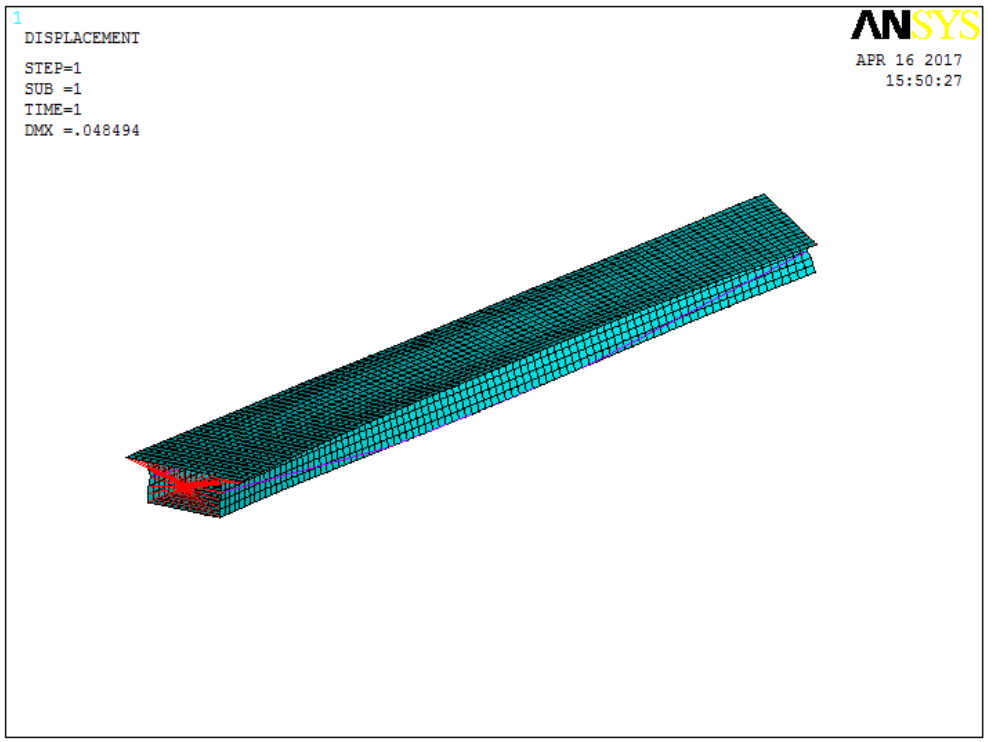

Figure (4.78) Deformed shape (UDL, prestress plus gravity, curved, delta =4m, case1)

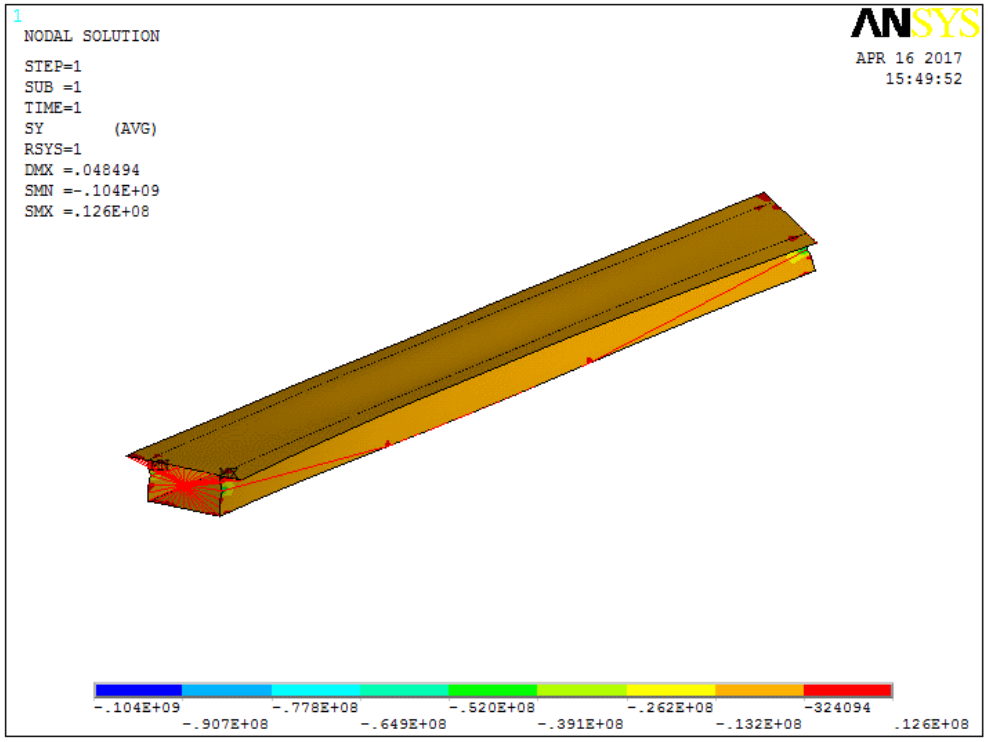

Figure (4.79) Longitudinal stresses (UDL, prestress plus gravity, curved, delta =4m, case1)

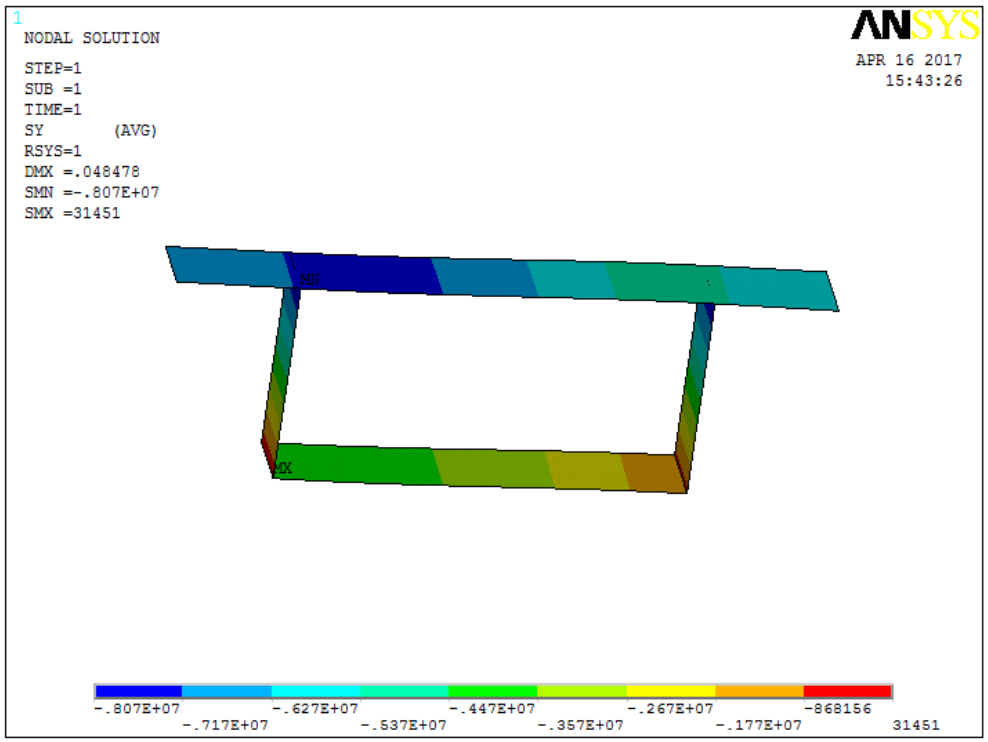

Figure (4.80) Longitudinal stresses at mid-span (UDL, prestress plus gravity, curved, delta =4m, case1)

Table (4.7) Reactions, torsional moments, prestress, mass and stresses for the mid-span section.

Delta (m) Load (kN/m^2)	Mass (Tonnes)	Reaction (kN)	M_y (kN.m)	Prestress (kN)	Stresses (kN/m^2)			
					Slab		Soffit	
delta=0					Interior	Exterior	Interior	Exterior
Load=6.2	840	-12100	0	15400	-8.43	-8.02	0.052	0.027
delta=1								
load =4.85	851	-11400	7950	15400	-8.24	-7.88	0.013	0.010
delta=2								
load 3.15	865	-10500	14900	15300	-8.07	-7.45	0.030	0.022
delta=3								
Load= 1.6	880	-9680	24200	15200	-8.01	-7.39	0.065	0.051
delta= 4								
load=0.1	896	-8860	26500	15200	-8.02	-7.30	0.029	0.018

Case 2 (prestressed force = 35000kN) curved box girder bridge (δ =5m) with an applied load of (0.2 kN/m^2) distributed on each element of the slab.

The deformed shape contour is shown in figure (4.81) and the longitudinal stress contours and longitudinal mid-span stresses are shown in figures (4.82) & (4.83). The longitudinal stresses for

the mid-span location for case 2 are presented in table (4.8). Figure (4.90) shows the relationship between load and curvature.

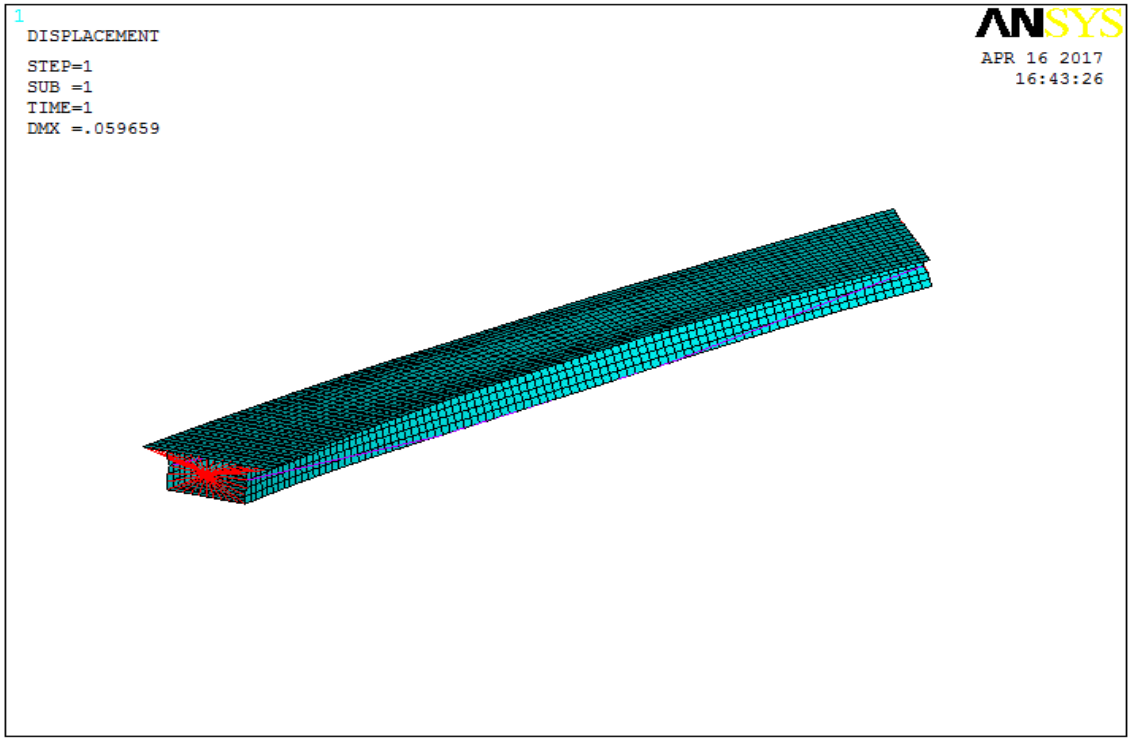

Figure (4.81) Deformed shape (UDL, prestress plus gravity, curved, delta =5m, case2)

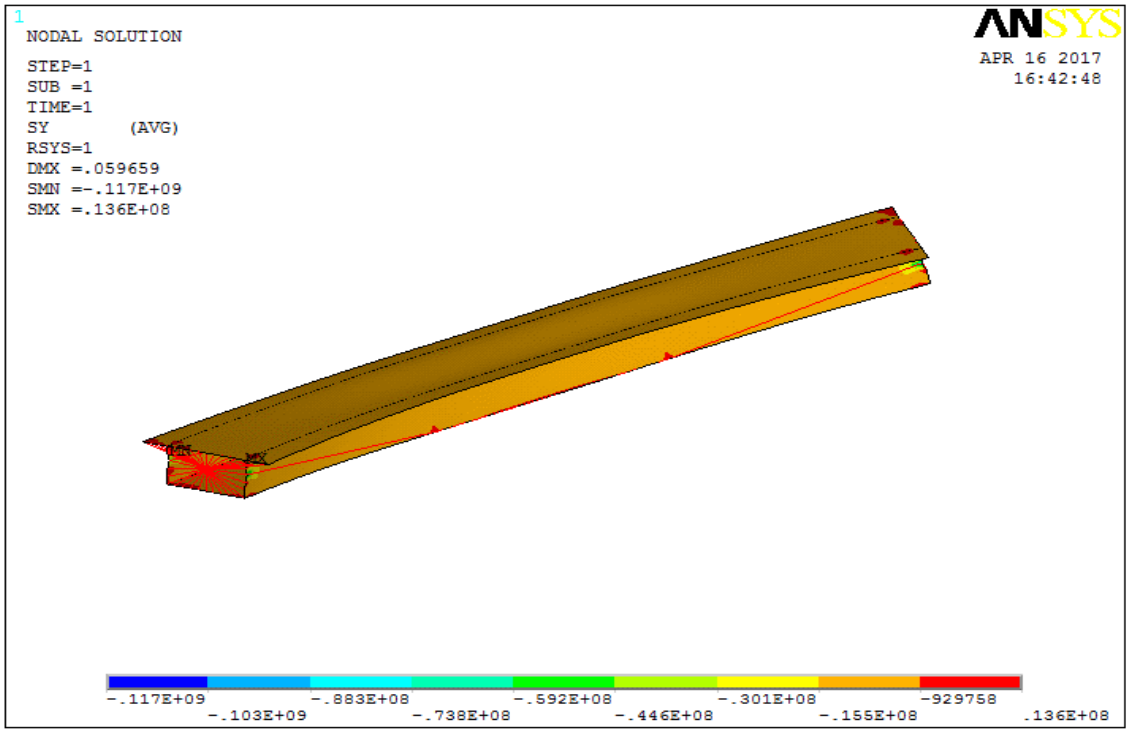

Figure (4.82) Longitudinal stresses (UDL, prestress plus gravity, curved, delta =5m, case2)

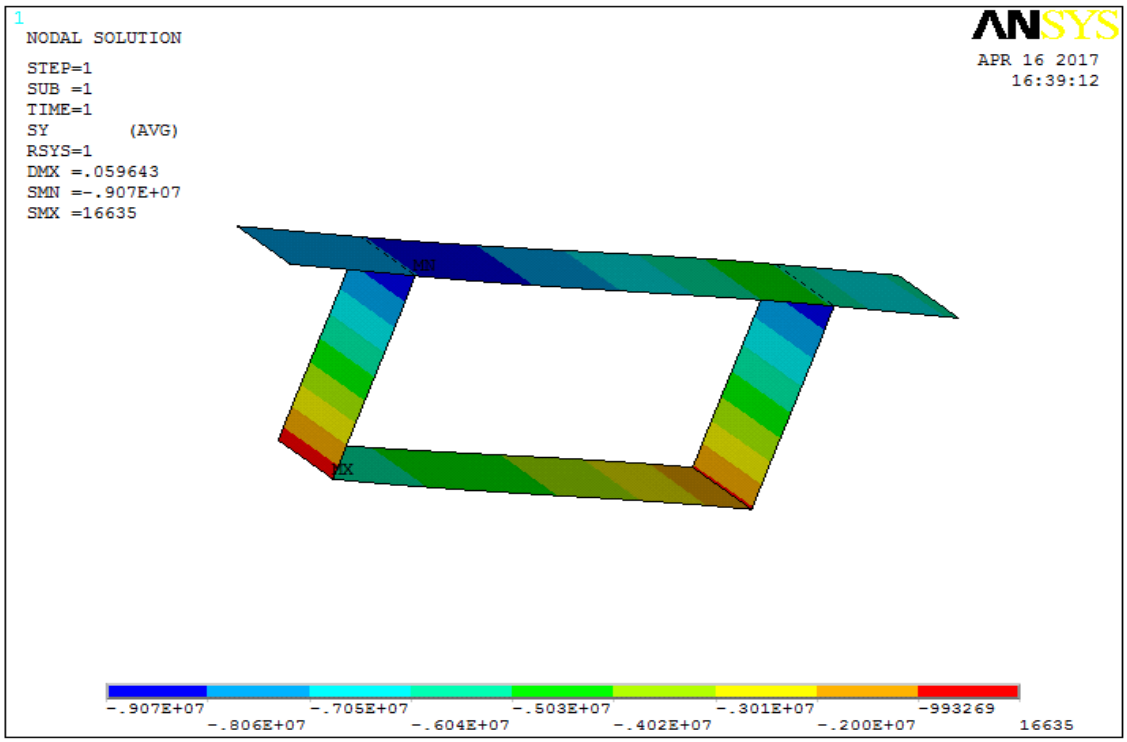

Figure (4.83) Longitudinal stresses at mid-span (UDL, prestress plus gravity, curved, delta =5m, case2)

Table (4.8) Reactions, torsional moments, mass, prestressand stresses for the mid-span section.

Delta (m) Load (kN/m^2)	Mass (Tonnes)	Reaction (kN)	M_y (kN.m)	Prestress (kN)	Stresses (N/mm^2)			
					Slab		Soffit	
delta=0					Interior	Exterior	Interior	Exterior
Load=8.7	840	-13700	0	17400	-9.25	-8.86	0.034	0.021
delta=1								
load =7.1	851	-12900	8950	17300	-9.32	-8.71	0.014	0.009
delta=2								
load =5.2	865	-11800	16800	17200	-9.12	-8.49	0.055	0.018
delta=3								
Load= 3.4	880	-10900	27200	17200	-9.01	-7.85	0.062	0.048
delta= 4								
load=1.7	896	-9930	29800	17100	-8.88	-7.81	0.010	0.006
delta=5								
Load=0.2	914	-9100	35300	17000	-8.77	-8.08	0.016	0.015

Case 3 (prestressed force = 39000 kN) curved box girder bridge (δ =6m) with an applied load (0.1kN/m^2) distributed on the deck of the box girder.

The curved box girder in this case is similar to case 1 the same philosophy. Deformed shape contour shows in figure (4.84) and the longitudinal stress contours and longitudinal mid-span stresses are shown in figures (4.85) & (4.86). The longitudinal stresses for the midspan location for case 3 are summarised in table (4.9). Figure (4.90) shows the relationship between load and curvature.

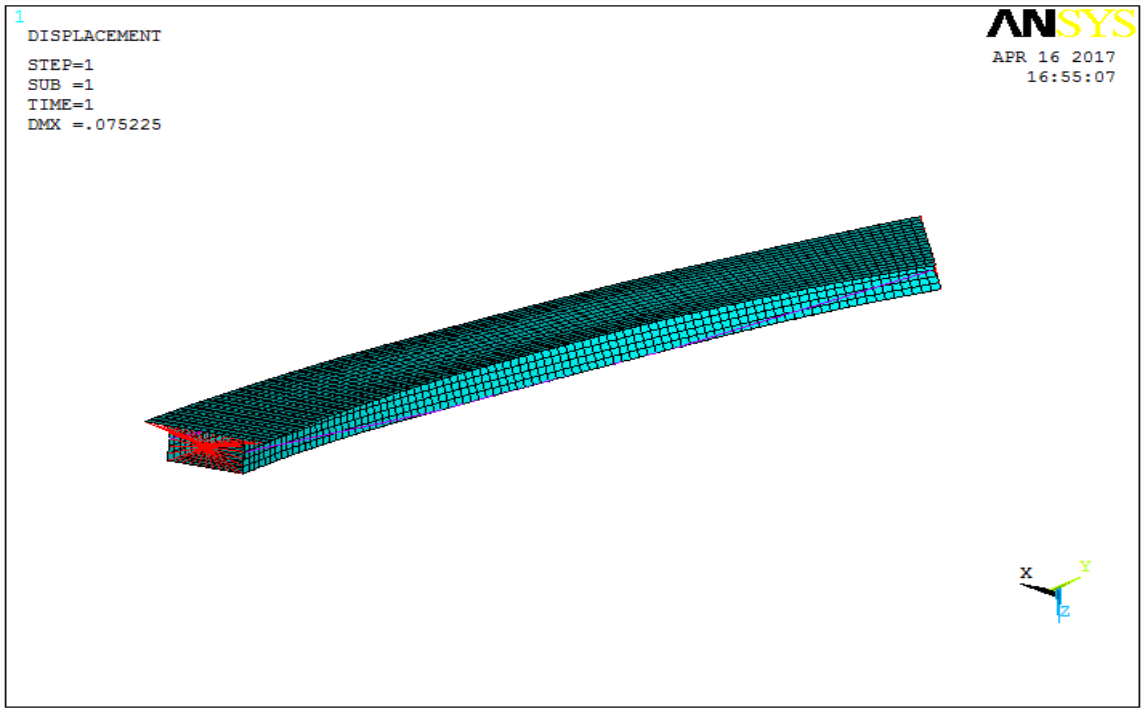

Figure (4.84) Deformed shape (UDL, prestress plus gravity, curved, delta =6m, case3)

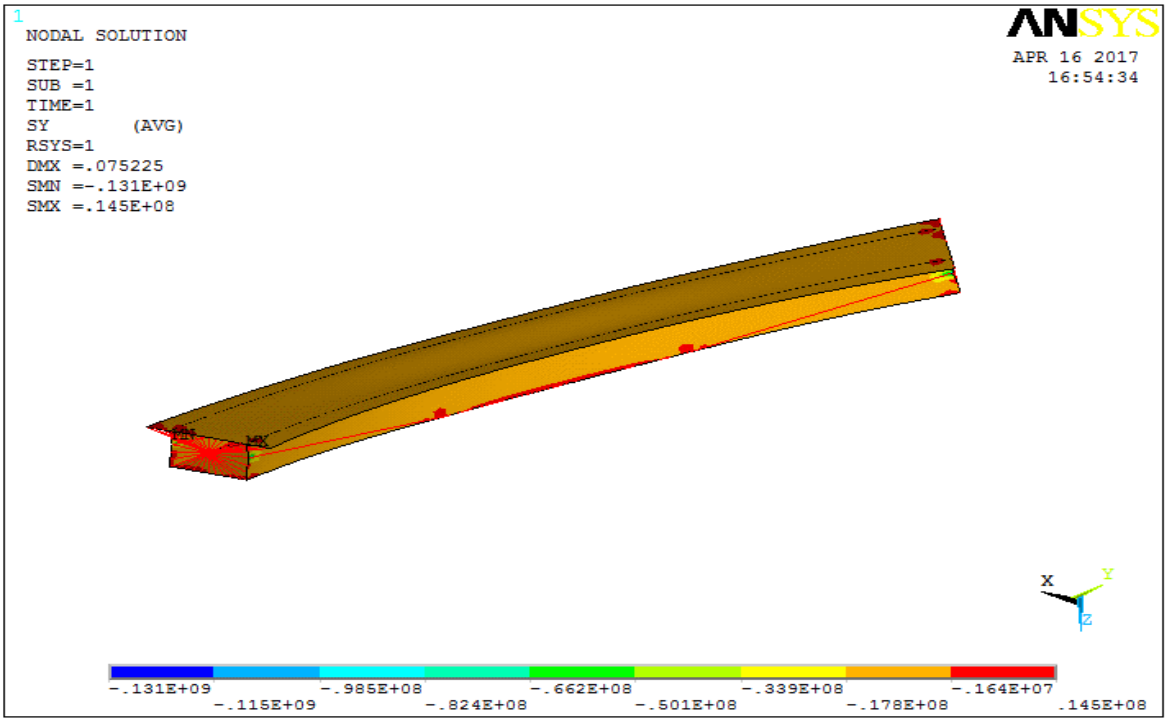

Figure (4.85) Longitudinal stresses (UDL, prestress plus gravity, curved, delta =6m, case3)

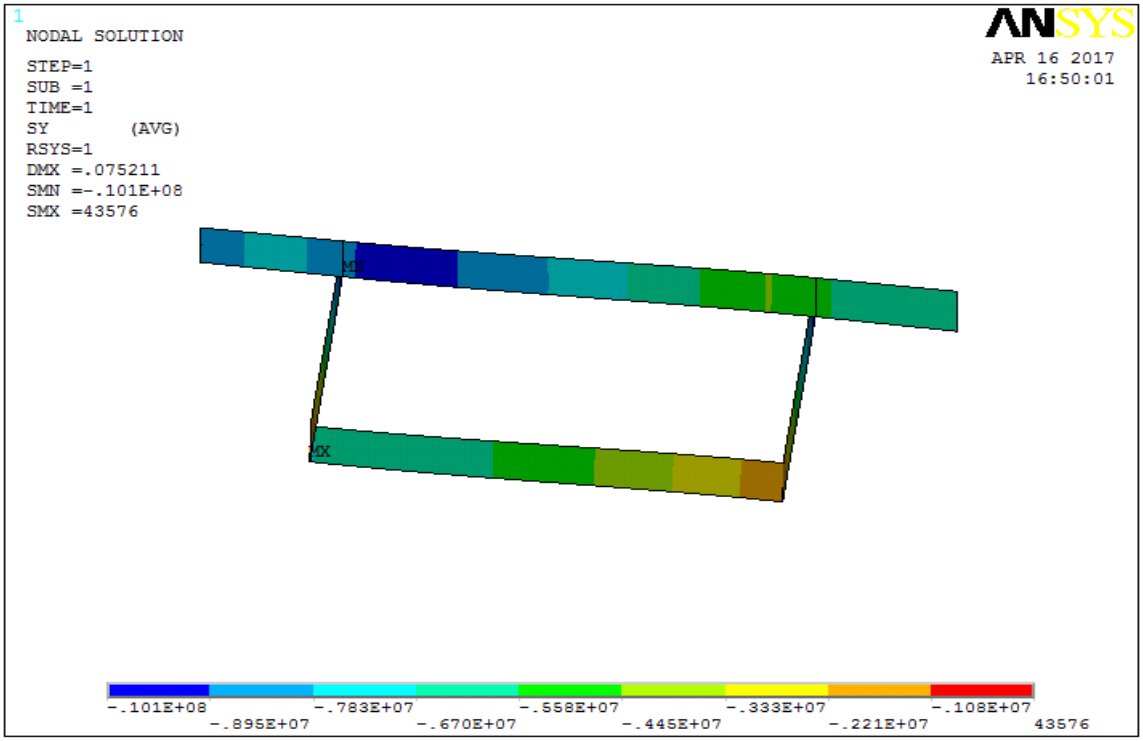

Figure (4.86) Longitudinal stresses at mid-span (UDL, prestress plus gravity, curved, delta =6m, case3)

Table (4.9) Reactions, torsional moments, mass, prestress and stresses for the mid-span section.

Delta (m) Load (kN/m^2)	Mass (Tonnes)	Reaction (kN)	M_y (kN.m)	Prestress (kN)	Stresses (kN/m^2)			
					Slab		Soffit	
delta=0					Interior	Exterior	Interior	Exterior
Load=11.2	840	-15200	0	19400	-10.67	-9.45	0.055	0.041
delta=1								
load =9.3	851	-14300	9920	19300	-10.40	-9.15	0.025	0.020
delta=2								
load =7.1	865	-13100	18600	19100	-10.18	-9.06	0.008	0.011
delta=3								
Load= 5.1	880	-12000	30000	19000	-9.85	-8.43	0.023	0.015
delta= 4								
load=3.3	896	-11000	33000	18900	-9.91	-8.45	0.024	0.021
delta=5								
Load=1.6	914	-10000	39000	18800	-9.78	-8.14	0.007	0.009
delta=6								
Load=0.1	932	-9220	44600	18700	-9.56	-7.80	0.41	0.25

Case 4 (prestressed force = 45000 kN) curved box girder bridge (δ =7m) with an applied load of (1.15kN/m^2) distributed on the deck.

Deformed shape contour shows in figure (4.87) and the longitudinal stress contours and longitudinal mid-span stresses are shown in figures (4.88) & (4.89). The longitudinal stresses for the mid-span location for case 4 are mentioned in table (4.10) and figure (4.90) shows the relationship between load and curvature.

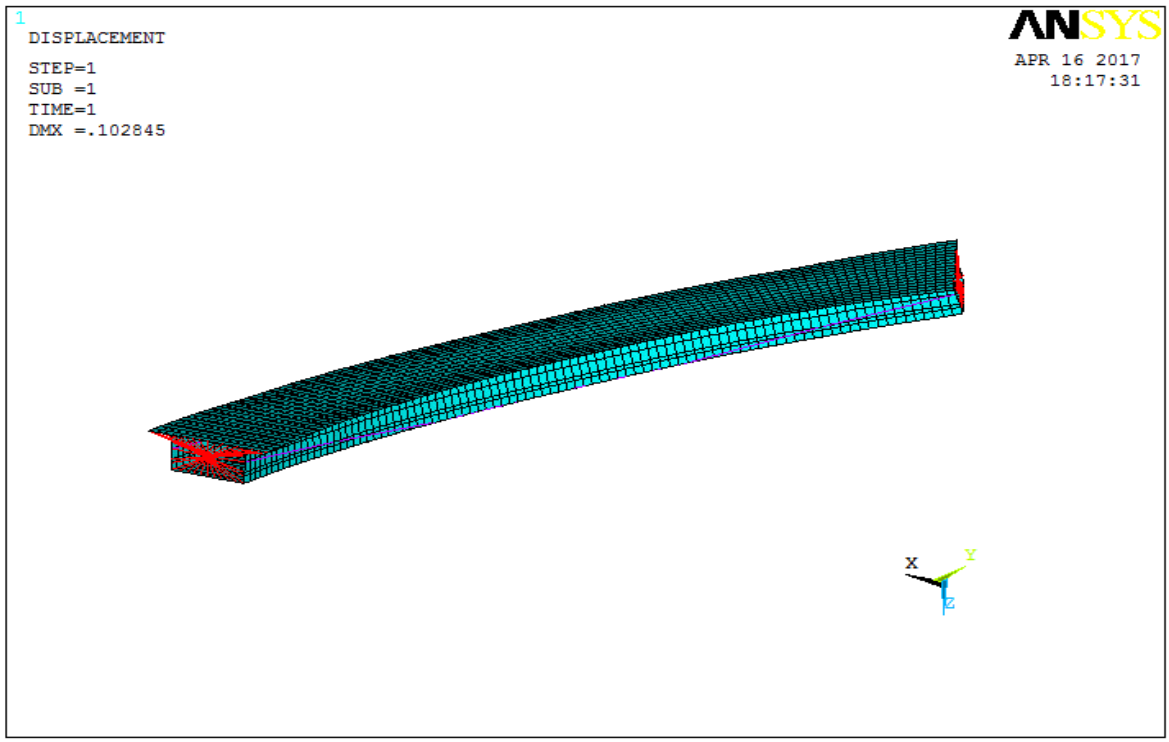

Figure (4.87) Deformed shape (UDL, prestress plus gravity, curved, delta =7m, case4)

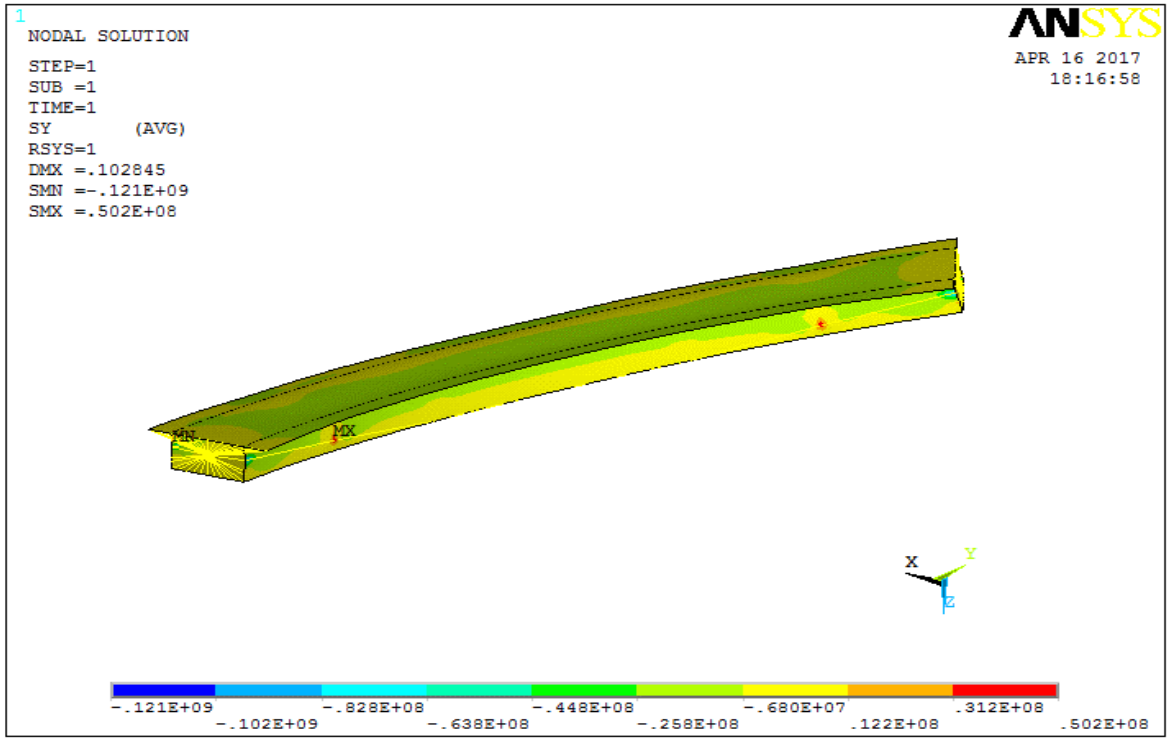

Figure (4.88) Longitudinal stresses (UDL, prestress plus gravity, curved, delta =7m, case4)

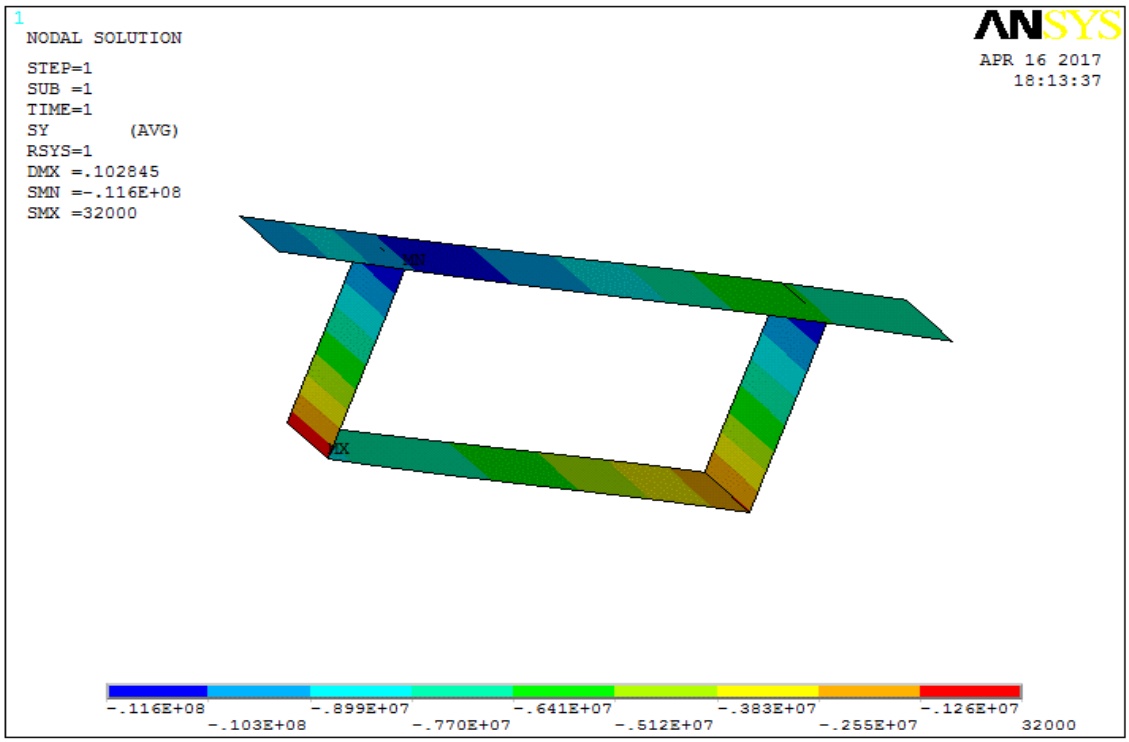

Figure (4.89) Longitudinal stresses at mid-span (UDL, prestress plus gravity, curved, delta =7m, case4)

Table (4.10) Reaction, torsional moments, mass, prestress and stresses for the mid-span section.

Delta (m) Load (kN/m^2)	Mass (Tonnes)	Reaction (kN)	M_y (kN.m)	Prestress (kN)	Stresses (N/mm^2)			
					Slab		Soffit	
delta=0					Interior	Exterior	Interior	Exterior
Load=15.3	840	-17800	0	22600	-12.23	-11.35	0.058	0.043
delta=1								
load =12.9	851	-16500	11500	22400	-11.65	-10.90	0.006	0.018
delta=2								
load =10.4	865	-15200	21600	22200	-11.17	-10.55	0.038	0.030
delta=3								
Load= 8	880	-13900	34800	22100	-11.46	-10.30	0.015	0.010
delta= 4								
load=5.9	896	-12700	38100	21900	-11.40	-10.03	0.010	0.016
delta=5								
Load=4	914	-11700	42600	21800	-11.36	-9.21	0.060	0.043
delta=6								
Load=2.2	932	-10700	51700	21700	-11.54	-8.73	0.066	0.050
delta=7								
Load=1.15	953	-10200	59900	21700	-11.24	-8.95	0.032	0.027

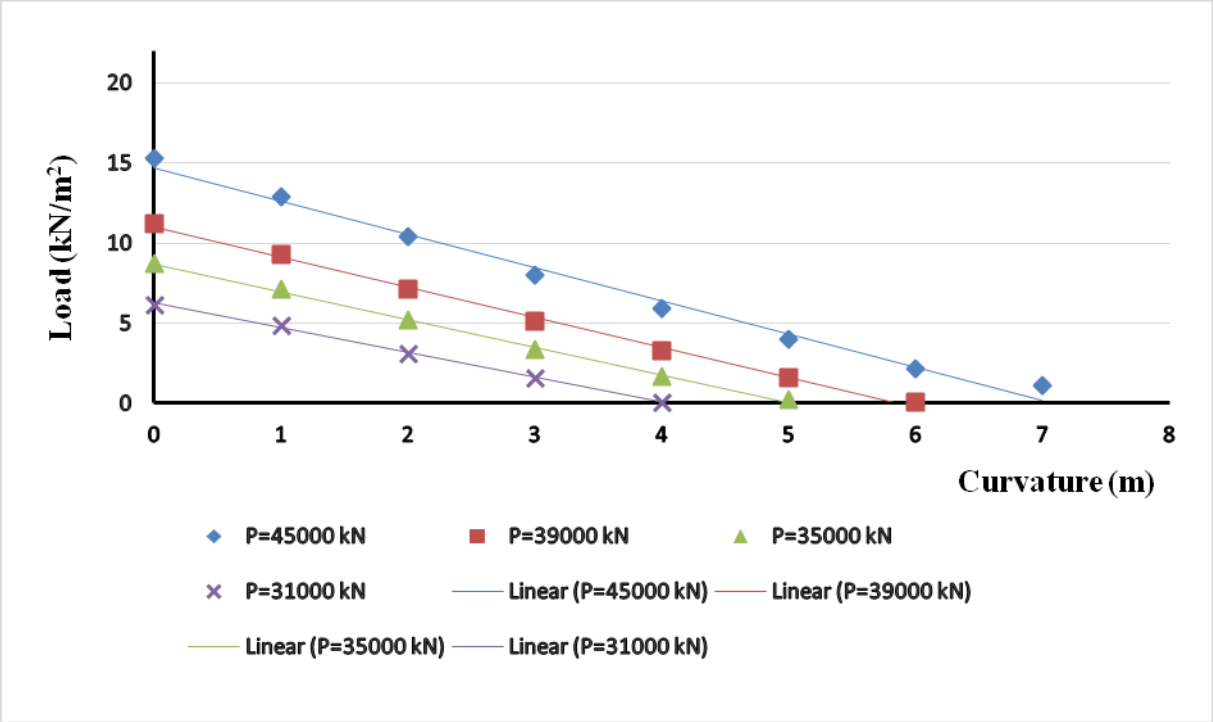

Figure (4.90) Relationship between load and curvature for all cases of box girder bridges.

There are a number of general observations which can be made from the results:

- The study is based purely on the mid-span stresses.
- The results are logical, the higher prestress provides more load capacity as governed by the mid-span section.
- There are areas of concentrated stress where the tendon profile changes direction. This is to be expected as there is equivalent loading applied in both the vertical and radial directions due to the angling of the tendon.
- At the mid-span of the beam the torsional moment from the curvature will theoretically be zero, hence the longitudinal stresses should be predominantly due to axial and bending effects of the applied loads and prestress. At the ends of the beam, the rotation about the longitudinal axis is zero, so warping is prevented and appears to be causing no warping stresses - as expected.
- The table shows that all prestress losses were lower that 20% and those losses mainly occur due to elastic shorting.

Chapter Five

Traffic Pattern

5.1 Traffic load patterning

This part of the study focusses on the variations of loading experienced by the bridge deck due to self-weight, prestress, additional UDL's and traffic patterning. Hence the traffic loadings considered in this chapter examine the effects of the location of the vehicles on the structural behaviour of the bridge.

The dead load of the girder is distributed on the decks based on the respective widths of the various structures. The dead load will be applied as superimposed dead loads. Superimposed dead loads will contain wearing course, future wearing surface, railings and barriers, except for footpath loads which will be distributed equally to all deck lines. Superimposed load (UDL) is calculated by multiplying the density of the material by the sectional area of the elements. Superimposed dead loads in this study were divided between parapet and pavement and the next section will explain the calculations of superimposed dead loads in detail. The sections are shown in figure (5.1). Complete dimensions of the section contained in figure (4.1).

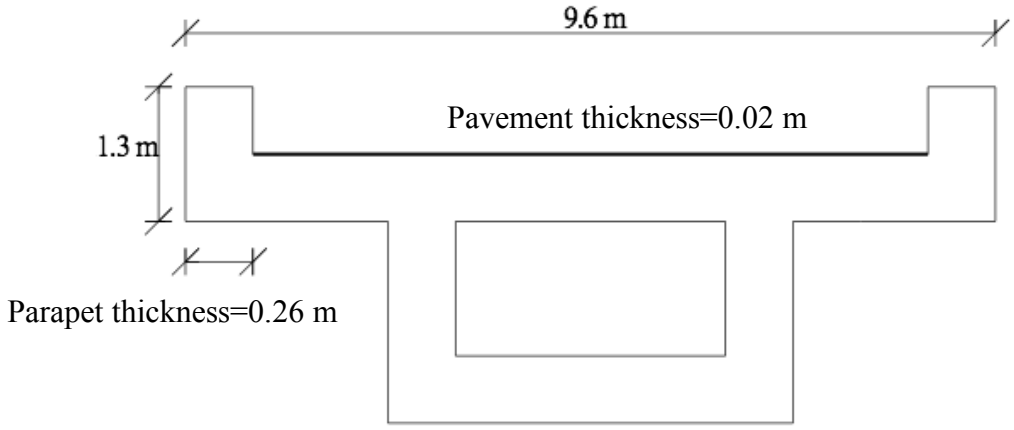

(A) Parapet and pavement.

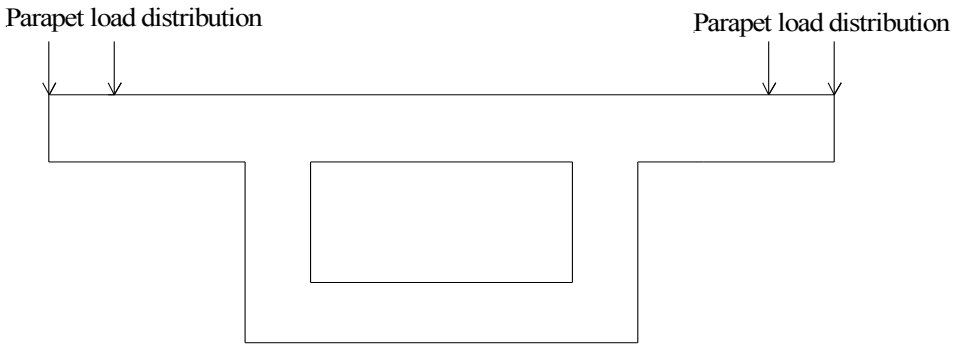

(B) Parapet load distribution.

Figure (5.1) Load distribution on box girder bridge.

The calculation of the superimposed dead load is as follows:

The parapet is assumed to be 1.3m high and 0.26m in width with a concrete unit weight of 24kN/m^3. This leads to a parapet UDL of approximately 8kN/m. The nodes are spaced at 0.6m apart in both the radial and tangential direction. Hence a tangential apportioning of force of 4.8 kN, split between two nodes in the radial direction leads to 2.4 kN per node.

- Parapet UDL=24×1.3×0.26= 8.11 approximately 8 kN/m.
- Parapet nodal loading on each flank of the span = 8×0.6= 4.8 kN.

The road surface (pavement) will be assumed 20mm thick with a unit weight of 22kN/m^3

- Road surface/pavement =0.02×22= 0.44 kN/m^2 and will be applied as a pressure on deck.

The traffic loading will be applied conservatively as a series of 25 ton lorries. This is in accordance with AASHTO. The standard values of vehicle load from this code of practice are shown in figure 5.2A. The chosen vehicle load that applied on the box girder is shown in figure 5.2B.

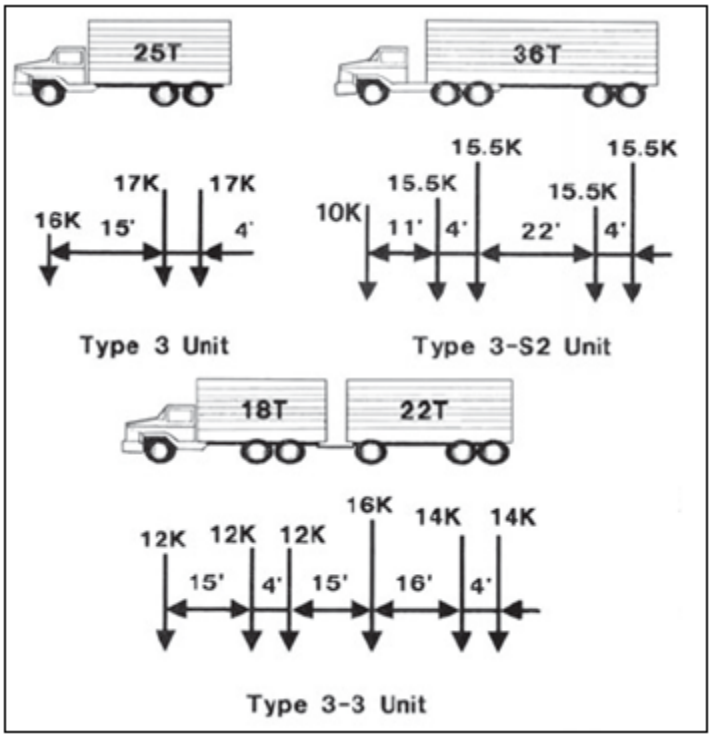

(A) Standard value of vehicle load from AASHTO

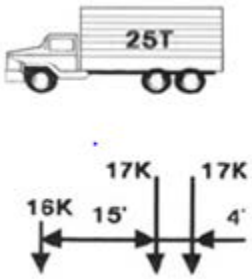

(B) Vehicle load

Figure (5.2) AASHTO vehicle load

Source: http://www.fhwa.dot.gov/publications/publicroads/05jul/09.cfm

- Vehicle loads in accordance with AASHTO are about 222.5 kN

In this study the vehicle load will be rounded to 225 kN

The vehicle length is 6 m long and has a width of 1.8m (AASHTO)

In terms of a patch UDL, the load will be $= \frac{225}{(1.8 \times 6)}$ = 20.83 kN/m^2

5.2Vehicle loads

There will be four cases of pattern loading to be analysed depending on the traffic location. In detail, this will be referred to as the left or right side, and location along the bridge, i.e. near end, middle or the far end. Figures (5.3) to (5.13) show the traffic location for each case of study.

1- Patterned traffic UDL

A- Near end

The traffic here will comprise two vehicles situated close to the cross-section axes end of the bridge deck as viewed in plan. These cases (near end patterned traffic UDL) are termed TL1 & TR1. TL1 & TR1 cases are left and right as shown in figures (5.3) & (5.4).

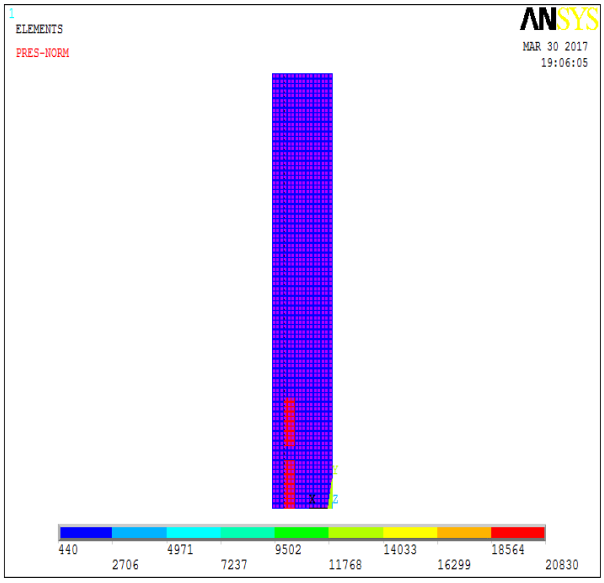

Figure (5.3) Load case (TL1) for traffic loads

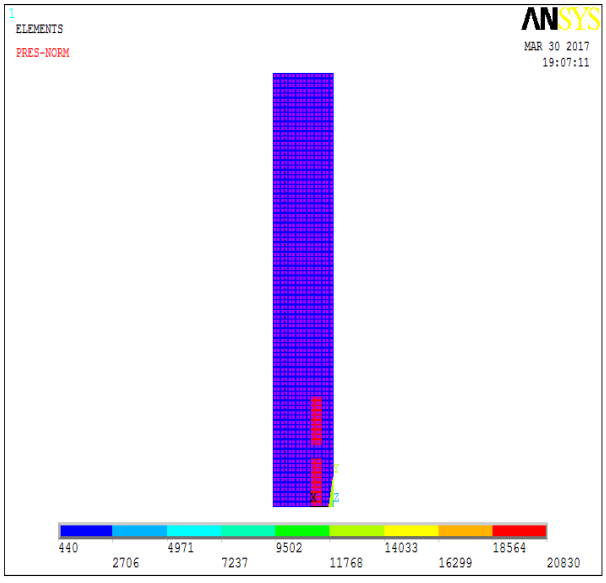

Figure (5.4) Load case (TR1) for traffic loads

B- Middle

Case B is similar to case A in terms of traffic load magnitude however the location of the traffic is on the left or the right side of mid-span (mid-length). These cases are TL2 & TR2, as shown in figures (5.5) & (5.6).

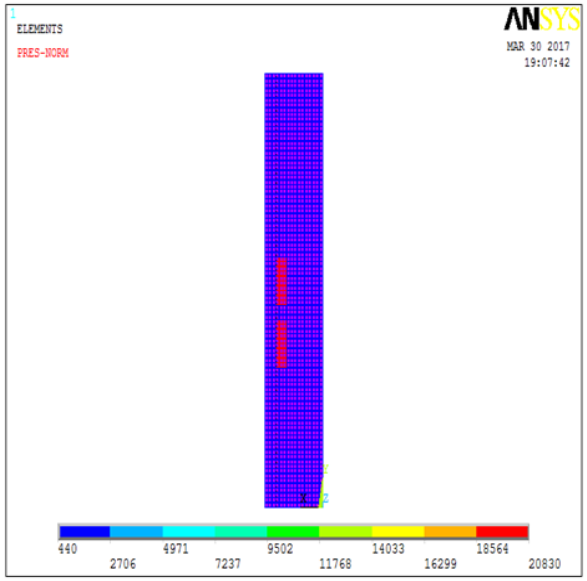

Figure (5.5) Load case (TL2) for traffic loads

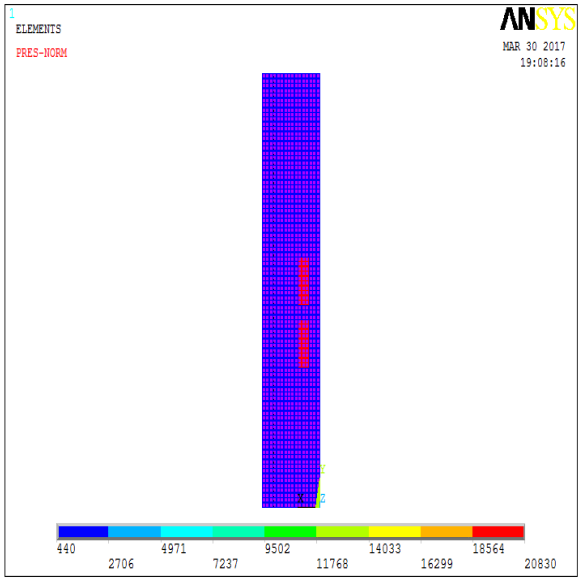

Figure (5.6) Load case (TR2) for traffic loads

C. Far end

The same as in A and B the two vehicles will move on left or right of the far span end. There will be also two cases TL3 & TR3 as shown in figures (5.7) & (5.8).

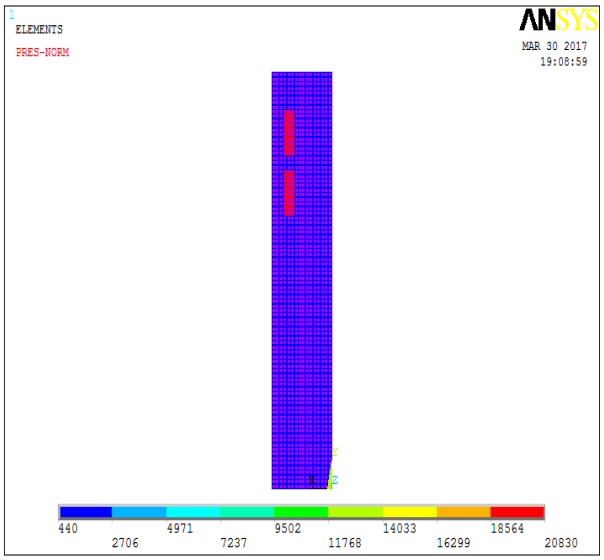

Figure (5.7) Load case (TL3) for traffic loads

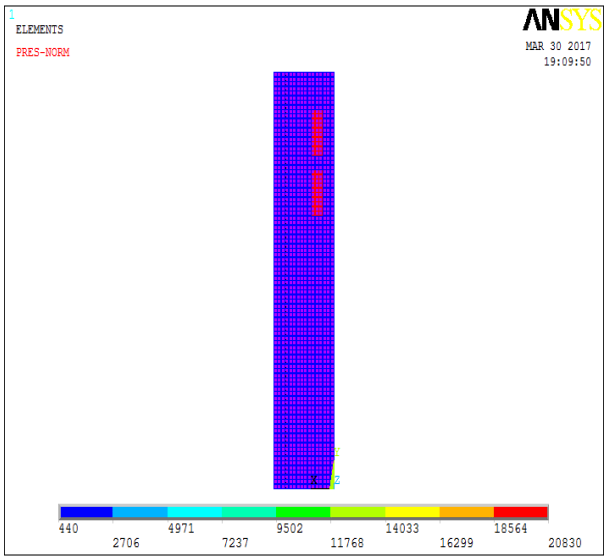

Figure (5.8) Load case (TR3) for traffic loads

2- Full Traffic UDL

The deck will be loaded with all the vehicles. This case is shown in figure (5.9) and will be represented as T4.

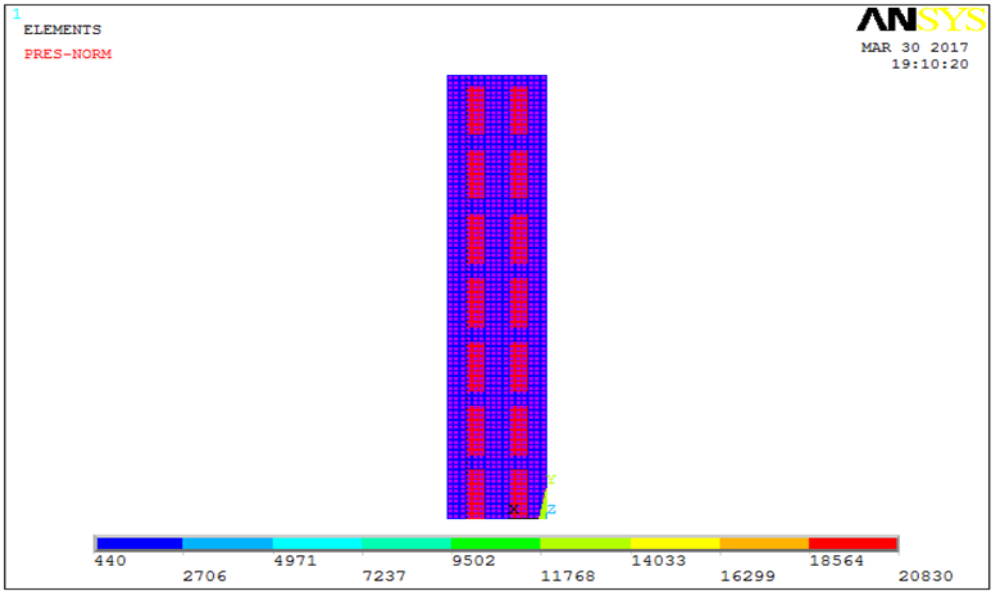

Figure (5.9) Load case (T4) for traffic loads

3- Near End+ Far End Traffic UDL

A- Left Near End + Right Far End Traffic

For this case, the traffic will be applied as shown in figure (5.10). This case will be called TL5.

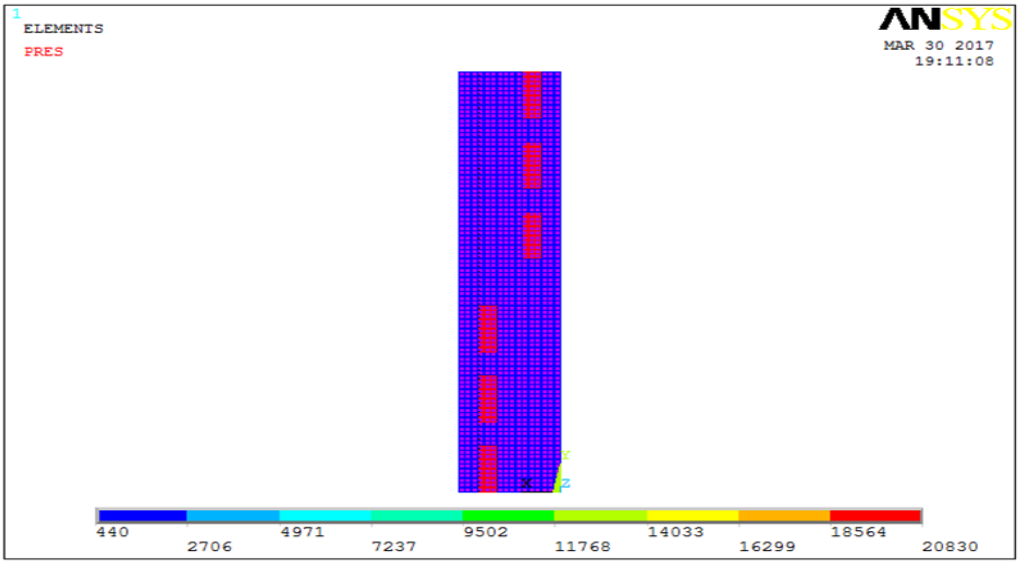

Figure (5.10) Load case (TL5) for traffic loads

B- Right Near End + Left Far End Traffic

For this case, the traffic will be applied as shown in figure (5.11). This case will be called TR5.

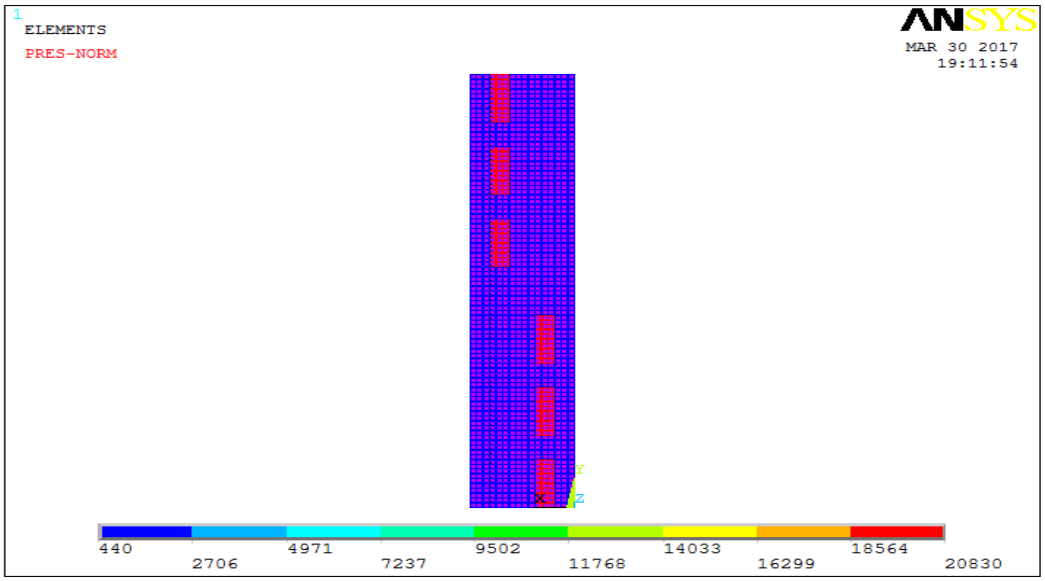

Figure (5.11) Load case (TR5) for traffic loads

4- Total traffic UDL

A- Total Traffic UDL Left

The traffic will be positioned all above the left side of the deck as shown in figure (5.12). This case will be called TL6.

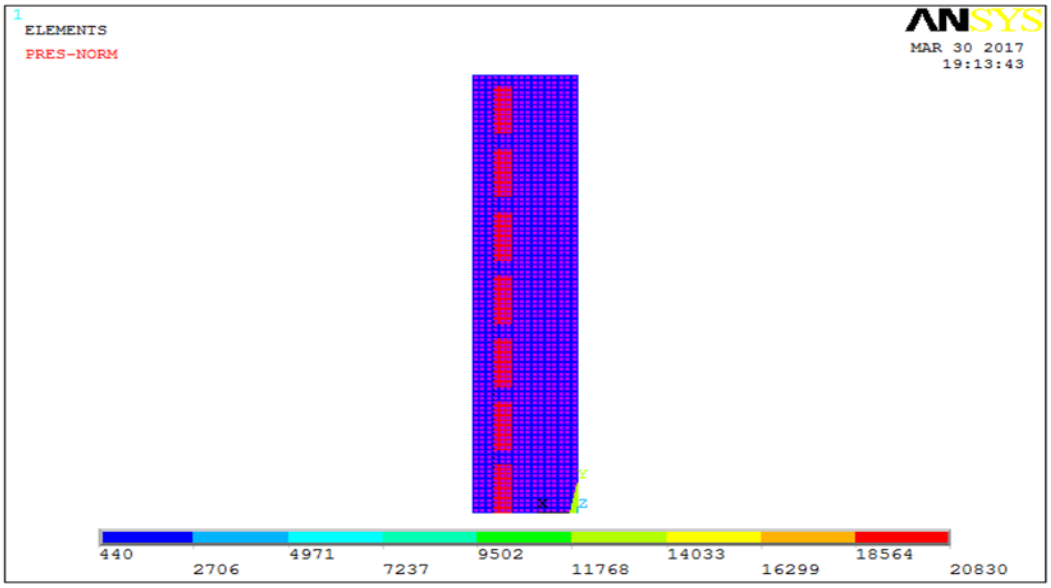

Figure (5.12) Load case (TL6) for traffic loads

B- Total traffic UDL Right

The traffic will be positioned all above the right side of the deck as shown in figure (5.13). This case will be called TR6.

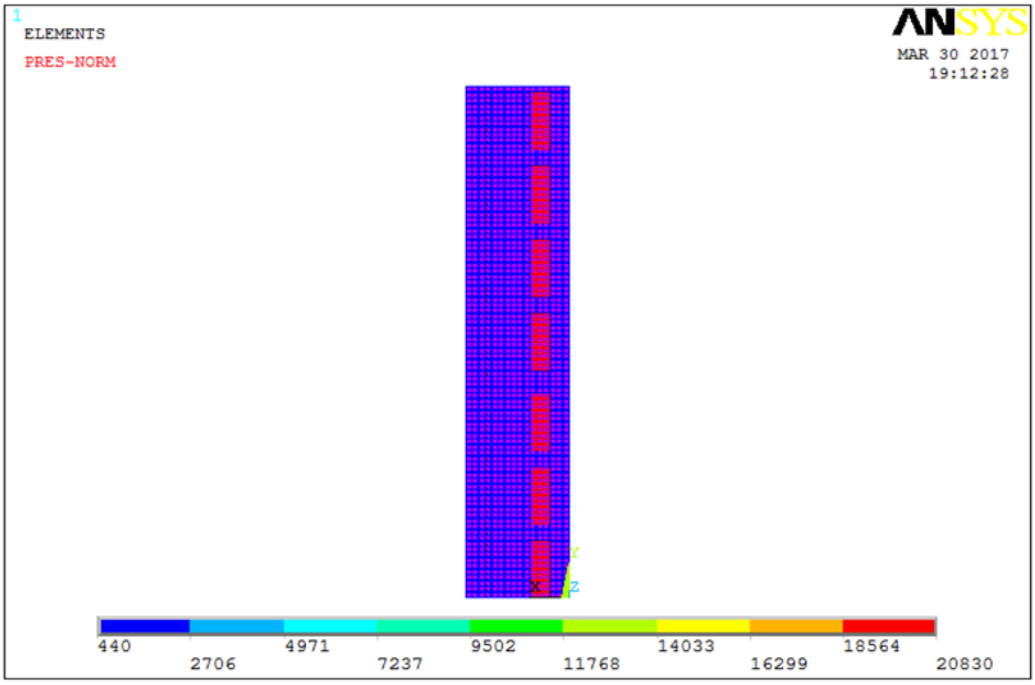

Figure (5.13) Load case (TR6) for traffic loads

5.3 Traffic patterning parametric models of varying curvature and prestressing.

The four cases with different prestress values that were investigated in chapter four will be developed in this chapter. Table 5.1. illustrates the various combinations of load patterning, prestress and curvature which were studied.

Table (5.1) Parametric combinations of traffic patterning, prestressing and curvature.

Delta m	Case 1 (P = 31000 kN)										
	TL1	TR1	TL2	TR2	TL3	TR3	T4	TL5	TR5	TL6	TR6
δ= 0	✓	✓	✓	✓	✓	✓	✓	✓	✓	✓	✓
δ= 1	✓	✓	✓	✓	✓	✓		✓	✓	✓	✓
δ= 2	✓	✓	✓	✓	✓	✓		✓	✓	✓	✓
δ= 3	✓	✓	✓		✓	✓					
Delta m	Case 2 (P = 35000 kN)										
	TL1	TR1	TL2	TR2	TL3	TR3	T4	TL5	TR5	TL6	TR6
δ= 0	✓	✓	✓	✓	✓	✓	✓	✓	✓	✓	✓
δ= 1	✓	✓	✓	✓	✓	✓	✓	✓	✓	✓	✓
δ= 2	✓	✓	✓	✓	✓	✓	✓	✓	✓	✓	✓
δ= 3	✓	✓	✓	✓	✓	✓		✓	✓	✓	✓
δ= 4	✓	✓	✓	✓	✓	✓					
Delta m	Case 3 (P = 39000 kN)										
	TL1	TR1	TL2	TR2	TL3	TR3	T4	TL5	TR5	TL6	TR6
δ= 0	✓	✓	✓	✓	✓	✓	✓	✓	✓	✓	✓
δ= 1	✓	✓	✓	✓	✓	✓	✓	✓	✓	✓	✓
δ= 2	✓	✓	✓	✓	✓	✓	✓	✓	✓	✓	✓
δ= 3	✓	✓	✓	✓	✓	✓	✓	✓	✓	✓	✓
δ= 4	✓	✓	✓	✓	✓	✓		✓	✓	✓	✓
δ= 5	✓	✓	✓	✓	✓	✓					
δ= 6						✓					
Delta m	Case 4 (P = 45000 kN)										
	TL1	TR1	TL2	TR2	TL3	TR3	T4	TL5	TR5	TL6	TR6
δ= 0	✓	✓	✓	✓	✓	✓	✓	✓	✓	✓	✓
δ= 1	✓	✓	✓	✓	✓	✓	✓	✓	✓	✓	✓
δ= 2	✓	✓	✓	✓	✓	✓	✓	✓	✓	✓	✓
δ= 3	✓	✓	✓	✓	✓	✓	✓	✓	✓	✓	✓
δ= 4	✓	✓	✓	✓	✓	✓	✓	✓	✓	✓	✓
δ= 5	✓	✓	✓	✓	✓	✓		✓	✓	✓	✓
δ= 6	✓	✓	✓	✓	✓	✓		✓	✓		
δ= 7	✓	✓									

5.4 Prestress = 31000 kN

The same bridge model presented in chapter four is analysed under the effects of moving loads (traffic) mentioned in the previous section. The prestress will be taken as 31000 kN and the results are shown in a similar way to the previous chapter i.e.:

1- Straight box shell model
2- Curved box shell model

For the straight box shell model

As in the previous chapter the deformed shape and longitudinal stress diagrams have been produced but with the addition of traffic loads moving along the span. These load patterns also allow the influence lines to be produced to look at the effect of deflection and stresses at a particular location as the load moves.

The following figures show the load cases as follows:

1-Case (TL2), deformed shape figure (5.14),). Longitudinal stresses figure (5.15), and mid-span longitudinal stresses figure (5.16).

2-Case (TR2), deformed shape figure (5.17). Longitudinal stresses figure (5.18) and mid-span longitudinal stresses figure (5.19).

3-Case (T4), deformed shape figure (5.20). Longitudinal stresses figure (5.21) and mid-span longitudinal stresses figure (5.22).

4-Case (TR5), deformed shape figure (5.23). Longitudinal stresses figure (5.24) and mid-span longitudinal stresses figure (5.25)

5-Case (TL6), deformed shape figure (5.26). Longitudinal stresses figure (5.27) and mid-span longitudinal stresses figure (5.28).

In order to investigate the effect of changing the locations of the traffic the influence lines have been produced. The influence lines are built up from the traffic load cases where the vehicles are moving from near end to mid-span and to the far end and from right to left side as shown in figure (5.29). The cases for influence lines are TL1, TL2 & TL3 and TR1, TR2 & TR3 and the investigation has carried out for both deflections and stresses:

1-Influence line for defection at mid-span for left and right are in figures (5.30) & (5.31), near end for left and right are in figures (5.34) & (5.35) and far end for left and right are in figures (5.38) & (5.39)
2-Influence line for stresses at mid-span for left and right are in figures (5.32) & (5.33), near end for left and right are in figures (5.36) & (5.37) and far end for left and right are in figures (5.40) & (5.41).

The final step through this study was to examine the deflections by introducing the deflection for each case (vehicle load cases) of study and comparing with the bridge original shape in the global section directions X and Z Also a comparison with the deflection of the bridge under prestressing, gravity, pavement and parapet loading. The deflection graphs show the bridge model cross-section with the deflection of the bridge under pavement loading and the deflection of the bridge under traffic loads (prestressed, gravity, pavement, parapet and vehicle loads). To magnify the effect of these deflections (so that they are discernible), they are multiplied by a factor of 20.

This part of the study will illustrate only two cases, those cases are:

1-Deflection at near end figure (5.42), mid-span figure (5.43) and far end figure (5.44) for case (TL2) and
2-Case (TR2), the deflection at near end figure (5.45), mid-span figure (5.46) and far end figure (5.47). The results are summarised in table (5.2).

Figure (5.29) provides a key for influence line graphs.

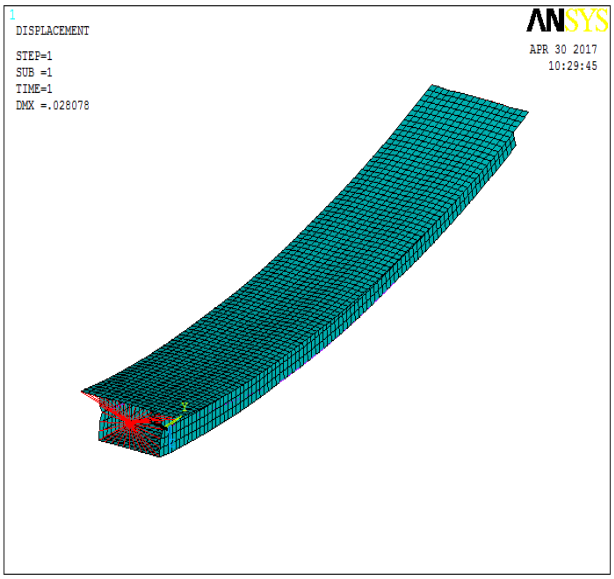

Figure (5.14) Deformed shape for load case (TL2)

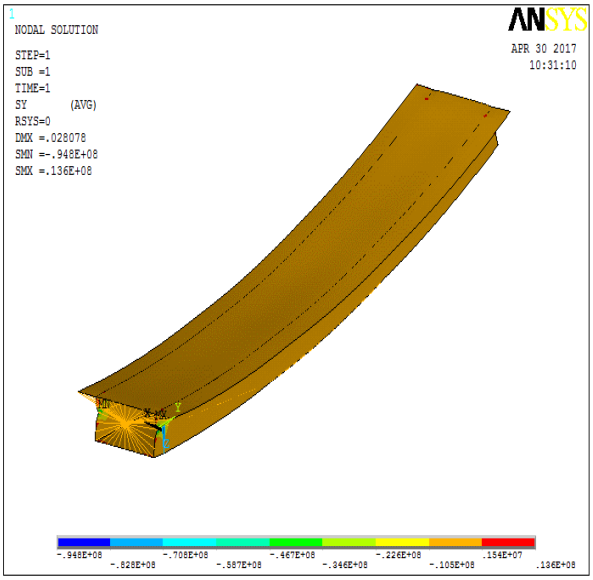

Figure (5.15) Longitudinal stresses for load case (TL2)

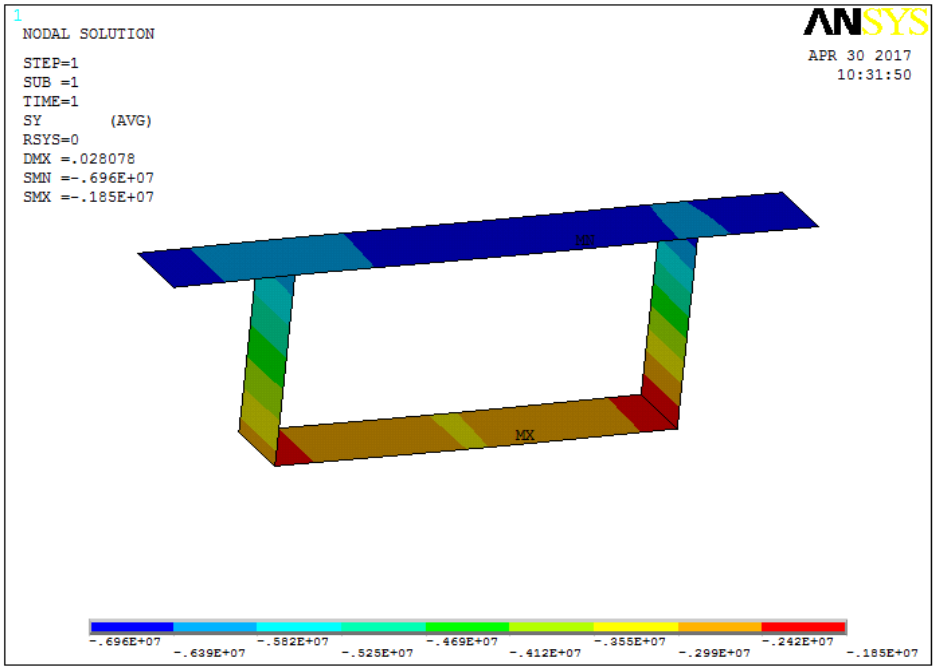

Figure (5.16) Longitudinal stresses at mid-span for load case (TL2), straight bridge model (N/m^2)

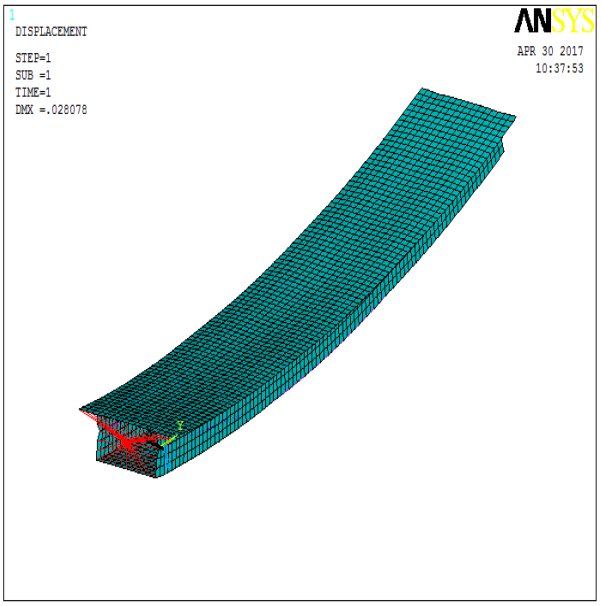

Figure (5.17) Deformed shape for load case (TR2)

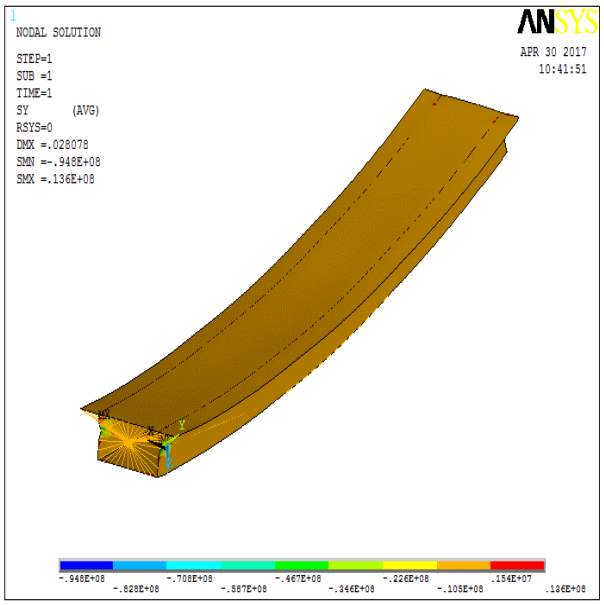

Figure (5.18) Longitudinal stresses for load case (TR2)

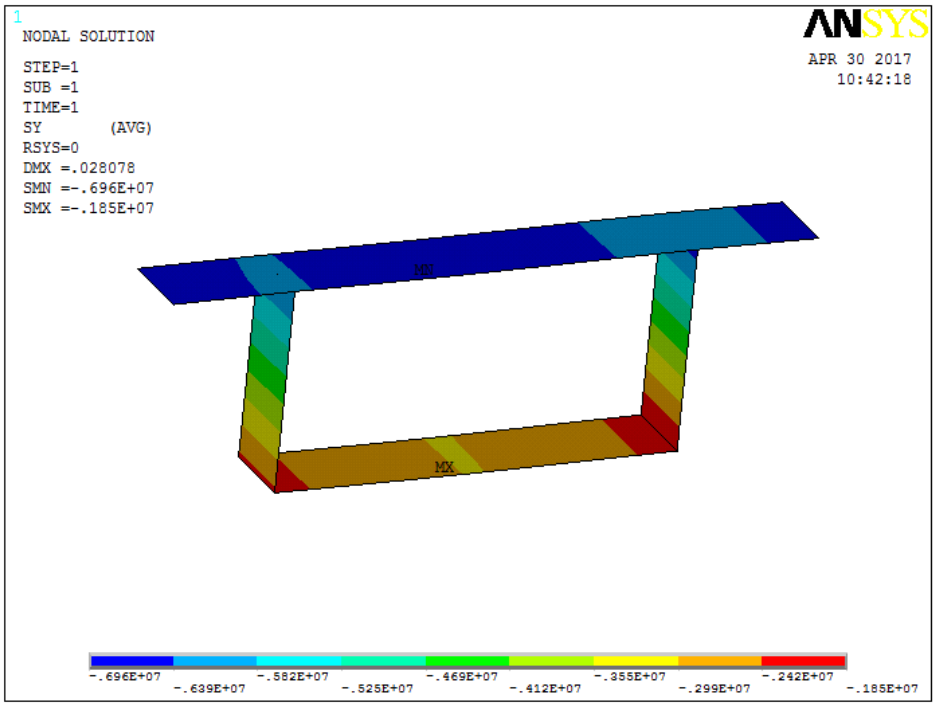

Figure (5.19) Longitudinal stresses at mid-span for load case (TR2), straight bridge model

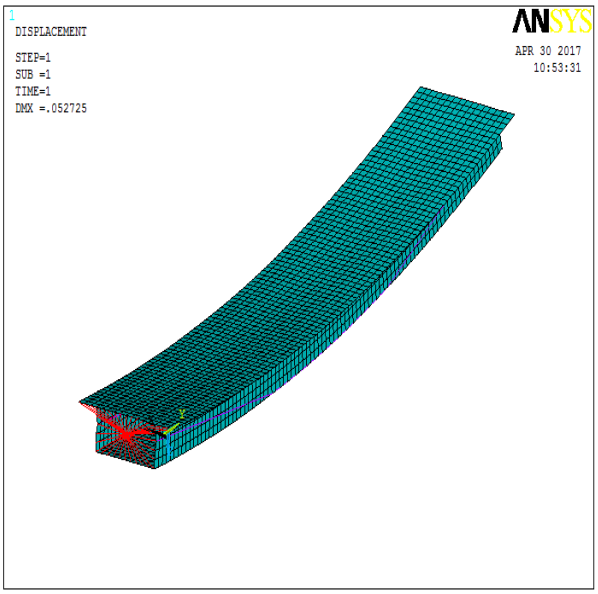

Figure (5.20) Deformed shape for load case (T4)

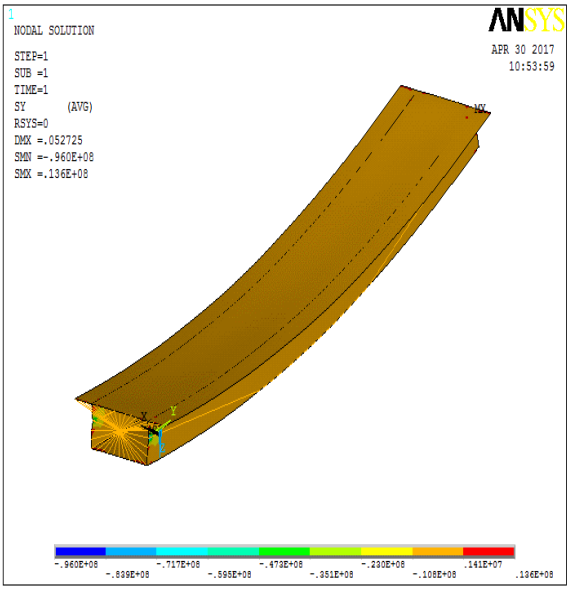

Figure (5.21) Longitudinal stresses for load case (T4)

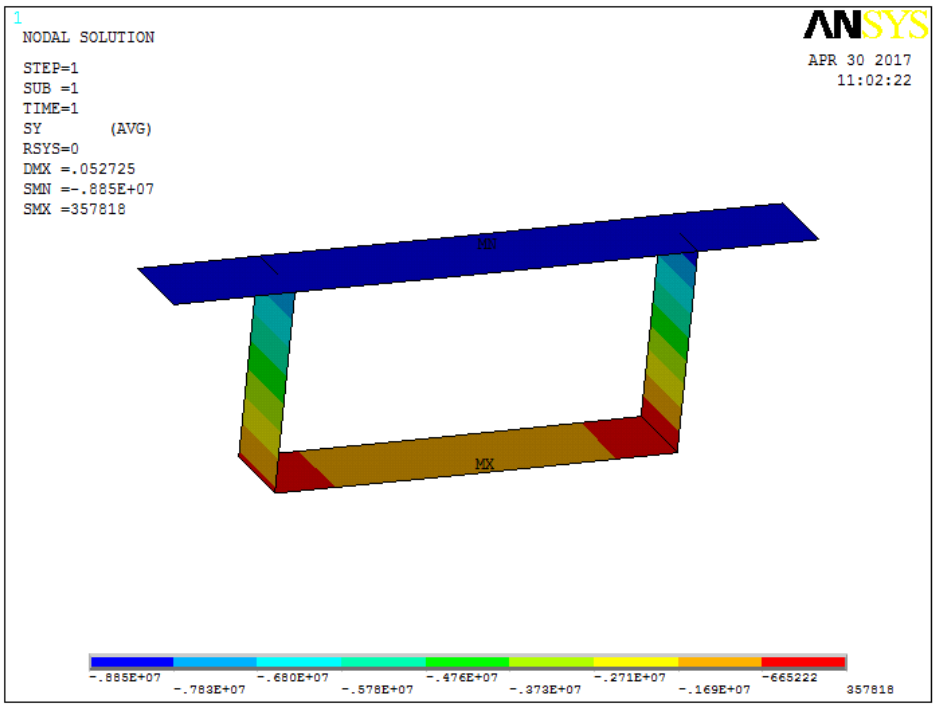

Figure (5.22) Longitudinal stresses at mid-span for load case (T4), straight bridge model

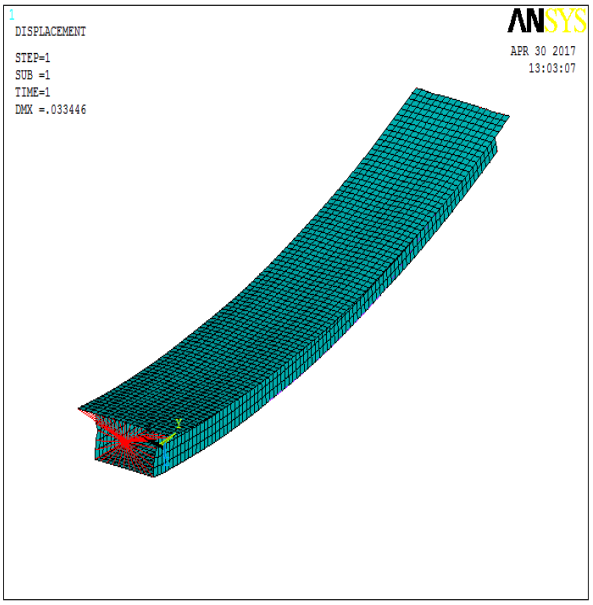

Figure (5.23) Deformed shape for load case (TR5)

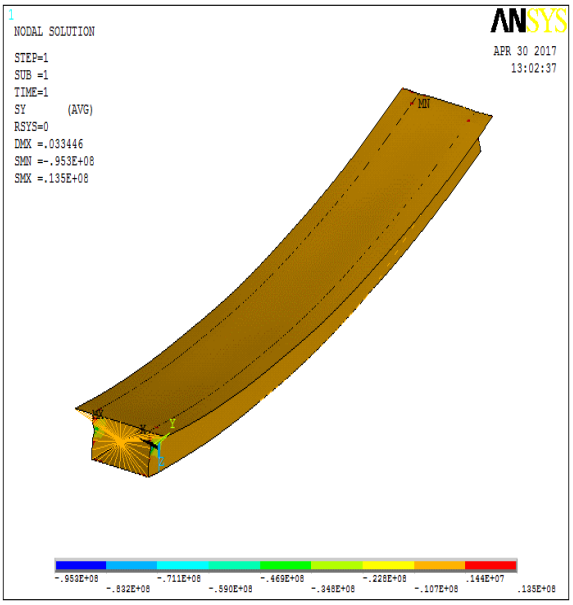

Figure (5.24) Longitudinal stresses for load case (TR5)

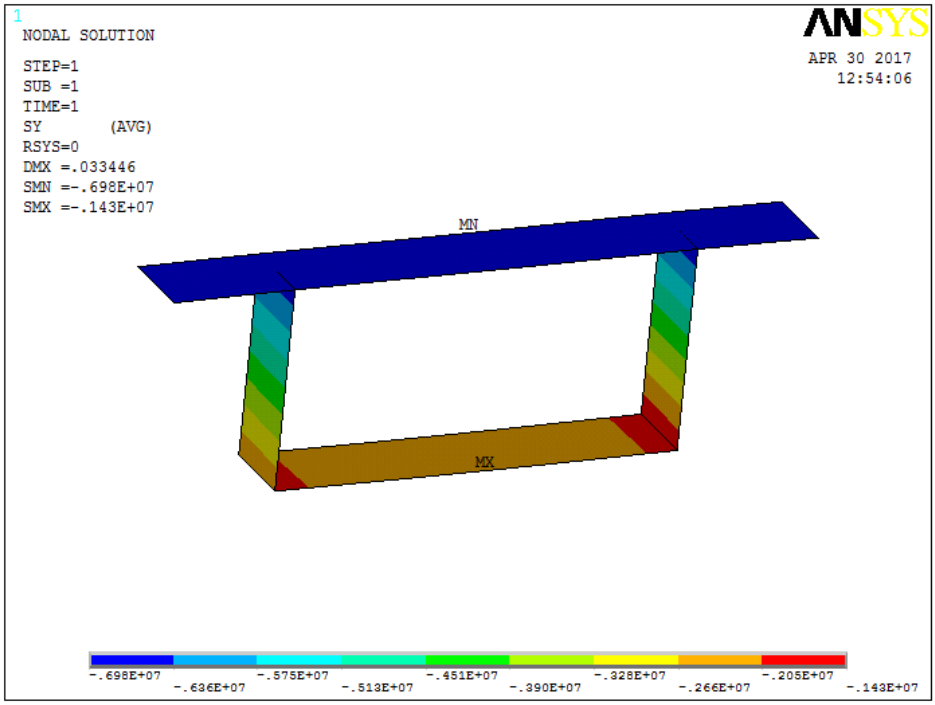

Figure (5.25) Longitudinal stresses at mid-span for load case (TR5), straight bridge model

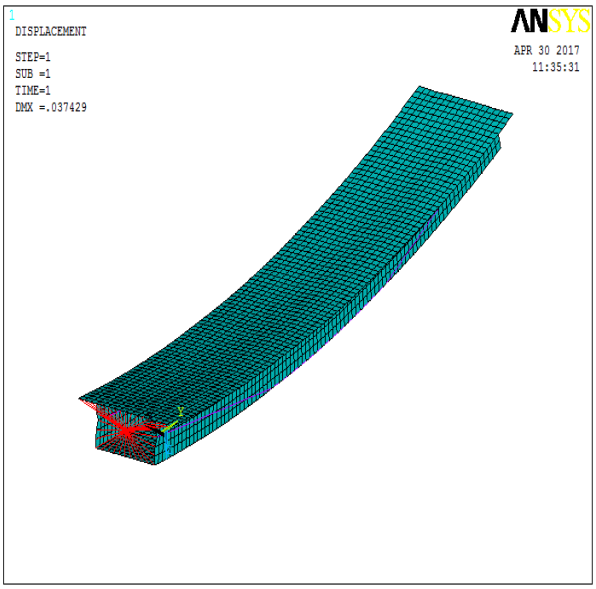

Figure (5.26) Deformed shape for load case (TL6)

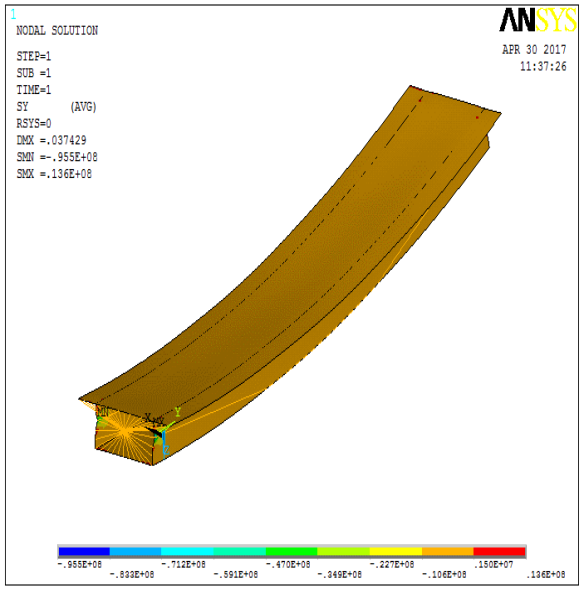

Figure (5.27) Longitudinal stresses for load case (TL6)

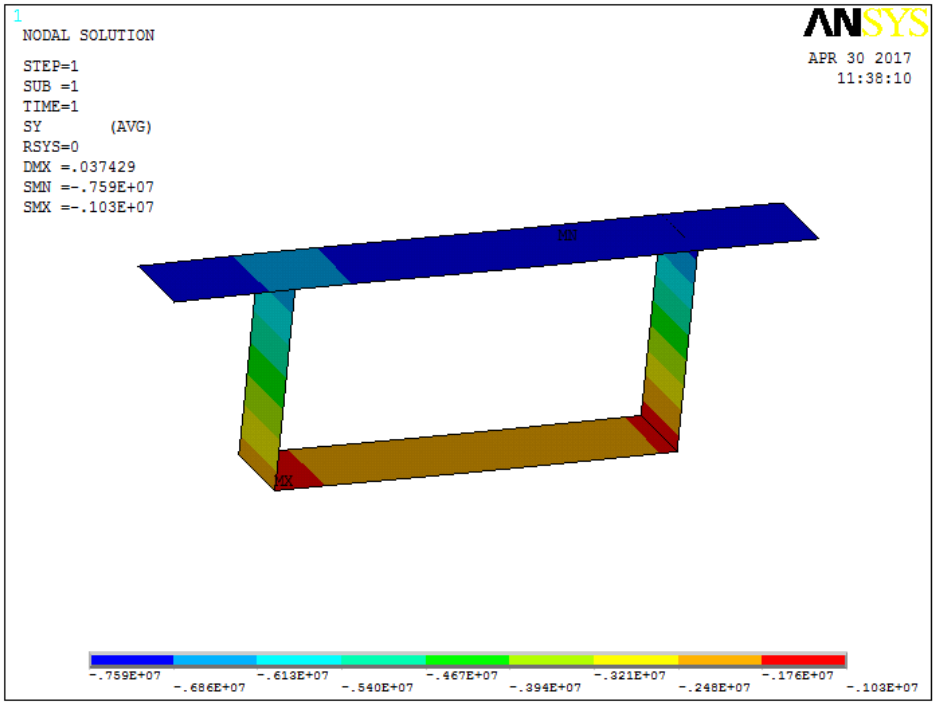

Figure (5.28) Longitudinal stresses at mid-span for load case (TL6), straight bridge model

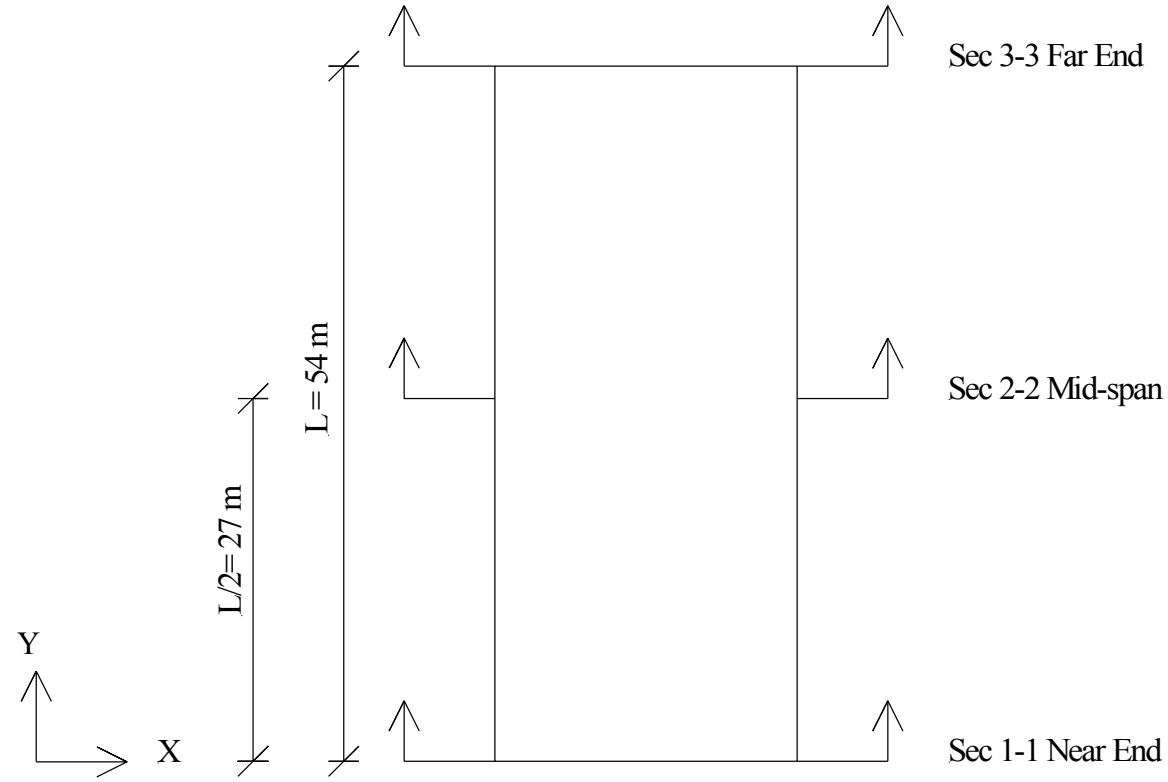

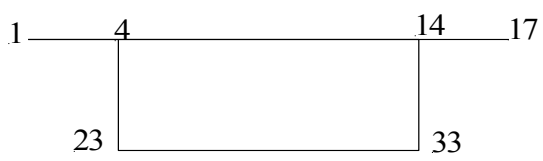

Sec 1-1 Near end

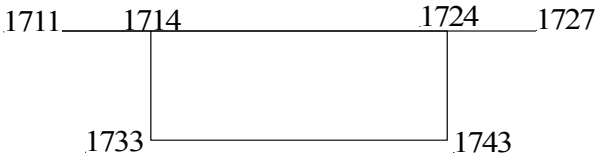

Sec 2-2 Mid-span

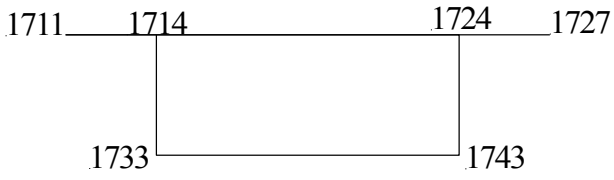

Sec 3-3 Far End

Figure (5.29) Influence lines (nodes location)

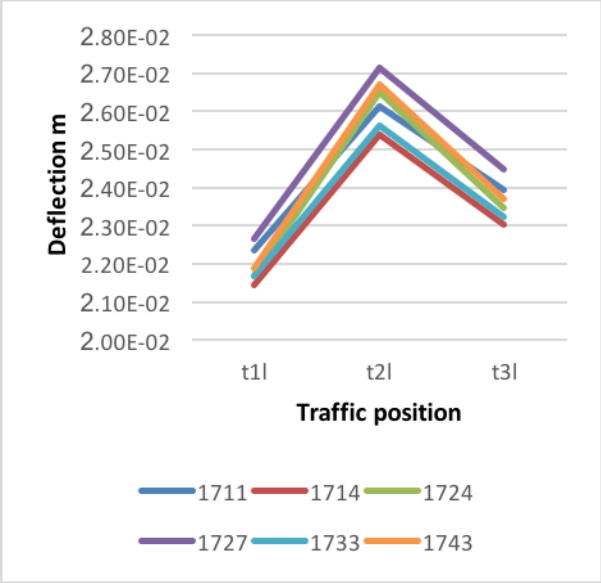

Figure (5.30) Influence line for deflection at mid-span for load cases (TL1, TL2 & TL3)

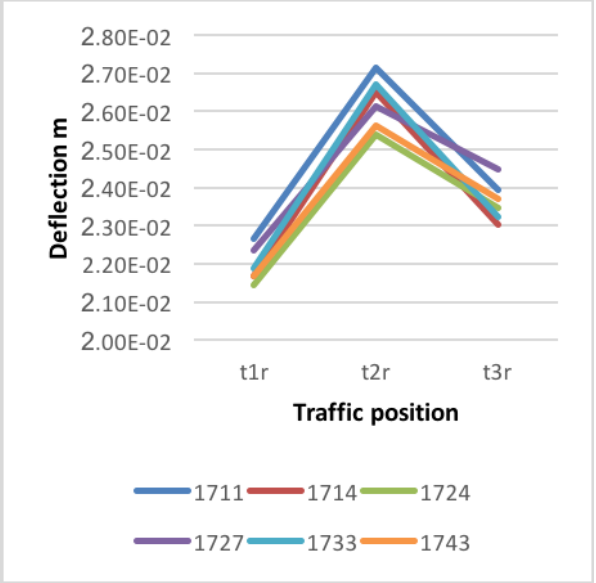

Figure (5.31) Influence line for deflection at mid-span for load cases (TR1, TR2 & TR3)

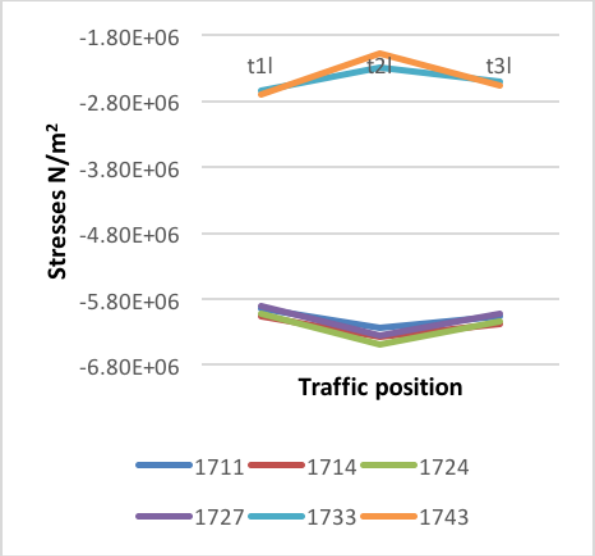

Figure (5.32) Influence line for stresses at mid-span for load cases (TL1, TL2 & TL3)

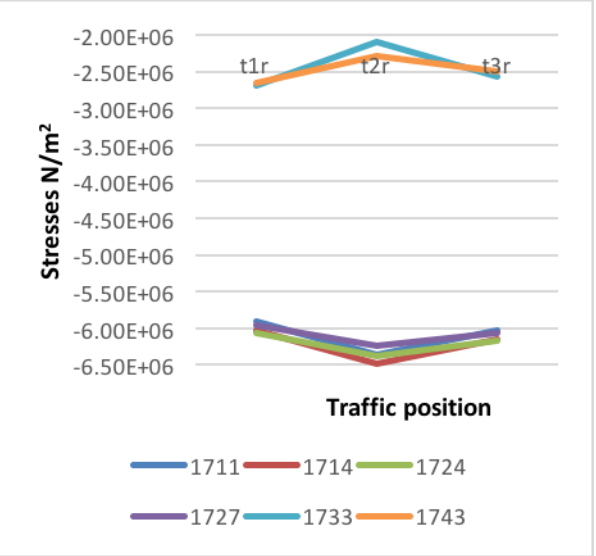

Figure (5.33) Influence line for stresses at mid-span for load cases (TR1, TR2 & TR3)

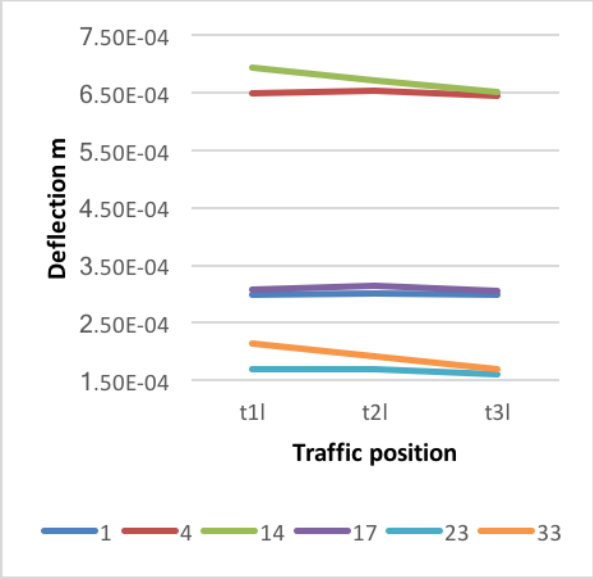

Figure (5.34) Influence line for deflection at near end for load cases (TL1, TL2 & TL3)

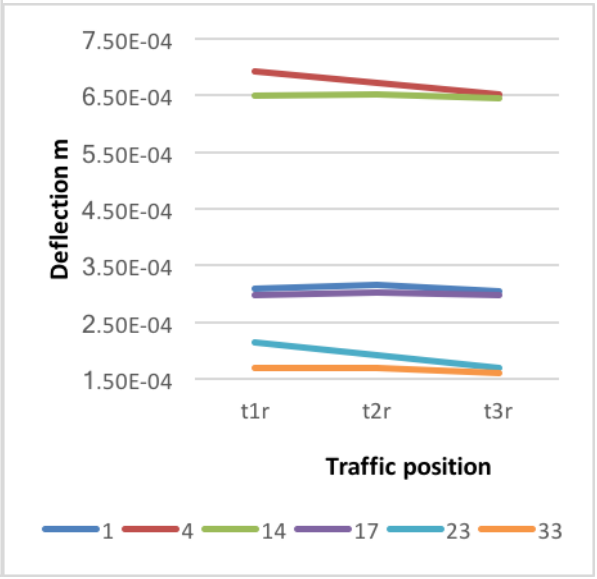

Figure (5.35) Influence line for deflection at near end for load cases (TR1, TR2 & TR3)

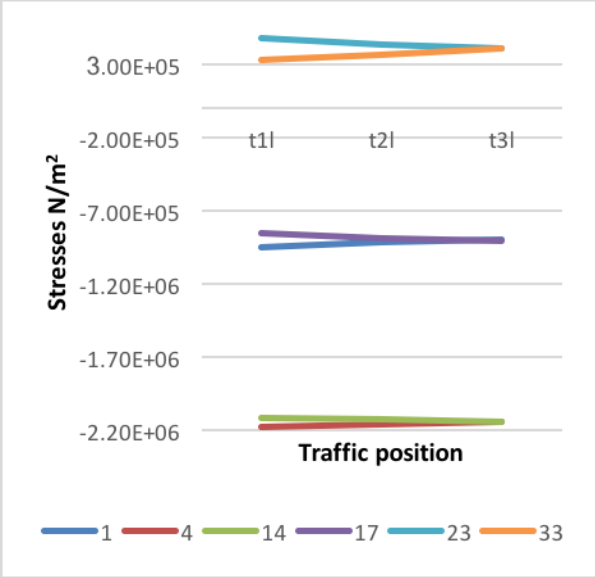

Figure (5.36) Influence line for stresses at near end for load cases (TL1, TL2 & TL3)

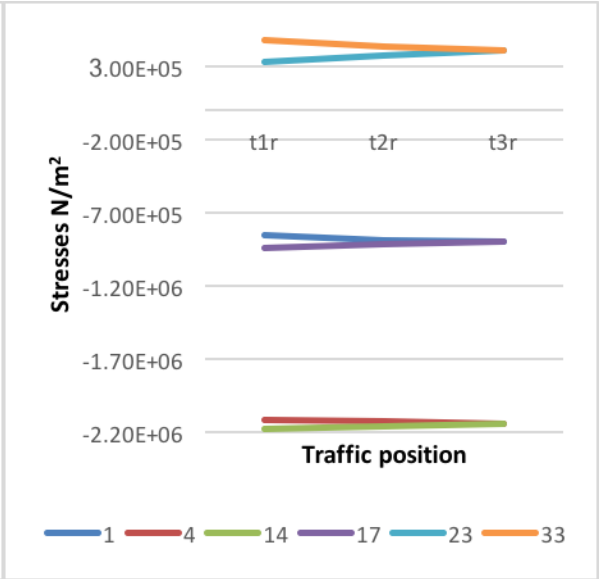

Figure (5.37) Influence line for stresses at near end for load cases (TR1, TR2 & TR3)

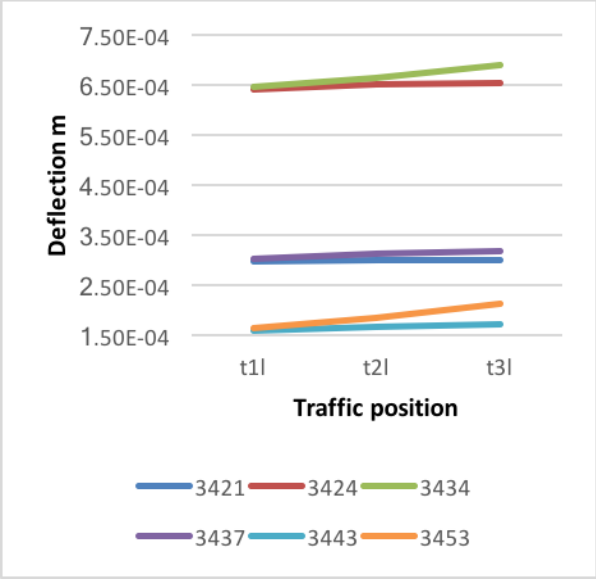

Figure (5.38) Influence line for deflection at far end for load cases (TL1, TL2 & TL3)

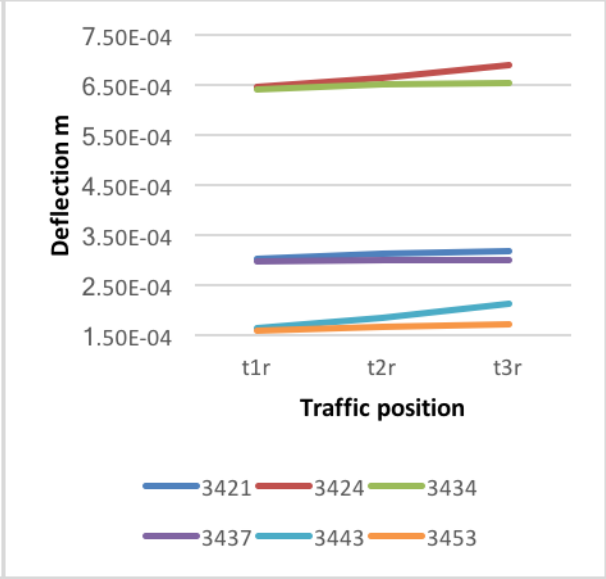

Figure (5.39) Influence line for deflection at far end for load cases (TR1, TR2 & TR3)

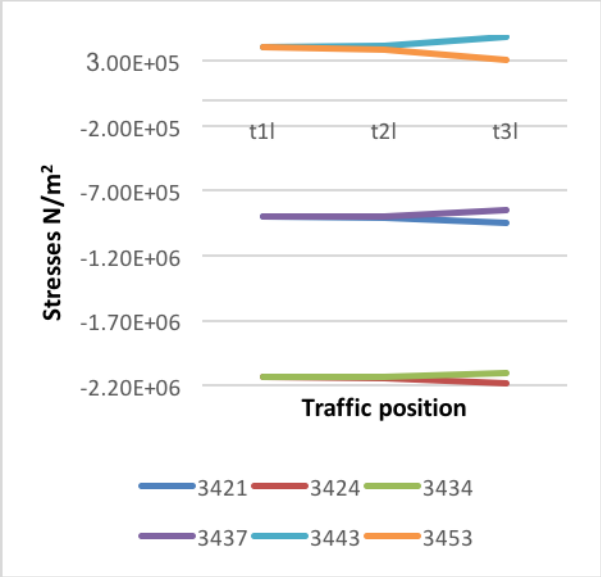

Figure (5.40) Influence line for stresses at far end for load cases (TL1, TL2 & TL3)

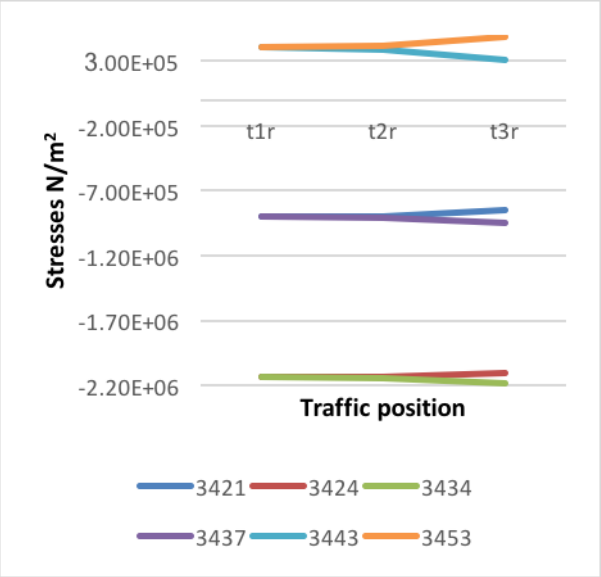

Figure (5.41) Influence line for stresses at far end for load cases (TR1, TR2 & TR3)

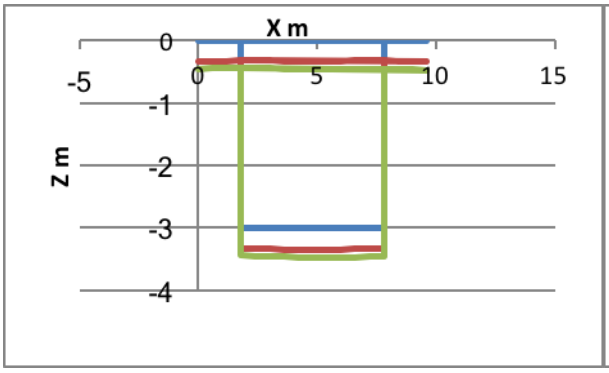

Figure (5.42) Deflected shape at near end for load cases (TL2)

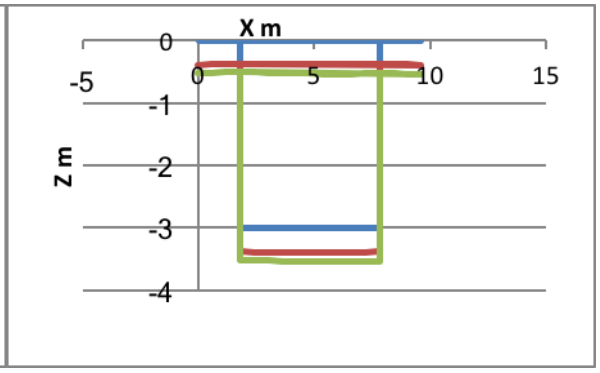

Figure (5.43) Deflected shape at mid-span for load cases (TL2)

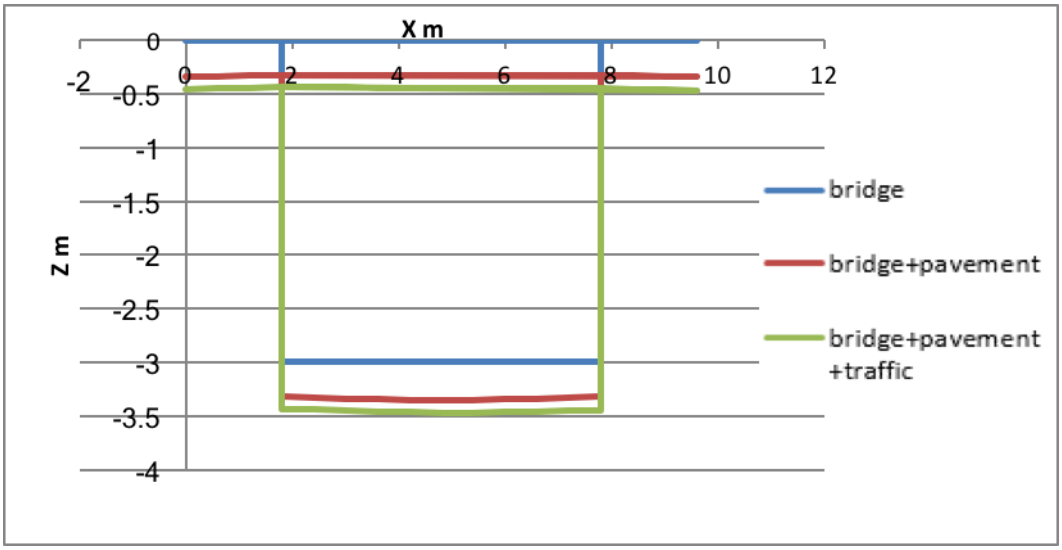

Figure (5.44) Deflected shape at far end for load cases (TL2)

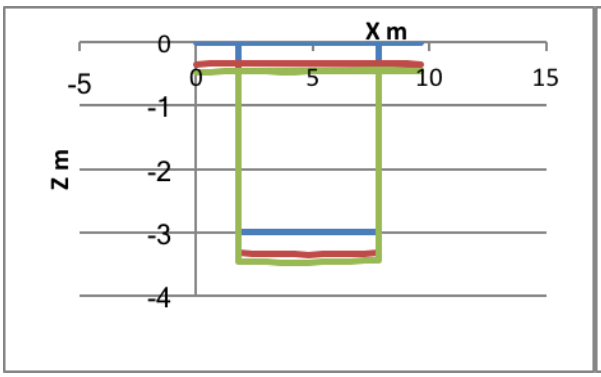

Figure (5.45) Deflected shape at near end for load cases (TR2)

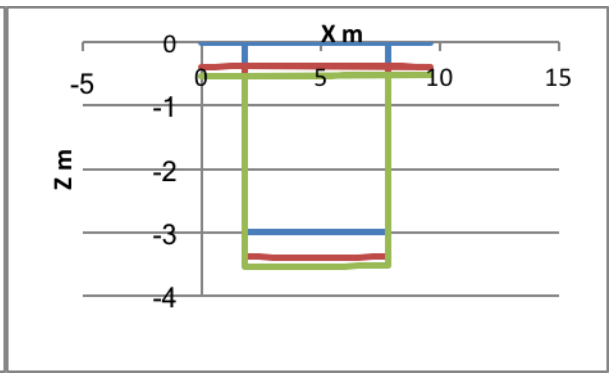

Figure (5.46) Deflected shape at mid-span for load cases (TR2)

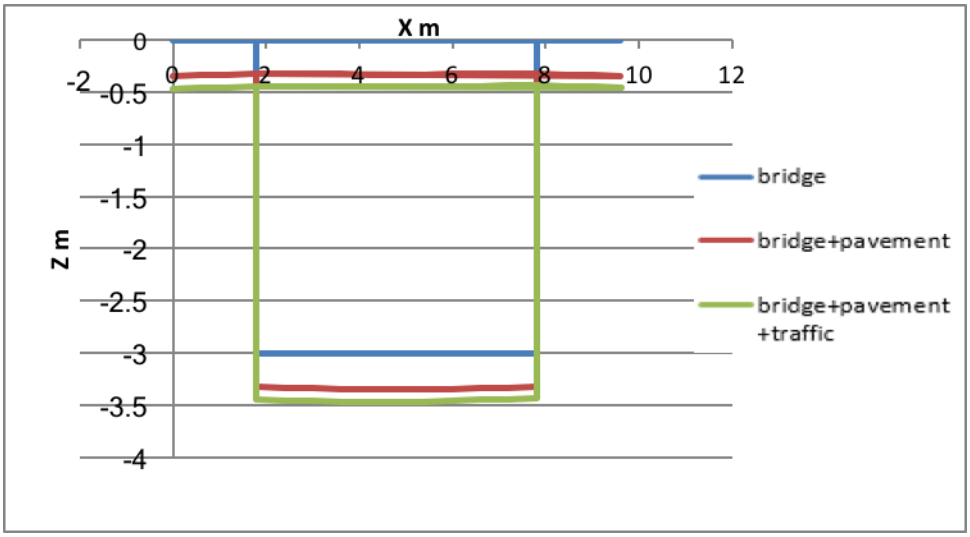

Figure (5.47) Deflected shape at far end for load cases (TR2)

Examining the results from this series of analyses, a number of observations can be made. Firstly, it can be seen that in proportion to the self-weight of the bridge, prestress and additional weight from the pavement and parapet, the traffic loading is considerably lower, However the effects of traffic volume and location on the deflection and longitudinal stresses are evident from the figures.

As curvature increases, so too does the rotation of the deck and hence the warping stress. Similarly, as curvature increases, so too does deflection and longitudinal stress. The most onerous deformations are associated with asymmetrical load cases.

When the load is asymmetrical, although the bridge section remains comfortably in compression across its entirety, the effects of torsion become clear from the mid-span contour plots, figure (5.19). The warping stresses in the deck are such that tension is produced at the loaded side and compression at the unloaded side (expected from the direction of twist). This is evident when observing the stresses across the deck, i.e. the compression is lower on the loaded side. When looking at the soffit, the lowest compression should therefore be on the opposite diagonal of the box section to the loaded deck side. This is corroborated by the contour plot.

The influence lines for stress are only meaningful for the moving load (2 lorries) along the deck span as presented in figures (5.32), (5.33), (5.36), (5.37), (5.40) and (5.41). Again, these support the presence of relatively low warping stresses, and the effects of twist can be seen clearly. As the loads for load cases 1 and 3 are asymmetrical about the mid-span, this accounts for the asymmetry in the influence line.

Load case T4 is effectively presents the worst case in terms of full loading, and produces tensile stresses. Therefore, case T4 will not be considered in the curved box girder studies for prestress force equal 31000 kN due to the heavy traffic loads applied.

Curved box shell model

The same philosophy used for the straight box model was adopted and the results are shown in the following figures for each of the load cases:

1-Case TL2, the boundary conditions for different load (traffic) are shown in figure (5.48). Deformed shape figure (5.49), longitudinal stresses figure (5.50) and mid-span longitudinal stresses figure (5.51).

2-Case TR2, the boundary conditions for different load (traffic) are shown in figure (5.52). Deformed shape figure (5.53), longitudinal stresses figure (5.54), and mid-span longitudinal stresses figure (5.55).

3-Case TR5, the boundary conditions for different load (traffic) are shown in figure (5.56). Deformed shape figure (5.57), longitudinal stresses figure (5.58) and mid-span longitudinal stresses figure (5.59).

4-Case TL6, the boundary conditions for different load (traffic) are shown in figure (5.60). Deformed shape figure (5.61), longitudinal stresses figure (5.62) and mid-span longitudinal stresses figure (5.63).

5-Influence line for defection at mid-span for left and right sides are shown in figures (5.64) & (5.65), near end figure (5.68) & (5.69) and far end figure (5.72) & (5.73).

6-Influence line for stresses at mid-span figures (5.66) & (5.67), near end figure (5.70) & (5.71) and far end figure (5.74) & (5.75).

7-Case TR5 deflection at near end figure (5.76), mid-span figure (5.77) and far end figure (5.78).

8-Case TL6 deflection at near end figure (5.79), mid-span figure (5.80) and far end figure (5.81).

The results are summarised in table 5.2.

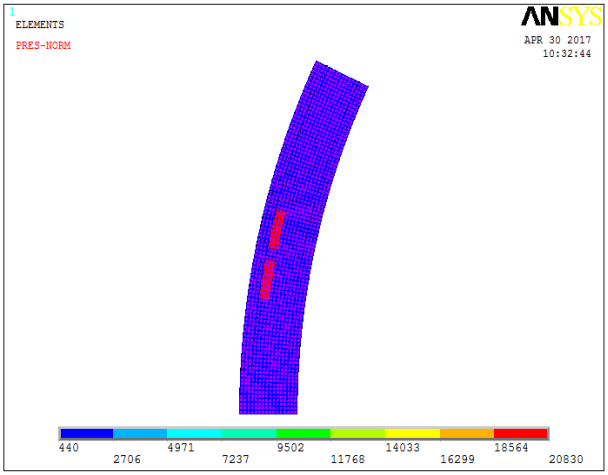

Figure (5.48) Load case TL2 for traffic loads, Delta = 3m

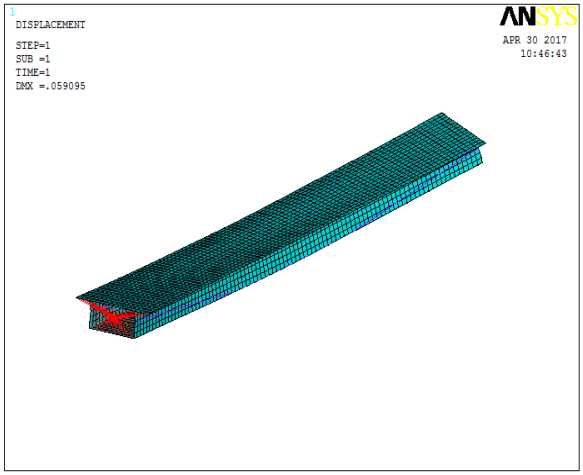

Figure (5.49) Deformed shape for load case TL2, Delta = 3 m

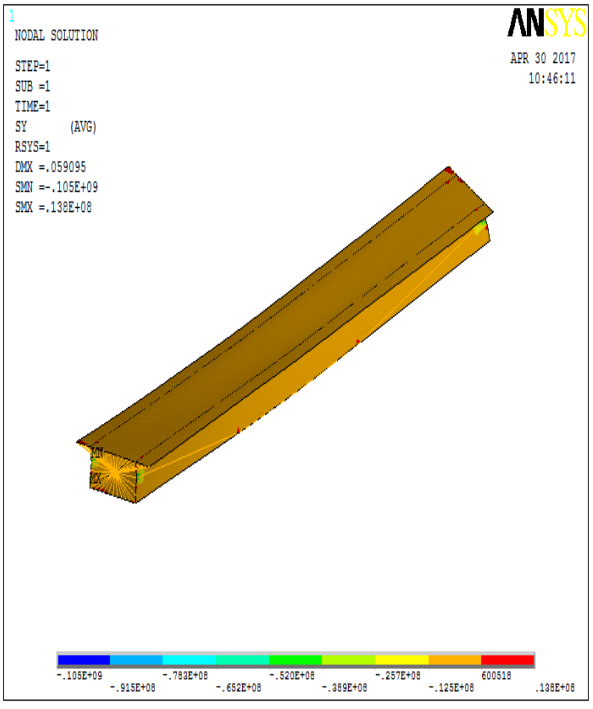

Figure (5.50) longitudinal stresses for load case TL2, Delta = 3 m

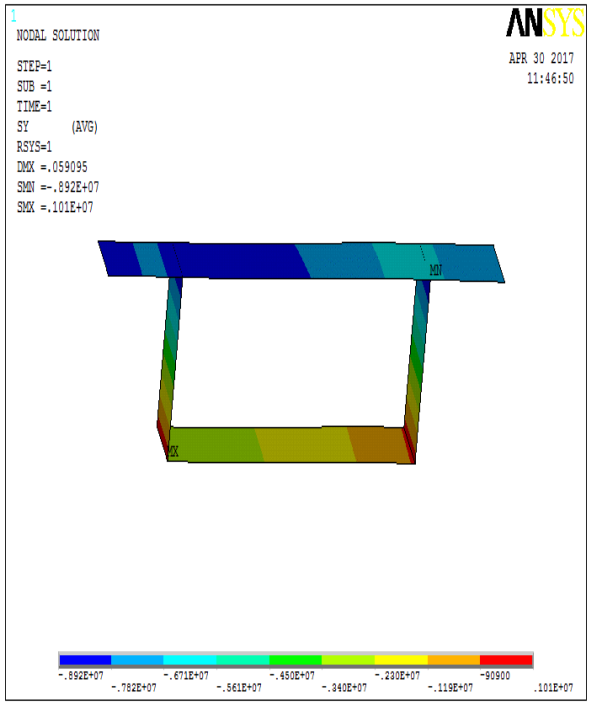

Figure (5.51) longitudinal stresses for load case TL2, Delta = 3 m

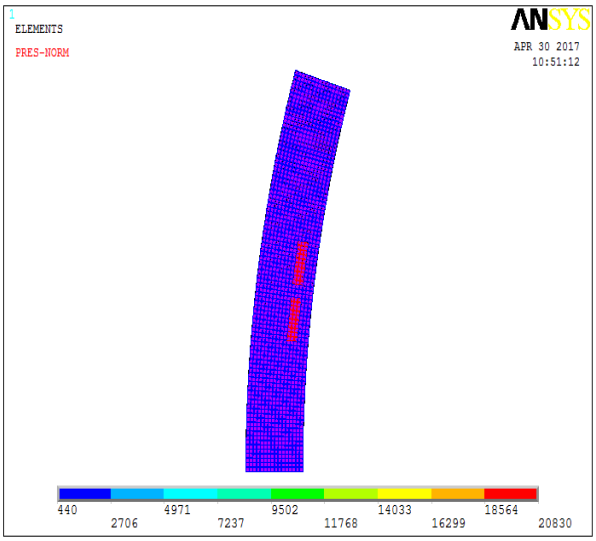

Figure (5.52) Load case TR2 for traffic loads, delta = 2m

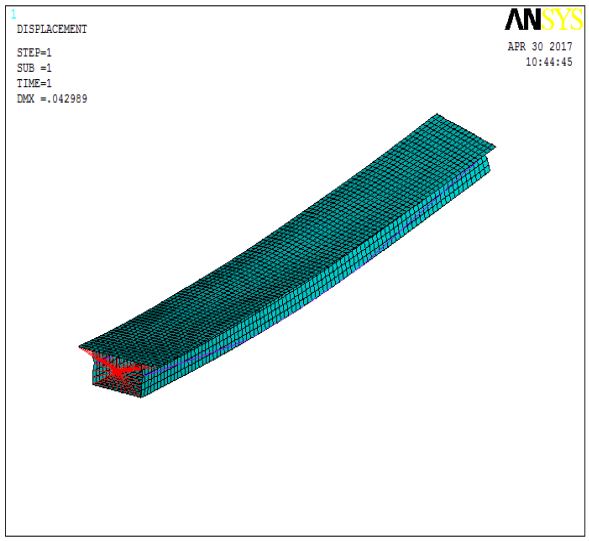

Figure (5.53) Deformed shape for load case TR2, Delta = 2 m

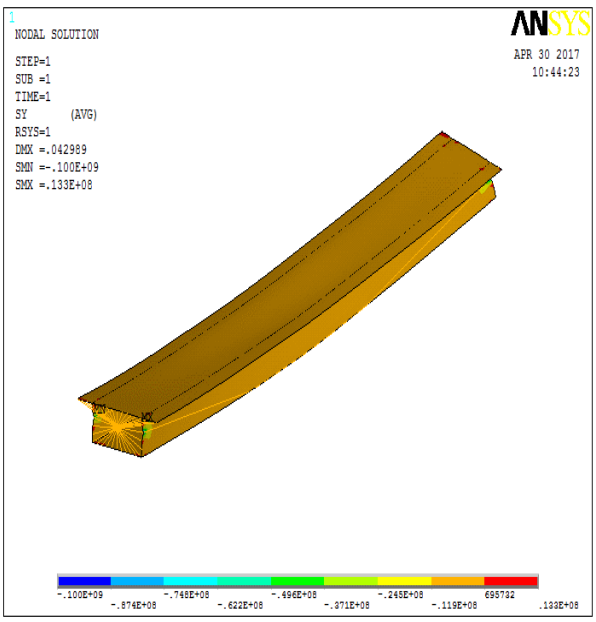

Figure (5.54) Longitudinal stresses for load case TR2, Delta = 2 m

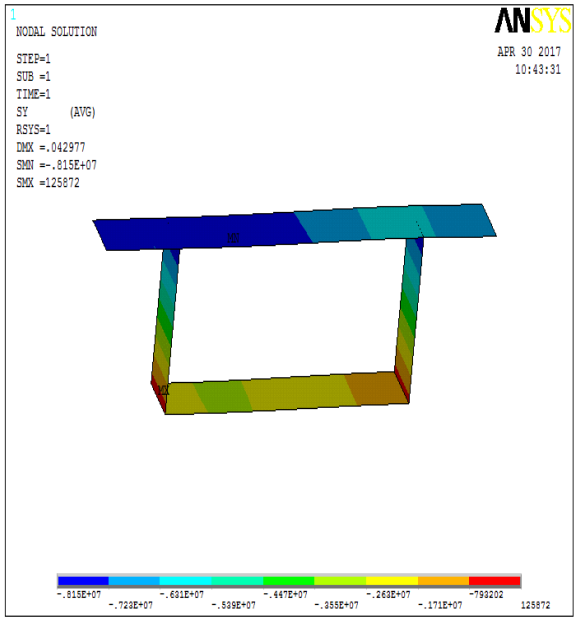

Figure (5.55) Longitudinal stresses at mid-span for Load case TR2, Delta = 2 m

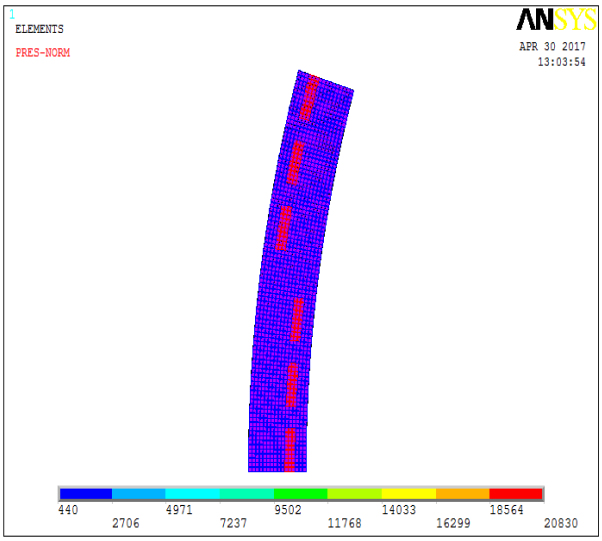

Figure (5.56) Load case TR5 for traffic loads, Delta = 2m

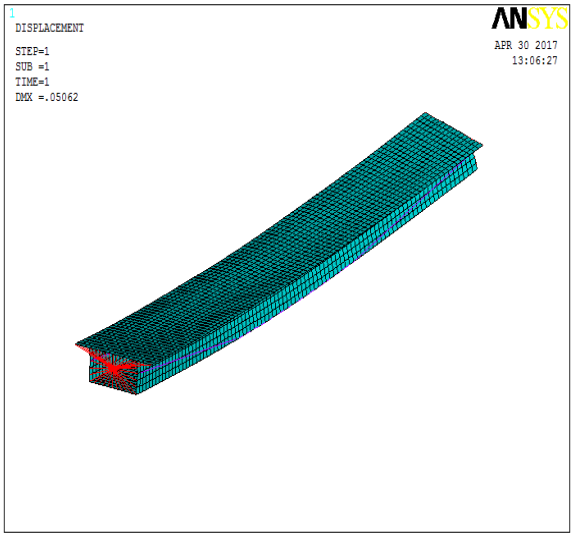

Figure (5.57) Deformed shape for load case TR5, Delta = 2 m

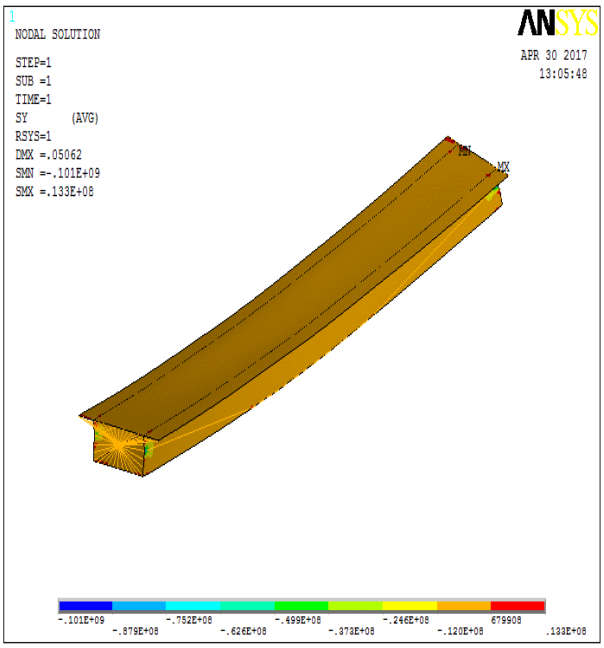

Figure (5.58) Longitudinal stresses for load case TR5, Delta = 2 m

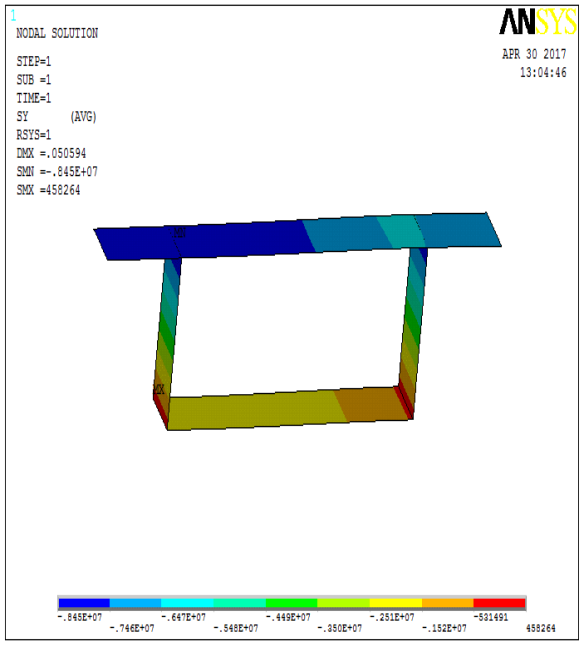

Figure (5.59) Longitudinal stresses at mid-span for Load case TR5, Delta = 2 m

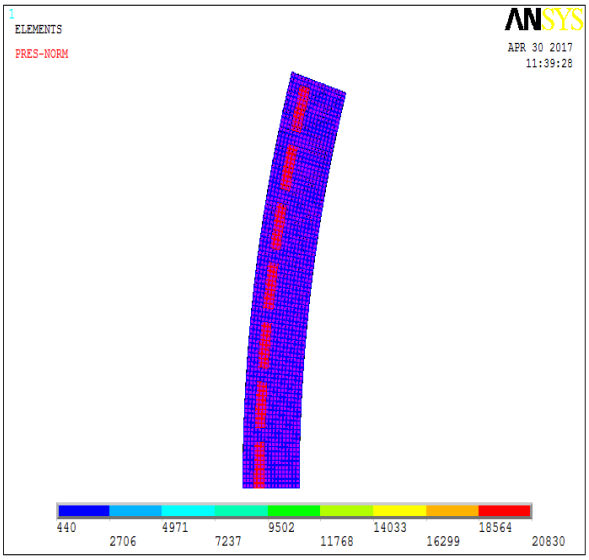

Figure (5.60) Load case TL6 for traffic loads, Delta = 2m

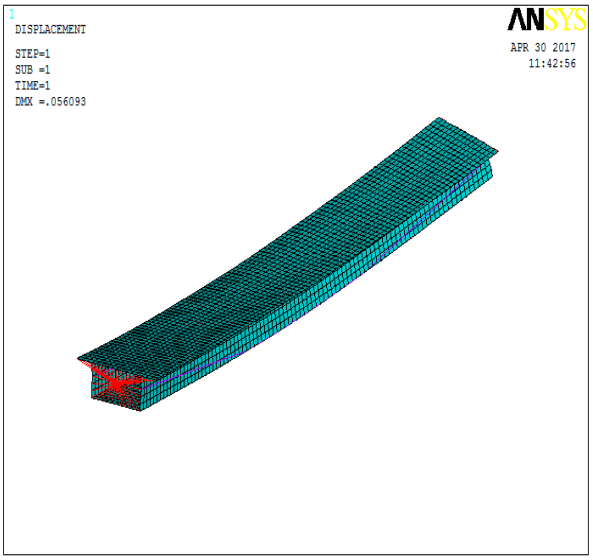

Figure (5.61) Deformed shape for load case TL6, Delta = 2 m

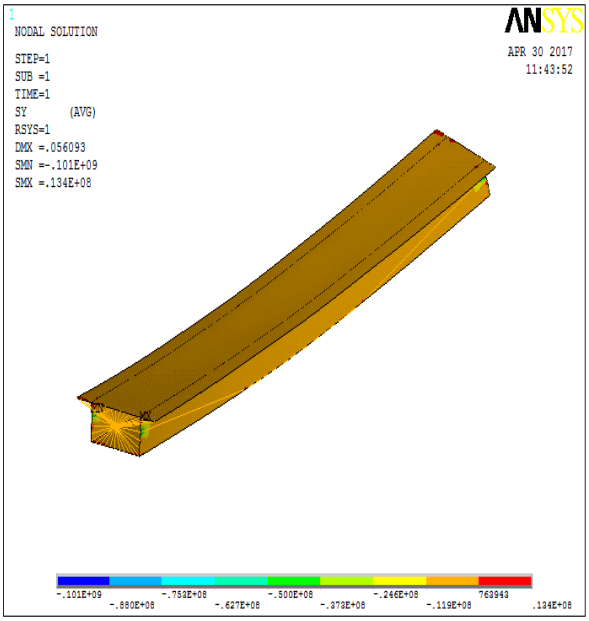

Figure (5.62) Longitudinal stresses for load case(TL6), Delta = 2 m

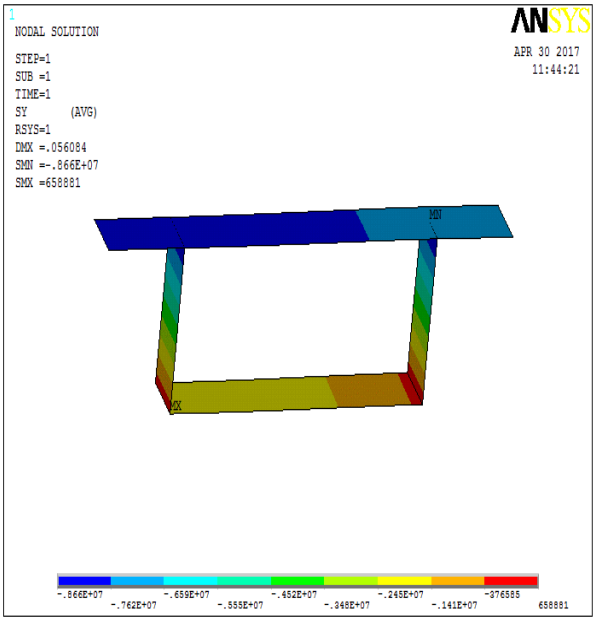

Figure (5.63) Longitudinal stresses at mid-span for load case TL6, Delta = 2 m

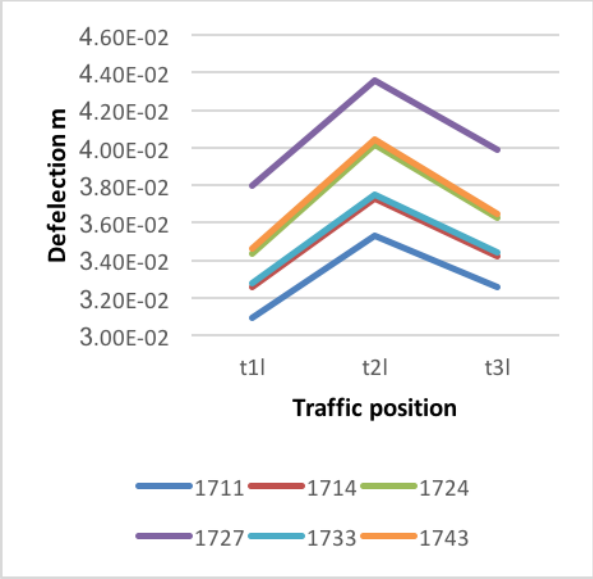

Figure (5.64) Influence line for deflection at mid-span for load cases (TL1, TL2 & TL3), Delta = 2m

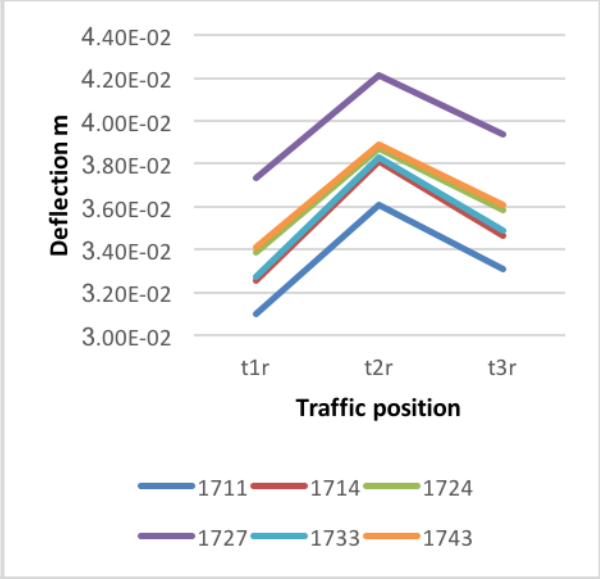

Figure (5.65) Influence line for deflection at mid-span for load cases (TR1, TR2 & TR3), Delta = 2m

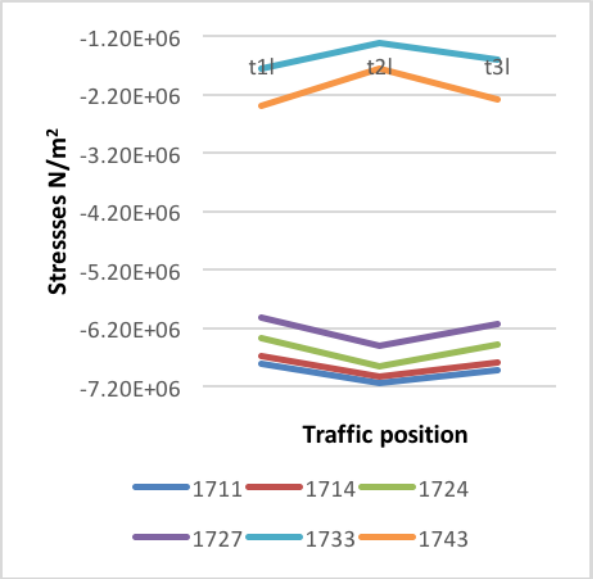

Figure (5.66) Influence line for stresses at mid-span for load cases (TL1, TL2 & TL3), Delta = 2m

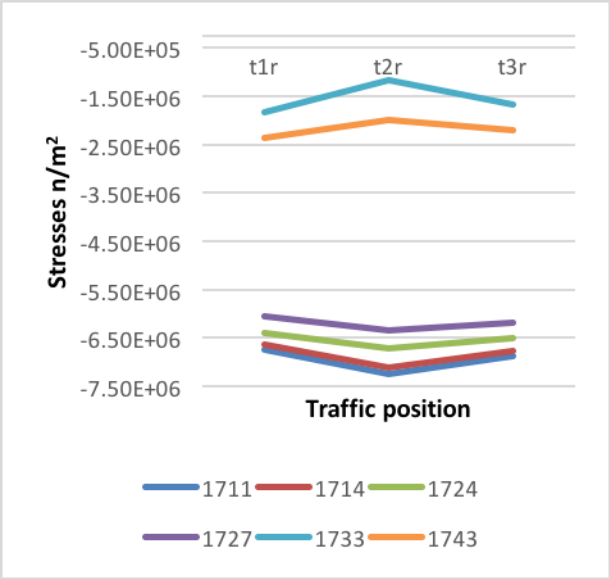

Figure (5.67) Influence line for stresses at mid-span for load cases (TR1, TR2 & TR3), Delta = 2m

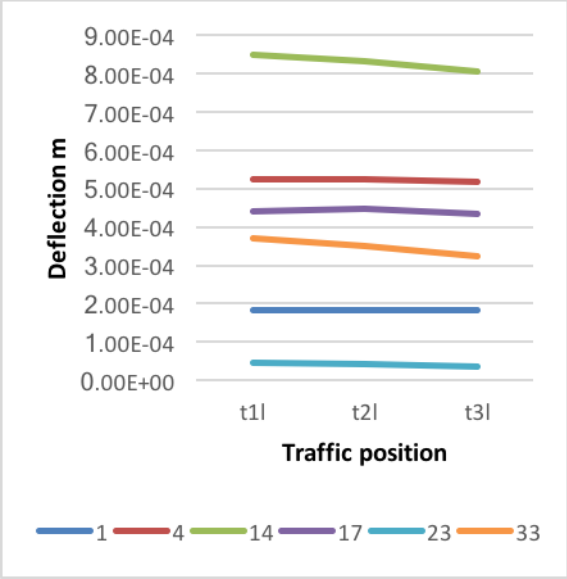

Figure (5.68) Influence line for deflection at near end for load cases (TL1, TL2 & TL3), Delta = 2m

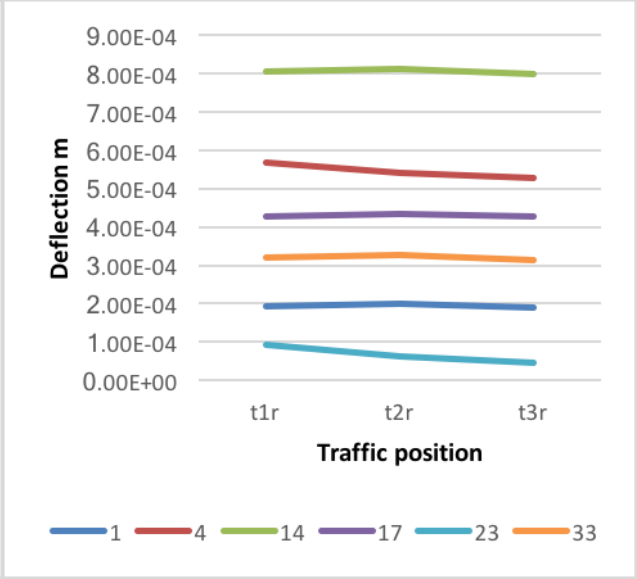

Figure (5.69) Influence line for deflection at near end for load cases (TR1, TR2 & TR3), Delta = 2m

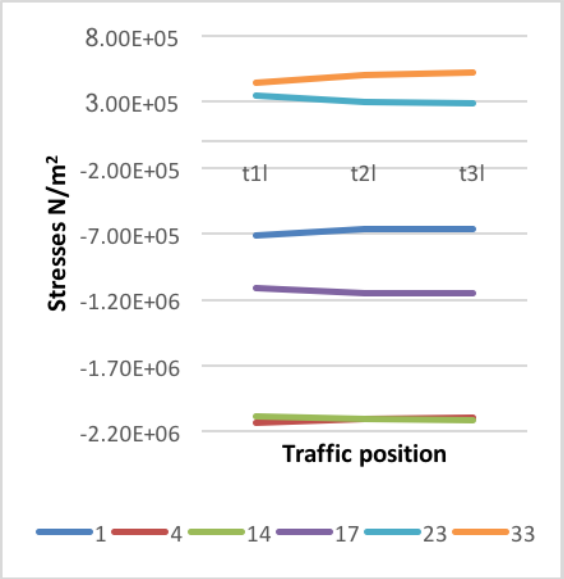

Figure (5.70) Influence line for stresses at near end for load cases (TL1, TL2 & TL3), Delta = 2m

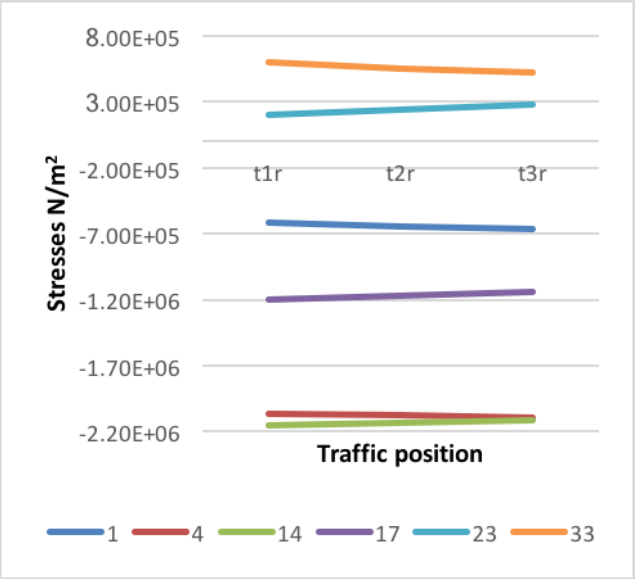

Figure (5.71) Influence line for stresses at near end for load cases (TR1, TR2 & TR3), Delta = 2m

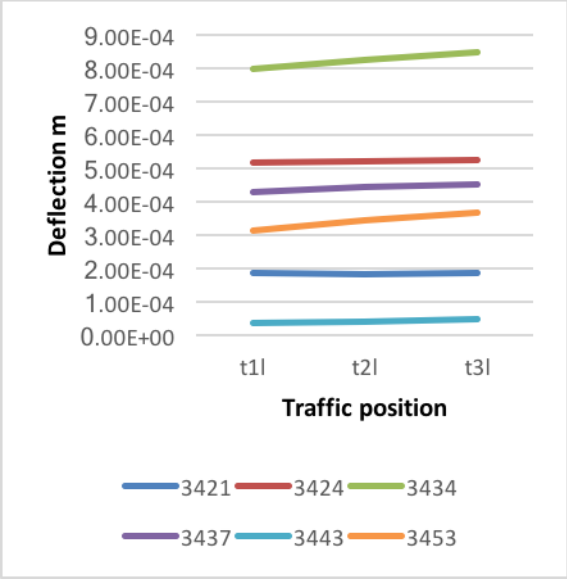

Figure (5.72) Influence line for deflection at far end for load cases (TL1, TL2 & TL3), Delta = 2m

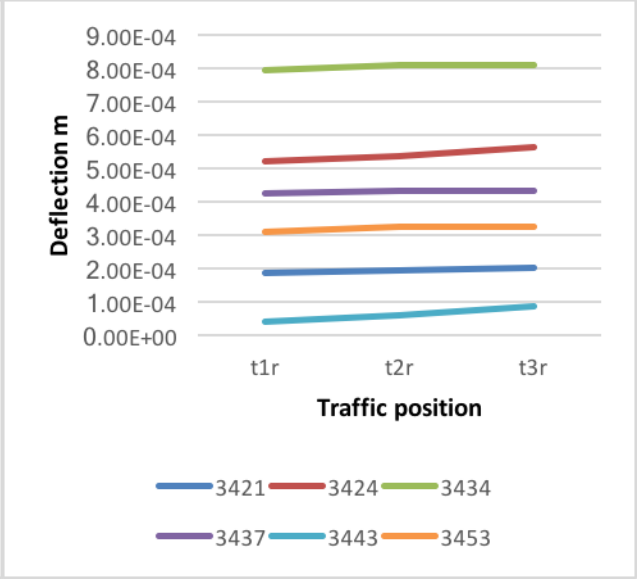

Figure (5.73) Influence line for deflection at far end for load cases (TR1, TR2 & TR3), Delta = 2m

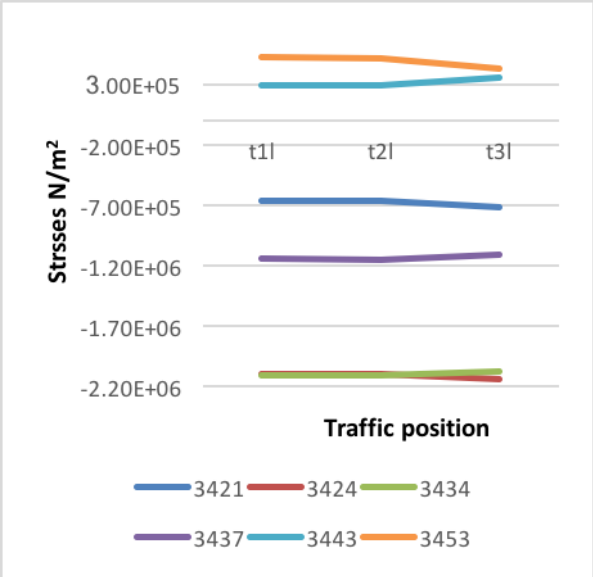

Figure (5.74) Influence line for stresses at far end for load cases (TL1, TL2 & TL3), Delta = 2m

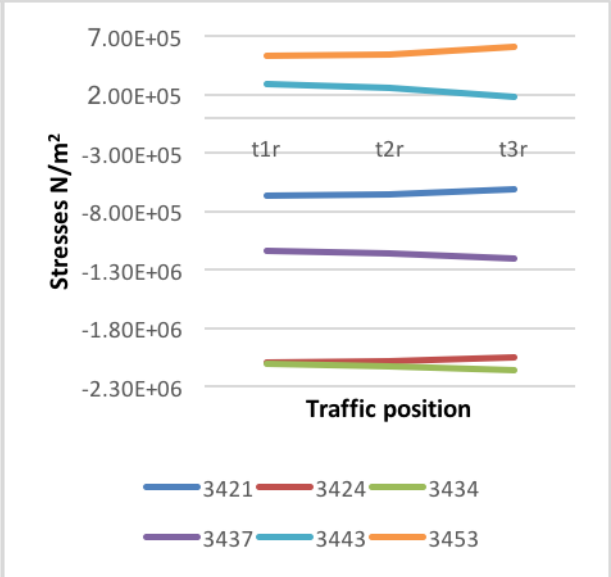

Figure (5.75) Influence line for stresses at far end for load cases (TR1, TR2 & TR3), Delta = 2m

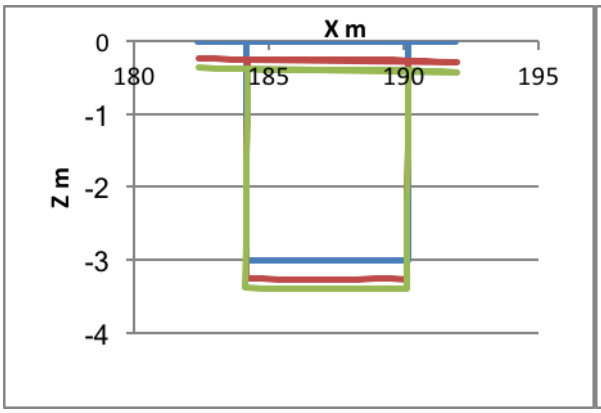

Figure (5.76) Deflection shape at near end for load case TR5, Delta = 2 m

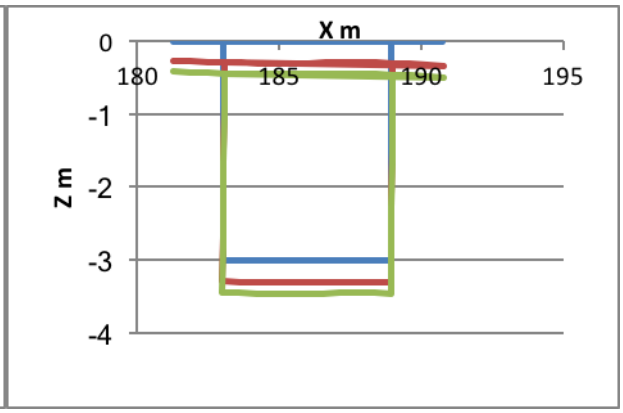

Figure (5.77) Deflection shape at mid-span for load case TR5, Delta = 2 m

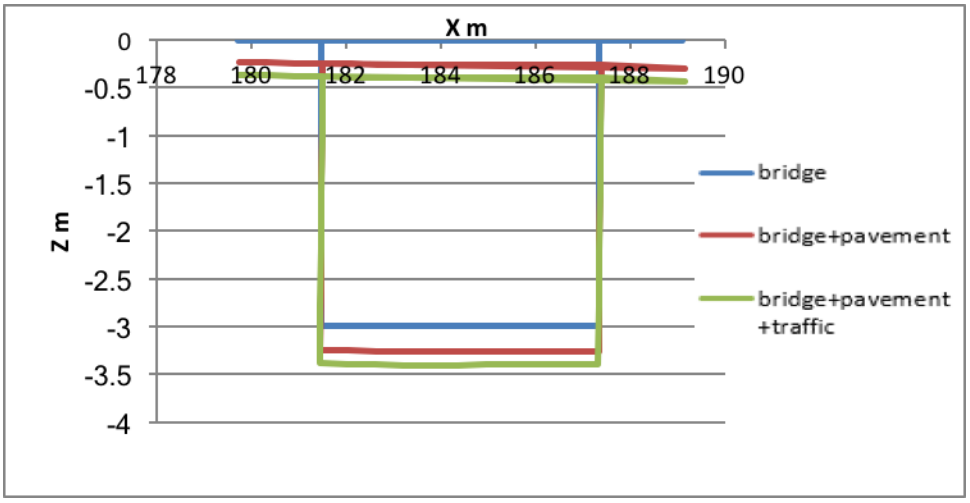

Figure (5.78) Deflection shape at far end for load case TR5, Delta = 2 m

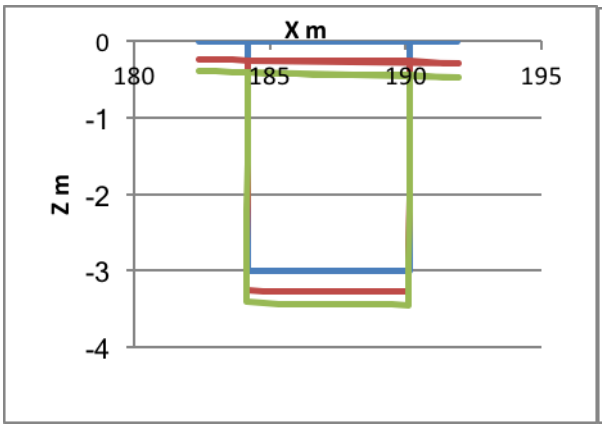

Figure (5.79) Deflection shape at near end for load case TL6, Delta = 2 m

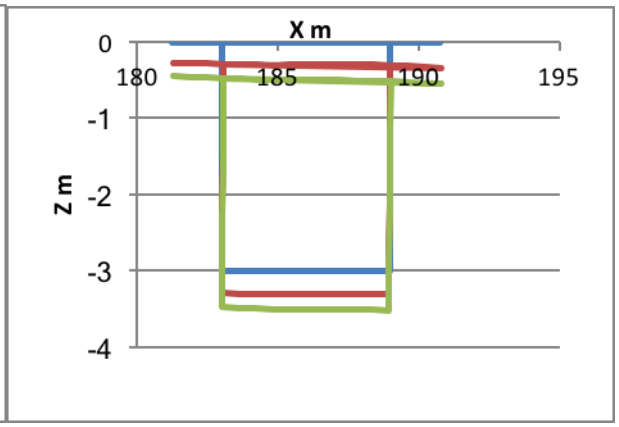

Figure (5.80) Deflection shape at mid-span for load case TL6, Delta = 2 m

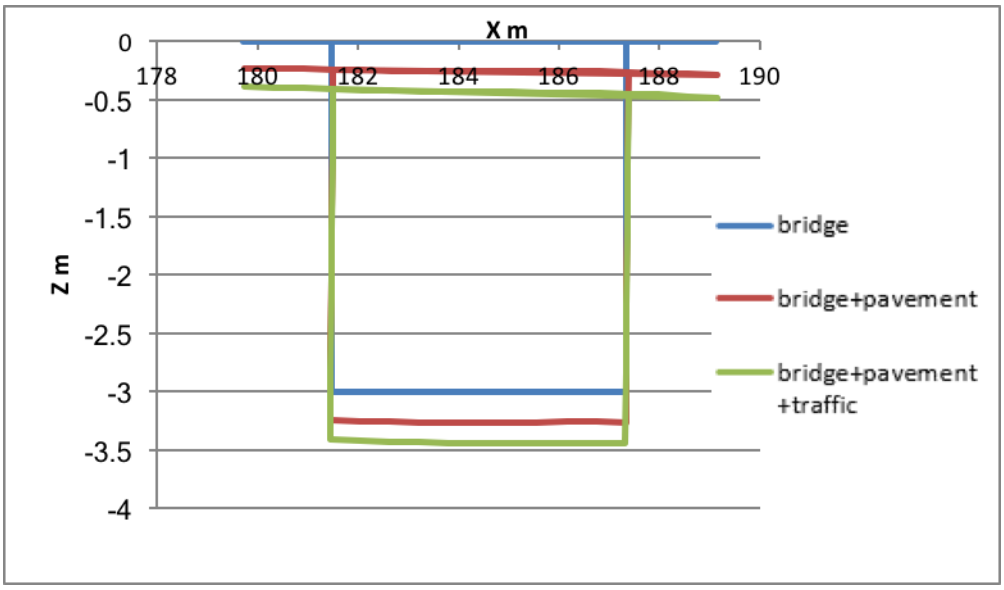

Figure (5.81) Deflection shape at far end for load case TL6, Delta = 2 m

Table (5.2) Stresses values at mid-span (prestress, P = 31000kN)

Traffic	Delta (m)	Location	Reaction (kN)	Moment (kN.m)	Prestress (kN)	Slab stresses (N/mm^2)		Soffit stresses (N/mm^2)	
						Interior	Exterior	Interior	Exterior
T1	δ=3	Left, TL1	-10280	28620	15290	-8.57	-7.70	0.55	0.30
	δ=3	Right, TR1	-10270	22400	15280	-8.55	-8.01	0.48	0.45
T2	δ=3	Left, TL2	-10280	27000	15370	-8.65	-7.90	0.95	0.40
	δ=2	Right, TR2	-10110	13600	15300	-8.46	-8.31	0.11	0.06
T3	δ=3	Left, TL3	-10280	26600	15320	-8.65	-8.16	0.72	0.55
	δ=3	Right, TR3	-10270	24500	15300	-7.99	-7.85	0.69	0.31
T4	δ= 0		-12500	0	15480	-8.76	-8.15	0.33	0.32
T5	δ=2	Left, TL5	-11000	15400	15350	-8.41	-8.10	0.45	0.31
	δ=2	Right, TR5	-11000	15400	15350	-8.39	-8.12	0.45	0.32
T6	δ=2	Left, TL6	-11300	19200	15410	-8.60	-8.22	0.66	0.41
	δ=2	Right, TR6	-11200	12500	15410	-8.82	-8.35	0.95	0.65

For the three others prestress forces (35000 kN, 39000kN and 45000 kN) the same philosophy was applied and the results have been illustrated through tables (5.3), (5.4) and (5.5).

Table (5.3) Stresses values at mid-span (prestress, P = 35000kN)

Traffic	Delta (m)	Location	Reaction (kN)	Moment (kN.m)	Prestress (kN)	Slab stresses (N/mm^2)		Soffit stresses (N/mm^2)	
						Interior	Exterior	Interior	Exterior
T1	δ=4	Left, TL1	-10460	31700	17110	-9.30	-8.95	0.40	0.31
	δ=4	Right, TR1	-10440	29600	17090	-9.42	-9.18	0.35	0.28
T2	δ=4	Left, TL2	-10460	32800	17200	-9.72	-8.85	0.90	0.75
	δ=4	Right, TR2	-10430	30700	17230	-9.85	-9.20	0.95	0.91
T3	δ=4	Left, TL3	-10460	32160	17140	-9.59	-9.07	0.62	0.41
	δ=4	Right, TR3	-10440	30100	17130	-9.43	-8.64	0.50	0.42
T4	δ=2		-12840	18100	17370	-9.92	-9.15	1.05	0.86
T5	δ=3	Left, TL5	-12000	27600	17180	-9.32	-9.01	0.28	0.21
	δ=3	Right, TR5	-12000	27600	17180	-9.32	-9.02	0.27	0.21
T6	δ=3	Left, TL6	-11500	31900	17250	-9.20	-8.51	0.55	0.48
	δ=3	Right, TR6	-11400	24900	17250	-9.68	-8.81	0.75	0.34

Table (5.4) Stresses values at mid-span (prestress = 39000kN)

Traffic	Delta (m)	Location	Reaction (kN)	Moment (kN.m)	Prestress (kN)	Slab stresses (N/mm^2)		Soffit stresses (N/mm^2)	
						Interior	Exterior	Interior	Exterior
T1	δ=5	Left, TL1	-10600	41400	18870	-9.89	-9.37	0.50	0.22
	δ=5	Right, TR1	-10600	39300	18870	-10.02	-9.41	0.46	0.26
T2	δ=5	Left, TL2	-10600	43000	18990	-10.68	-10.05	1.05	0.54
	δ=5	Right, TR2	-10600	40700	18910	-10.70	-9.94	1.28	0.73
T3	δ=5	Left, TL3	-10600	42000	251.6	-10.32	-9.67	0.68	0.45
	δ=6	Right, TR3	-10800	51000	216.9	-11.48	-10.85	0.15	0.09
T4	δ=3		-13000	32400	19210	-10.66	-9.83	0.11	0.10
T5	δ=4	Left, TL5	-11400	33600	18940	-9.99	-8.91	0.30	0.24
	δ=5	Right, TR5	-11400	23600	18940	-10.01	-9.06	0.33	0.24
T6	δ=5	Left, TL6	-11600	38300	19110	-9.75	-8.98	0.67	0.55
	δ=5	Right, TR6	-11600	30900	19010	-10.51	-8.17	0.95	0.72

Table (5.5) Stresses values at mid-span (prestress = 45000kN)

Traffic	Delta (m)	Location	Reaction (kN)	Moment (kN.m)	Prestress (kN)	Slab stresses (N/mm^2)		Soffit stresses (N/mm^2)	
						Interior	Exterior	Interior	Exterior
T1	δ=7	Left, TL1	-11100	65000	21860	-12.45	-11.70	1.10	0.95
	δ=7	Right, TR1	-11000	62700	21840	-12.30	-11.28	0.95	0.63
T2	δ=6	Left, TL2	-10900	54400	21800	-12.14	-10.92	0.61	0.47
	δ=6	Right, TR2	-10800	52000	218.2	-12.32	-11.75	0.87	0.72
T3	δ=6	Left, TL3	-10900	53300	21720	-11.95	-11.68	0.22	0.20
	δ=6	Right, TR3	-10800	51000	21700	-11.82	-10.85	0.15	0.14
T4	δ=4		-13300	39500	22050	-12.00	-11.05	0.65	0.55
T5	δ=6	Left, TL5	-11800	56300	21950	-12.87	-11.45	0.13	0.85
	δ=6	Right, TR5	-11800	56200	21940	-12.89	-11.50	0.14	0.92
T6	δ=5	Left, TL6	-11900	49400	21840	-11.25	-10.91	0.12	0.09
	δ=5	Right, TR6	-11800	41700	251.6	-11.89	-11.25	0.34	0.30

For the curved bridge model, it can be seen that the effects of horizontal curvature exaggerate the variation of longitudinal stress around the section. The results demonstrate the effects of the various parameters on the behaviour of the member.

For the prestress, the level of pretension appears to act in a similar fashion whether the bridge is curved or not. The level of pretension is usually selected on a desired longitudinal stress profile under service loading, and as the pretension varies the balance of the vertically applied loading is altered accordingly (the lower prestress values in the study present under-balanced conditions). As the bridge curves on plan the line of the prestressing tendons generally follow the horizontal centroid, and therefore do not impose any equivalent horizontal load. Essentially, they apply compression to the section akin to a prestressed arch on plan. In the vertical plane, eccentricity from the section centroid does apply an upward equivalent load which can balance a portion of the downward UDL.

Considering the traffic positioning (influence lines), it can be seen that the increased curvature causes more disparity in the longitudinal (tangential) stresses at the four corners of the box section, as demonstrated by larger gaps between the influence lines. As curvature increases, so too does rotation of the deck, hence so too does warping stress. Also, the size of the traffic loading when compared to self-weight is such that it has minimal effect on the stresses. The stresses at sab edges are very similar along the deck because shear leg and flange cross bending permit stress relief. However, at the soffit, the section is torsionally very stiff and stresses are almost ten times larger at mid-span, see figure (5.82). However, the influence lines do show how the torsional warping stresses change across the section as the position of the applied torque from the traffic alters, for example the influence lines for the stresses at mid-span in figures (5.66) and (5.67).

The deflections have been factored to enhance the visualization. Again, the physical twist is slightly evident from the date for the unsymmetrical loading conditions when viewing the displaced section diagrams.

Hence, it is still the horizontal curvature of the bridge which appears to have the most effect on the results. As the curvature increases, the torsional effects of both UDL loading and traffic are increased accordingly. As the horizontal eccentricity of the load from the supports increases as the curvature increases and the torsional moment increases too.

For example, δ= 2 m where σ_1 is stress for TR2 and σ_2 is stress for TR6

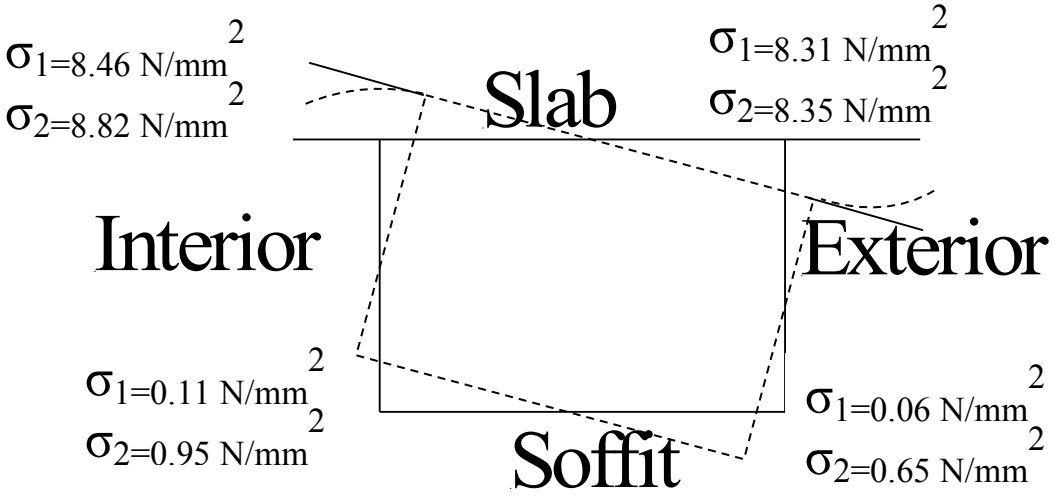

Figure (5.82) Stresses for mid-span box girder bridge, TR2 & TL6, Delta = 2 m

Chapter Six

Conclusion and Recommendations

6.1 Conclusion

The aim of the study was to develop and present a readily scriptable finite element representation of a concrete box girder bridge with a particular prestress, that can be curved in plan. This was achieved and validated against published works Khaloo & Kafimosavi (2007). The model was then successfully modified and subject to a number of parametric studies to provide insight to the influence of curvature, prestress and traffic load patterning. The results were presented in terms of section stresses, deflections and influence lines for traffic loading.

The various effects of the parameters are discussed in the following five sections:

6.1.1 Effects of curvature

The straight bridge exhibits symmetrical behaviour about its vertical section centreline acting as expected as a simply supported beam subject to a UDL (i.e. a parabolic bending moment profile). The longitudinal stresses in the section are uniform and vary linearly with the section depth. The combination of bending stresses from the applied UDL, prestress and direct compression, governs the final stress profile. The FE model was successfully validated in this sense with a balanced self-weight in terms of approximately uniform compression from top to bottom.

As the bridge takes on a curved profile on plan, the geometric volume of the bridge increases, hence the mass of the bridge will be larger as the curvature increases hence an increased UDL will also be experienced. The vertical load now has an eccentricity which increases toward mid-span, causing a twist or torque. So, this is present in addition to the normal vertical bending effects and can possibly cause some degree of warping. All of this contributes to a change in direct stresses within the section which at increased curvatures cause the beam to violate service stress limits. This has clearly been shown in the studies carried out in Chapter 4. From figure 4.90 in Chapter 4, the relationships clearly show that the higher levels of prestress do allow the

bridge to take on more load at increased curvature, however this trend might also be expected of straight bridges as long as transfer stresses were kept within acceptable limits (to avoid applying too much prestress).

6.1.2 Effects of prestress

As eluded to already, the level of prestressing tends to allow increased curvatures to be acceptable in terms of keeping the longitudinal stress (figure 4.89) within class 1 levels (i.e. no cracking present). Specifying these design criteria allows the FE model to remain linear.

The tendon profile represented as piecewise linear does not balance the applied load as a continuously curved tendon would do (upward point loads at third points in opposition to a downward UDL), but provides a reasonable balance in light of the modelling/meshing issues a continuously curved tendon would produce.

The prestress as represented in the finite element model is akin to a pretensioned beam. Full compatibility between the nodes of the concrete beam and the prestressing tendon ensure that this is the case. Loss of prestress would be expected whether the beam was post or pretensioned (elastic shortening would occur in pretensioned beams), hence as long as the level of prestress is known in the FE model after any losses, the cause and type of losses is not of concern. By way of validation a sample calculation of elastic shortening prestress losses is presented in Appendix 5.

From the box girder shell FE model with an initial prestressing force of 45000kN, the reported prestressing forces in the steel without and with the applied self-weight are approximately 37000kN and 42000kN respectively. This equates to a loss of around 18% From the design calculations provided in Appendix 5 it can be seen that the predicted losses are quite close to the losses obtained (within 1% at 36385kN and 41788kN respectively). It was also observed that the elastic shortening prestress loss is insensitive to the amount of horizontal curvature of the bridge deck.

It should be noted that long term losses such as creep, shrinkage and relaxation are not accounted for in the model. Also, friction and anchorage draw-in are also not applicable as these are associated with post-tensioned members. No anchorage strengthening was considered, but as the model was linear, this was not problematic (also the tendons terminate close to the centroid of the section so will spread the anchorage loading). Transmission lengths (the length over which

the force builds up from zero at the beam end to its full value within the beam span) are short and have no significant effects on the performance of the bridge deck.

6.1.3 Boundary conditions

Considering the boundary conditions, the intention was to maintain the beam as simply supported as the form of the bridge became horizontally curved in plan. Initially a range of supports were tried and tested, but these would generate a range of design issues with tendon profiles and consistency of support conditions as the bridge curved in plan. To achieve this consistency, the rigid beam structure at the ends provides a single node point at the section centroid which is a means of conveniently providing a range of support conditions.

Having taken the decision to provide a simple span with zero moments at the ends of the bridge, it was evident that the six degrees of freedom (three translational and three rotational) would need to be orientated in accordance with the radial and tangential directions of the curve, i.e. rotated into cylindrical coordinates. If the boundary conditions remained in the Cartesian directions this would have provided complications with varying degrees of moment fixity at the ends. Hence the nodes were rotated into the cylindrical co-ordinate system so that with the boundary rotation about the tangential direction prevented global rotation of the curved structure. It is accepted that in practice the curved spans are likely to be one of a set of continuous members with continuity over intermediate supports, however an understanding of the structural behaviour of the basic curved bending element is required before the number of parameters and details are built up.

6.1.4 Traffic patterning

The results from Chapter 5 regarding the load patterning from traffic suggest that the traffic loading is significantly lower than the bridge self-weight loading. Unsymmetrical load patterning causes disruption in the uniform flow of torque along the bridge and hence can present itself as warping stresses. As expected the stresses become more pronounced and disparate at higher curvatures as the torque (and loading) increases.

6.2 Discussion

6.2.1 Shell vs Beam models

The decision was made to model the box girder using shell elements. It can be seen that this allows for stresses and local behaviour to be captured within the model, as well as allowing the profile of the prestressing tendon to be altered as desired.

Stress resultants (such as bending moments, shearing forces and axial forces) are harder to process with such detailed models, but are usually readily available from beam element models. As a small additional exercise a beam element model was developed using ANSYS to examine, compare and contrast with the shell element model. A brief description follows:

The beam element model nodes were laid out using cylindrical coordinates on plan. To represent the section properties in the correct manner, Beam 44 was used (which is a 3D tapered beam element). This element allowed the input of individual section properties with centroidal offsets at each end of the element. To represent the prestress, a link element (Link 8) was applied across the nodes and an initial strain input to create the prestress.

When the prestress is applied in this manner, it tends to create only a precompression akin to a straight tendon positioned along the centroid of the section. To capture the additional bending effects of a profiled tendon, an equivalent transverse load was also applied to the model.

The boundary conditions for the model at the ends of the beam are exactly the same as for the shell model, i.e. restrained in torsion about the longitudinal/tangential axis, restrained in radial and vertical translation at both ends, and in tangential translation at one end only

As an example, the bridge with a sector dimension delta of 5m (curvature of 0.0133 per metre) is shown as an example (refer to Chapter 4 for dimensions and section properties). Figure (6.1) shows the general bridge arrangement constructed from beam elements and the deflected shape under self-weight. The maximum deflection is 31mm which compares well with the 29mm reported for the shell model.

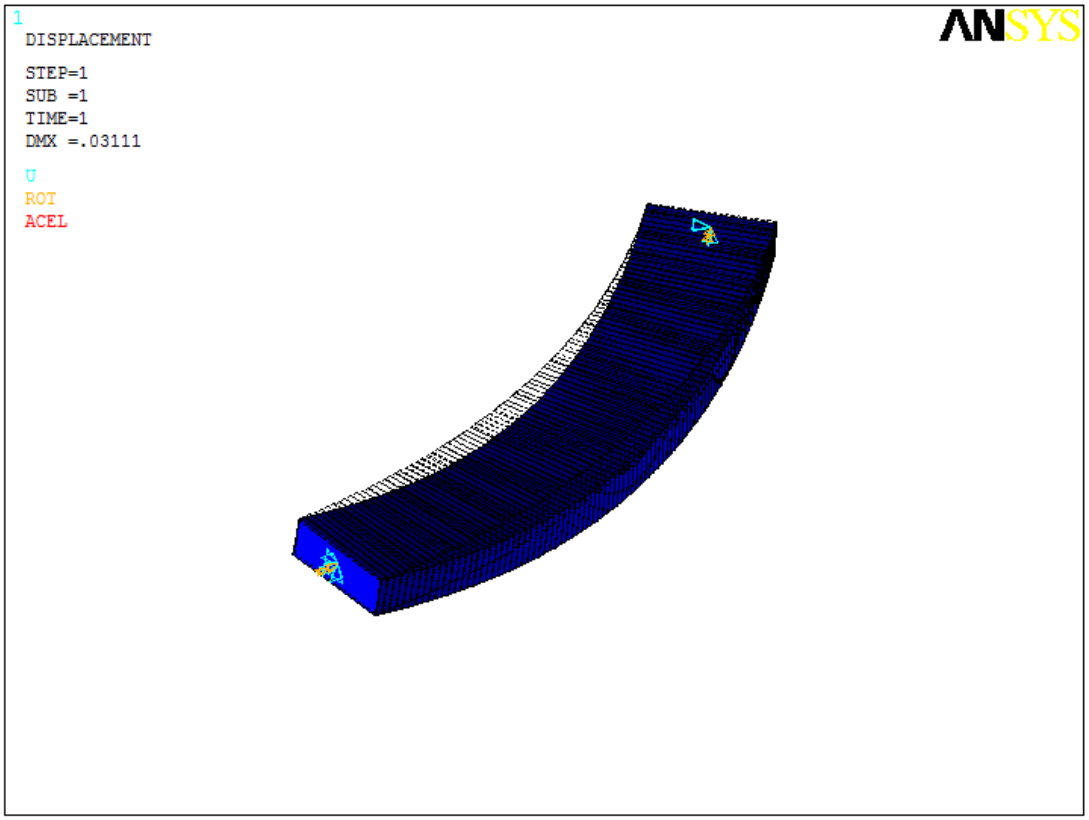

Figure (6.1) Deflection of bridge under self-weight, delta = 5m

The bending and torsional moment diagrams are shown in figures (6.2) and (6.3) respectively:

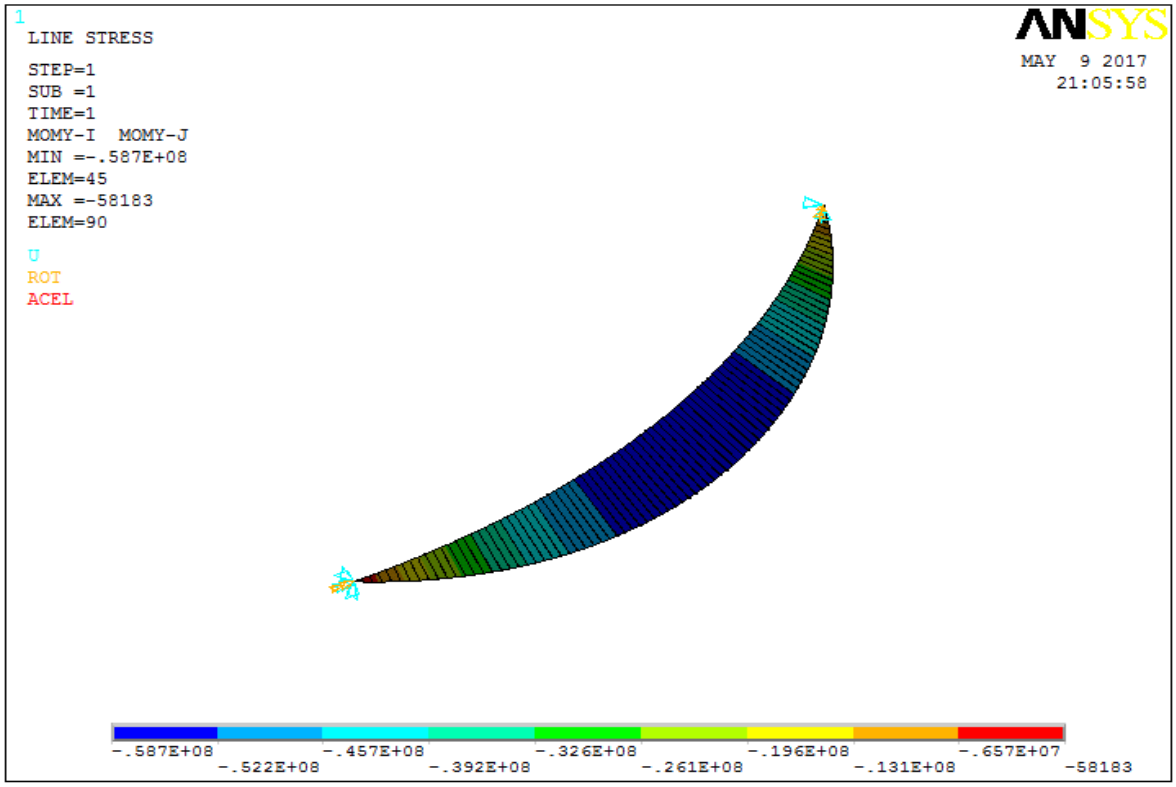

Figure (6.2) Vertical bending moment of bridge under self-weight, delta = 5m

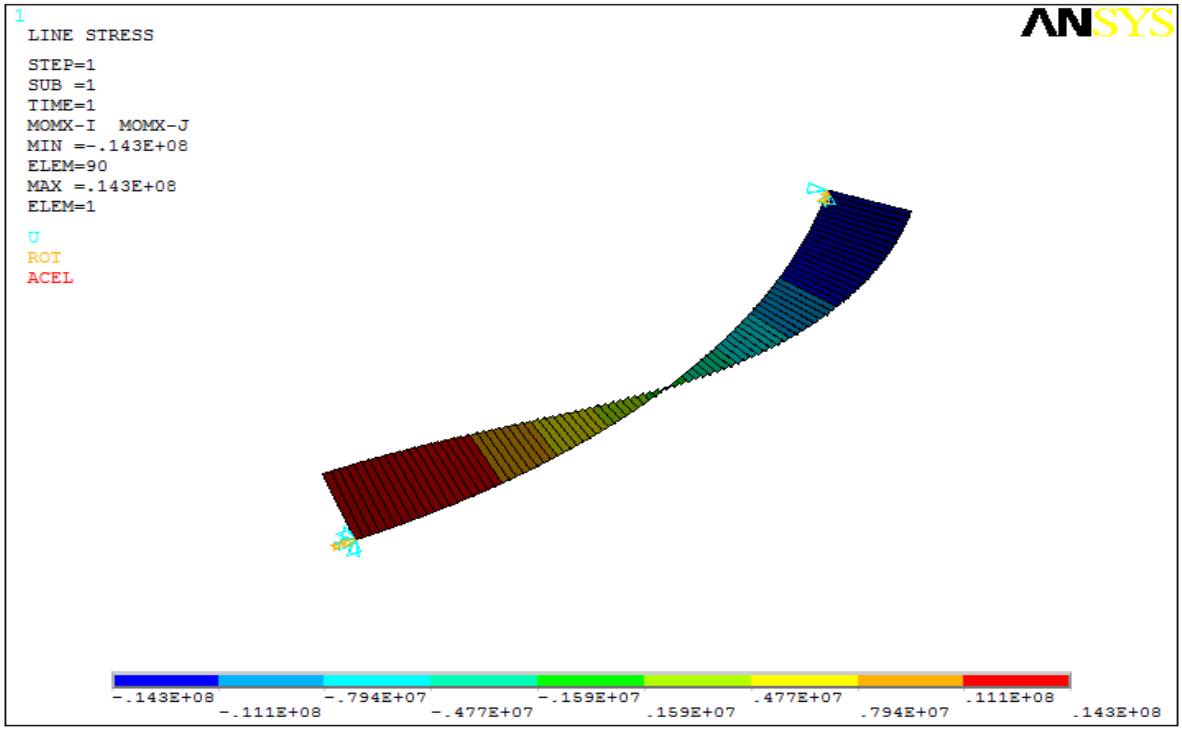

Figure (6.3) Torsion of bridge under self-weight, delta = 5m

The form of the bending moment diagram and torsion moment diagrams are as expected for a curved member subject to a UDL. The maximum bending moment occurs at the mid-span (58700 kNm) and the maximum torsion occurs at the end (14300 kNm). Compared to the shell model reactions, there is a marginal difference between the reported torsions at the boundaries, with the shell model being slightly higher. On closer inspection, as the shell model represents the deck in 2D on plan, then as the arc length (as viewed on plan) increases moving from the inner to the outer radius, there will naturally be more mass toward the outer edge. Therefore, there is an increased weight distribution across the deck from the inner to the outer radius causing a torsion which would not be considered in the beam element model. This additional torsion will register at the supports.

The torsion will cause St. Venant shear stresses and in-plane warping stresses along the length of the beam. However, as the section is of a closed box form the effects of warping should be minimal, and only prevalent at the ends of the beam.

A calculation for the equivalent transverse point loading created by the piecewise linear prestress is presented in Appendix 5. This has been subsequently applied to the model as shown in figure (6.4). The vertical bending moment is shown in figure (6.5) and the torsion is shown in figure (6.6). This shows that the conventional load balancing is affected to a degree by the curvature of the bridge in so much that this needs to be considered in the calculation in terms of the developed length of the curve. Hence the equivalent loads calculated using the straight beam geometry will tend to overestimate the bending moment required to balance the applied downward UDL. The upward deflection due to the prestress is approximately 34mm, hence the combined effects produce an upward camber of approximately 3mm as seen in figure (6.4).

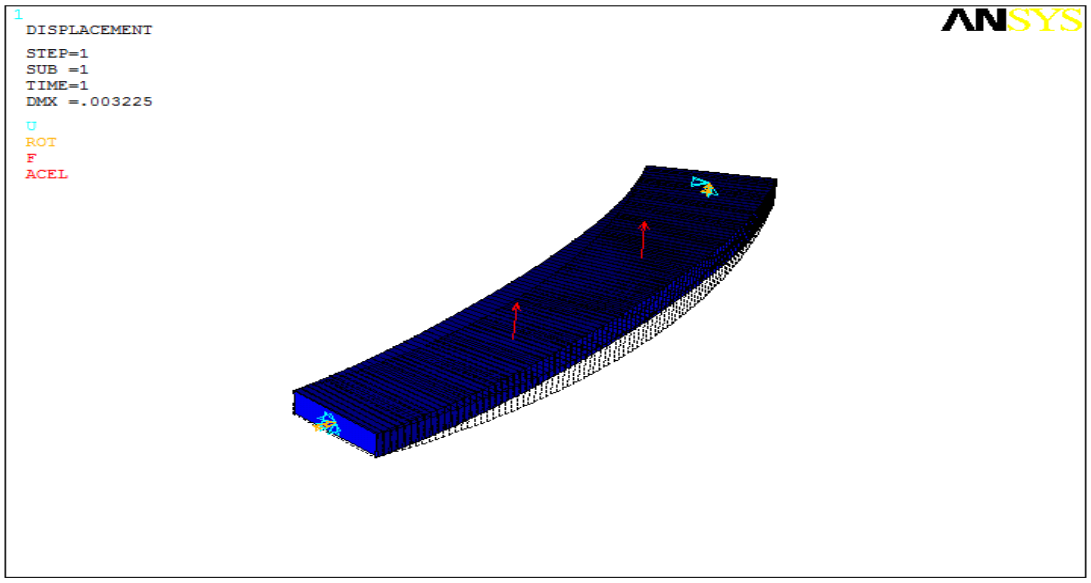

Figure (6.4) Deflection of bridge under self-weight and equivalent load, delta = 5m

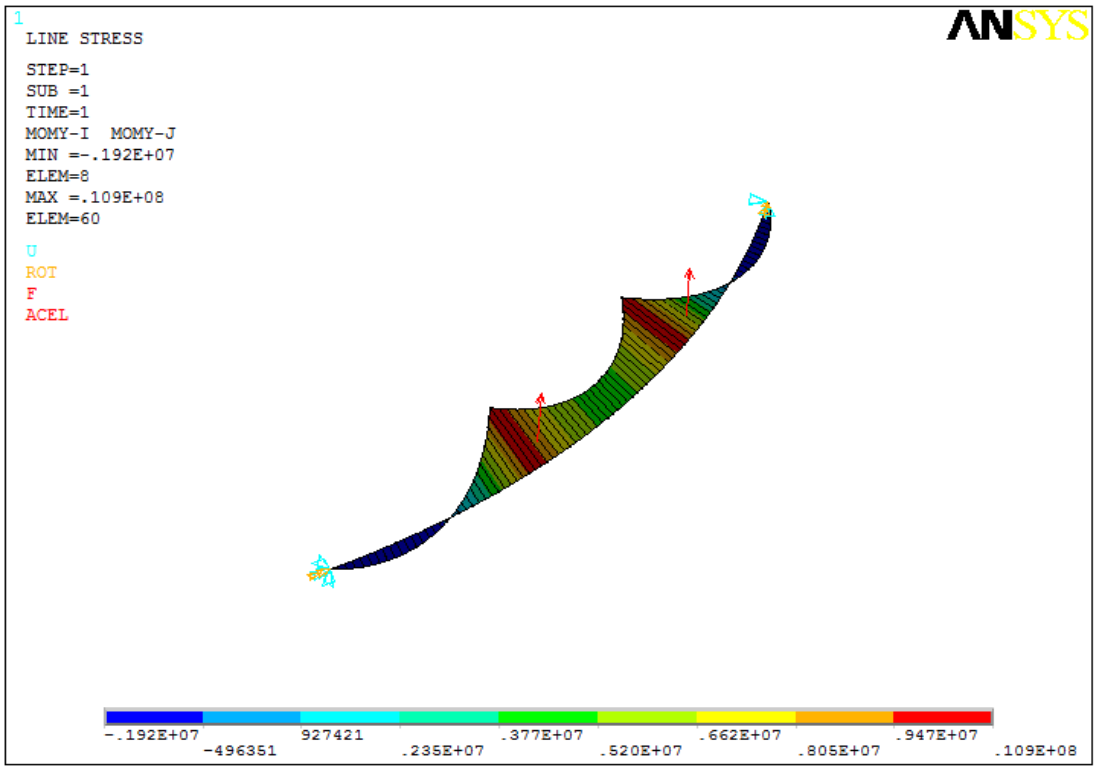

Figure (6.5) Vertical bending moment of bridge under self-weight and equivalent load, delta = 5m

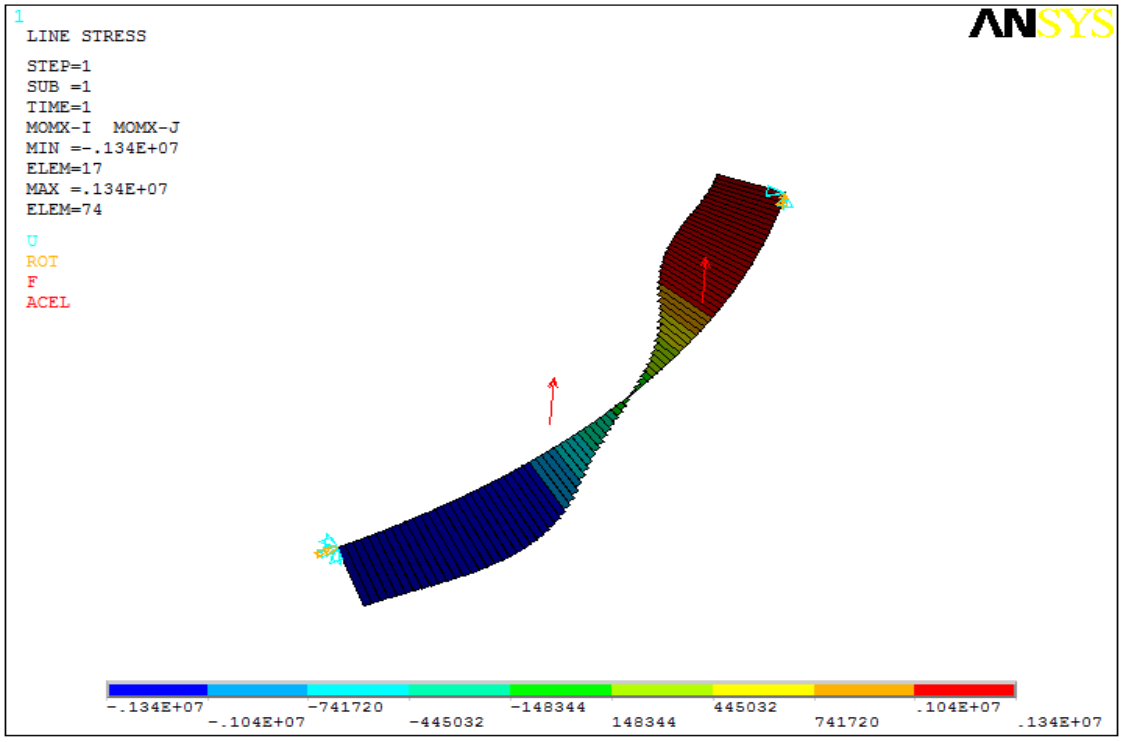

Figure (6.6) Torsion of bridge under self-weight and equivalent load, delta = 5m

It can be seen that the effects of abrupt changes in tendon profile causing point equivalent loads will also cause abrupt changes in torsion along the bridge axis (as seen in figure 6.6). As stated earlier the effects of torsion are generally resisted by the closed geometric box form of the section.

6.3 Further work

Clearly, with just a simply supported model there are many further parameters which can be examined. In terms of application to a real bridge structure, the following presents some recommendations for further study:

- Introduce fixed boundary conditions. This would necessitate that the tendon profiles would need to rise above the centroid at supports. This would then serve as preliminary work for investigating the effect of continuity and the presence of a degree of rotational stiffness at supports.
- Introduce continuity with intermediate piers/supports. These would be likely to require reversed curvature of the tendon over the support sections and local thickening of the deck

soffit to cope with increased bearing stresses. The added complication of secondary (parasitic) moments would arise, so the effects of these would be interesting to investigate (a parametric study could be conducted through linear transformation of the tendon profile).

- Consider the implications of partial prestressing, i.e. allow tension to develop in the section (class 2 and 3 sections). The material would also need to capture the effects of concrete cracking. With ANSYS this would mean exploring a model constructed from solid elements, so an alternative code such as ABAQUS might be preferable.

6.4 Recommendations for practice

The procedure presented in this work has highlighted that modern FE software packages can be programmed/scripted to quickly provide shell based finite element models which can be used to either validate a design or as part of the design process.

For class 1 sections it is recommended that the usual prestressing design processes are carried out to a code of practice for a straight deck in plan. Once an FE model has been validated against this design, the desired curvature can be introduced and the FE model will allow the user to examine a range of prestressing options rapidly.

The use of FEA within design practice should become routine procedure rather than considered as a specialist process, although this will require greater understanding of advanced modelling amongst industrialists.

References

Abeer A.M., A.A., Allawi & K.H., Chai. (2013). Theoretical Study on Torsional Strengthening of Multi-cell RC Box Girders. *World Academy of Science, Engineering and Technology International Journal of Civil, Environmental, Structural, Construction and Architectural Engineering*, 7 (2), 92-99.

Al-Wazeer, A., Harris, B, & Nutakor, C. (2007). CoRe Concerns. Retrieved February 2007, from https://www.fhwa.dot.gov/publications/publicroads/07jan/04.cfm

Ahirwar, K., Khan, M. & Kumar, A. (2016). Review on Analysis and Behavior Investigation of Box Girder Bridges. *International Research Journal of Engineering and Technology (IRJET),* 3(4), 2339–2342.

Al-Rifaie, W. N., and Evans, H. R. (1979). An approximate method for the analysis of box girder bridges that are curved in plan. *Proc., Int. Association of Bridges and Structural Engineering, Int. Association for Bridge and Structural Engineering (IABSE*), 1–21.

Alawneh, M. (2013). *Curved precast prestressed concrete girder bridges*. (PhD thesis), University of Nebraska - Lincoln. Retrieved from http://digitalcommons.unl.edu/dissertations/AAI3591522

American Association of State Highway and Transportation Officials AASHTO. (2004). *AASHTO LRFD Bridge Design Specifications*. 3rd Ed. Washington, DC. Retrieved from :http://www.fhwa.dot.gov/publications/publicroads/05jul/09.cfm

Angomas, F. (2009). *Behavior of Prestressed Concrete Bridge Girders*. (MSc thesis). Retrieved from Utah State University. https://www.scribd.com/document/323707409/Behavior-of-Prestressed-Concrete-Bridge-Girders

ANSYS Element Reference, 001084, Tenth Edition, SAS IP Inc.

Benaim, R. (2008). *The Design of Prestressed Concrete Bridges Concepts and Principles*. Retrieved from http://197.14.51.10:81/pmb/ARCHITECTURE/The%20Design%20of%20Prestressed%20Concrete%20Bridges.pdf

Bourne, S. (2013). Prestressing: recovery of the lost art. *The Structural Engineer*, 91(2), 12-22.

Chan, S.L. & Teng, J.G. (2002). *Advances in Steel Structures.* Third international conference on advanced steel structures, Hong Kong, China. Retrieved from https://www.elsevier.com/books/advances-in-steel-structures/chung/978-0-08-044017-0

Chapman, J. C., Dowling, P. J., Lim, P. T. K., & Billington, C. J. (1971). The structural behaviour of steel and concrete box girder bridges. *The Structural Engineer, 49(*3), 111–120.

Cheung, Y. K. (1976). The Finite-Strip Method in Structural Analysis. Headington Hill Hall, Oxford: Pergamos Press Ltd.

Childs, D. (2015). *Bridge Abutment Design Tutorial*. Retrieved 4 January 2016, from http://www.bridgedesign.org.uk/tutorial/abutmentu.html

Chourasia, M., & Akhtar, S. (2015). Design and Analysis of Prestressed Concrete Box Girder by Finite Element Method (4 Cells & 1 Cell). *International Journal of Civil and Structural Engineering Research, 3*(1), 413–421.

Chung C. Fu and Daili Yang (2001). Torsional Analysis for Prestressed Concrete Multiple Cell Box. *Journal of Engineering Mechanics, 127*(1), 1-20.

Civil Engineering, (2015). Box Girder Bridges. Retrieved, 4 March 2015, from https://erkrishneelram.wordpress.com/2015/03/12/box-girder-bridges/

Corven, J. (2016). *Post-Tensioned Box Girder Design Manual.* Department of Transportation Federal Highway Administration, USA.

Dabrowski, R.(1968). *Curved thin-walled girders—Theory and analysis.* New York: Springer.

Darji, A.R., Parikh, K.B., & Shah, V.J. (2016). Curved Span PSC Box Girder Bridges: A Review *International Journal of Engineering Innovation & Research. 5*(2), 153–159.

DeSantiago, E., Mohammadi, J. & Albaijat H. M. O. (2005). Analysis of Horizontally Curved Bridges Using Simple Finite-Element Models. *Journal of Practice Periodical on Structural Design and Construction, ASCE.* 10(1), 18-21.

Dey, S. S.& Balasubramanian N. (1984). Dynamic Response of Orthotropic Curved Bridge Decks Due to Moving Loads. *Journal Computers and Structures.* 18(1), 27-32.

Engineeringcivil.com (2013). *Analysis and design of prestressed concrete box girder bridge*. Retrieved 27 September 2015, from http://www.engineeringcivil.com/analysis-and-design-of-prestressed-concrete-box-girder-bridge.html

Evans, H., & Shanmugam, N. (1984). Simplified Analysis for Cellular Structures. *Journal of Structural Engineering.* 110(3), 531-543.

Fangping, L. & Jianting, Z. (2012). The Deformation Analysis of the Curved Box Girder Bridges under Different Radius. *Modern Applied Science.* 6(4), 71-76.

Galambos, T.V., Hajjar, J. F., Huang, W-H., Pulver, B. E., Leon, R.T., & Rudie, B.J. (2000). Comparison of Measured and Computed Stresses in a Steel Curved Girder Bridge. *Journal of Bridge Engineering. ASCE.* 5(3), 191-199.

Gupta, P. K., Singh, K.K., & Mishra, A. (2010). Parametric Study on Behaviour of Box-Girder Bridges Using Finite Element Method. *Asian Journal of Civil Engineering (Building and Housing).* 11(1), 135–148.

Harik, I.E., & Pashanasangi, S. (1985). Curved Bridge Decks: Analytical Strip Solution. *Journal of Structural Engineering. ASCE.* 111(7), 1517-1533.

Hsu, T.T.C. (1988). Softening Truss Model Theory for Shear and Torsion. *ACI Structural Journal.* 85(6), 624-635.

Hurst, M. (1998). Prestressed concrete design. 1st ed. London: E&FN Spon.

International Database for Civil and Structural Engineering. (2015). *Risorgimento Bridge (Rome, 1911)*. Retrieved 3 December 2015, from http://structurae.net/structures/risorgimento-bridge

International Database for Civil and Structural Engineering. (2015). *Sclayn Bridge (Sclayn / Vezin, 1950)*. Retrieved 3 December 2015, from http://structurae.net/structures/sclayn-bridge

Jain, R., & Singh, A. (2016). Parametric Study of Horizontally Curved Box Girders for Torsional Behavior and Stability. *International Research Journal of Engineering and Technology (IRJET).* 3(6), 1431–1436.

Jaramilla, B. & Huo, S. (2005). *Looking to Load and Resistance Factor Rating*. Retrieved August 2005 from http://www.fhwa.dot.gov/publications/publicroads/05jul/09.cfm

John, S. & Prasad, R. (2017). An Overview on Box Girder Bridges. *International Research Journal of Engineering and Technology (IR JET).* 4*(*1), 522-524.

Khairmode, A.S., & Kulkarni, D.B. (2016). Analysis of prestressed concrete multi-cell box girder curved bridge. *International Journal of Science and Research (IJSR).* 5(6), 2455–2459. doi:10.21275/v5i6.art20162

Khaloo, A.R. & Kafimosavi, M. (2007). Enhancement of Flexural Design of Horizontally Curved Prestressed Bridges. *Journal of Bridge Engineering, ASCE.* 12(5), 585-590.

Kolbrunner, C.F. & Basler, K. (1969). *Torsion in Structures: An Engineering Approach*. Berlin. Springer-Verlag.

Kou, C. (1989). *Static and dynamic analysis of curved continuous box-girder bridges.* (PhD thesis). Brigham Young University, Utah.

Kou, C., Benzely, S.E., Huang, J., and Firmage, D. A. (1992). Free vibration analysis of curved thin-walled girder bridges. *Journal of Structural Engineering, ASCE.* 118 *(*10), 2890–2910.

Kumar.Ch, P., M.Tech, S., & M.Tech, D. (2016). Analysis and Design of Prestressed Box Girder Bridge by IRC: 112-2011. *International Journal of Constructive Research in Civil Engineering,* 2(2), 1-10.

Lin, T. & Burns, N. (1981). *Design of prestressed concrete structures*. 1st ed. New York: Wiley.

Linzell, D., Leon, R., & Zureick, A. (2004). Experimental and Analytical Studies of a Horizontally Curved Steel I-Girder Bridge during Erection. *Journal of Bridge Engineering, 9*(6), 521-530.

Maisel, B.I., Rowe, R.E. & Swann, R.A. (1973). Concrete box girder bridges. *Journal of Structural Engineering.* 51(10), 363-376.

Maisel, B.I. (1970). Review of literature related to the analysis and design of thin-walled beams, *Tech. Rep. No. 42440, Cement and Concrete Association.* London.

Maisel, B. I. (1982). *Analysis of concrete box beams sing small-computer capacity*. Cement and Concrete Association Retrieved 12-1982, from http://worldcat.org/isbn/0721012531

Marsh, J. G. & Taylor, P. (1990). PC program for orthotropic plate box girder bridges. Australia. *Second National Structural Engineering Conference, Institution of Engineers, Australia.* 224–235.

Meyer, C. & Scordelis, A.C. (1971). Analysis of curved folded plate structures. *Journal. Structural Division.* 97(10), 2459–2480.

Mosley, W.H., Bungey, J.H. & Hulse, R. (2012). Reinforced concrete design to Eurocode 2. *Basingstoke: Palgrave Macmillan*.

National Cooperative Highway Research Program (2008). *Development of Design Specifications and Commentary for Horizontally Curved Concrete Box-Girder Bridges*. Washington D.C.: Research sponsored by the American Association of State Highway and Transportation Officials in Cooperation with the Federal Highway Administration.

O'Brien, E., Dixon, A. & Sheils, E. (2012). *Reinforced and prestressed concrete design to EC2*. 1st ed. Abingdon, Oxon: Spon Press.

Okeil, A. M. & El-Tawil, S. (2004). Warping stresses in curved box girder bridges: Case study. *Journal of Bridge Engineering.* 9(5), 487–496.

Ontario Ministry of Transportation and Communications. (2000) *Canadian highway bridge design code (CHBDC)*. Ontario, Canada.

Patil, Y.S. & Shinde, S.B. (2013). Comparative Analysis of Box Girder Bridge with Two Different Codes. *Engineering and Technology (IJCIET) International Journal of Civil Engineering and Technology (IJCIET)*. 4(3), 111–120.

Prayash Gomdenn, B. P. J. (2012). *Box girder bridges. Rak-11.3001 Design of Bridges*. Aalto University. Retrieved from https://www.scribd.com/doc/215010342/Notes-Bridge-Design-Box-Girder-Bridges.

Rajagopalan, N. (2002). *Prestressed concrete*. 1st ed. Pang Bourne: Alpha Science.

Sali, J. & Mohan, R.P. (2017). Parametric Study of Single Cell Box Girder Bridge under Different Radii of Curvature. *Applied Mechanics and Materials.* 857, 165-170.

Sali, J., Inqualabi, K.Q.I. & Mohan, R.P. (2016). Parametric study of behaviour of box girder bridges under different radius of curvature. *International Journal of Science and Research (IJSR).* 5(6), 487–492.

Sarode, A. & Vesmawala, G. (2014). Parametric study of horizontally curved box girders for torsional behaviour and stability. *International Refereed Journal of Engineering and Science (IRJES).* 3(2), 50-55.

Sasidharan, N.P. & Johny, B. (2015). Finite element analysis and parametric study of curved concrete box girder using Abaqus software. *International Journal of Research in Engineering and Technology.* 04(10), 425–429. doi:10.15623/ijret.2015.0410069.

Schlaich, J. & Scheef, H. (1982). *Concrete Box Girder Bridges*. 1st Edition. Switzerland: International Association for Bridge and Structural Engineering.

Scordelis, A.C. (1961). *A matrix Formulation of the Folded Plate Equations.* The American Society of Civil Engineers, *ASCE.* 126(2), 579-600.

Sennah, K. & Kennedy, J. (2002). Literature Review in Analysis of Box-Girder Bridges. *Journal of Bridge Engineering.* 7(2), 134-143.

Shah, R.J., Darji, A.R., & Parikh, K.B. (2016). Parametric study of curved span psc box girder bridges as per IRC: 112: 2011. *Journal of Emerging Technologies and Innovative Research (JETIR).* 3*(*6), 177–182.

Shanmugam, N.E., Thevendran, V. & Liew, J.Y.R. (1995). Experimental Study on Steel Beams curved in Plan. *Journal of Structural Engineering, ASCE.* 121(2), 249-258.

Shen, Y., Song, T.Y. & Li, G.P. (2015). Advances of external prestressing tendons in multi-span box-girder bridges. *International Conference on Multi-Span Large Bridges.* Retrieved 1-3 July 2015, Porto, Portugal, 1255-1262.

Swann, R.A. (1972). *A feature survey of concrete spine-beam bridges.* London: Cement and Concrete Association.

Thakai, R., Deshpande, R. & Bedkihal, S. (2016). Parametric Study on Behavior of Box-Girder Bridges Using Finite Element Method. *International Research Journal of Engineering and Technology (IRJET).* 3(1), 211–218.

Vlasov, V.Z. (1965). *Thin-walled elastic beams*. 2nd Edition. Washington D. C.: National Science Foundation.

Zienkeiwicz, O.C. (1977). *The finite-element method.* 3rd Edition. California: McGraw-Hill Book Company.

Appendix

Appendix1

- Paper's calculation for stresses

Second Moment of Area $I = 15.24\ m^4$
Cross Sectional Area $A = 8.64\ m^2$
Distance from Soffit to Centroid $Y_{bar} = 1.822$ m
concrete unit weight $\rho = 2400\ kg.\ m^{-3}$
Depth of Section $D = 3.3$ m
Width of Deck $B = 12$ m
Length of Deck $L = 54$ m
Acceleration $g = 9.81\ m.sec^{-2}$
Applied load $UDL = 25\ kN.m^{-2}$
Load per unit length $W = UDL \times B$
$W = 300\ kN.\ m^{-1}$
Moment at Midspan From Gravity

$$M_g = \frac{W \times L^2}{8}$$

$M_g = 1.093 \times 10^5$ kN.m
Prestressing force from all tendons P 45000 kN
Eccentricity ecc= 1.822 m
Moment at midspan from prestress $M_p = P \times ecc$
$M_p = 8.199 \times 10^4$ kN.m
Gravity Load Stresses

$$\sigma_{tg} = \frac{-M_g \times (D - Y_{Bar})}{I}$$

$\sigma_{tg} = -10.605\ N.mm^{-2}$

$$\sigma_{bg} = \frac{Mg \times Y_{Bar}}{I}$$

$\sigma_{bg} = 13.073\ N.mm^{-2}$
Prestress Stresses

$$\sigma_{tp} = \frac{P}{A} + \frac{M_p \times (D - Y_{Bar})}{I}$$

$\sigma_{tp} = 2.743 N.mm^{-2}$

$$\sigma_{bp} = \frac{P}{A} - \frac{M_p \times Y_{Bar}}{I}$$

$\sigma_{bp} = -15\ N.mm^2$
Total Stresses:
$\sigma_{tg} + \sigma_{tp} = -7.86\ N.mm^{-2}$
$\sigma_{bg} + \sigma_{bp} = 1.94\ N.mm^{-2}$

Appendix 2

- **Box girder model (APDL)**

A- APDL for the straight box girder

```
!Example Input deck for Box girder section
!Trapezoid bottom Flange Width
*ask,TBFW,Trapezoid bottom Flange Width (m),8.4
!Trapezoid bottom Flange thickness
*ask,TBFT,Trapezoid bottom Flange Thickness (m),0.3
!Trapezoid top Flange Width1
*ask,TTFW,Trapezoid Top Flange Width (m),8.4
!Trapezoid top deck thickness
*ask,TTFT,Trapezoid Top Deck Thickness (m),0.3
!Trapezoid web thickness
*ask,TWT,Trapezoid Web thickness (m),0.3
!Trapezoid web depth
*ask,TWD,Trapezoid Web Depth (m),3.3
!Extra wing width
*ask,EWW,Extra wing width (m),1.8
!Extra wing thickness
*ask,EWT,Extra wing thickness (m),0.3
!Span
*ask,SPAN,span(m),54
!No Elems in Extra wing
*ask,NEEW, No of elements in Extra wing,3
!No Elems in trapezoid top flange
*ask,NETTF,No of elements trapezoid top flange,14
!No Elems in trapezoid bottom flange
*ask,NETBF,No of elements trapezoid bottom flange,14
!No Elems in trapezoid web
*ask,NETW,No of elements trapezoid web,5
!No Elems in Span
*ask,NES, No of elements in span,90
/PREP7
ET,1,SHELL63
KEYOPT,1,3,0
KEYOPT,1,4,0
KEYOPT,1,5,0
KEYOPT,1,6,0
R,1,TBFT,TBFT,TBFT,TBFT,,
R,2,TTFT,TTFT,TTFT,TTFT, ,
R,3,TWT,TWT,TWT,TWT, ,
R,4,EWT,EWT,EWT,EWT, ,
MP,EX,1,17e9
MP,PRXY,1,0.3
!*************************
!***NODES FOR TOP DECK********
```

```
!*****************************
n,1,0,0,0
ngen,NEEW+1,1,1,,1,EWW/NEEW
ngen,NETTF+1,1,NEEW+1,,1,TTFW/NETTF
ngen,NEEW+1,1,NEEW+NETTF+1,,1,EWW/NEEW
!*********************************************
!***GENERATE NODE AT TOP OF WEB ON DECK********
!*********************************************
n,NEEW+NETTF+NEEW+2,EWW,0,0
!*****************************
!***NODES FOR BOX SECTION********
!*****************************
ngen,NETW+1,1,NEEW+NETTF+NEEW+2,,1,,,TWD/NETW
NGEN,NETBF+1,1,NEEW+NETTF+NEEW+NETW+2,,1,TBFW/NETBF
ngen,NETW+1,1,NEEW+NETTF+NEEW+NETW+NETBF+2,,1,,,-TWD/NETW
!*************************************************************
n,NEEW+NETTF+NEEW+NETW+NETBF+NETW+3,(EWW+0.5*TTFW),0,TWD
ngen,NETW+1,1,NEEW+NETTF+NEEW+NETW+NETBF+NETW+3,,,,,-TWD/NETW
!*************************************************************
ngen,NES+1,NEEW+NETTF+NEEW+NETW+NETBF+NETW+NETW+4,1,NEEW+NETTF+
NEEW+NETW+NETBF+NETW+NETW+4,1,0,SPAN/NES,0
Type,1
Mat,1
Real,2
e,1,2,NEEW+NETTF+NEEW+NETW+NETBF+NETW+NETW+6,NEEW+NETTF+NEEW+N
ETW+NETBF+NETW+NETW+5
egen,NEEW+NETTF+NEEW,1,1,
Real,1
e,(2*NEEW)+NETTF+2,(2*NEEW)+NETTF+3,(2*NEEW)+NETTF+(3*NETW)+NETBF+NE
TTF+(2*NEEW)+7,(2*NEEW)+NETTF+(3*NETW)+NETBF+NETTF+(2*NEEW)+6
egen,(2*NETW)+NETBF,1,NEEW+NETTF+NEEW+1
e,(2*NEEW)+NETTF+(2*NETW)+NETBF+3,(2*NEEW)+NETTF+(2*NETW)+NETBF+4,4*
NEEW+2*NETTF+4*NETW+2*NETBF+13,4*NEEW+2*NETTF+4*NETW+2*NETBF+12
egen,NETW,1,2*NEEW+NETTF+2*NETW+NETBF+1
egen,NES,2*NEEW+NETTF+3*NETW+NETBF+4,1,2*NEEW+NETTF+3*NETW+NETBF
```

B- APDL curved box girder

1- Delta (δ =1 m)

```
!Example Input deck for Box girder section
!Trapezoid bottom Flange Width
*ask,TBFW,Trapezoid bottom Flange Width (m),8.4
!Trapezoid bottom Flange thickness
*ask,TBFT,Trapezoid bottom Flange Thickness (m),0.3
!Trapezoid top Flange Width1
*ask,TTFW,Trapezoid Top Flange Width (m),8.4
!Trapezoid top deck thickness
```

```
*ask,TTFT,Trapezoid Top Deck Thickness (m),0.3
!Trapezoid web thickness
*ask,TWT,Trapezoid Web thickness (m),0.3
!Trapezoid web depth
*ask,TWD,Trapezoid Web Depth (m),3.3
!Extra wing width
*ask,EWW,Extra wing width (m),1.8
!Extra wing thickness
*ask,EWT,Extra wing thickness (m),0.3
*ask,THETA,Angle(deg),8.48
*ask,RD,Radius(m),365
!Span
*ask,SPAN,span(m),54
!No Elems in Extra wing
*ask,NEEW, No of elements in Extra wing,3
!No Elems in trapezoid top flange
*ask,NETTF,No of elements trapezoid top flange,14
!No Elems in trapezoid bottom flange
*ask,NETBF,No of elements trapezoid bottom flange,14
!No Elems in trapezoid web
*ask,NETW,No of elements trapezoid web,5
CSYS,1
!No Elems in Span
*ask,NES, No of elements in span,90
/PREP7
ET,1,SHELL63
KEYOPT,1,3,0
KEYOPT,1,4,0
KEYOPT,1,5,0
KEYOPT,1,6,0
R,1,TBFT,TBFT,TBFT,TBFT,,
R,2,TTFT,TTFT,TTFT,TTFT, ,
R,3,TWT,TWT,TWT,TWT, ,
R,4,EWT,EWT,EWT,EWT, ,
MP,EX,1,17e9
MP,PRXY,1,0.3
!*****************************
!***NODES FOR TOP DECK********
!*****************************
n,1,RD,0,0
ngen,NEEW+1,1,1,,1,EWW/NEEW
ngen,NETTF+1,1,NEEW+1,,1,TTFW/NETTF
ngen,NEEW+1,1,NEEW+NETTF+1,,1,EWW/NEEW
!*********************************************
!***GENERATE NODE AT TOP OF WEB ON DECK********
!*********************************************
```

```
n,NEEW+NETTF+NEEW+2,RD+EWW,0,0
!*****************************
!***NODES FOR BOX SECTION********
!*****************************
ngen,NETW+1,1,NEEW+NETTF+NEEW+2,,1,,,TWD/NETW
NGEN,NETBF+1,1,NEEW+NETTF+NEEW+NETW+2,,1,TBFW/NETBF
ngen,NETW+1,1,NEEW+NETTF+NEEW+NETW+NETBF+2,,1,,,-TWD/NETW
!*************************************************************
n,NEEW+NETTF+NEEW+NETW+NETBF+NETW+3,RD+(EWW+0.5*TTFW),0,TWD
ngen,NETW+1,1,NEEW+NETTF+NEEW+NETW+NETBF+NETW+3,,,,,-TWD/NETW
!*************************************************************
ngen,NES+1,NEEW+NETTF+NEEW+NETW+NETBF+NETW+NETW+4,1,NEEW+NETTF+
NEEW+NETW+NETBF+NETW+NETW+4,1,0,THETA/NES,0
Type,1
Mat,1
Real,2
e,1,2,NEEW+NETTF+NEEW+NETW+NETBF+NETW+NETW+6,NEEW+NETTF+NEEW+N
ETW+NETBF+NETW+NETW+5
egen,NEEW+NETTF+NEEW,1,1,
Real,1
e,(2*NEEW)+NETTF+2,(2*NEEW)+NETTF+3,(2*NEEW)+NETTF+(3*NETW)+NETBF+NE
TTF+(2*NEEW)+7,(2*NEEW)+NETTF+(3*NETW)+NETBF+NETTF+(2*NEEW)+6
egen,(2*NETW)+NETBF,1,NEEW+NETTF+NEEW+1
e,(2*NEEW)+NETTF+(2*NETW)+NETBF+3,(2*NEEW)+NETTF+(2*NETW)+NETBF+4,4*
NEEW+2*NETTF+4*NETW+2*NETBF+13,4*NEEW+2*NETTF+4*NETW+2*NETBF+12
egen,NETW,1,2*NEEW+NETTF+2*NETW+NETBF+1
egen,NES,2*NEEW+NETTF+3*NETW+NETBF+4,1,2*NEEW+NETTF+3*NETW+NETBF
```

2- Delta (δ=2 m)

The same as delta=1 but with different radius (RD) and Angle (THETA)

```
*ask,THETA,Angle(deg),8.48
*ask,RD,Radius(m),365
```

3- Delta (δ =3 m)

```
*ask,THETA,Angle(deg),25.361
*ask,RD,Radius(m),123
```

4- Delta (δ =4 m)

```
*ask,THETA,Angle(deg),33.708
*ask,RD,Radius(m),93.125
```

5- Delta (δ = 5 m)

```
*ask,THETA,Angle(deg),41.966
*ask,RD,Radius(m),75.4
```

6- Delta (δ =6 m)

*ask,THETA,Angle(deg),50.115
*ask,RD,Radius(m),63.75

7- Delta (δ = 7 m)
*ask,THETA,Angle(deg),58.138
*ask,RD,Radius(m),55.571

8- Delta (δ = 8 m)
*ask,THETA,Angle(deg),66.017
*ask,RD,Radius(m),49.563

9- Delta (δ =9 m)
*ask,THETA,Angle(deg),73.74
*ask,RD,Radius(m),45

10- Delta (δ =10 m)
*ask,THETA,Angle(deg),81.293
*ask,RD,Radius(m),41.45

11- Delta (δ = 11 m)
*ask,THETA,Angle(deg),88.665
*ask,RD,Radius(m),38.636

Appendix 3
Calculate (Delta δ, Theta ɵ and Radius R) for cases (2, 3, 4, 6, 7, 8, 9, 10)

A. Case 2

Length L =54 m
Delta $\delta_{step} = 2$ m

Radius $R = \left[\frac{\delta_{step}{}^2+(0.5\times L)^2}{2\times\delta_{step}}\right]$ R= 183.25 m

Theta $\theta = 2\times \tan^{-1}\left[\frac{0.5\times L}{\sqrt{R^2-(0.5\times L)^2}}\right]$ θ = 16.946°

B- Case 3

Length L =54 m
Delta $\delta_{step} = 3$ m

Radius $R = \left[\frac{\delta_{step}{}^2+(0.5\times L)^2}{2\times\delta_{step}}\right]$ R= 123 m

Theta $\theta = 2\times \tan^{-1}\left[\frac{0.5\times L}{\sqrt{R^2-(0.5\times L)^2}}\right]$ θ = 25.361°

C- Case 4

Length L =54 m
Delta $\delta_{step} = 4$ m

Radius $R = \left[\frac{5\times L)^2}{2\times\delta_{step}}\right]$ R= 93.125 m

Theta $\theta = 2\times \tan^{-1}\left[\frac{0.5\times L}{\sqrt{R^2-(0.5\times L)^2}}\right]$ θ = 33.708°

D- Case 6

Length L =54 m
Delta $\delta_{step} = 6$ m

Radius $R = \left[\frac{\delta_{step}{}^2+(0.5\times L)^2}{2\times\delta_{step}}\right]$ R= 63.75 m

Theta $\theta = 2\times \tan^{-1}\left[\frac{0.5\times L}{\sqrt{R^2-(0.5\times L)^2}}\right]$ $\theta = 50.115^{\circ}$

E- Case 7

Length L =54 m
Delta $\delta_{step} = 7$ m

Radius $R = \left[\frac{\delta_{step}{}^2+(0.5\times L)^2}{2\times\delta_{step}}\right]$ R= 55.571 m

Theta $\theta = 2\times \tan^{-1}\left[\frac{0.5\times L}{\sqrt{R^2-(0.5\times L)^2}}\right]$ $\theta = 58.138^{\circ}$

F- Case 8

Length L =54 m
Delta $\delta_{step} = 8$ m

Radius $R = \left[\frac{\delta_{step}{}^2+(0.5\times L)^2}{2\times\delta_{step}}\right]$ R= 49.563 m

Theta $\theta = 2\times \tan^{-1}\left[\frac{0.5\times L}{\sqrt{R^2-(0.5\times L)^2}}\right]$ $\theta = 66.017^{\circ}$

G- Case 9

Length L =54 m
Delta $\delta_{step} = 9$ m

Radius $R = \left[\frac{\delta_{step}{}^2+(0.5\times L)^2}{2\times\delta_{step}}\right]$ R= 45 m

Theta $\theta = 2\times \tan^{-1}\left[\frac{0.5\times L}{\sqrt{R^2-(0.5\times L)^2}}\right]$ $\theta = 73.74^{\circ}$

H- Case 10

Length L =54 m
Delta $\delta_{step} = 10$ m

Radius $R = \left[\frac{5\times L)^2}{2\times\delta_{step}}\right]$ R= 41.45 m

Theta $\theta = 2\times \tan^{-1}\left[\frac{0.5\times L}{\sqrt{R^2-(0.5\times L)^2}}\right]$ $\theta = 81.293^{\circ}$

Appendix 4

- **Box girder model (APDL)**

A- APDL for the straight box girder

```
!Example Input deck for Box girder section
!Trapezoid bottom Flange Width
*ask,TBFW,Trapezoid bottom Flange Width (m),6
!Trapezoid bottom Flange thickness
*ask,TBFT,Trapezoid bottom Flange Thickness (m),0.3
!Trapezoid top Flange Width1
*ask,TTFW,Trapezoid Top Flange Width (m),6
!Trapezoid top deck thickness
*ask,TTFT,Trapezoid Top Deck Thickness (m),0.3
!Trapezoid web thickness
*ask,TWT,Trapezoid Web thickness (m),0.3
!Trapezoid web depth
*ask,TWD,Trapezoid Web Depth (m),3
!Extra wing width
*ask,EWW,Extra wing width (m),1.8
!Extra wing thickness
*ask,EWT,Extra wing thickness (m),0.3
!Span
*ask,SPAN,span(m),54
!No Elems in Extra wing
*ask,NEEW, No of elements in Extra wing,3
!No Elems in trapezoid top flange
*ask,NETTF,No of elements trapezoid top flange,10
!No Elems in trapezoid bottom flange
*ask,NETBF,No of elements trapezoid bottom flange,10
!No Elems in trapezoid web
*ask,NETW,No of elements trapezoid web,5
!No Elems in Span
*ask,NES, No of elements in span,90
/PREP7
ET,1,SHELL63
KEYOPT,1,3,0
KEYOPT,1,4,0
KEYOPT,1,5,0
KEYOPT,1,6,0
R,1,TBFT,TBFT,TBFT,TBFT,,
R,2,TTFT,TTFT,TTFT,TTFT, ,
R,3,TWT,TWT,TWT,TWT, ,
R,4,EWT,EWT,EWT,EWT, ,
MP,EX,1,17e9
```

```
MP,PRXY,1,0.3
!*****************************
!***NODES FOR TOP DECK********
!*****************************
n,1,0,0,0
ngen,NEEW+1,1,1,,1,EWW/NEEW
ngen,NETTF+1,1,NEEW+1,,1,TTFW/NETTF
ngen,NEEW+1,1,NEEW+NETTF+1,,1,EWW/NEEW
!*********************************************
!***GENERATE NODE AT TOP OF WEB ON DECK********
!*********************************************
n,NEEW+NETTF+NEEW+2,EWW,0,0
!*****************************
!***NODES FOR BOX SECTION********
!*****************************
ngen,NETW+1,1,NEEW+NETTF+NEEW+2,,1,,,TWD/NETW
NGEN,NETBF+1,1,NEEW+NETTF+NEEW+NETW+2,,1,TBFW/NETBF
ngen,NETW+1,1,NEEW+NETTF+NEEW+NETW+NETBF+2,,1,,,-TWD/NETW
!*************************************************************
ngen,NES+1,NEEW+NETTF+NEEW+NETW+NETBF+NETW+2,1,NEEW+NETTF+NEEW+
NETW+NETBF+NETW+3,1,0,SPAN/NES,0
Type,1
Mat,1
Real,2
e,1,2,NEEW+NETTF+NEEW+NETW+NETBF+NETW+4,NEEW+NETTF+NEEW+NETW+N
ETBF+NETW+3
egen,NEEW+NETTF+NEEW,1,1,
Real,1
e,(2*NEEW)+NETTF+2,(2*NEEW)+NETTF+3,(2*NEEW)+NETTF+(2*NETW)+NETBF+NE
TTF+(2*NEEW)+5,(2*NEEW)+NETTF+(2*NETW)+NETBF+NETTF+(2*NEEW)+4
egen,(2*NETW)+NETBF,1,NEEW+NETTF+NEEW+1
egen,NES,2*NEEW+ !Example Input deck for Box girder section
!Trapezoid bottom Flange Width
*ask,TBFW,Trapezoid bottom Flange Width (m),6
!Trapezoid bottom Flange thickness
*ask,TBFT,Trapezoid bottom Flange Thickness (m),0.3
!Trapezoid top Flange Width1
*ask,TTFW,Trapezoid Top Flange Width (m),6
!Trapezoid top deck thickness
*ask,TTFT,Trapezoid Top Deck Thickness (m),0.3
!Trapezoid web thickness
*ask,TWT,Trapezoid Web thickness (m),0.3
!Trapezoid web depth
*ask,TWD,Trapezoid Web Depth (m),3
!Extra wing width
*ask,EWW,Extra wing width (m),1.8
```

```
!Extra wing thickness
*ask,EWT,Extra wing thickness (m),0.3
!Span
*ask,SPAN,span(m),54
!No Elems in Extra wing
*ask,NEEW, No of elements in Extra wing,3
!No Elems in trapezoid top flange
*ask,NETTF,No of elements trapezoid top flange,10
!No Elems in trapezoid bottom flange
*ask,NETBF,No of elements trapezoid bottom flange,10
!No Elems in trapezoid web
*ask,NETW,No of elements trapezoid web,5
!No Elems in Span
*ask,NES, No of elements in span,90
/PREP7
ET,1,SHELL63
KEYOPT,1,3,0
KEYOPT,1,4,0
KEYOPT,1,5,0
KEYOPT,1,6,0
R,1,TBFT,TBFT,TBFT,TBFT,,
R,2,TTFT,TTFT,TTFT,TTFT, ,
R,3,TWT,TWT,TWT,TWT, ,
R,4,EWT,EWT,EWT,EWT, ,
MP,EX,1,17e9
MP,PRXY,1,0.3
!*****************************
!***NODES FOR TOP DECK********
!*****************************
n,1,0,0,0
ngen,NEEW+1,1,1,,1,EWW/NEEW
ngen,NETTF+1,1,NEEW+1,,1,TTFW/NETTF
ngen,NEEW+1,1,NEEW+NETTF+1,,1,EWW/NEEW
!*********************************************
!***GENERATE NODE AT TOP OF WEB ON DECK********
!*********************************************
n,NEEW+NETTF+NEEW+2,EWW,0,0
!*****************************
!***NODES FOR BOX SECTION********
!*****************************
ngen,NETW+1,1,NEEW+NETTF+NEEW+2,,1,,,TWD/NETW
NGEN,NETBF+1,1,NEEW+NETTF+NEEW+NETW+2,,1,TBFW/NETBF
ngen,NETW+1,1,NEEW+NETTF+NEEW+NETW+NETBF+2,,1,,,-TWD/NETW
!*************************************************************
ngen,NES+1,NEEW+NETTF+NEEW+NETW+NETBF+NETW+2,1,NEEW+NETTF+NEEW+
NETW+NETBF+NETW+3,1,0,SPAN/NES,0
```

```
Type,1
Mat,1
Real,2
e,1,2,NEEW+NETTF+NEEW+NETW+NETBF+NETW+4,NEEW+NETTF+NEEW+NETW+N
ETBF+NETW+3
egen,NEEW+NETTF+NEEW,1,1,
Real,1
e,(2*NEEW)+NETTF+2,(2*NEEW)+NETTF+3,(2*NEEW)+NETTF+(2*NETW)+NETBF+NE
TTF+(2*NEEW)+5,(2*NEEW)+NETTF+(2*NETW)+NETBF+NETTF+(2*NEEW)+4
egen,(2*NETW)+NETBF,1,NEEW+NETTF+NEEW+1
egen,NES,2*NEEW+NETTF+2*NETW+NETBF+2,1,2*NEEW+NETTF+2*NETW+NETBF+
NETBF+2,1,2*NEEW+NETTF+2*NETW+NETBF
```

B- APDL curved box girder

1- Delta (δ =1 m)

```
!Example Input deck for Box girder section
!Trapezoid bottom Flange Width
*ask,TBFW,Trapezoid bottom Flange Width (m),6
!Trapezoid bottom Flange thickness
*ask,TBFT,Trapezoid bottom Flange Thickness (m),0.3
!Trapezoid top Flange Width1
*ask,TTFW,Trapezoid Top Flange Width (m),6
!Trapezoid top deck thickness
*ask,TTFT,Trapezoid Top Deck Thickness (m),0.3
!Trapezoid web thickness
*ask,TWT,Trapezoid Web thickness (m),0.3
!Trapezoid web depth
*ask,TWD,Trapezoid Web Depth (m),3
!Extra wing width
*ask,EWW,Extra wing width (m),1.8
!Extra wing thickness
*ask,EWT,Extra wing thickness (m),0.3
*ask,THETA,Angle(deg),8.48
*ask,RD,Radius(m),365
!Span
*ask,SPAN,span(m),54
!No Elems in Extra wing
*ask,NEEW, No of elements in Extra wing,3
!No Elems in trapezoid top flange
*ask,NETTF,No of elements trapezoid top flange,10
!No Elems in trapezoid bottom flange
*ask,NETBF,No of elements trapezoid bottom flange,10
!No Elems in trapezoid web
*ask,NETW,No of elements trapezoid web,5
CSYS,1
```

```
!No Elems in Span
*ask,NES, No of elements in span,90
/PREP7
ET,1,SHELL63
KEYOPT,1,3,0
KEYOPT,1,4,0
KEYOPT,1,5,0
KEYOPT,1,6,0
R,1,TBFT,TBFT,TBFT,TBFT,,
R,2,TTFT,TTFT,TTFT,TTFT, ,
R,3,TWT,TWT,TWT,TWT, ,
R,4,EWT,EWT,EWT,EWT, ,
MP,EX,1,17e9
MP,PRXY,1,0.3
!*****************************
!***NODES FOR TOP DECK********
!*****************************
n,1,RD,0,0
ngen,NEEW+1,1,1,,1,EWW/NEEW
ngen,NETTF+1,1,NEEW+1,,1,TTFW/NETTF
ngen,NEEW+1,1,NEEW+NETTF+1,,1,EWW/NEEW
!*********************************************
!***GENERATE NODE AT TOP OF WEB ON DECK********
!*********************************************
n,NEEW+NETTF+NEEW+2,RD+EWW,0,0
!*****************************
!***NODES FOR BOX SECTION********
!*****************************
ngen,NETW+1,1,NEEW+NETTF+NEEW+2,,1,,,TWD/NETW
NGEN,NETBF+1,1,NEEW+NETTF+NEEW+NETW+2,,1,TBFW/NETBF
ngen,NETW+1,1,NEEW+NETTF+NEEW+NETW+NETBF+2,,1,,,-TWD/NETW
!*************************************************************
ngen,NES+1,NEEW+NETTF+NEEW+NETW+NETBF+NETW+2,1,NEEW+NETTF+NEEW+
NETW+NETBF+NETW+3,1,0,THETA/NES,0
Type,1
Mat,1
Real,2
e,1,2,NEEW+NETTF+NEEW+NETW+NETBF+NETW+4,NEEW+NETTF+NEEW+NETW+N
ETBF+NETW+3
egen,NEEW+NETTF+NEEW,1,1,
Real,1
e,(2*NEEW)+NETTF+2,(2*NEEW)+NETTF+3,(2*NEEW)+NETTF+(2*NETW)+NETBF+NE
TTF+(2*NEEW)+5,(2*NEEW)+NETTF+(2*NETW)+NETBF+NETTF+(2*NEEW)+4
egen,(2*NETW)+NETBF,1,NEEW+NETTF+NEEW+1
egen,NES,2*NEEW+NETTF+2*NETW+NETBF+2,1,2*NEEW+NETTF+2*NETW+NETBF
```

2- Delta (δ =2 m)

The same as delta=1 but with different radius (RD) and Angle (THETA)

*ask,THETA,Angle(deg),16.946
*ask,RD,Radius(m),183.25

3- Delta (δ=3 m)

*ask,THETA,Angle(deg),25.361
*ask,RD,Radius(m),123

4- Delta (δ=4 m)

*ask,THETA,Angle(deg),33.708
*ask,RD,Radius(m),93.125

5- Delta (δ=5 m)

*ask,THETA,Angle(deg),41.966
*ask,RD,Radius(m),75.4

6- Delta (δ=6 m)

*ask,THETA,Angle(deg),50.115
*ask,RD,Radius(m),63.75

7- **Delta (δ= 7 m)**

*ask,THETA,Angle(deg),58.138
*ask,RD,Radius(m),55.571

8- Delta (δ= 8 m)

*ask,THETA,Angle(deg),66.017
*ask,RD,Radius(m),49.563

Appendix 5

- **Prestress Loss due to Elastic Shortening**

Elastic Modulus of Steel $E_s := 200 \cdot kN \cdot mm^{-2}$

Elastic Modulus of Concrete $E_{cm} := 17 \cdot kN \cdot mm^{-2}$

Modular ratio

$m_r := \frac{E_s}{E_{cm}}$ $m_r = 11.765$

Initial Prestress $P_0 := 45000\,kN$

Cross Sectional Area of $A_p := 41660\,mm^2$

Initial stress in tendons

$\sigma_{p0} := \frac{P_0}{A_p}$ $\sigma_{p0} = 1080.173\,N \cdot mm^{-2}$

Eccentricity of tendons $e := 1.715\,m$

Cross Sectional Area of Concrete Section $A_c := 6.21 \cdot m^2$

Second moment of Area of Section $I_c := 9.133 \cdot m^4$

Radius of gyration

$r := \sqrt{\frac{I_c}{A_c}}$ $r = 1.213\,m$

Stress in the concrete at the level of the tendons

$$\sigma_{cg} := \frac{\sigma_{p0}}{\left[m_r + \frac{A_c}{A_p \cdot \left(1 + \frac{e^2}{r^2} \right)} \right]} \qquad \sigma_{cg} = 17.577\,N \cdot mm^{-2}$$

Change in tendon stress

$\Delta\sigma_p := m_r \cdot \sigma_{cg}$ $\Delta\sigma_p = 206.786\,N \cdot mm^{-2}$

Loss of tendon force

$\Delta P := \Delta\sigma_p \cdot A_p$ $\Delta P = 8.615 \times 10^3 \cdot kN$

Tendon force after elastic shortening loss

$P_{eff} := P_0 - \Delta P$ $P_{eff} = 36385\,kN$

Elastic shortening losses with the addition of applied UDL

Bending moment due to UDL (from FE model)

$M_{applied} := 58703\,kN \cdot m$

Stress in the concrete at the level of the tendons

$$\sigma_{cg} := \frac{\sigma_{p0}}{\left[m_r + \frac{A_c}{A_p \cdot \left(1 + \frac{e^2}{r^2} \right)} \right]} - \frac{M_{applied} \cdot e}{I_c} \qquad \sigma_{cg} = 6.554 \cdot N \cdot mm^{-2}$$

Change in tendon stress

$\Delta\sigma_p := m_r \cdot \sigma_{cg}$ $\qquad \Delta\sigma_p = 77.1 \cdot N \cdot mm^{-2}$

Loss of tendon force

$\Delta P := \Delta\sigma_p \cdot A_p$ $\qquad \Delta P = 3.212 \times 10^3 \cdot kN$

Tendon force after elastic shortening loss in addition to applied UDL

$P_{eff} := P_0 - \Delta P$ $\qquad P_{eff} = 41788\,kN$

- **<u>Equivalent Load Calculation for Piecewise Linear Prestressing</u>**

Length of Span $\qquad Span := 54 \cdot m$

Calculate Equivalent Loads at third points to produce the same moment as the UDL at midspan

$W := \frac{3M_{applied}}{Span}$ $\qquad W = 3261\,kN$